
Mixed QCD–electroweak $\mathcal{O}(\alpha_s\alpha)$ corrections to Drell–Yan processes in the resonance region

Alexander Huss



PHYSIKALISCHES INSTITUT
FAKULTÄT FÜR MATHEMATIK UND PHYSIK
ALBERT-LUDWIGS-UNIVERSITÄT FREIBURG

September 2014

Mixed QCD–electroweak $\mathcal{O}(\alpha_s\alpha)$ corrections to Drell–Yan processes in the resonance region

Alexander Huss

DISSERTATION

zur Erlangung des Doktorgrades
der Fakultät für Mathematik und Physik der

ALBERT-LUDWIGS-UNIVERSITÄT

Freiburg im Breisgau

vorgelegt von

Alexander Huss

September 2014

Dekan: Prof. Dr. Michael Růžička

Referent: Prof. Dr. Stefan Dittmaier

Koreferent: Prof. Dr. Thomas Filk

Tag der mündlichen Prüfung: 8. Dezember 2014

Contents

Introduction and motivation	1
1. Theoretical preliminaries	7
1.1. The Standard Model of particle physics	7
1.1.1. The Lagrangian and quantisation	8
1.1.2. Renormalization	16
1.1.3. Electroweak input-parameter schemes	22
1.2. Unstable particles in QFT	24
1.3. Infrared singularities in NLO calculations	28
1.3.1. IR singularities in one-loop amplitudes	28
1.3.2. IR singularities in real-emission cross sections	29
1.4. The parton model and perturbative QCD	31
I. The Drell–Yan process at NLO and the pole expansion	37
2. The Drell–Yan process at the LHC	39
2.1. Conventions and leading-order results	39
2.2. Survey of NLO corrections	43
3. The dipole subtraction formalism	47
3.1. Conventions and general remarks	48
3.2. The dipole subtraction formalism for photon radiation off massless fermions . . .	52
3.2.1. Final-state emitter and final-state spectator	53
3.2.2. Final-state emitter and initial-state spectator and vice versa	54
3.2.3. Initial-state emitter and initial-state spectator	57
3.3. The dipole subtraction formalism for the production of massive particles	58
3.4. The dipole subtraction formalism for particle decays	60
3.4.1. General properties	60
3.4.2. Subtraction function for massive final-state fermions	62
3.4.3. Subtraction function for massless final-state fermions	66
3.4.4. Extension to non-collinear-safe observables	68
4. Pole expansion of the NLO $\mathcal{O}(\alpha)$ corrections to Drell–Yan processes	71
4.1. Concept of the pole expansion	71
4.2. Calculation of the $\mathcal{O}(\alpha)$ corrections in the pole approximation	73
4.2.1. Virtual corrections	73
4.2.2. Real corrections	76
4.3. Complete result for the NLO EW corrections in the pole approximation	81
4.3.1. The factorizable corrections to the production	81

4.3.2.	The factorizable corrections to the decay	82
4.3.3.	The non-factorizable corrections	83
4.4.	QCD corrections	85
4.5.	Numerical results at NLO	88
4.5.1.	Input parameters and setup	88
4.5.2.	Phase-space cuts and event selection	89
4.5.3.	Results	90
II.	Pole expansion for the mixed QCD–electroweak $\mathcal{O}(\alpha_s\alpha)$ corrections	95
5.	Concept of the pole expansion and classification of contributions	97
5.1.	Survey of NNLO corrections	97
5.2.	Classification of corrections in the pole approximation	100
6.	The non-factorizable $\mathcal{O}(\alpha_s\alpha)$ corrections	103
6.1.	Calculation of the non-factorizable corrections	103
6.1.1.	Soft-photon radiation off a quark line—the YFS approach	103
6.1.2.	Double-virtual corrections	109
6.1.3.	Real QCD \times virtual EW corrections	115
6.1.4.	Virtual QCD \times real photonic corrections	117
6.1.5.	Double-real corrections	118
6.2.	Complete result for the non-factorizable corrections	120
6.3.	Numerical results for non-factorizable corrections	124
7.	The factorizable initial–final $\mathcal{O}(\alpha_s\alpha)$ corrections	127
7.1.	Calculation of the factorizable initial–final corrections	127
7.1.1.	Double-virtual corrections	127
7.1.2.	Real \times virtual corrections	129
7.1.3.	Double-real corrections	130
7.2.	Complete result for the factorizable initial–final corrections	132
7.3.	Numerical results for the factorizable initial–final corrections	137
	Summary and outlook	143
	Appendix	145
A.	Conventions and notation	145
A.1.	General conventions	145
A.2.	The Weyl–van-der-Waerden spinor formalism	148
A.3.	Feynman rules	152
A.4.	Kinematics and phase-space integration	155
B.	Virtual corrections	157
B.1.	Scalar one-loop integrals	157
B.1.1.	Mellin–Barnes method	158

B.1.2. Expansion of one-loop integrals	159
B.2. Electroweak vertex corrections	163
B.2.1. Charged-current interactions	163
B.2.2. Neutral-current interactions	164
B.3. Non-factorizable corrections	167
C. The soft phase-space slicing method	171
D. Explicit form of the IR-safe contributions to $\mathcal{O}(\alpha_s\alpha)$ corrections in the PA	173
D.1. Non-factorizable corrections	173
D.2. Factorizable initial-final corrections	175
Bibliography	179
Acknowledgements	187
List of publications	189

Introduction and motivation

The Standard Model of particle physics

The primary objective of particle physics is to identify the elementary constituents of matter and to understand the fundamental laws that govern them. The Standard Model of particle physics (SM) accommodates most of our present knowledge about elementary particles and their interactions. Ever since the SM took its present form in the 1970s, a multitude of experiments have continuously challenged its predictions at ever higher accuracies and energies, and so far, the experimental results have shown remarkable agreement with the theoretical predictions. The SM incorporates the description of three of the four known fundamental forces of nature: electromagnetism, the weak interactions, and the strong force. The matter content of the SM consists of three generations of spin- $\frac{1}{2}$ fermions, each made up of two quarks, one charged lepton, and one lepton-neutrino. They interact with each other by the exchange of spin-1 force carriers, where the photon describes the electromagnetic interactions, the massive W^\pm and Z bosons the weak interactions, and eight gluons represent the mediators of the strong force. On a formal level, the SM is formulated as a quantized, spontaneously broken gauge theory with the underlying gauge group $SU(3)_C \times SU(2)_W \times U(1)_Y$ and consists of two parts: the electroweak (EW) theory and quantum chromodynamics (QCD).

The Glashow–Salam–Weinberg [1–3] (GSW) model provides a unified description of the electromagnetic and weak interactions. It is described by the $SU(2)_W \times U(1)_Y$ component of the SM gauge group and the spontaneous breaking to the residual $U(1)_{\text{em}}$ symmetry of electromagnetism is modelled by the so-called Higgs mechanism, which further renders the gauge bosons W^\pm and Z massive in this process. The prediction and subsequent experimental discovery of these massive gauge bosons at the “Super Proton Synchrotron” at the European Organization for Nuclear Research (CERN) in 1983 [4–7] constitutes one of the major successes of the SM. As a remnant of the Higgs mechanism, the SM predicts a neutral scalar (spin-0) particle called the Higgs boson. The discovery of such a boson was announced on July 4th 2012 by the two experiments ATLAS and CMS at the Large Hadron Collider (LHC) at CERN with a mass of approximately 125 GeV [8, 9]. Further measurements have begun to analyse its properties which are so far consistent with the SM prediction. The discovery of a Higgs boson with SM-like properties completes the particle spectrum of the SM and marks the beginning of a new era of particle physics.

QCD describes the strong interactions between quarks and gluons and introduces a new quantum number called *colour*, which transforms under the $SU(3)_C$ component of the SM gauge group. Its most peculiar feature is that of confinement, which expresses the empirical fact that no particle that carries an open colour charge can be observed as a free particle. Coloured particles are always confined within bound states of the strong interaction, called hadrons, which cannot be described using perturbative methods. On the other hand, the property of *asymptotic freedom* [10, 11] states that if a hadron is probed at energies far above the confining scale of QCD, its constituents behave as if they were free particles. Moreover, the information on the non-perturbative behaviour in high-energy scattering of the hadron can then be encoded in universal parton distribution functions (PDFs) and fragmentation functions which can be

extracted from experiments. These fundamental properties enable us to calculate reliable predictions within perturbative QCD which can be compared to experiment.

Despite its huge success, the SM is broadly accepted only as a low-energy approximation of a more fundamental description of nature. First and foremost, it does not incorporate the gravitational force in its description, for which no consistent quantized theory exists to date. However, this does not represent a serious limitation for collider phenomenology, since particle accelerators will not be able to probe matter particles at such short distances where gravity will be sizeable enough to be measured. Further shortcomings of the SM include the explanation for the large hierarchy observed in the fermion masses, the prediction for the number of three fermion generations, and the explanation for dark matter and dark energy, evidence of which is present in cosmological data [12]. Various models and extensions to the SM have been proposed in order to address these and further issues of the SM with the aim to provide a more fundamental description of nature at shorter distances. Many of these models have been tested and severely constrained by the experiments at the LHC in the past years. With the restart of the programme next year with a centre-of-mass energy of 13 TeV, an unprecedented energy regime will become accessible to further challenge such models.

The Drell–Yan process

One of the most prominent processes at the LHC is the so-called Drell–Yan process [13] which describes the production of a lepton pair in hadronic collisions. It represents the first hadron–hadron cross section that was calculated from first principles and greatly contributed to the understanding of the hadron structure and the validation of the parton model, see e.g. Ref. [14] for a historic review. The LHC at CERN collides two proton beams at a centre-of-mass energy that is almost four orders of magnitude higher than the protons rest mass. W and Z bosons are abundantly produced, and the corresponding Drell–Yan processes are classified into the charged- and neutral-current processes,

$$\begin{aligned} p p &\rightarrow W \rightarrow \ell \nu_\ell, \\ p p &\rightarrow Z/\gamma \rightarrow \ell^+ \ell^-, \end{aligned}$$

respectively. The LHC operating at the design luminosity of $\mathcal{L} = 10^{34} \text{ cm}^{-2}\text{s}^{-1}$, for instance, will produce ≈ 20 events per second for each lepton flavour of the neutral-current process, and even an order of magnitude more events for the charged-current processes.

This large production rate in combination with the clean experimental signature of the leptonic vector-boson decay allows this process to be measured with great precision. Moreover, the Drell–Yan-like production of W or Z bosons is one of the theoretically best understood and most precisely predicted processes. As a consequence, EW gauge-boson production is among the most important classes of “standard-candle” processes at the LHC (see, e.g. Refs. [15, 16]). Its total cross section can be used as a luminosity monitor, and the measurement of the mass and width of the Z boson represents a powerful tool for detector calibration, as it was used e.g. in the determination of the W-boson mass at the Tevatron collider at Fermilab [17, 18]. Furthermore, the W charge asymmetry and the rapidity distribution of the Z boson deliver important constraints in the fit of the quark PDFs [19], which represents a crucial ingredient for almost all predictions at the LHC. For instance, a recent measurement of rapidity distributions in W and Z production has revealed a novel sensitivity to the strange quark distribution which indicate that their contribution may be larger than represented by current PDF sets [20]. Moreover, several extensions of the SM predict new heavy gauge bosons (W' , Z') which may

be produced through the Drell–Yan mechanism and be observed, e.g., in the high-energy tails of distributions [16]. Here the SM prediction constitutes an irreducible background in these searches and must be predicted with highest possible precision in order to enhance the discovery potential of the LHC.

Furthermore, the Drell–Yan process at the LHC allows for high-precision measurements in the resonance regions, where the weak mixing angle $\sin^2 \theta_{\text{eff}}^\ell$ might be extracted from data with LEP precision [21] and the W-boson mass M_W is expected to be measured with the highest accuracy ever. At present, the most precise determination for the W-boson mass results from the measurements by the two experiments CDF [17] and D0 [18] at the Tevatron, where their combined data yields a value of $M_W = 80.387(16)$ GeV [22]. The experimental uncertainty of $\Delta M_W = 16$ MeV significantly surpasses combined LEP precision of 33 MeV [23] and dominates the value of the world average which is given by $M_W = 80.385(15)$ GeV. This measurement represents a remarkable achievement by hadron-collider experiments. In hadronic collisions, the W-boson mass can be determined from a fit to the distributions of the lepton transverse momentum ($p_{T,\ell}$) and the transverse mass of the lepton pair ($M_{T,\ell\nu}$) which exhibit a Jacobian peak around M_W and $M_W/2$, respectively, and allow for a precise extraction of the mass. The anticipated precision for the M_W measurement at the LHC further exceeds the Tevatron measurements with a sensitivity of about 7 MeV [24] or even lower [25]. The comparison of the direct measurement of M_W with the indirect measurements from a global fit to EW precision data represents a powerful test of the validity of the SM. Any deviations from the SM prediction may deliver crucial hints about physics beyond the SM. Prior to the discovery of the Higgs boson, the W-boson mass in combination with the top-quark mass (m_t) provided indirect constraints on the mass of the Higgs boson (M_H) through quantum-loop corrections. After its discovery in 2012, such relations can be exploited to over-constrain the Higgs sector of the SM, which will be of great importance in order to establish that the discovered particle is indeed the SM Higgs boson and to further scrutinize the SM.

To fully exploit the potential of the extraordinary experimental precision that is achievable for the Drell–Yan process, it is necessary to have theoretical predictions that match (or even surpass) the required accuracy. In the past two decades, great effort was made in the theory community to deliver such precise predictions: QCD corrections are known up to next-to-next-to-leading order (NNLO) [26–33], EW corrections up to next-to-leading order (NLO) [34–45].¹ Both on the QCD and on the EW sides, there are further refinements such as leading higher-order effects [44, 45, 47–53] and generalizations to the supersymmetric extension of the SM [44, 45]. The treatment of small transverse momenta requires a resummation of large logarithms through matched parton showers [54–56] or dedicated calculations supplemented with fits to non-perturbative functions [57, 58] that are available at next-to-next-to-leading logarithmic accuracy [59–61]. First approaches to the combination of QCD and EW corrections can be found in Refs. [62–67]. In view of fixed-order calculations, the largest missing piece seems to be the mixed QCD–EW corrections of $\mathcal{O}(\alpha_s\alpha)$. Knowing the contribution of this order will also answer the question how to properly combine QCD and EW corrections in predictions. In Ref. [68] this issue is quantitatively discussed with special emphasis on observables that are relevant for the M_W determination, revealing percent corrections of $\mathcal{O}(\alpha_s\alpha)$ that should be calculated. First steps towards this direction have been taken by calculating two-loop contributions [69–71], the full $\mathcal{O}(\alpha_s\alpha)$ corrections to the W and Z decay widths [72, 73], the $\mathcal{O}(\alpha)$ EW corrections to W/Z + jet production [74–79], and the $\mathcal{O}(\alpha_s)$ QCD corrections to W/Z + γ production [76, 80–86].

¹A recent update with QED-corrected PDFs has been presented in Ref. [46].

Outline of the thesis

In this work, we present the calculation of the $\mathcal{O}(\alpha_s\alpha)$ corrections to Drell–Yan processes in the resonance region via the so-called *pole approximation* (PA). It is based on a systematic expansion of the cross section about the resonance pole and aims at improving the theoretical prediction in the vicinity of the gauge-boson resonance where the higher precision is especially relevant. The PA leads to simplifications in the calculation and, moreover, decomposes the calculation into distinct well-defined contributions that can be tackled successively. More precisely, the contributions can be classified into two types: the factorizable and the non-factorizable corrections. In the former, the production and the subsequent decay of the gauge boson proceed independently, whereas in the latter, the production and decay sub-processes are linked by the exchange of soft photons.

We begin with the application of the PA to the EW corrections at NLO where the full corrections without approximation are known [34–45]. This allows us to establish our methods and to assess the validity of the approximation by a detailed comparison with the full calculation. We consistently apply the PA to all parts of the NLO calculation, in particular, also the real-emission corrections. This is necessary in order to discuss the different contributions of factorizable and non-factorizable corrections separately and prepares for the extension to the mixed QCD–EW corrections. Furthermore, disentangling the individual contributions in a consistent way allows to identify the dominant contributions at $\mathcal{O}(\alpha)$, which can give valuable insights on the expected sizes of the individual contributions at NNLO.

Motivated and guided by the successful construction of the PA at $\mathcal{O}(\alpha)$, we establish its framework at $\mathcal{O}(\alpha_s\alpha)$ for the calculation of the mixed QCD–EW corrections. Analogously to the NLO case, the calculation can be classified in terms of the factorizable and non-factorizable corrections. The non-factorizable corrections comprise the conceptually most challenging contribution to the PA and are discussed first. They turn out to be very small and, thus, demonstrate that for phenomenological purposes the $\mathcal{O}(\alpha_s\alpha)$ corrections can be factorized into terms associated with initial-state and/or final-state corrections. From the investigation of the PA at NLO, we identify the factorizable corrections of the type “initial–final” to deliver the dominant contribution at $\mathcal{O}(\alpha_s\alpha)$. This class of corrections which we calculate in this work combine large QCD corrections to the production with large EW corrections to the decay of the W/Z boson. The remaining factorizable corrections are expected to deliver only a small contribution to the $\mathcal{O}(\alpha_s\alpha)$ corrections and are isolated by the PA in a well-defined way and not further considered in this work.

In general, calculations of radiative corrections involving massless particles pose several technical challenges. Specifically, they involve the evaluation of loop integrals and phase-space integrations which contain so-called infrared (IR) singularities that are associated with configurations involving soft and/or collinear particles. The isolation and cancellation of these singularities is a non-trivial task and requires a careful treatment. At NLO, general techniques have been developed in the past decades which allow for the analytical control over these singularities in a process-independent manner without sacrificing the flexibility of a fully differential Monte Carlo approach for the evaluation of the cross section. These techniques can be essentially classified into two approaches: the phase-space-slicing method and the subtraction method. The calculation of the non-factorizable corrections is performed using the soft-slicing method and the remaining corrections employ the subtraction method, more specifically the so-called dipole subtraction method. The consistent application of the PA to the NLO and NNLO corrections requires the extension of the dipole subtraction formalism to cover decay kinematics in order to handle the decay sub-process of the W or Z boson. A part of this thesis

is devoted to such an extension which was developed within this work by explicitly constructing a process-independent subtraction term for decay processes. The treatment of IR singularities at NNLO is not yet as well established as in the case of calculations at NLO and constitutes one of the main bottlenecks in the progress of NNLO calculations. Although the cancellation of IR singularities in the $\mathcal{O}(\alpha_s\alpha)$ corrections presented in this work is accomplished by using a combined approach of the techniques developed for NLO calculations, it represents one of the main technical difficulties in the calculation and we devote special attention to its discussion.

The results on the non-factorizable corrections of the mixed QCD–EW $\mathcal{O}(\alpha_s\alpha)$ corrections and the application of the PA to the EW corrections have been published to a large extent in Ref. [87] and were presented in Ref. [88]. First preliminary numerical results for the factorizable initial–final corrections were shown in conference proceedings in Ref. [89].

This thesis is organized as follows:

In Chap. 1 we give a brief overview of the Standard Model of elementary particle physics. We begin in Sect. 1.1 with the motivation and construction of the classical SM Lagrangian and sketch the steps towards a quantized theory. We further discuss the renormalization of the SM and the different choices of input parameter schemes in this context. After addressing the issues associated with unstable particles in Sect. 1.2, we devote Sect. 1.3 to the discussion of IR singularities that arise in NLO calculations. Finally, we describe the calculation of hadronic cross sections in Sect. 1.4 and introduce the parton model and its perturbative extensions. In the remainder of this work we present the calculation of the various corrections to the Drell–Yan processes in the PA which is divided into two parts:

Part I is dedicated to the calculation of the NLO corrections in the PA, and we begin by setting up our notation and conventions in Chap. 2 which are used throughout this work. Chapter 3 contains a technical discussion of the dipole subtraction formalism which allows for an organized treatment of IR singularities. We first review the formalism for massless external fermions and move on to present the relevant subtraction terms for the production of charged massive particles that are needed in this work. The extension of this formalism to cover decay processes has been developed in the context of this work and is presented in Sect. 3.4. In Chap. 4 we describe the concept of the pole expansion at NLO, give explicit results for the EW and QCD corrections that will be used as building blocks in the calculation of the $\mathcal{O}(\alpha_s\alpha)$ corrections, and establish the numerical accuracy of the PA by comparing it to the full NLO EW results.

In Part II we establish the pole expansion for the mixed QCD–EW $\mathcal{O}(\alpha_s\alpha)$ corrections and begin with a classification of the different contributions to the factorizable and non-factorizable corrections in Chap. 5. Chapter 6 is dedicated to the calculation of the non-factorizable $\mathcal{O}(\alpha_s\alpha)$ corrections, where we encounter non-trivial gauge cancellations that allow to write the corrections in terms of one-loop EW and QCD results. We describe our treatment of IR singularities in detail and give a final formula for the corrections that is suitable for a numerical evaluation. The numerical results of the non-factorizable corrections are discussed in Sect. 6.3. In Chapter 7 we present the calculation of the initial–final factorizable corrections, where we observe that many parts of the calculation exhibit a reducible form of a product of NLO QCD and EW corrections. We discuss the construction of an IR-finite final result in detail with a special focus on the overlapping IR singularities between the QCD and EW corrections in Sect. 7.2. Before we conclude, we present the numerical results of the factorizable initial–final corrections in Sect. 7.3, and compare them to different versions of a naive product ansatz obtained by multiplying NLO QCD and EW corrections factors.

In Appendix A we collect the notations and conventions used throughout this work. The explicit expressions for the virtual corrections are given in Appendix B. Appendix C gives a brief review of the soft phase-space-slicing method that is employed in the calculation of the non-factorizable corrections. Last, we give the explicit form of the IR-safe contributions to the $\mathcal{O}(\alpha_s\alpha)$ corrections in the PA in Appendix D.

Theoretical preliminaries

The purpose of this chapter is to provide a brief introduction into the Standard Model (SM) of particle physics and to set up the theoretical framework for the calculation presented in the remainder of the work. Further details on the topics addressed in this chapter can be found, e.g. in Refs. [90, 91]. In Sect. 1.1 we begin with the construction of the classical SM Lagrangian and after briefly sketching the quantization procedure we move on to discuss the renormalization of the SM and review the different choices of input-parameter schemes. In Sect. 1.2 we address the conceptual problems associated with unstable particles in quantum field theories with an emphasis on the different mass definitions. Section. 1.3 covers the infrared divergences that arise in higher-order calculation involving massless particles and Sect. 1.4 gives a review of the QCD-improved parton model. The conventions used throughout this work are collected in Appendix A.

1.1. The Standard Model of particle physics

The SM unifies the description of three of the four fundamental interactions of nature, electromagnetism, the weak force, and the strong interactions, as a consistent relativistic quantum field theory. It fully respects the Poincaré symmetry and is most conveniently formulated in the Lagrangian formalism in terms of a Lorentz-invariant local functional \mathcal{L} , the Lagrangian density. The quantum-mechanical particle states belong to infinite-dimensional irreducible representations of the Poincaré group and can be characterised by a real positive number m and a half-integer number s which can be identified with the mass and spin of the associated particles, respectively. The corresponding fields belong to irreducible finite-dimensional representations of the Lorentz group and obey the equations-of-motion given by the Euler–Lagrange equations, which determine the dynamics of the theory. Besides the space-time symmetries, so-called internal symmetries play a crucial role in the SM which comprise transformations among the fields themselves. Explicitly, the SM is formulated as a spontaneously broken non-Abelian gauge theory with the underlying gauge group

$$SU(3)_C \times SU(2)_W \times U(1)_Y, \tag{1.1}$$

where the different groups correspond to the colour group of the strong interactions, the weak isospin, and the hypercharge phase symmetry, respectively. After briefly reviewing the concept of local (gauge) symmetries as the guiding principle to describe the interactions between fundamental particles, we will motivate the construction of the SM Lagrangian $\mathcal{L}_{\text{SM}}^{\text{cl}}$ which emerges as the minimal theory satisfying the restrictions imposed by symmetry principles and the requirement of renormalizability. The remainder of this section is then dedicated to the aspect of renormalization and the choice of input parameters.

1.1.1. The Lagrangian and quantisation

The electroweak (EW) sector of the SM is described by the Glashow–Salam–Weinberg [1–3] (GSW) model of electroweak interactions where the underlying gauge group $SU(2)_W \times U(1)_Y$ is spontaneously broken to the residual electromagnetic $U(1)_{\text{em}}$ symmetry. The strong interaction couples to the colour quantum numbers and is described by quantum chromodynamics [10, 11, 92, 93] (QCD) with the associated gauge group $SU(3)_C$. The classical SM Lagrangian can be divided into the following parts,

$$\mathcal{L}_{\text{SM}}^{\text{cl}} = \mathcal{L}_{\text{Yang-Mills}} + \mathcal{L}_{\text{Fermion}} + \mathcal{L}_{\text{Higgs}} + \mathcal{L}_{\text{Yukawa}}, \quad (1.2)$$

which will be examined successively in the following. Further terms need to be added in order to obtain a Lagrangian suitable for quantization, which will be discussed in the end.

Gauge theories and the Yang–Mills Lagrangian

The guiding principle in the construction of the SM Lagrangian is the postulate of local (gauge) symmetries. To this end, we first consider the Lagrangian $\mathcal{L}_{\Phi}(\Phi, \partial_{\mu}\Phi)$ of a generic field multiplet $\Phi(x) = (\Phi_1(x), \dots, \Phi_n(x))^T$ which is invariant under global symmetry transformations of the SM gauge group (1.1),

$$\Phi(x) \rightarrow \Phi'(x) = U(\theta)\Phi(x) \equiv U(\theta_C, \theta_W, \theta_Y)\Phi(x). \quad (1.3)$$

The transformation $U(\theta)$ can be parametrized in terms of a set of real group parameters $\theta = (\theta_C, \theta_W, \theta_Y)$,

$$U(\theta_C, \theta_W, \theta_Y) = \exp \left[-ig_s \theta_C^a \hat{T}_C^a + ig \theta_W^i \hat{T}_W^i - ig' \theta_Y \hat{T}_Y \right] \equiv U_C(\theta_C) U_W(\theta_W) U_Y(\theta_Y), \quad (1.4)$$

where \hat{T}_C^a ($a = 1, \dots, 8$), \hat{T}_W^i ($i = 1, 2, 3$), and \hat{T}_Y denote the generators of the Lie algebras of the groups $SU(3)_C$, $SU(2)_W$, and $U(1)_Y$, respectively. Furthermore, independent gauge coupling constants g_s , g , and g' are introduced for each group in the product of Eq. (1.1). The explicit form of the generators \hat{T} depends on the representation under which the field Φ transforms. In particular, for fields that belong to the singlet representation of one of the groups \mathcal{G}_X in Eq. (1.1), i.e. which transform trivially under the respective group transformation U_X , the associated generators vanish, $\hat{T}_X \equiv 0$.

Promoting Eq. (1.4) to a local transformation by allowing the group parameters to depend on the space-time coordinate x ($\theta \rightarrow \theta(x)$) inevitably destroys the covariant transformation property of the derivative of the field, $\partial_{\mu}\Phi$, which will in general disturb the invariance of \mathcal{L}_{Φ} . The gauge-covariant derivative D_{μ} is a generalization of the ordinary derivative ∂_{μ} in such a way that the variation of the field induced by the locality of the gauge transformation is taken into account so that $D_{\mu}\Phi$ transforms covariantly. It is defined as follows,

$$D_{\mu} = \partial_{\mu} + ig_s G_{\mu}^a(x) \hat{T}_C^a - ig W_{\mu}^i(x) \hat{T}_W^i + ig' B_{\mu}(x) \hat{T}_Y, \quad (1.5)$$

with the fields G_{μ}^a ($a = 1, \dots, 8$), W_{μ}^i ($i = 1, 2, 3$), and B_{μ} accompanying the generators called the

gauge fields. They have the following transformation properties under gauge transformations,¹

$$G_\mu^a \hat{T}_C^a \rightarrow G_\mu'^a \hat{T}_C^a = U_C(\boldsymbol{\theta}_C(x)) \left(G_\mu^a \hat{T}_C^a - \frac{i}{g_s} \partial_\mu \right) U_C(\boldsymbol{\theta}_C(x))^\dagger, \quad (1.6a)$$

$$W_\mu^i \hat{T}_W^i \rightarrow W_\mu'^i \hat{T}_W^i = U_W(\boldsymbol{\theta}_W(x)) \left(W_\mu^i \hat{T}_W^i + \frac{i}{g} \partial_\mu \right) U_W(\boldsymbol{\theta}_W(x))^\dagger, \quad (1.6b)$$

$$B_\mu \rightarrow B_\mu' = B_\mu + \partial_\mu \theta_Y(x), \quad (1.6c)$$

so that D_μ transforms covariantly,

$$D_\mu \rightarrow D_\mu' = U(\boldsymbol{\theta}(x)) D_\mu U(\boldsymbol{\theta})^\dagger. \quad (1.7)$$

With this property at hand, performing the replacement $\partial_\mu \rightarrow D_\mu$ inside \mathcal{L}_Φ , also known as the method of minimal substitution, guarantees that the resulting Lagrangian will be invariant under gauge transformations. The requirement of gauge invariance automatically induces interaction terms, where the gauge fields act as the mediators.

In order to incorporate dynamics for the gauge fields into the theory, a gauge-invariant kinetic term is added, given by the Yang–Mills Lagrangian

$$\mathcal{L}_{\text{Yang–Mills}} = -\frac{1}{4} G_{\mu\nu}^a G^{a,\mu\nu} - \frac{1}{4} W_{\mu\nu}^i W^{i,\mu\nu} - \frac{1}{4} B_{\mu\nu} B^{\mu\nu}, \quad (1.8)$$

where the field strength tensors are defined as

$$\begin{aligned} G_{\mu\nu}^a &= \partial_\mu G_\nu^a - \partial_\nu G_\mu^a - g_s f^{abc} G_\mu^b G_\nu^c, \\ W_{\mu\nu}^i &= \partial_\mu W_\nu^i - \partial_\nu W_\mu^i + g \varepsilon^{ijk} W_\mu^j W_\nu^k, \\ B_{\mu\nu} &= \partial_\mu B_\nu - \partial_\nu B_\mu. \end{aligned} \quad (1.9)$$

Here f^{abc} and ε^{ijk} are the structure constants of the $SU(3)$ and $SU(2)$ algebras, respectively. The gauge invariance of $\mathcal{L}_{\text{Yang–Mills}}$ can be easily seen from the relation of the field-strength tensors to the commutator

$$[D_\mu, D_\nu] = ig_s G_{\mu\nu}^a \hat{T}_C^a - ig W_{\mu\nu}^i \hat{T}_W^i + ig' B_{\mu\nu}, \quad (1.10)$$

which transforms covariantly according to Eq. (1.7). The bilinear terms in the Lagrangian $\mathcal{L}_{\text{Yang–Mills}}$ describe the free motion of the fields, however, in case of a non-Abelian group also terms cubic and quartic in the gauge fields arise, i.e. the gauge fields interact among themselves. Furthermore, any naive mass term of the gauge fields is forbidden, as it would spoil gauge invariance.

Fermionic part

The spin- $\frac{1}{2}$ matter content of the SM can be classified into the leptons (ν_ℓ, ℓ) , which are only subject to the electromagnetic and weak interactions, and the quarks (q_u, q_d) , which also interact strongly. The fermions come in three generations, which have identical properties under the gauge interactions, but differ in their mass and flavour. The three generations of quarks and

¹ From Eq. (1.6) it can be seen that for global symmetry transformations the gauge fields transform under the adjoint representation of the associated group.

		generation			representation	charges		
		1 st	2 nd	3 rd		I_w^3	Y	Q
leptons	$\Psi_L^{L'_i}$	$\begin{pmatrix} \nu_e' \\ e' \end{pmatrix}_L$	$\begin{pmatrix} \nu_\mu' \\ \mu' \end{pmatrix}_L$	$\begin{pmatrix} \nu_\tau' \\ \tau' \end{pmatrix}_L$	$(\mathbf{1}, \mathbf{2})_{-1}$	$\frac{1}{2}$ $-\frac{1}{2}$	-1 -1	0 -1
	$\Psi_R^{\ell'_i}$	e'_R	μ'_R	τ'_R	$(\mathbf{1}, \mathbf{1})_{-2}$	0	-2	-1
quarks	$\Psi_L^{Q'_i}$	$\begin{pmatrix} u' \\ d' \end{pmatrix}_L$	$\begin{pmatrix} c' \\ s' \end{pmatrix}_L$	$\begin{pmatrix} t' \\ b' \end{pmatrix}_L$	$(\mathbf{3}, \mathbf{2})_{\frac{1}{3}}$	$\frac{1}{2}$ $-\frac{1}{2}$	$\frac{1}{3}$ $\frac{1}{3}$	$\frac{2}{3}$ $-\frac{1}{3}$
	$\Psi_R^{u'_i}$	u'_R	c'_R	t'_R	$(\mathbf{3}, \mathbf{1})_{\frac{4}{3}}$	0	$\frac{4}{3}$	$\frac{2}{3}$
	$\Psi_R^{d'_i}$	d'_R	s'_R	b'_R	$(\mathbf{3}, \mathbf{1})_{-\frac{2}{3}}$	0	$-\frac{2}{3}$	$-\frac{1}{3}$

Table 1.1.: The fermionic matter content of the SM arranged by the three generations of leptons and quarks. The representation of the fields with respect to the SM gauge group (1.1) is denoted by $(SU(3)_C, SU(2)_W)_{U(1)_Y}$. I_w^3 and Y denote the third component of the weak isospin and the hypercharge, respectively. The electric charge Q is related to the above via Eq. (1.13). The colour degrees of freedom of the quarks are suppressed in the notation.

leptons are listed in Table. 1.1 together with their representation under the SM gauge group (1.1) and EW quantum numbers. The left- and right-handed fermions, defined via the projection operators ω_\pm given in Eq. (A.9),

$$\Psi_L(x) \equiv \omega_- \Psi(x), \quad \Psi_R(x) \equiv \omega_+ \Psi(x), \quad \Psi(x) = \Psi_L(x) + \Psi_R(x), \quad (1.11)$$

are assigned to different representations owing to the chiral nature of the weak interactions. As a consequence, any explicit mass terms for the fermions are forbidden, as they mix the two chiralities and, as such, would spoil gauge invariance. The Lagrangian for the fermionic fields is thus obtained by applying the procedure of minimal substitution to the free Dirac theory of massless fermions, leading to

$$\mathcal{L}_{\text{Fermion}} = \sum_{i=1}^3 \left(\bar{\Psi}_L^{L'_i} \not{D} \Psi_L^{L'_i} + \bar{\Psi}_R^{\ell'_i} \not{D} \Psi_R^{\ell'_i} + \bar{\Psi}_L^{Q'_i} \not{D} \Psi_L^{Q'_i} + \bar{\Psi}_R^{u'_i} \not{D} \Psi_R^{u'_i} + \bar{\Psi}_R^{d'_i} \not{D} \Psi_R^{d'_i} \right). \quad (1.12)$$

The primes on the fermion fields indicate that they are eigenstates with respect to the gauge interactions in order to distinguish them from the mass eigenstates.

Note that the explicit form of the covariant derivatives that appear in Eq. (1.12) differ for fermion fields that belong to different representations of the gauge group, cf. Eq. (1.5): The quarks carry charges of the strong interactions, referred to as colour, and come in three variants (red, green, and blue) arranged in triplets which is suppressed in the notation above. They transform under the fundamental representation of the $SU(3)_C$ colour group ($\mathbf{3}$) and the generators can be chosen as $\hat{T}_C^a = t^a \equiv \frac{\lambda^a}{2}$, where λ^a denote the Gell-Mann matrices. The group

$SU(2)_W$ is associated with the weak isospin, where only the left-handed fermions transform non-trivially. They are arranged in doublets (see Table 1.1) and transform under the fundamental representation (**2**) where the generators are given by the Pauli matrices σ^i , $\hat{T}_W^i \equiv I_W^i = \frac{\sigma^i}{2}$. Lastly, the generator of the $U(1)_Y$ group is given by $\hat{T}_Y \equiv \frac{Y}{2}$, where Y denotes the so-called hypercharge. Its value is determined by the Gell-Mann–Nishijima relation

$$Q = I_W^3 + \frac{Y}{2}, \quad (1.13)$$

where Q is the relative electric charge of the particle. Further information regarding the group $SU(3)$ and the explicit expressions for the generators can be found in Appendix A.1.

Spontaneous symmetry breaking and the Higgs mechanism

As already stated above, any naive mass terms for the gauge bosons are forbidden due to gauge invariance. They can be, however, accommodated in a gauge theory by the mechanism of spontaneous symmetry breaking (SSB). Here, the vacuum state of the theory only respects the symmetry of a smaller subgroup, without disturbing the full symmetry of the Lagrangian. This is accomplished by allowing a field to develop a non-vanishing vacuum expectation value (vev), which has to be a scalar in order to preserve Lorentz invariance. In the SM a scalar weak isospin doublet is introduced which is conventionally parametrized as follows,

$$\Phi(x) = \begin{pmatrix} \phi^+(x) \\ \phi^0(x) \end{pmatrix}, \quad (1.14)$$

with hypercharge $Y_\Phi = 1$. The most general Lagrangian of Φ which satisfies the restrictions imposed by gauge invariance, renormalizability, and the stability of the vacuum reads

$$\mathcal{L}_{\text{Higgs}} = (D_\mu \Phi)^\dagger (D^\mu \Phi) + \mu^2 (\Phi^\dagger \Phi) - \frac{\lambda}{4} (\Phi^\dagger \Phi)^2, \quad \lambda > 0. \quad (1.15)$$

For $\mu^2 > 0$ the field develops a non-vanishing vev Φ_0 with

$$|\Phi_0|^2 = \Phi_0^\dagger \Phi_0 = \frac{2\mu^2}{\lambda} \equiv \frac{v^2}{2}, \quad (1.16)$$

which is illustrated in Fig. 1.1(b). In order to preserve the electromagnetic gauge symmetry $U(1)_{\text{em}}$, only the neutral component ϕ^0 of $\Phi(x)$ can develop the vev ($Q\Phi_0 \equiv 0$), and further parametrizing the field in terms of displacements from the vacuum we obtain

$$\Phi(x) = \begin{pmatrix} \phi^+(x) \\ \frac{1}{\sqrt{2}}(v + H(x) + i\chi(x)) \end{pmatrix}. \quad (1.17)$$

Here, the real field $H(x)$ corresponds to the massive mode associated with the physical Higgs boson, a neutral spin-0 particle with mass

$$M_H = \sqrt{2}\mu. \quad (1.18)$$

The complex and real fields $\phi^+(x)$ and $\chi(x)$ would correspond to the massless Nambu–Goldstone [94, 95] bosons in the case of a global symmetry. For local symmetries, however, these would-be

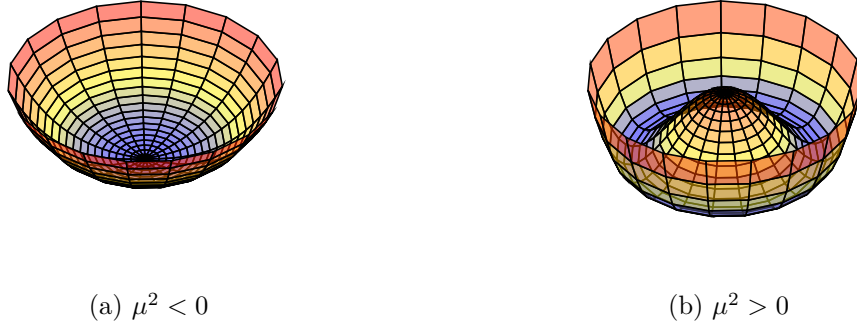


Figure 1.1.: The Higgs potential for the two possible signs of the quadratic term in Eq. (1.15) for fixed values of λ and μ^2 . For $\mu^2 > 0$ (b) the configuration $|\Phi| = 0$ is unstable and the potential develops a degenerate minimum at some Φ with $|\Phi| = v/\sqrt{2}$.

Nambu–Goldstone modes are transformed into the longitudinal polarization states of the gauge bosons associated with the broken symmetries and render them massive. This mechanism of generating mass terms for the gauge fields through SSB is known as the Higgs mechanism [96–99].

The Higgs mechanism induces mixing terms among the gauge fields and it is convenient to perform field redefinitions to make the physical content of the theory manifest: Since the strong interaction is unaffected by SSB in the EW sector, the gauge coupling parameter g_s can be directly identified with the strong coupling and $\alpha_s \equiv \frac{g_s^2}{4\pi}$ is defined analogous to the fine-structure constant. Correspondingly, the eight gauge fields G_μ^a are identified with the eight gluons g , the mediators of the strong force. The mass matrix of the EW gauge bosons is given by the terms in $\mathcal{L}_{\text{Higgs}}$ that are bilinear in the gauge fields and originate from the vev part of the Higgs doublet.² It is diagonalized by the following rotation among the fields B_μ and W_μ^3

$$\begin{pmatrix} A_\mu \\ Z_\mu \end{pmatrix} = \begin{pmatrix} \cos \theta_w & -\sin \theta_w \\ \sin \theta_w & \cos \theta_w \end{pmatrix} \begin{pmatrix} B_\mu \\ W_\mu^3 \end{pmatrix}, \quad (1.19)$$

with the weak mixing angle θ_w given by

$$\cos \theta_w \equiv c_w = \frac{g}{\sqrt{g^2 + g'^2}}, \quad \sin \theta_w \equiv s_w = \frac{g'}{\sqrt{g^2 + g'^2}}. \quad (1.20)$$

By construction, a residual $U(1)_{\text{em}}$ symmetry remains unbroken after SSB with the generator given by the relative electric charge Q as defined in Eq. (1.13). The associated massless gauge boson A_μ is identified with the photon and the field Z_μ corresponds to the massive, electrically neutral Z boson. The elementary charge e and hence the fine-structure constant α can be expressed in terms of the couplings g and g' ,

$$e = \frac{gg'}{\sqrt{g^2 + g'^2}}, \quad \alpha \equiv \frac{e^2}{4\pi}. \quad (1.21)$$

² The bilinear terms that mix the gauge bosons with the would-be Goldstone bosons are not considered here. They can be removed by the transition to the unitary gauge or by the choice of the gauge-fixing condition as shown below.

Further, taking the two linear combinations of the mass degenerate fields $W_\mu^{1,2}$

$$W_\mu^\pm = \frac{1}{\sqrt{2}} \left(W_\mu^1 \mp i W_\mu^2 \right), \quad Q W_\mu^\pm = I_W^3 W_\mu^\pm = \pm W_\mu^\pm, \quad (1.22)$$

delivers the $U(1)_{\text{em}}$ eigenstates of the electrically charged gauge bosons. The masses of the gauge bosons W^\pm , Z , γ , and g are then given by

$$M_W = \frac{vg}{2} = \frac{ve}{2s_w}, \quad M_Z = \frac{v\sqrt{g^2 + g'^2}}{2} = \frac{ve}{2s_w c_w}, \quad M_\gamma \equiv 0, \quad M_g \equiv 0, \quad (1.23)$$

respectively.

Fermion masses and Yukawa couplings

As a consequence of the distinct transformation properties of the two fermion chiralities, any explicit fermion mass term is forbidden in the SM. The solution to this problem is again provided by the Higgs doublet which was already responsible for the mass generation of the gauge bosons as described above. To this end, we define the charge conjugate of the Higgs doublet

$$\Phi^c = i\sigma^2 \Phi^* = \left((\phi^0)^*, -\phi^- \right)^T, \quad (1.24)$$

and construct the most general gauge-invariant interaction between the fermions and the Higgs field,

$$\mathcal{L}_{\text{Yukawa}} = - \sum_{i,j=1}^3 \left(\bar{\Psi}_L^{L'i} G_{ij}^\ell \Psi_R^{\ell'j} \Phi + \bar{\Psi}_L^{Q'i} G_{ij}^u \Psi_R^{u'j} \Phi^c + \bar{\Psi}_L^{Q'i} G_{ij}^d \Psi_R^{d'j} \Phi + \text{h.c.} \right), \quad (1.25)$$

where “h.c.” stands for the hermitian conjugate of the terms preceding it. The Yukawa couplings G_{ij}^f are complex 3×3 matrices in generation space. The vev part of the Higgs field generates mass terms of the fermions that can be diagonalized by a bi-unitary transformation

$$m_{f,i} \delta_{ij} = \frac{v}{\sqrt{2}} \sum_{k,l=1}^3 U_{L,ik}^f G_{kl}^f U_{R,lj}^{f\dagger}, \quad f = \ell, u, d. \quad (1.26)$$

Hence, the transition of the primed eigenstates of the gauge interactions to the unprimed mass eigenstates is given by

$$\Psi_L^{f_i} = \sum_{j=1}^3 U_{L,ij}^f \Psi_L^{f'_j}, \quad \Psi_R^{f_i} = \sum_{j=1}^3 U_{R,ij}^f \Psi_R^{f'_j}. \quad (1.27)$$

In the original formulation of the SM all neutrinos are assumed to be massless³ and as such, mass degenerate. Consequently, it is possible to choose the same transformation for the neutrino

³ This assumption has to be revisited in view of the observation of neutrino oscillations. Dirac masses of the neutrinos can be incorporated into the SM by mimicking the construction in the quark sector, which requires the introduction of right-handed neutrinos. However, the construction of neutrino mass terms is much less restricted than in the quark sector owing to the fact that the neutrinos are electrically neutral. As a consequence, there exist more general possibilities to incorporate neutrino masses, see e.g. Ref. [100] and references therein.

fields as for the leptons,

$$\Psi_L^{\nu_i} = \sum_{j=1}^3 U_{L,ij}^\ell \Psi_L^{\nu_j}, \quad (1.28)$$

thus, eliminating all occurrences of U_L^ℓ induced by the transition to the mass eigenstates. In the quark sector, on the other hand, a residual dependence from the transition given in Eq. (1.27) remains in the charged-current interactions. The quark mixing matrix, parametrizing the transition between different generations of the mass eigenstates, is given by the Cabibbo–Kobayashi–Maskawa [101, 102] (CKM) matrix defined as follows

$$U_L^u U_L^{d\dagger} \equiv \mathbf{V}_{\text{CKM}} = \begin{pmatrix} V_{ud} & V_{us} & V_{ub} \\ V_{cd} & V_{cs} & V_{cb} \\ V_{td} & V_{ts} & V_{tb} \end{pmatrix}. \quad (1.29)$$

It appears only in the charged-current interactions but not in the neutral-current interactions and can be parametrized in terms of three angles and a complex phase, where the latter is the only source of \mathcal{CP} violation in the SM.

Quantization of gauge theories—the Faddeev–Popov procedure

Although the gauge symmetry was the guiding principle in the construction of the classical SM Lagrangian discussed so far, it gives rise to a redundancy in the description of the theory stemming from the over-counting of the physically equivalent field configurations which are related to each other by gauge transformations. As a result, the straight-forward application of a quantization procedure, for instance provided by the path-integral formalism, fails in this case. This issue can be circumvented by a method proposed by Faddeev and Popov [103] which we briefly sketch in the following. In the first step, gauge-fixing conditions (F^\pm , F^Z , F^A , $F^{G,a}$) are imposed by adding a term \mathcal{L}_{fix} to the Lagrangian which explicitly breaks the gauge symmetry,

$$\mathcal{L}_{\text{fix}} = -\frac{1}{\xi_W} F^+ F^- - \frac{1}{2\xi_Z} (F^Z)^2 - \frac{1}{2\xi_A} (F^A)^2 - \frac{1}{2\xi_G} (F^{G,a})^2. \quad (1.30)$$

The gauge-fixing functionals can be chosen linear in the fields

$$\begin{aligned} F^\pm &= \partial^\mu W_\mu^\pm \mp i\xi'_W M_W \phi^\pm, & F^Z &= \partial^\mu Z_\mu - \xi'_Z M_Z \chi, \\ F^A &= \partial^\mu A_\mu, & F^{G,a} &= \partial^\mu G_\mu^a, \end{aligned} \quad (1.31)$$

and all bilinear vector–scalar mixing terms induced by the Higgs mechanism are removed by setting $\xi'_V = \xi_V$ ($V = W, Z$), a choice which is known as the 't Hooft gauge. Further setting $\xi_V = 1$ ($V = W, Z, A, G$) in the 't Hooft–Feynman gauge, the masses of the unphysical would-be Nambu–Goldstone bosons equal those of the respective physical counterparts,

$$M_{\phi^\pm} = \sqrt{\xi_W} M_W \xrightarrow{\xi_W \rightarrow 1} M_W, \quad M_\chi = \sqrt{\xi_Z} M_Z \xrightarrow{\xi_Z \rightarrow 1} M_Z, \quad (1.32)$$

Moreover, this results in particularly simple expressions for the propagators,

$$\frac{-ig_{\mu\nu}}{k^2 - M_V^2} + \frac{i(1 - \xi_V)k_\mu k_\nu}{(k^2 - M_V^2)(k^2 - \xi_V M_V^2)} \xrightarrow{\xi_V \rightarrow 1} \frac{-ig_{\mu\nu}}{k^2 - M_V^2}. \quad (1.33)$$

making this the preferred choice in higher-order calculations.⁴ The inclusion of \mathcal{L}_{fix} to the classical Lagrangian effectively promotes the unphysical degrees of freedom of the gauge fields to dynamical modes of the theory. They are compensated in the Faddeev–Popov procedure by the contributions of the so-called ghost fields u^α and \bar{u}^α . The additional term to the Lagrangian from these fields is given by

$$\mathcal{L}_{\text{ghost}} = -\bar{u}^\alpha(x) \frac{\delta F^\alpha}{\delta \theta^\beta(x)} u^\beta(x), \quad \alpha, \beta \in \{\pm, Z, A, (G, a)\}, \quad (1.34)$$

which is derived from the variation of the gauge-fixing conditions (1.31) with respect to infinitesimal gauge transformations $\delta\theta^\alpha$. The auxiliary Grassmann-valued ghost fields violate the spin-statistics theorem, however, this poses no problem as they only appear as virtual particles within loops, but not as external physical states. We therefore arrive at the effective Lagrangian of the SM,

$$\begin{aligned} \mathcal{L}_{\text{SM}} &= \mathcal{L}_{\text{SM}}^{\text{cl}} + \mathcal{L}_{\text{fix}} + \mathcal{L}_{\text{ghost}} \\ &= \mathcal{L}_{\text{Yang–Mills}} + \mathcal{L}_{\text{Fermion}} + \mathcal{L}_{\text{Higgs}} + \mathcal{L}_{\text{Yukawa}} + \mathcal{L}_{\text{fix}} + \mathcal{L}_{\text{ghost}}, \end{aligned} \quad (1.35)$$

which is suitable for quantization. A remnant of the local gauge symmetry, which is explicitly broken by this procedure, manifests itself in form of a global Becchi–Rouet–Stora (BRS) symmetry [104, 105].

If the interactions are small, the SM can be evaluated perturbatively about the free field theory. The free theory is described by the bilinear terms of the Lagrangian and the solutions of the corresponding field equations are given by the one-particle wave functions of the respective field. Note however, that the self-interacting nature of the fields still influences the free part of the theory by a shift of the bare mass to the renormalized mass and a modified normalization of the one-particle states. This aspect is related to renormalization which will be discussed in more detail in the next section. In the so-called *weak asymptotic limit* the interactions are assumed to be negligible long before and after the scattering reaction ($t \rightarrow \pm\infty$), where the particles are considered to be far apart. As a consequence, the particles entering/exiting the reaction can be described by the free one-particle states. The S -matrix transforms the incoming configuration for $t \rightarrow -\infty$ into the outgoing configuration for $t \rightarrow +\infty$ and encapsulates the information of the scattering reaction. The Lehmann–Symanzik–Zimmermann (LSZ) reduction formula [106] further establishes a relation between the S -matrix element and the n -point Green functions of the theory. The latter can be evaluated perturbatively and its expansion can be organized pictorially in terms of so-called Feynman diagrams, where different line types are used to distinguish the fields. The Feynman diagrams are assembled from two types of building blocks: the propagators and the vertices. The former are represented by lines and are derived from the free, bilinear part of the Lagrangian, and the latter emerge from the remaining interaction terms and are represented by dots (“vertices”) that join multiple lines. The associated analytic expressions can be directly derived from the effective Lagrangian (1.35) and gives rise to the

⁴ The unitary gauge corresponds to taking the limit $\xi_V \rightarrow \infty$, which effectively eliminates the would-be Nambu–Goldstone bosons from the theory.

Feynman rules. Lastly, the external legs translate into the one-particle wave functions. All Feynman rules that are needed in the calculation of the LO and real-emission amplitudes are collected in Appendix A.3. Further details on the perturbative expansion and the LSZ reduction formula can be found e.g. in Refs. [90,91]. A complete set of the Feynman rules of the SM is also given there.

1.1.2. Renormalization

The SM Lagrangian in Eq. (1.35) depends on a set of independent parameters which can be chosen as the strong and electromagnetic coupling constants, the masses of the particles, and the entries of the CKM matrix:

$$g_s, e, M_W, M_Z, M_H, m_{f,i}, \mathbf{V}_{\text{CKM}}. \quad (1.36)$$

All remaining parameters can be derived from this set. In particular, the weak mixing angle is fixed through the relation,

$$c_w^2 = 1 - s_w^2 = \frac{M_W^2}{M_Z^2}. \quad (1.37)$$

Although we have identified the parameters in Eq. (1.36) with the couplings and the masses of the particles, in order to make theoretical predictions, it is first necessary to relate these parameters to independent measurable quantities. This set of experimental input parameters need not coincide with the choice of Eq. (1.36) but are instead preferably chosen as the set of parameters that are measured with the highest precision or are favoured from a theoretical standpoint, as will be discussed in more detail in Sect. 1.1.3. After establishing the relation between the parameters appearing in the Lagrangian and the experimentally measured quantities, any further theoretical prediction can be made in terms of the input parameters. This step of reparametrizing the theory in terms of physically measured quantities is known as *renormalization*. In fact, in the calculation of higher-order corrections divergences may arise which forbid any direct physical interpretation of the (bare) parameters appearing in the Lagrangian. The divergences have their origin in the virtual loop corrections, in particular in the infinite-momentum region of the unconstrained loop momenta, and are therefore called ultraviolet (UV) divergences. In a renormalizable theory, all divergences drop out in relations that express physical observables in terms of measurable (renormalized) quantities. The renormalizability of a theory is therefore a crucial property in order to obtain predictions using perturbation theory. It was shown by ‘t Hooft [107] that spontaneously broken non-Abelian gauge theories, and therefore also the SM, are renormalizable. In the remainder of this section we will outline the renormalization of the EW part of the SM in the on-shell scheme essentially following Ref. [108], however, restrict ourselves only to the discussion of the parts that are needed in this work.

First, the parameters initially appearing in the Lagrangian are considered to be so-called “bare” quantities (denoted with a subscript “0” in the following) which can receive divergent contributions at higher orders. In the counterterm approach, these bare parameters are split according to

$$e_0 = Z_e e = (1 + \delta Z_e) e, \quad (1.38a)$$

$$M_{Z,0}^2 = M_Z^2 + \delta M_Z^2, \quad (1.38b)$$

$$M_{W,0}^2 = M_W^2 + \delta M_W^2, \quad (1.38c)$$

into the finite renormalized parameters and the respective renormalization constants which can become divergent. We have omitted the renormalization of the top-quark mass m_t in Eq. (1.38), as it does not appear in the Drell–Yan processes at lowest order. All light fermion masses are set equal to zero throughout this work⁵ and receive no higher-order corrections owing to the additional chiral symmetry. As will be argued in more detail in Sect. 2.1, the dependence on the non-diagonal structure of the CKM matrix can be isolated globally, which allows to utilize a diagonal CKM matrix ($\mathbf{V}_{\text{CKM}} = \mathbf{1}$) in the rest of the calculation, in particular in the radiative corrections. Therefore, no renormalization of the CKM matrix is required and no flavour transitions between different quarks generations need to be considered. Although the renormalization constants introduced so far are sufficient in order to obtain finite S -matrix elements, an additional field renormalization is performed,

$$W_0^\pm = \sqrt{Z_W} W^\pm = \left(1 + \frac{1}{2}\delta Z_W\right) W^\pm, \quad (1.39a)$$

$$\begin{pmatrix} Z_0 \\ A_0 \end{pmatrix} = \begin{pmatrix} \sqrt{Z_{ZZ}} & \sqrt{Z_{ZA}} \\ \sqrt{Z_{AZ}} & \sqrt{Z_{AA}} \end{pmatrix} \begin{pmatrix} Z \\ A \end{pmatrix} = \begin{pmatrix} 1 + \frac{1}{2}Z_{ZZ} & \frac{1}{2}Z_{ZA} \\ \frac{1}{2}Z_{AZ} & 1 + \frac{1}{2}Z_{AA} \end{pmatrix} \begin{pmatrix} Z \\ A \end{pmatrix}, \quad (1.39b)$$

$$\Psi_{\sigma,0}^f = \sqrt{Z_f^\sigma} \Psi_\sigma^f = \left(1 + \frac{1}{2}\delta Z_f^\sigma\right) \Psi_\sigma^f, \quad \sigma = \text{L, R}, \quad (1.39c)$$

which additionally renders all Greens functions finite. These wave-function renormalization constants allow for additional constraints to be imposed on the renormalized fields which can be exploited to simplify the later calculations significantly. Inserting the renormalization transformations above into the bare Lagrangian in Eq. (1.35), the contributions can be rearranged into the original Lagrangian written in terms of the renormalized quantities and an extra counterterm Lagrangian

$$\mathcal{L}_{\text{SM},0} = \mathcal{L}_{\text{SM}} + \delta\mathcal{L}, \quad (1.40)$$

where \mathcal{L}_{SM} has the same functional dependence on the renormalized fields Φ as $\mathcal{L}_{\text{SM},0}$ on the bare fields Φ_0 . The counterterm Lagrangian $\delta\mathcal{L}$ collects all the potentially divergent renormalization constants and gives rise to additional Feynman rules which are visually distinguished by crosses on the vertices. Finally, the renormalized quantities are fixed by imposing renormalization conditions, and their numerical values are determined through experimental input. The choice of independent input parameters together with the renormalization conditions defines a renormalization scheme. Before proceeding to define the on-shell renormalization scheme, it is first necessary to introduce a regularization procedure in order to map the divergences to some finite expression in a mathematically well-defined way, which is discussed in the following.

Dimensional regularization

Although many different regularisation schemes were proposed in the literature, dimensional regularisation [109, 110] established itself as the preferred method owing to its property to preserve Lorentz and gauge invariance and due to its simplicity and applicability to infrared-divergences. In a nutshell, dimensional regularization consists of the analytic continuation of

⁵ One exception is the case of non-collinear safe observables which depend logarithmically on the physical mass of the leptons and will be covered in Sect. 3.

the dimensionality of space-time into $d = 4 - 2\epsilon$ dimensions,

$$\int \frac{d^4 q}{(2\pi)^4} \rightarrow \int \frac{d^d q}{(2\pi)^d} = \int \frac{d^{(4-2\epsilon)} q}{(2\pi)^{(4-2\epsilon)}}, \quad (1.41)$$

where ϵ is an arbitrary complex number. The integrals become analytic functions in the regulator ϵ , and the divergences in four space-time dimensions manifest themselves as poles in ϵ . The consistent evaluation of the integrand requires the generalisation of the metric and the Dirac algebra to d dimensions,

$$g_{\mu\nu} = (1, \underbrace{-1, \dots, -1}_{d-1}), \quad g^\mu{}_\mu = d, \quad \{\gamma^\mu, \gamma^\nu\} = 2g^{\mu\nu} \mathbb{1}. \quad (1.42)$$

An arbitrary mass scale μ is introduced in order to keep the coupling constants dimensionless after the transition to $d \neq 4$ dimensions,⁶

$$e \rightarrow \mu^{\frac{4-d}{2}} e = \mu^\epsilon e, \quad g_s \rightarrow \mu^{\frac{4-d}{2}} g_s = \mu^\epsilon g_s. \quad (1.43)$$

In practice, there are several variants of the dimensional-regularisation prescription, e.g. the original formulation by 't Hooft and Veltman (tHV) [109], conventional dimensional regularization (CDR) [111], and dimensional reduction (DR). They vary in the dimensionality of the momenta of the external particles and in the treatment of the spin degrees of freedom for the internal and external states. Throughout this work we employ the CDR scheme which considers not only the internal, but also the external momenta and polarization vectors consistently in d dimensions. The photon and gluon therefore have $(d-2)$ helicities and the massive gauge bosons $(d-1)$ polarisation states. However, the fermions continue to have two spin states despite their momenta being d dimensional. This is in line with the freedom to choose a value for the trace of the Dirac unit matrix, which is chosen to take its canonical value of four.

A complete definition of the scheme further requires a prescription for the treatment of the chirality matrix γ^5 , which is defined in Eq. (A.8) for the case of four space-time dimensions. However, a generalisation of the γ^5 matrix to d dimensions which fully respects the four-dimensional properties does not exist, thereby making the proper treatment of γ^5 within dimensional regularization a delicate issue. For instance in Ref. [109], the anti-commutation relation (A.8) was abandoned in favour of a γ^5 definition that commutes on the extended $(d-4)$ -dimensional subspace. In practice, for one-loop calculations within an anomaly-free theory, however, a totally anti-commuting γ^5 can be employed as was shown in Ref. [112] as long as Dirac traces with γ^5 in closed fermion loops are evaluated in the same way where fermions just belong to different generations. An overview on the different prescriptions to treat γ^5 within dimensional regularization can be found in Ref. [113] and references therein.

Finally, we briefly comment on a further advantage of dimensional regularization which is its applicability to simultaneously regularize so-called infrared divergences. These divergences arise in higher-order calculations which involve massless particles and will be discussed in more detail in Sect. 1.3. In this context, a consistent treatment that does not distinguish between internal and external states proves to be useful, as it is provided by the CDR scheme. In particular, the

⁶ This mass scale can alternatively be absorbed into the integration measure of the loop momentum by a factor $\mu^{4-d} = \mu^{2\epsilon}$ on the r.h.s. of Eq. (1.41).

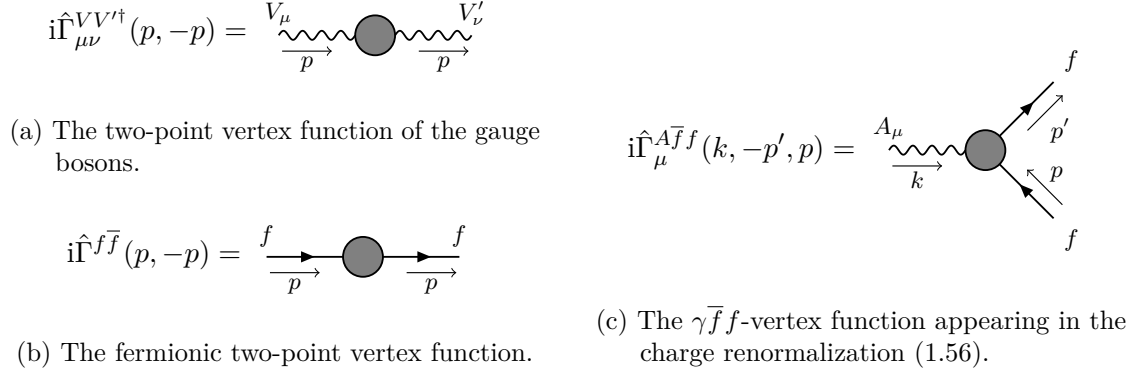


Figure 1.2.: The one-particle irreducible vertex functions that enter the renormalization conditions in Eqs. (1.45), (1.46), and (1.56).

continuation of the invariant phase-space measure into d dimensions, cf. Eq. (A.52),

$$d\phi^{(d)}(k_1, \dots, k_n; Q) = \prod_{i=1}^n \left[\frac{d^d k_i}{(2\pi)^{(d-1)}} \delta_+(k_i^2 - m_i^2) \right] (2\pi)^4 \delta^{(d)}\left(\sum_{i=1}^n k_i - Q\right), \quad (1.44)$$

will be extensively used in the dipole subtraction formalism covered in Sect. 3. Further details on dimensional regularization can be found in Ref. [111].

The on-shell renormalization of the EW part of the SM

The on-shell scheme is specified in terms of the input parameters given in Eq. (1.36) and the renormalization conditions are formulated for external fields on their mass shell, thus, allowing for a direct physical interpretation of the renormalised parameters. As stated above, we will restrict our discussion to the renormalization of the SM as far as it is needed in our calculation, i.e. we will only discuss the conditions to determine the renormalization constants given in Eqs. (1.38) and (1.39), and refer to Ref. [108] for a more exhaustive treatment of the renormalization of the SM in the on-shell scheme.

The renormalized masses are required to be equal to the physical masses, defined as the real parts of the locations of the propagator poles in the complex p^2 plane. This requirement translates into conditions for the zeros of the respective two-point vertex functions shown in Figs. 1.2(a) and 1.2(b),

$$\text{Re } \hat{\Gamma}_{\mu\nu}^{VV'\dagger}(p, -p) \varepsilon^\nu(p) \Big|_{p^2=M_V^2} = 0, \quad V, V' \in \{W, Z, A\}, \quad (1.45a)$$

$$\text{Re } \hat{\Gamma}^{f\bar{f}}(p, -p) u_f(p) \Big|_{p^2=m_f^2} = 0, \quad (1.45b)$$

where the polarization vector $\varepsilon^\mu(k)$ and spinor $u(p)$ serve as projectors onto physical states. The calculation of the mass renormalization constants can be greatly simplified by fixing the field renormalization constants in Eq. (1.39) in such a way to prevent mixings between on-shell particles. Furthermore, choosing the normalization of the fields so that the corresponding

propagators have residue one at their mass pole leads to the conditions

$$\lim_{p^2 \rightarrow M_V^2} \frac{1}{p^2 - M_V^2} \text{Re } \hat{\Gamma}_{\mu\nu}^{VV'\dagger}(p, -p) \varepsilon^\nu(p) = -i\varepsilon_\mu(p), \quad (1.46a)$$

$$\lim_{p^2 \rightarrow m_f^2} \frac{\not{p} + m_f}{p^2 - m_f^2} \text{Re } \hat{\Gamma}^{f\bar{f}}(p, -p) u_f(p) = iu_f(p). \quad (1.46b)$$

With this choice no external self-energy corrections need to be taken into account when calculating scattering amplitudes. These renormalization conditions translate to the following conditions on the self-energies of the gauge bosons,

$$\text{Re } \hat{\Sigma}_T^W(M_W^2) = 0, \quad (1.47a)$$

$$\text{Re } \hat{\Sigma}_T^{ZZ}(M_Z^2) = 0, \quad \text{Re } \hat{\Sigma}_T^{AZ}(M_Z^2) = 0, \quad (1.47b)$$

$$\hat{\Sigma}_T^{AZ}(0) = 0, \quad \hat{\Sigma}_T^{AA}(0) = 0, \quad (1.47c)$$

$$\text{Re } \left. \frac{\partial \hat{\Sigma}_T^W(p^2)}{\partial p^2} \right|_{p^2=M_W^2} = 0, \quad (1.48a)$$

$$\text{Re } \left. \frac{\partial \hat{\Sigma}_T^{ZZ}(p^2)}{\partial p^2} \right|_{p^2=M_Z^2} = 0, \quad \text{Re } \left. \frac{\partial \hat{\Sigma}_T^{AA}(p^2)}{\partial p^2} \right|_{p^2=0} = 0, \quad (1.48b)$$

and the fermions,

$$\hat{\Sigma}_L^f(0) = 0, \quad \hat{\Sigma}_R^f(0) = 0. \quad (1.49)$$

Only the transverse part $\hat{\Sigma}_T$ of the gauge bosons enter as a result of the contraction with the polarisation vectors $\varepsilon^\mu(k)$ in Eq. (1.45a) and (1.46a). The dependence on the renormalization constants enter the renormalized self-energies as follows,

$$\hat{\Sigma}_T^W(p^2) = \Sigma_T^W(p^2) + (p^2 - M_W^2)\delta Z_W - \delta M_W^2, \quad (1.50a)$$

$$\hat{\Sigma}_T^{ZZ}(p^2) = \Sigma_T^{ZZ}(p^2) + (p^2 - M_Z^2)\delta Z_{ZZ} - \delta M_Z^2, \quad (1.50b)$$

$$\hat{\Sigma}_T^{AZ}(p^2) = \Sigma_T^{AZ}(p^2) + \frac{1}{2}p^2\delta Z_{AZ} + \frac{1}{2}(p^2 - M_Z^2)\delta Z_{ZA}, \quad (1.50c)$$

$$\hat{\Sigma}_T^{AA}(p^2) = \Sigma_T^{AA}(p^2) + p^2\delta Z_{AA}, \quad (1.50d)$$

$$\hat{\Sigma}_\sigma^f(p^2) = \Sigma_\sigma^f(p^2) + \delta Z_f^\sigma, \quad \sigma = R, L, \quad (1.50e)$$

where the explicit expressions for the unrenormalized self-energies Σ can be found in Appendix B of Ref. [108]. Inserting the renormalized self-energies in Eq. (1.50) into the renormalization conditions of Eqs. (1.47), (1.48), and (1.49), and solving for the renormalization constants delivers

$$\delta M_W^2 = \text{Re } \Sigma_T^W(M_W^2), \quad \delta Z_W = -\text{Re } \left. \frac{\partial \Sigma_T^W(p^2)}{\partial p^2} \right|_{p^2=M_W^2}, \quad (1.51)$$

$$\delta M_Z^2 = \text{Re } \Sigma_T^{ZZ}(M_Z^2), \quad \delta Z_{ZZ} = -\text{Re } \left. \frac{\partial \Sigma_T^{ZZ}(p^2)}{\partial p^2} \right|_{p^2=M_Z^2}, \quad (1.52)$$

$$\delta Z_{AZ} = -2 \text{Re } \frac{\Sigma_T^{AZ}(M_Z^2)}{M_Z^2}, \quad \delta Z_{ZA} = 2 \frac{\Sigma_T^{AZ}(0)}{M_Z^2}, \quad (1.53)$$

$$\delta Z_{AA} = - \left. \frac{\partial \Sigma_T^{AA}(p^2)}{\partial p^2} \right|_{p^2=0}, \quad (1.54)$$

$$\delta Z_f^\sigma = -\Sigma_\sigma^f(0), \quad \sigma = R, L. \quad (1.55)$$

The electric charge e is defined as the coupling of the full on-shell $\gamma e^+ e^-$ vertex in the Thomson limit, i.e. for vanishing momentum transfer of the photon. Owing to the field renormalization conditions chosen above, no external-leg corrections and photon-Z mixings need to be considered, and the renormalization condition can be expressed in terms of the one-particle irreducible (1PI) vertex function $\hat{\Gamma}_\mu^{Ae^+e^-}$ shown in Fig. 1.2(c),

$$\bar{u}(p) i \hat{\Gamma}_\mu^{Ae^+e^-}(k=0, -p, p) u(p) \Big|_{p^2=m_e^2} = \bar{u}(p) i e \gamma_\mu u(p). \quad (1.56)$$

From this, the renormalization constant δZ_e is determined as [108]

$$\delta Z_e = -\frac{1}{2} \delta Z_{AA} - \frac{s_w}{c_w} \frac{1}{2} \delta Z_{ZA} = \frac{1}{2} \Pi^{AA}(0) - \frac{s_w}{c_w} \frac{\Sigma_T^{AZ}(0)}{M_Z^2}, \quad (1.57)$$

with

$$\Pi^{AA}(p^2) = \frac{\Sigma_T^{AA}(p^2)}{p^2} \quad (1.58)$$

denoting the photon vacuum polarization. Although the weak mixing angle is a derived quantity in the on-shell scheme (see Eq. (1.37)) it is convenient to introduce the following renormalization constants

$$s_{w,0} = s_w + \delta s_w, \quad c_{w,0} = c_w + \delta c_w, \quad (1.59)$$

which are directly related to the renormalization constants of the gauge-boson masses and given by

$$\frac{\delta c_w}{c_w} = -\frac{s_w^2}{c_w^2} \frac{\delta s_w}{s_w} = \frac{1}{2} \text{Re} \left(\frac{\Sigma_T^W(M_W^2)}{M_W^2} - \frac{\Sigma_T^{ZZ}(M_Z^2)}{M_Z^2} \right). \quad (1.60)$$

For the renormalization of the strong coupling constant g_s , no analogue to the Thomson limit (1.56) exists since the $g\bar{q}q$ interaction for vanishing gluon momentum is far outside the realm of perturbative QCD and not accessible experimentally due to the confinement of the quarks and gluons within hadronic bound states. A simple alternative is to only subtract the divergent terms (including universal constants) proportional to

$$\frac{c_\epsilon}{\epsilon} = \frac{1}{\epsilon} - \gamma_E + \ln(4\pi) + \mathcal{O}(\epsilon) \quad (1.61)$$

into the renormalization constants which defines the modified minimal-subtraction ($\overline{\text{MS}}$) scheme. However, this scheme introduces an explicit dependence on the arbitrary mass scale μ from Eq. (1.43), which in this context is also referred to as the *renormalization scale* and denoted μ_R . Since physical quantities must be independent of the renormalization scheme, also any dependence on the arbitrary scale μ_R must drop out in the final result. This condition naturally leads to the formulation of so-called renormalization group equations (RGE), which are e.g. discussed in detail in Ref. [111]. In this context, the beta function is defined as

$$\beta(\alpha_s) = \frac{\partial \alpha_s}{\partial \ln \mu_R^2}, \quad (1.62)$$

and describes the dependence of the coupling α_s on the renormalization scale, which cancels against the explicit dependence on μ_R in Green functions and S -matrix elements introduced by the renormalization scheme. In practice, however, a truncation of the perturbation series at some fixed order induces a dependence on μ_R which is of the next higher order. Therefore, it is possible to obtain an estimate for the missing higher-order correction through the variation of the renormalization scale. The perturbative expansion of the β function reads [114]

$$\beta(\alpha_s) = -b\alpha_s^2 [1 + b'\alpha_s + \mathcal{O}(\alpha_s^2)], \quad b = \frac{33 - 2N_f}{12\pi}, \quad b' = \frac{153 - 19N_f}{2\pi(33 - 2N_f)}, \quad (1.63)$$

where b and b' correspond to the 1-loop and 2-loop contributions, respectively, and N_f denotes the number of active flavours. For $N_f < 17$ the 1-loop coefficient is negative, and as a consequence, the strong coupling α_s becomes smaller at short distances. This property is known as *asymptotic freedom* [10, 11] and turns perturbative QCD into a reliable calculational tool at high scales. Lastly, we note that the use of a variable scale $\mu_R^2 = Q^2$ instead of an arbitrarily fixed one ($\mu_R = \mu_{\text{fix}}$), with Q^2 denoting a typical scale of the hard scattering, automatically resums the potentially large logarithms $\ln(Q^2/\mu_{\text{fix}}^2)$ to all orders. As a result, employing a running coupling $\alpha_s(Q^2)$ effectively absorbs all such logarithms into the lower-order prediction and renders the corrections smaller, which in turn leads to a more stable perturbative expansion.

In the section that follows, it will be described how further leading universal higher-order corrections can be absorbed into a redefinition of the EW couplings via an appropriate choice of an input-parameter scheme.

1.1.3. Electroweak input-parameter schemes

The electromagnetic coupling was defined in the previous section via the on-shell renormalization in the Thomson limit. The fine-structure constant determined in this way defines the “ $\alpha(0)$ -scheme”, which reflects the scale of the UV subtraction point given by the vanishing photon momentum transfer $Q = 0$. A closer inspection of the renormalization constant in Eq. (1.57) reveals that this scheme introduces a dependence on the light-fermion masses through logarithms $\sim \alpha \ln(m_f^2/s)$ that appear in the photon vacuum polarisation $\Pi^{AA}(0)$. They remain uncanceled in the final S -matrix element if the corresponding coupling e does not result from an external photon.⁷ Not only do these logarithms represent large universal corrections which should be absorbed into an appropriate redefinition of the coupling, moreover, the sensitivity to the

⁷ For the coupling to external photons, this dependence exactly cancels against the external wave-function renormalization, reflecting that the interaction effectively occurs at the low scale $Q^2 = 0$, and that $\alpha(0)$ is the appropriate coupling in this case.

fermion masses touches on a conceptual problem regarding the definition of light-quark masses within perturbation theory: The quarks are treated as free particles in the SM Lagrangian (1.2), however, due to the non-perturbative nature of the strong interaction at small scales they are confined within colourless bound states. Therefore, the masses m_q ($q = u, d, c, s, b$) appearing in the Lagrangian should be rather understood as effective parameters which are directly determined from experimental data. In high-energy experiments ($s \gg M_Z^2$) it is feasible to treat the light quarks as massless particles, as it is done throughout this work. The dependence on the quark masses only enters through the hadronic vacuum polarization and can be completely removed by a clever choice of an input-parameter scheme. What follows is an outline of the two common schemes used in predictions for high-energy experiments: the $\alpha(M_Z)$ -scheme and G_μ -scheme.

In the “ $\alpha(M_Z)$ -scheme”, see e.g. Ref. [115], the universal logarithms of the light-fermion masses are re-summed to all orders via the replacement

$$\alpha(0) \rightarrow \alpha(M_Z) \equiv \frac{\alpha(0)}{1 + \Delta\alpha(M_Z)}, \quad \delta Z_e \rightarrow \delta Z_e - \frac{1}{2} \Delta\alpha(M_Z) \equiv \delta Z_e^{\alpha(M_Z)}. \quad (1.64)$$

The UV-finite quantity

$$\Delta\alpha(M_Z) = \Pi_{f \neq t}^{AA}(0) - \text{Re} \Pi_{f \neq t}^{AA}(M_Z^2) \quad (1.65)$$

describes the running of the coupling α from the Thomson limit to the scale $Q^2 = M_Z^2$, induced by the light fermions in the photon vacuum polarization. In this scheme all light-fermion logarithms that originate from the charge renormalization cancel in the EW corrections as can be seen from the modification to the renormalization constant δZ_e given in Eq. (1.64). In particular, the dependence on the perturbatively ill-defined light-quark masses drops out.

Secondly, in the “ G_μ -scheme” the electromagnetic coupling constant is derived from the muon decay constant G_μ , which is very accurately measured from the muon lifetime τ_μ . At leading order, the relation between α and the Fermi constant can be directly inferred from the SM Lagrangian by a comparison with the four-fermion interaction in the Fermi model,

$$\frac{4G_\mu}{\sqrt{2}} = \frac{e^2}{2s_w^2 M_W^2}. \quad (1.66)$$

At higher orders, calculating the muon lifetime in the SM and comparing it to the the QED improved Fermi model yields the following relation [108, 116],

$$G_\mu = \frac{\pi\alpha}{\sqrt{2}s_w^2 M_W^2} (1 + \Delta r), \quad (1.67)$$

where

$$\begin{aligned} \Delta r &= \Pi^{AA}(0) - \frac{c_w^2}{s_w^2} \left(\frac{\Sigma_T^{ZZ}(M_Z^2)}{M_Z^2} - \frac{\Sigma_T^W(M_W^2)}{M_W^2} \right) \\ &\quad + \frac{\Sigma_T^W(0) - \Sigma_T^W(M_W^2)}{M_W^2} + 2 \frac{c_w}{s_w} \frac{\Sigma_T^{AZ}(0)}{M_Z^2} + \frac{\alpha}{4\pi s_w^2} \left(6 + \frac{7 - 4s_w^2}{2s_w^2} \ln c_w^2 \right) \\ &\equiv \Delta\alpha(M_Z) - \frac{c_w^2}{s_w^2} \Delta\rho + \Delta r_{\text{rem}}, \end{aligned} \quad (1.68)$$

with

$$\Delta\rho = \frac{\Sigma_{\text{T}}^{ZZ}(M_Z^2)}{M_Z^2} - \frac{\Sigma_{\text{T}}^W(M_W^2)}{M_W^2}. \quad (1.69)$$

The quantity Δr comprises all higher-order corrections *excluding* the contributions that constitute QED corrections in the Fermi model, which are included in the definition of the muon decay constant G_μ . The leading-order relation (1.66) is then promoted to a definition of the electromagnetic coupling in the G_μ -scheme,

$$\alpha(0) \rightarrow \alpha_{G_\mu} \equiv \frac{\sqrt{2}G_\mu M_W^2 s_w^2}{\pi} = \alpha(0) (1 + \Delta r), \quad \delta Z_e \rightarrow \delta Z_e - \frac{1}{2}\Delta r \equiv \delta Z_e^{G_\mu}, \quad (1.70)$$

where Δr is subtracted in the renormalization constant in order to avoid double-counting. Since the quantity $\Delta\alpha(M_Z)$ is contained in Δr , the light-fermion logarithms are correctly absorbed into the coupling α_{G_μ} and the dependence on the problematic light-quark masses is removed. Furthermore, this input-parameter scheme includes the corrections $\Delta\rho$ to the ρ -parameter, which are related to the renormalization of the weak mixing angle (1.60). They arise from large mass splittings within the isospin doublets and give contributions enhanced by the large top-quark mass m_t^2 [117]. The recipe to include the dominant corrections from $\Delta\rho$ via a substitution $s_w^2 \rightarrow s_w^2 + \Delta\rho c_w^2$ is exactly absorbed in this scheme for the combination α/s_w^2 , which is naturally appearing in the charged-current processes. In the neutral-current processes this absorption is only partial, since couplings such as $\alpha/(s_w^2 c_w^2)$ appear.

Throughout this work we employ the G_μ -scheme if not explicitly stated otherwise. The impact of the different input-parameter schemes to the neutral- and charged-current Drell–Yan processes was studied in Refs. [45] and [37], respectively.

1.2. Unstable particles in QFT

The purpose of this section is to review the treatment of unstable particles in quantum field theories and the conceptual problems associated with their description. A general overview on unstable particles can be found e.g. in Ref. [90], which we follow closely.

Most particles in the SM, such as the weak gauge bosons (W^\pm , Z), the Higgs particle H , and the top quark t have a short lifetime τ , and as such, can only be observed through their decay products. These unstable particles then manifest themselves through resonances in certain observables, e.g. the invariant-mass distribution (Q^2) of the decay products where the resonance is described by a Breit–Wigner shape around the mass M of the decaying particle,

$$\frac{d\sigma}{dQ^2} \underset{Q^2 \rightarrow M^2}{\sim} \frac{\text{const}}{(Q^2 - M^2)^2 + \Gamma^2 M^2}, \quad (1.71)$$

with $\Gamma = \tau^{-1}$ denoting the finite decay width of the resonance.

In the following, we consider the case of a scalar particle ϕ for simplicity, however, the discussion is analogously applicable to other particles with different spin. In the end of this section, we discuss the special case of the weak gauge bosons W and Z in more detail with a particular emphasis on the numerical impact of different mass definitions. The perturbative evaluation of quantum field theories is formulated as an expansion about the free theory where

$$\frac{\phi}{p} \text{---} \bigcirc \text{---} \phi = \text{---} + \text{---} \bullet \text{---} + \text{---} \bullet \bullet \text{---} + \dots$$

Figure 1.3.: Dyson-summed propagator of a scalar particle ϕ with momentum p . The filled blobs represent the one-particle irreducible self-energy insertions $i\hat{\Sigma}^\phi(p^2)$.

all particles are considered to be stable. As a consequence, the tree-level propagator $i/(p^2 - M^2)$ with momentum transfer p becomes divergent at the on-shell point $p^2 = M^2$, which leads to a non-integrable infinity in the theoretical prediction if the particle can kinematically be on its mass shell. The decay of an unstable particle constitutes a higher-order effect and its decay width is related to the imaginary part of its self-energy via the unitarity. A realistic theoretical description of the resonance therefore requires at least a partial resummation of self-energy insertions as illustrated in Fig. 1.3. Performing this so-called Dyson summation, the propagator can be written in the following form,

$$\begin{aligned} G^{\phi\phi}(p^2) &= \frac{i}{p^2 - M^2} + \frac{i}{p^2 - M^2} i\hat{\Sigma}^\phi(p^2) \frac{i}{p^2 - M^2} + \dots = \frac{i}{p^2 - M^2} \sum_{n=0}^{\infty} \left(\frac{-\hat{\Sigma}^\phi(p^2)}{p^2 - M^2} \right)^n \\ &= \frac{i}{p^2 - M^2 + \hat{\Sigma}^\phi(p^2)} = - \left(\hat{\Gamma}^{\phi\phi}(p, -p) \right)^{-1}, \end{aligned} \quad (1.72)$$

where M and $\hat{\Sigma}^\phi(p^2)$ denote the renormalized mass and self-energy of the scalar particle ϕ , respectively. We do not further specify the specific renormalization conditions and, in particular, we do not assume that field renormalization of the field ϕ has been performed at this point. In case ϕ corresponds to a stable particle, the propagator $G^{\phi\phi}(p^2)$ develops a pole on the real axis at the physical mass $p^2 = M_{\text{phys}}^2$ owing to $\text{Im} \hat{\Sigma}^\phi(M_{\text{phys}}^2) = 0$ for stable particles. The on-shell mass M_{OS} defined through the renormalization condition, cf. Eqs. (1.45),

$$\text{Re} \hat{\Gamma}^{\phi\phi}(p, -p) \Big|_{p^2=M_{\text{OS}}^2} = 0, \quad \Rightarrow \quad \text{Re} \hat{\Sigma}^\phi(M_{\text{OS}}^2) = 0, \quad (1.73)$$

is therefore correctly identified with the physical mass, $M_{\text{OS}} = M_{\text{phys}}$. For unstable particles, however, the pole of the propagator $G^{\phi\phi}(p^2)$ is shifted into the complex p^2 plane because of the non-vanishing absorptive part in the self-energy, $\text{Im} \hat{\Sigma}^\phi(M_{\text{OS}}^2) \neq 0$, and the Dyson-summed propagator takes the following form in the vicinity of the on-shell mass,

$$G^{\phi\phi}(p^2) \underset{p^2 \rightarrow M_{\text{OS}}^2}{\sim} \frac{iR_{\text{OS}}}{p^2 - M_{\text{OS}}^2 + iM_{\text{OS}}\Gamma_{\text{OS}}}, \quad (1.74)$$

with the residue⁸

$$R_{\text{OS}} = 1 + \text{Re} \hat{\Sigma}'^\phi(M_{\text{OS}}^2), \quad \hat{\Sigma}'^\phi(p^2) = \frac{\partial \hat{\Sigma}^\phi(p^2)}{\partial p^2}, \quad (1.75)$$

and the on-shell width given by

$$\Gamma_{\text{OS}} = \frac{\text{Im} \hat{\Sigma}^\phi(M_{\text{OS}}^2)}{M_{\text{OS}} R_{\text{OS}}}. \quad (1.76)$$

⁸ In case an on-shell field renormalization of the field ϕ is performed, $R_{\text{OS}} = 1$.

The mass and width defined in this scheme is gauge dependent beyond the one-loop level, as was shown in Ref. [118]. Alternatively, the location of the propagator pole in the complex p^2 plane can be used to define the so-called pole mass and pole width as follows,

$$\mu^2 - M^2 + \hat{\Sigma}^\phi(\mu^2) = 0, \quad \mu^2 \equiv M_{\text{pole}}^2 - iM_{\text{pole}}\Gamma_{\text{pole}}. \quad (1.77)$$

Since the pole location is a property of the S -matrix, the pole mass and width are gauge independent quantities [118–121] and the propagator takes the following form in the vicinity of the complex pole,

$$G^{\phi\phi}(p^2) \underset{p^2 \rightarrow \mu^2}{\sim} \frac{iR_{\text{pole}}}{p^2 - M_{\text{pole}}^2 + iM_{\text{pole}}\Gamma_{\text{pole}}}, \quad R_{\text{pole}} = 1 + \text{Re} \hat{\Sigma}'^\phi(\mu^2). \quad (1.78)$$

The relation between the perturbative definition of the pole and the on-shell mass is given by [90]

$$M_{\text{OS}}^2 = M_{\text{pole}}^2 + \text{Im} \left[\hat{\Sigma}^\phi(M_{\text{pole}}^2) \right] \text{Im} \left[\hat{\Sigma}'^\phi(M_{\text{pole}}^2) \right] + \mathcal{O}(\alpha^3), \quad (1.79)$$

$$\begin{aligned} M_{\text{OS}}\Gamma_{\text{OS}} = M_{\text{pole}}\Gamma_{\text{pole}} + \text{Im} \left[\hat{\Sigma}^\phi(M_{\text{pole}}^2) \right] \left\{ \left(\text{Im} \left[\hat{\Sigma}'^\phi(M_{\text{pole}}^2) \right] \right)^2 \right. \\ \left. + \frac{1}{2} \text{Im} \left[\hat{\Sigma}^\phi(M_{\text{pole}}^2) \right] \text{Im} \left[\hat{\Sigma}''^\phi(M_{\text{pole}}^2) \right] \right\} + \mathcal{O}(\alpha^4), \end{aligned} \quad (1.80)$$

i.e. the two mass and width definitions agree with each other up to gauge-dependent corrections starting at the two-loop order.

The conventional definition of the decay width is given by the expression

$$\Gamma_{\text{conv}} = \frac{1}{2M} \sum_f \int d\Phi_f \left| \mathcal{M}^{\phi \rightarrow f} \right|^2, \quad f = \{ f_1, \dots, f_n \}, \quad d\Phi_f = d\phi(k_1, \dots, k_n; M) \quad (1.81)$$

where the sum over f extends over all possible decay channels of the unstable particle ϕ and the phase-space measure $d\phi$ is defined in Eq. (A.52). This definition of the decay width can be shown to correspond to the on-shell width Γ_{OS} given in Eq. (1.76) and as a consequence, the conventional decay width Γ_{conv} is also gauge dependent beyond the one-loop level. Furthermore, Eq. (1.81) exposes a conceptual problem associated with unstable particles appearing as external states in the transition amplitudes: As mentioned briefly in the end of Sect. 1.1.1, the matrix element \mathcal{M} is defined as the transition amplitude of asymptotic states which are thought to be prepared long before/after ($t \rightarrow \pm\infty$) the process under consideration. However, such states become ill-defined in case of unstable particles which have a finite life time τ , and therefore, the application of the LSZ reduction formula to obtain Eq. (1.81) is not justified. Important work to address this conceptual problem was done by Veltman [122], who has shown that excluding such external states associated with unstable particles and further defining their propagators by a full Dyson summation leads to an S -matrix that respects unitarity, renormalizability, and causality on the space of stable particles.

The remainder of this section is dedicated to the discussion of the special case of the weak gauge bosons W and Z , which only decay into light fermions. For $p^2 \sim M_V^2$ it is feasible to neglect the masses of the light fermions and the imaginary part of the gauge-boson self-energies

can be approximated by the the following simple form,

$$\text{Im } \hat{\Sigma}_T^V(p^2) = \frac{\Gamma_{V,\text{OS}}}{M_{V,\text{OS}}} p^2 \Theta(p^2), \quad V = W, Z, \quad (1.82)$$

where the on-shell scheme was extended to the wave-function renormalization of the field ϕ , i.e. $R_{\text{OS}} \equiv 1$. The Dyson-summed propagator leads to a “running width” description of the resonance given by the following expression,

$$G^{\phi\phi}(p^2) \sim \frac{i}{p^2 - M_{\text{OS}}^2 + i \frac{\Gamma_{\text{OS}}}{M_{\text{OS}}} p^2}. \quad (1.83)$$

Although the mass and width defined via this scheme are known to be gauge dependent beyond the one-loop level as discussed above, this running-mass scheme has been employed in the determination of the W- and Z-boson masses at LEP and the Tevatron. Owing to its gauge independence, the pole mass and width is the preferred scheme from a theoretical point of view. Rewriting Eq. (1.83) as follows,

$$\frac{i}{p^2 - M_{\text{OS}}^2 + i \frac{\Gamma_{\text{OS}}}{M_{\text{OS}}} p^2} = \frac{i \left(1 + i \frac{\Gamma_{V,\text{OS}}}{M_{V,\text{OS}}}\right)^{-1}}{p^2 - \mu_V^2}, \quad \mu_V^2 = \frac{M_{V,\text{OS}}^2 - i M_{V,\text{OS}} \Gamma_{V,\text{OS}}}{1 + \frac{\Gamma_{V,\text{OS}}^2}{M_{V,\text{OS}}^2}} \quad (1.84)$$

results in the simple conversion formula between the two schemes given by

$$M_{V,\text{pole}} = \frac{M_{V,\text{OS}}}{c_V}, \quad \Gamma_{V,\text{pole}} = \frac{\Gamma_{V,\text{OS}}}{c_V}, \quad c_V = \sqrt{1 + \frac{\Gamma_{V,\text{OS}}^2}{M_{V,\text{OS}}^2}}. \quad (1.85)$$

The numerical impact of the difference in the mass definitions is given by

$$M_{W,\text{OS}} \approx 80 \text{ GeV}, \quad \Gamma_{W,\text{OS}} \approx 2.2 \text{ GeV}, \quad \Rightarrow \quad (M_{W,\text{OS}} - M_{W,\text{pole}}) \approx 27 \text{ MeV}, \quad (1.86)$$

$$M_{Z,\text{OS}} \approx 91 \text{ GeV}, \quad \Gamma_{Z,\text{OS}} \approx 2.5 \text{ GeV}, \quad \Rightarrow \quad (M_{Z,\text{OS}} - M_{Z,\text{pole}}) \approx 34 \text{ MeV}. \quad (1.87)$$

Comparing these values with the current experimental accuracy of the mass measurements [123]

$$\Delta M_{W,\text{exp}} = 15 \text{ MeV}, \quad \Delta M_{Z,\text{exp}} = 2.1 \text{ MeV}, \quad (1.88)$$

reveals that the scheme choice has an impact that is larger than the experimental accuracy. It is therefore important to be careful with the scheme that is used in the calculations and the respective input values obtained from the measurements.

So far, we have discussed the two mass and width definitions given by the on-shell and the pole schemes, which lead to the parametrizations of the gauge-boson resonance in terms of a running and a fixed width, respectively. The transition from one to the other scheme is given in Eq. (1.85) for the weak gauge bosons. However, in a gauge theory where gauge invariance and unitarity hold order-by-order, performing a Dyson summation (1.72) inevitably mixes perturbative orders and, in general, leads to gauge-dependent results. Different approaches have been proposed to cope with this issue in order to obtain gauge-independent predictions. In Sect. 4.1, we describe the so-called *pole approximation* that was used in this work and refer to Sect. 2.8 of Ref. [124] for an overview on the most frequently used schemes in LHC physics. A

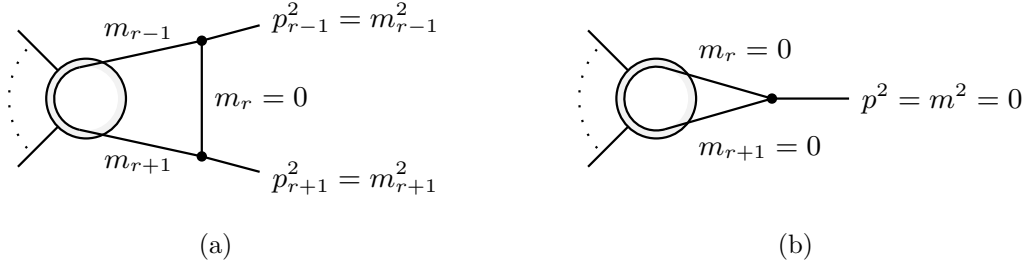


Figure 1.4.: Generic one-loop diagrams illustrating the configurations that lead to the two types of infrared singularities: the soft (a) and collinear (b) singularities.

detailed comparison between the *complex-mass scheme*, the *pole scheme*, and the *factorization scheme* in the application of the neutral-current Drell–Yan process can be found in Ref. [45].

1.3. Infrared singularities in NLO calculations

Section 1.1.2 dealt with the treatment of UV divergences in radiative corrections, which are associated with the infinite-momentum region of the loop momenta and are removed by the procedure of renormalization. Apart from UV divergences, virtual corrections can also develop singularities for finite loop momenta, called the Landau singularities, where the necessary condition for their occurrence is described by the Landau equations [125]. A special type of Landau singularities are the infrared (IR) singularities, which are pathological solutions of the Landau equations that are independent of the external momenta and related to vanishing particle masses.⁹ Infrared singularities do not only occur in loop integrals, but also arise from the phase-space integration of the associated real-emission corrections over the unresolved regions, where the radiated particle becomes soft and/or collinear to another particle. The inclusive treatment of such degenerate states leads to the exact cancellation of all IR singularities between the virtual and the real contributions in physical observables. This is the statement of the Kinoshita–Lee–Nauenberg (KLN) theorem [126, 127] which is a consequence of unitarity.

In the following, we discuss the structure of IR singularities that occur in the virtual and real corrections in NLO calculations in Sects. 1.3.1 and 1.3.2, respectively. A more detailed treatment of IR singularities and their cancellation can be found in Ref. [126]. The discussion of the IR singularity structure that goes beyond NLO, which will become relevant in the calculation of the mixed QCD–electroweak $\mathcal{O}(\alpha_s \alpha)$ corrections, is postponed to Sect. 6.1.1 in Part II where these corrections will be discussed in detail.

1.3.1. IR singularities in one-loop amplitudes

At the one-loop level, two types of IR singularities can be distinguished: the soft and collinear singularities. The two generic one-loop diagrams that lead to the respective divergences are shown in Fig. 1.4 and discussed in the following.

First, *soft* singularities occur in configurations where a massless virtual particle is exchanged between two external on-shell legs. The divergence originates from the integration region

⁹ The arbitrariness of external momenta in this context refers to the relative orientation keeping their squares fixed. There can be restrictions on the magnitude of momenta that arise e.g. from mass-shell conditions. Due to the connection to vanishing masses, these singularities are also often referred to as “mass singularities”.

where the momentum of the massless particle tends to zero (i.e. is soft) and requires the three neighbouring propagators in the loop to satisfy the conditions as indicated in Fig. 1.4(a). If the exchanged particle is a fermion, the additional momentum dependence in the numerator of the fermion propagator leads to a suppression, so that no soft singularity occurs.

Second, a *collinear* singularity arises from a configuration where an external massless on-shell particle splits into two massless virtual particles inside the loop. The divergence results from the region of the loop integral in which the two virtual particles have momenta collinear to the external leg. This situation is illustrated in Fig. 1.4(b) together with the kinematic requirements that lead to this singularity.

The above two cases can also occur simultaneously, giving rise to overlapping soft and collinear singularities. We note that at most three neighbouring loop propagators are involved in the conditions that describe the occurrence of IR singularities and it was shown in Ref. [128] that the complete IR singular structure of an arbitrary one-loop diagram can be expressed in terms of only three-point integrals. Since IR singularities arise in the massless limit, a straight-forward approach to regularize them in case of Abelian groups is by introducing infinitesimal masses. The singularities then manifest themselves as logarithms of these small regulator masses. In this work, however, we will employ the method of dimensional regularization as already used in the context of regularizing UV divergences in Sect. 1.1.2. Here, the soft and collinear singularities appear as poles in ϵ , and the overlapping case gives rise to $\frac{1}{\epsilon^2}$ poles.

1.3.2. IR singularities in real-emission cross sections

The IR singularities that appear in the phase-space integration of the real-emission corrections can be divided into the soft and collinear singularities as well, in direct correspondence to the one-loop case discussed in the previous section. These divergences have their origin in the integration over the unresolved regions of phase space and it is required that such degenerate configurations are treated inclusively so that the cancellation of all IR singularities is guaranteed by the KLN theorem. As reviewed in the following, the real-emission corrections exhibit a factorization property in the singular limits which allows for the isolation of the IR-singular behaviour in a process-independent manner. This property is an essential ingredient in the construction of general algorithms for the analytic cancellation of IR singularities in higher-order calculations, such as the dipole subtraction formalism which is discussed in Chap. 3. We will restrict ourselves to the discussion of the IR singularities that appear in NLO QED corrections and refer the reader to Refs. [129, 130] where the analogous case for QCD is discussed.

A soft singularity occurs in the bremsstrahlung process involving the additional emission of a photon, when the energy of the radiated photon tends to zero. We denote the corresponding real-emission amplitude by $\mathcal{M}_R^\gamma(k)$, where k is the momentum of the photon and the dependence on the remaining momenta is suppressed in the notation. The singular behaviour in the soft-photon limit¹⁰ ($k^\mu \rightarrow 0$) is then described by the well-known eikonal currents (see e.g. Refs. [108, 131]) and the squared real-emission matrix element, summed over all photon polarizations λ_γ , can be

¹⁰ Note that the energy of the photon (k^0) must be much smaller than all relevant scales of the hard process, so that its consistent omission in the regular terms does not have a sizeable impact. In particular, if the considered process contains a narrow resonance, the eikonal approximation is only valid for $k^0 \ll \Gamma$, where Γ denotes the width of the resonance.



Figure 1.5.: Photon radiation off an incoming (a) and outgoing (b) fermion line.

written as

$$\begin{aligned}
 \sum_{\lambda_\gamma} |\mathcal{M}_R^\gamma(k)|^2 &\underset{k \rightarrow 0}{\sim} -4\pi\mu^{2\epsilon}\alpha \sum_{I,J} \eta_I Q_I \eta_J Q_J \frac{p_I \cdot p_J}{(p_I \cdot k)(p_J \cdot k)} |\mathcal{M}_0|^2 \\
 &= -4\pi\mu^{2\epsilon}\alpha \sum_{\substack{I,J \\ I \neq J}} \eta_I Q_I \eta_J Q_J \frac{1}{p_I \cdot k} \left[\frac{2(p_I \cdot p_J)}{p_I \cdot k + p_J \cdot k} - \frac{m_I^2}{p_I \cdot k} \right] |\mathcal{M}_0|^2. \quad (1.89)
 \end{aligned}$$

Here, the summation over the indices I, J extends over all external charged legs, and \mathcal{M}_0 denotes the matrix element of the process without photon emission. We have further introduced the sign factors $\eta_I = \pm$ describing the charge flow, which are defined as $\eta_I = +1$ for incoming particles and outgoing anti-particles and $\eta_I = -1$ for incoming anti-particles and outgoing particles. Equation (1.89) only depends on the momenta and charges of the external legs, which can be both massive and massless, and the generalisation to the d -dimensional treatment amounts to the additional global factor $\mu^{2\epsilon}$. The second line in Eq. (1.89) is obtained by using charge conservation

$$\sum_I \eta_I Q_I = 0 \quad (1.90)$$

and further rearrangements. It serves the purpose to disentangle the collinear singularities in the two limits $p_I \cdot k \rightarrow 0$ and $p_J \cdot k \rightarrow 0$ which occurs in the case of vanishing masses $m_{I,J} \rightarrow 0$ and when the soft photon becomes collinear to either of the particles I and J .

The collinear singularities arise from configurations in the phase-space integration where the radiated photon becomes collinear to an external massless charged particle. In the following, we only consider the case of photon radiation off fermions and distinguish the two cases with incoming and outgoing fermions as illustrated in Figs. 1.5(a,b), respectively. The asymptotic behaviour of the squared transition matrix element in these collinear limits takes the following form [132]

$$\sum_{\lambda_\gamma} |\mathcal{M}_R^\gamma(p_i, k)|^2 \underset{p_i \cdot k \rightarrow 0}{\sim} \frac{4\pi\mu^{2\epsilon}\alpha}{p_i \cdot k} \hat{P}_{\text{QED}}^{ff}(z_i) |\mathcal{M}_0(p_i + k)|^2, \quad z_i = \frac{p_i^0}{p_i^0 + k^0}, \quad (1.91a)$$

$$\sum_{\lambda_\gamma} |\mathcal{M}_R^\gamma(p_a, k)|^2 \underset{p_a \cdot k \rightarrow 0}{\sim} \frac{4\pi\mu^{2\epsilon}\alpha}{x_a(p_a \cdot k)} \hat{P}_{\text{QED}}^{ff}(x_a) |\mathcal{M}_0(p_a - k)|^2, \quad x_a = \frac{p_a^0 - k^0}{p_a^0}, \quad (1.91b)$$

where our notation makes the dependence on the momentum of the fermion explicit that is involved in the respective limits. The variables z_i and x_a correspond to the momentum fractions that is carried away by the fermions after the collinear splittings $f \rightarrow f\gamma$ and the d dimensional

splitting function $\hat{P}_{\text{QED}}^{ff}$ is given by

$$\hat{P}_{\text{QED}}^{ff}(z) = Q_f^2 \left(\frac{1+z^2}{1-z} - \epsilon(1-z) \right). \quad (1.92)$$

The analogous expression for the case using finite masses as regulators can be found in Ref. [133], and the limiting formulae for the collinear limits associated with the various splittings that are not covered here, such as the splitting process $\gamma \rightarrow \bar{f}f$ can be found in Ref. [134].

1.4. The parton model and perturbative QCD

As it was briefly outlined in Sect. 1.1.2, the running of the strong coupling α_s leads to the property of asymptotic freedom which turns perturbation theory into a reliable calculational tool for QCD at high scales. However, it also induces the growth of the coupling with decreasing scales which eventually leads to a breakdown of perturbation theory.¹¹ QCD therefore becomes strongly coupled at long distances and the empiric fact that quarks and gluons never appear as asymptotic states, also known as *colour confinement*, only allows for scattering experiments to be performed involving external colourless bound states of the strong interaction, called hadrons. These hadrons cannot be solely described using perturbation theory and the ability to predict their structure from QCD is limited. As a consequence, the determination of their properties almost entirely relies on experimental input. In order to study the fundamental interactions governing the quarks and gluons we therefore require a precise prescription to identify the perturbatively accessible hard scattering process between these elementary constituents in the scattering reactions with external hadrons. Such a description is provided by the parton model and will be described in the following for the case of hadron–hadron collisions. Further details and field-theoretical background can be found e.g. in Ref. [114].

The naive parton model

The “naive” parton model [135, 136] describes the hadron as a composite object made up of point-like constituents called the partons (*parts* of hadrons) which are identified with the quarks and gluons. For high-energy collisions, the masses of the hadrons and their constituents can be neglected, and additionally, the hadron is Lorentz contracted in the longitudinal direction and all its internal interactions are time dilated in this *infinite momentum frame*. From these considerations, during the brief moment in which the hadron is probed by the scattering reaction, it can be assumed that the number density of the partons is constant and that each parton carries a definite momentum fraction x ($0 < x < 1$) of the hadron’s momentum. The distribution of the momentum of the hadron among its constituents is described by the *parton distribution function* (PDF) $f_{a|A}^{(0)}(x_a)$ which plays the role of a generalized number density to find a parton of species a carrying the longitudinal momentum fraction x_a of the parent hadron A . For collisions with a momentum transfer much larger than the confining scale Λ_{QCD} , the interaction between the hadrons is described by the incoherent scattering between two constituent partons which can be assumed to be free. As a result, the cross section for the scattering process $A + B \rightarrow f + X$

¹¹ The characteristic scale of QCD which signals the transition between the perturbative and the non-perturbative regime is given by the Λ_{QCD} parameter which is typically of the order of a few hundred MeV. It is the scale where, by extrapolation into the non-perturbative domain, the strong coupling α_s would formally become divergent.

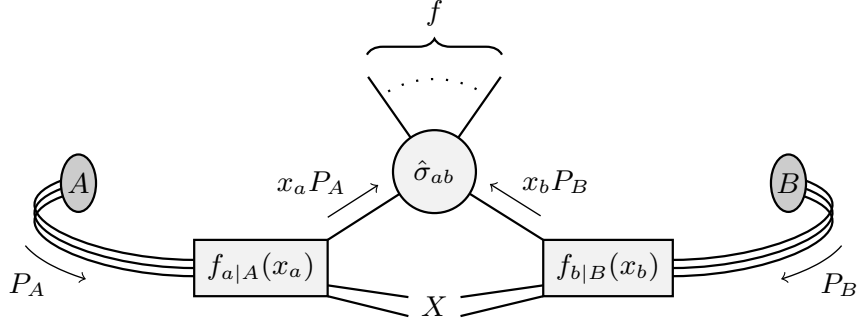


Figure 1.6.: A schematic representation of the hadronic scattering process $A + B \rightarrow f + X$, where f denotes the final-state configuration of interest and X captures any additional hadronic activity from the hadron remnants.

initiated by two hadrons with momenta P_A and P_B can be written as the incoherent sum over all partonic sub-processes that contribute to the final state f under consideration, convoluted with the respective PDFs (see Fig. 1.6),

$$\sigma_{AB}(P_A, P_B) = \sum_{a,b} \int_0^1 dx_a \int_0^1 dx_b f_{a|A}^{(0)}(x_a) f_{b|B}^{(0)}(x_b) \hat{\sigma}_{ab}^0(p_a, p_b). \quad (1.93)$$

The momenta of the partons that participate in the hard scattering are given by $p_a = x_a P_A$ and $p_b = x_b P_B$, and $\hat{\sigma}_{ab}^0$ denotes the partonic cross section at leading order. As pointed out in the introduction of this section, the PDFs are outside of the perturbative regime of QCD and have to be extracted from experiment. They are, however, universal in the sense that they only capture the structure of the hadron, but do not depend on the actual scattering reaction that probes them. As a result, they can be extracted, e.g. from lepton–nucleon deep-inelastic scattering (DIS) experiments, and used to calculate predictions for hadron–hadron collisions.

The QCD improved parton model

The critical shortcoming of the naive parton model described so far is the fact that the hadronic cross section defined through Eq. (1.93) is not IR safe.¹² The parton model is devised for high-energy scattering reactions and is formulated in the limit where all partons are considered to be massless. In general, this gives rise to IR singularities at higher orders, as was outlined in Sect. 1.3, and the cancellation of these divergences is ruled by the KLN theorem which requires the inclusive treatment of all external degenerate states. This requirement of inclusiveness is, however, not fulfilled in the case at hand because a collinear splitting in the initial-state will modify the momentum that enters the hard scattering process. What the naive parton model therefore fails to capture is the degenerate configuration where a parton inside the hadron undergoes a collinear splitting before entering the hard scattering reaction. As a consequence, going beyond the leading-order description for the partonic scattering process will, in general, contain uncanceled divergences of collinear origin in the hadronic cross section given in Eq. (1.93).

¹² For this reason, the partonic cross section in Eq. (1.93) must be restricted to the Born-level prediction $\hat{\sigma}_{ab}^0$, which is guaranteed to be free of any IR singularities.

However, these initial-state collinear singularities corresponds to long-distance interactions which should be attributed to the description of the hadrons, and thus, to the PDFs. In the QCD-improved parton model, these divergences are absorbed into the PDFs via a procedure very reminiscent to renormalization discussed in Sect. 1.1.2. To this end, the PDFs $f_{a|A}^{(0)}$ in Eq. (1.93) are considered to be bare distributions and the collinear singularities are absorbed by a redefinition procedure, which at NLO QCD amounts to the following replacement

$$f_{a|A}^{(0)}(x) \rightarrow f_{a|A}^{\text{F.S.}}(x, \mu_F^2) - \frac{\alpha_s}{2\pi} \frac{1}{\Gamma(1-\epsilon)} \sum_b \int_x^1 \frac{dz}{z} f_{b|A}^{\text{F.S.}}\left(\frac{x}{z}, \mu_F^2\right) \left[-\frac{1}{\epsilon} \left(\frac{4\pi\mu^2}{\mu_F^2} \right)^\epsilon P^{ba}(z) + K_{\text{F.S.}}^{ba}(z) \right]. \quad (1.94)$$

The functions $P^{ab}(z)$ are the four-dimensional regularized Altarelli–Parisi probabilities for the splitting process $a(p) \rightarrow b(zp) + c((1-z)p)$ which can be calculated perturbatively and are given in Appendix C of Ref. [129]. This procedure further introduces a new scale μ_F , called the *factorization scale*, which separates the long-distance from the short-distance physics in such a way that collinear splitting processes which involve transverse momenta up to μ_F are attributed to the description of the hadron.

The ability to separate the initial-state collinear singularities in a process-independent manner so that they can be absorbed into the universal density functions is ruled by *factorization theorems* and represents a crucial properties of the theory, besides asymptotic freedom, which gives us the ability to calculate reliable predictions in QCD. For many important processes factorization is proven to all orders in α_s [137], such as DIS and the Drell–Yan processes.

The ambiguity in distributing finite contributions between the renormalized PDFs and the partonic cross section is fixed by the choice of the coefficient functions $K_{\text{F.S.}}^{ab}$ and defines the *factorization scheme*. The standard choice in QCD calculations is the $\overline{\text{MS}}$ scheme, where only the divergent terms (plus additional universal constants as in Eq. (1.61)) are absorbed into the PDFs and corresponds to the choice

$$K_{\overline{\text{MS}}}^{ab} \equiv 0. \quad (1.95)$$

After performing the redefinition of the PDFs (1.94), the hadronic cross section takes the following form,

$$\sigma_{AB}(P_A, P_B) = \sum_{a,b} \int_0^1 dx_a \int_0^1 dx_b f_{a|A}^{\text{F.S.}}(x_a, \mu_F^2) f_{b|B}^{\text{F.S.}}(x_b, \mu_F^2) \hat{\sigma}_{ab}(p_a, p_b; \mu_F^2), \quad (1.96)$$

which is a direct generalisation of Eq. (1.93). The perturbatively calculable hard scattering cross section for the scattering between two partons a and b is denoted by $\hat{\sigma}_{ab}$, which is free from all IR singularities. It is derived from the “bare” (but UV renormalized) partonic cross section σ_{ab} by removing the long-distance pieces that correspond to the collinear singularities that were absorbed into the redefinition of the PDFs (1.94). At NLO QCD it is given by

$$\hat{\sigma}_{ab}(p_a, p_b; \mu_F^2) = \sigma_{ab}(p_a, p_b) + \sigma_{ab}^{\text{C}}(p_a, p_b; \mu_F^2), \quad (1.97)$$

with the so-called collinear counterterm

$$\begin{aligned} \sigma_{ab}^C(p_a, p_b; \mu_F^2) = & -\frac{\alpha_s}{2\pi} \frac{1}{\Gamma(1-\epsilon)} \sum_{cd} \int_0^1 dz_c \int_0^1 dz_d \sigma_{cd}^0(z_c p_a, z_d p_b) \\ & \times \left\{ \delta_{bd} \delta(1-z_d) \left[-\frac{1}{\epsilon} \left(\frac{4\pi\mu^2}{\mu_F^2} \right)^\epsilon P^{ac}(z_c) + K_{\text{F.S.}}^{ac}(z_c) \right] \right. \\ & \left. + \delta_{ac} \delta(1-z_c) \left[-\frac{1}{\epsilon} \left(\frac{4\pi\mu^2}{\mu_F^2} \right)^\epsilon P^{bd}(z_d) + K_{\text{F.S.}}^{bd}(z_d) \right] \right\}. \end{aligned} \quad (1.98)$$

Note that the universality of PDFs as described in the context of the naive parton model above is modified in the QCD improved parton model due to the additional dependence on the factorization scale μ_F . However, in complete analogy to the derivation of the renormalization group equations sketched in Sect. 1.1.2, any dependence on μ_F must drop out in physical quantities if all orders in perturbation theory are taken into account. This condition is equivalent to the statement that the bare PDFs (1.94) are independent of μ_F and leads to the Dokshitzer–Gribov–Lipatov–Altarelli–Parisi [138–140] (DGLAP) evolution equations for the PDFs,

$$\frac{\partial}{\partial(\ln \mu_F^2)} f_{a|H}(x, \mu_F^2) = \frac{\alpha_s}{2\pi} \sum_b \int_x^1 \frac{dz}{z} f_{b|H}(z, \mu_F^2) P^{ba} \left(\frac{x}{z} \right). \quad (1.99)$$

These integro-differential equations describe the dependence of the PDFs on the factorization scale, where the evolution kernels are given by the splitting functions introduced in Eq. (1.94). In practice, the perturbation series is truncated at a certain order and translates into a μ_F dependence of the theoretical prediction, which represents an essential part of theoretical uncertainties in precision predictions. To conclude, not only is the universality of the PDFs undisturbed by the additional dependence on the factorization scale μ_F , but from the scale dependence that is calculable perturbatively, further predictions arise that can be tested experimentally. Turning this argument around, if no experimental data is available for a direct extraction of the PDFs at a given scale, the evolution equations can be used to extrapolate known PDFs measured at different scales to the desired one in order to make theoretical predictions.

The QED-corrected PDFs

Turning now to the inclusion of NLO EW $\mathcal{O}(\alpha)$ corrections to hadronic cross sections, the residual initial-state collinear singularities in the partonic cross sections σ_{ab} can be absorbed into the renormalized PDFs following the same procedure as in the QCD case described above. In addition to the quarks and gluons which we identified with the partons so far, now also the photon appears as a constituent of the hadron and, thus, a photon PDF $f_{\gamma|H}$ is introduced. The redefinition of the PDFs that take into account collinear splittings induced by photonic corrections is given by [141]¹³

$$\begin{aligned} f_{q|A}^{(0)}(x) \rightarrow & f_{q|A}^{\text{F.S.}}(x, \mu_F^2) \\ & - \frac{\alpha}{2\pi} \frac{1}{\Gamma(1-\epsilon)} \int_x^1 \frac{dz}{z} f_{q|A}^{\text{F.S.}} \left(\frac{x}{z}, \mu_F^2 \right) \left[-\frac{1}{\epsilon} \left(\frac{4\pi\mu^2}{\mu_F^2} \right)^\epsilon P_{\text{QED}}^{qq}(z) + C_{\text{F.S.}}^{qq}(z) \right] \end{aligned}$$

¹³ The expression given in Ref. [141] uses infinitesimal quark masses as regulators for the collinear singularities and the expression given here was obtained by a proper conversion to dimensional regularization.

$$-\frac{\alpha}{2\pi} \frac{1}{\Gamma(1-\epsilon)} \int_x^1 \frac{dz}{z} f_{\gamma|A}^{\text{F.S.}}\left(\frac{x}{z}, \mu_F^2\right) \left[-\frac{1}{\epsilon} \left(\frac{4\pi\mu^2}{\mu_F^2} \right)^\epsilon P_{\text{QED}}^{\gamma q}(z) + C_{\text{F.S.}}^{\gamma q}(z) \right], \quad (1.100)$$

with an analogous expression for the anti-quark PDFs $f_{\bar{q}|A}^{(0)}(x)$. The four-dimensional regularized QED splitting kernels are given by (cf. Eq. (1.92))

$$P_{\text{QED}}^{ff}(z) = Q_f^2 \left(\frac{1+z^2}{1-z} \right)_+, \quad P_{\text{QED}}^{\gamma f}(z) = 3 Q_f^2 \left[z^2 + (1-z)^2 \right], \quad (1.101)$$

and the coefficient functions $C_{\text{F.S.}}$ define the factorization scheme in the same way as the functions $K_{\text{F.S.}}$ for the case of QCD corrections,

$$\begin{aligned} C_{\overline{\text{MS}}}^{ff}(z) &= C_{\overline{\text{MS}}}^{\gamma f}(z) = 0, \\ C_{\text{DIS}}^{ff}(z) &= Q_q^2 \left[P_{\text{QED}}^{ff}(z) \left(\ln \left(\frac{1-z}{z} \right) - \frac{3}{4} \right) + \frac{9+5z}{4} \right]_+, \\ C_{\text{DIS}}^{\gamma f}(z) &= 3 Q_q^2 \left[P_{\text{QED}}^{\gamma f}(z) \ln \left(\frac{1-z}{z} \right) - 8z^2 + 8z - 1 \right]. \end{aligned} \quad (1.102)$$

The collinear counterterm for the QED corrections is then given by

$$\begin{aligned} \sigma_{ab}^{\text{C}}(p_a, p_b; \mu_F^2) &= -\frac{\alpha}{2\pi} \frac{1}{\Gamma(1-\epsilon)} \sum_{cd} \int_0^1 dz_c \int_0^1 dz_d \sigma_{cd}^0(z_c p_a, z_d p_b) \\ &\quad \times \left\{ \delta_{bd} \delta(1-z_d) \left[-\frac{1}{\epsilon} \left(\frac{4\pi\mu^2}{\mu_F^2} \right)^\epsilon P_{\text{QED}}^{ac}(z_c) + C_{\text{F.S.}}^{ac}(z_c) \right] \right. \\ &\quad \left. + \delta_{ac} \delta(1-z_c) \left[-\frac{1}{\epsilon} \left(\frac{4\pi\mu^2}{\mu_F^2} \right)^\epsilon P_{\text{QED}}^{bd}(z_d) + C_{\text{F.S.}}^{bd}(z_d) \right] \right\}, \end{aligned} \quad (1.103)$$

in direct correspondence to the QCD case. As it was argued in Refs. [141, 142], the omission of EW corrections in the PDF fit to data more closely follows a DIS-like factorization scheme. We therefore employ a mixed prescription using the $\overline{\text{MS}}$ scheme for QCD and the DIS scheme for the EW NLO calculations which is in line with the recommendation given in Sect. 2.4 of Ref. [124].

Throughout this work, we consistently use the parton distribution functions provided by the NNPDF collaboration in the NNPDF2.3 sets [143] which also contain PDFs that incorporate the QED corrections discussed above [142]. In Fig. 1.7 the x dependence of the momentum distributions $x f_{a|p}(x, \mu_F^2)$ is shown for the NNPDF2.3QED NLO set and for the factorization scale $\mu_F = M_Z$.

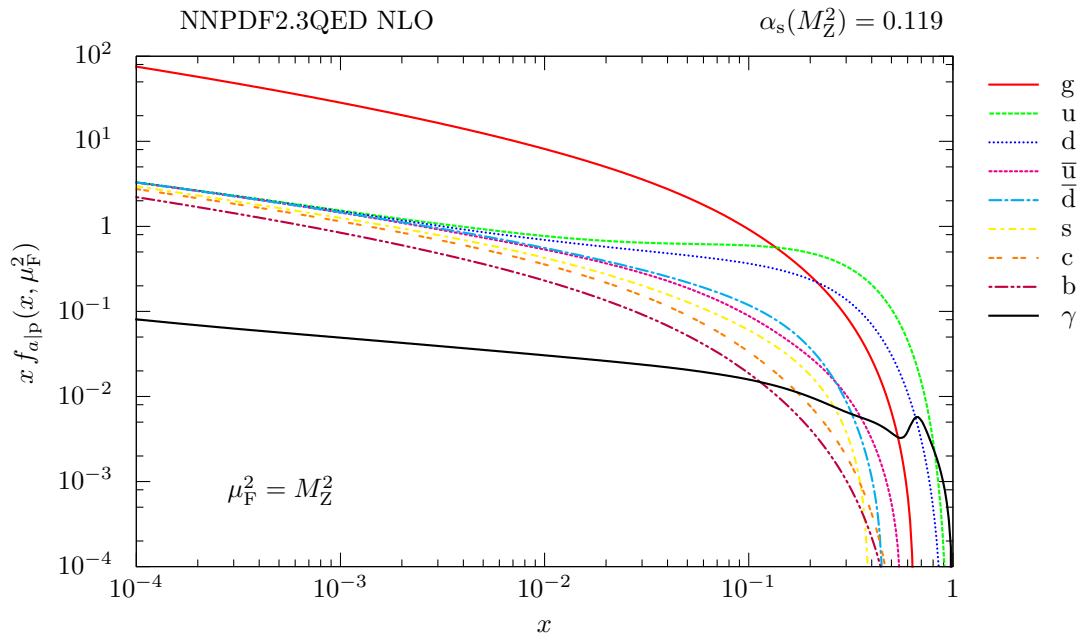


Figure 1.7.: The momentum distribution of the partons inside the proton as described by the NNPDF2.3QED NLO PDF set.

Part I.

The Drell–Yan process at NLO and the pole expansion

The Drell–Yan process at the LHC

In this work, we calculate radiative corrections to the Drell–Yan-like processes at the LHC where two protons are brought to collision to produce a pair of leptons, $pp \rightarrow \ell_1 \bar{\ell}_2$. The purpose of this chapter is to set up our conventions that are used in the remainder of this work and to outline the strategy for the calculation of the NLO corrections. In Sect. 2.1 we review the approximations that have been used in the calculation and justify their validity and discuss their implications. Furthermore, we will lay out the details of our calculational setup and use the Drell–Yan processes at lowest order to discuss the calculation of the helicity amplitudes using the Weyl–van-der-Warden (WvdW) spinor formalism in some detail. The notation and conventions introduced here will be employed for all helicity amplitudes presented in this work and are intended to serve as a reference for the reader. Section 2.2 reviews the general structure of the calculation of NLO corrections with the emphasis on the analytical cancellation of IR singularities. We will briefly motivate the two methods that are commonly employed in NLO calculations, which both find an application in our calculation: the phase-space slicing method and the subtraction method.

2.1. Conventions and leading-order results

The Drell–Yan-like production of lepton pairs at the LHC is given by the following hadronic scattering reaction,

$$p(P_A) + p(P_B) \rightarrow \ell_1(k_1) + \bar{\ell}_2(k_2) + X, \quad (2.1)$$

where the assignment of the momenta of the respective particles is given in parentheses and any additional hadronic activity arising from the proton remnants is denoted generically by X . As discussed in Sect. 1.4, the hadronic cross section is given by the incoherent sum over the different partonic scattering reactions that contribute to the final state under consideration,

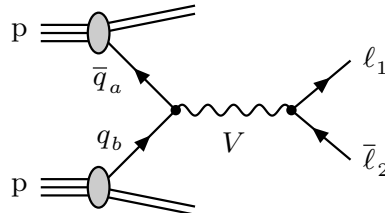


Figure 2.1.: The Drell–Yan process at the LHC at lowest order. For each of the the charged-current processes only one diagram with $V = W^\pm$ exists, whereas in the neutral-current process two diagrams with $V = Z$ and $V = \gamma$ contribute.

each convoluted with the respective PDFs (see Eq. (1.93)),

$$\sigma_{\text{pp}}^{\text{LO}}(P_A, P_B) = \sum_{a,b} \int_0^1 dx_a \int_0^1 dx_b f_{a|p}^{(0)}(x_a, \mu_F^2) f_{b|p}^{(0)}(x_b, \mu_F^2) \hat{\sigma}_{ab}^0(p_a, p_b). \quad (2.2)$$

The cross section $\hat{\sigma}_{ab}^0$ is obtained from the squared LO matrix element $|\mathcal{M}_0|^2$ according to Eq. (A.49) and after performing the phase-space integration. The partons entering the hard scattering reaction carry the fractions $x_{a/b}$ of the parent hadrons' momenta $P_{A/B}$ where the mass of the proton (m_p) is neglected, i.e. $P_{A/B}^2 = 0$. We work in the five-flavour scheme with $N_f = 5$ massless quarks $q = u, d, c, s, b$, where the bottom quark is also considered as a possible incoming particle. Correspondingly, the running of the strong coupling constant α_s is induced by the five light quarks, as described by Eq. (1.63).

In Born approximation, the hadronic scattering reaction is given by the diagram shown in Fig. 2.1 and the partonic scattering reaction is given by the following generic process,

$$\bar{q}_a(p_a) + q_b(p_b) \rightarrow \ell_1(k_1) + \bar{\ell}_2(k_2), \quad (2.3)$$

with the four-momenta of the respective particles given in parentheses. Quarks are consistently taken as massless ($p_a^2 = p_b^2 = 0$), and the small lepton masses are only retained to regularize mass singularities in collinear final-state radiation, otherwise $k_1^2 = k_2^2 = 0$. The Mandelstam variables are defined by

$$\hat{s} = (p_a + p_b)^2, \quad s_{ij} = (k_i + k_j)^2, \quad t_{ij} = (p_i - k_j)^2. \quad (2.4)$$

We consider the charged-current process with $\ell_1 \bar{\ell}_2 = \nu_e e^+ / \nu_\mu \mu^+$ and intermediate vector boson $V = W^+$, its charge conjugate with $\ell_1 \bar{\ell}_2 = e^- \bar{\nu}_e / \mu^- \bar{\nu}_\mu$ and $V = W^-$, as well as the neutral-current process with $\ell_1 \bar{\ell}_2 = e^- e^+ / \mu^- \mu^+$ and $V = Z$,

$$\bar{d}_i + u_j \rightarrow W^+ \rightarrow \nu_\ell + \ell^+, \quad (2.5a)$$

$$\bar{u}_i + d_j \rightarrow W^- \rightarrow \ell^- + \bar{\nu}_\ell, \quad (2.5b)$$

$$\bar{q} + q \rightarrow Z/\gamma \rightarrow \ell^- + \ell^+, \quad (2.5c)$$

where u_i and d_i denote the light up-type and down-type quarks of the i -th generation, respectively (see Table 1.1). The photon-induced process $\gamma\gamma \rightarrow \ell^- \ell^+$ that appears for the neutral-current process as well, was not considered here since it only delivers a small contribution [45] and furthermore, is not enhanced in the resonance region which is the main focus of this work.

For the quark mixing matrix we ignore all flavour transitions that involve the third generation, which is justified due to the numerically small values of the entries V_{ub} , V_{cb} , V_{td} , V_{ts} in the CKM matrix ($V_{tb} \approx 1$). Furthermore, owing to the mass degeneracy of the light quarks ($m_q = 0$) and the unitarity of the CKM matrix, the effect of a non-diagonal CKM matrix vanishes in most contributions after taking the flavour sums. The only exception is the case of the quark–anti-quark annihilation channels of the charged-current processes, where the CKM matrix appears as a global factor $|V_{ij}|^2$ multiplying the respective PDFs of the incoming quarks. Note that this statement also holds at the level of NLO $\mathcal{O}(\alpha)$ EW corrections. We therefore absorb the global factor $|V_{ij}|^2$ into the parton luminosities and set the CKM matrix to the unit matrix in the remaining parts of the calculation. This leads to significant simplifications and a speed-up in the numerical evaluation, where the flavour sum is shifted into the convolution with the PDFs

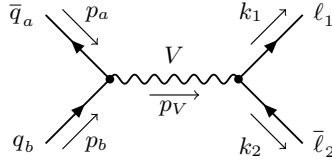


Figure 2.2.: The Feynman diagram for the process $\bar{q}_a q_b \rightarrow \ell_1 \bar{\ell}_2$. The momentum p_V of the intermediate vector boson V is given by $p_V = p_a + p_b = k_1 + k_2$.

and only one generic scattering amplitude needs to be computed.

The calculation presented in this work is based on a Feynman-diagrammatic approach in the 't Hooft–Feynman gauge. In order to ensure the correctness of the results, a second independent calculation has been performed also employing the Feynman-diagrammatic approach, and furthermore, the virtual corrections have been also calculated by a third independent calculation following an effective-field-theory approach as described in more detail in Ref. [87]. For the numerical evaluation, a fully flexible Monte Carlo program was developed which implements all results presented in this work and that allows for the calculation of total cross sections as well as arbitrary differential distributions. All helicity amplitudes were calculated using the Weyl–van-der-Waerden spinor formalism (see Appendix. A.2), resulting in very compact expressions and a fast numerical code. The evaluation of the one-loop integrals is performed using the *Collier* library [144], which is based on the results of Refs. [145, 146]. The numerical integration is performed using an independent implementation of the *Vegas* [147, 148] Monte Carlo algorithm and a specific phase-space parametrization. A second independent implementation uses the program *Rady* based on Refs. [37, 44, 45] which has been extended to include the $\mathcal{O}(\alpha_s \alpha)$ corrections presented in Part II. The numerical results obtained from the two programs are in mutual agreement.

The leading-order helicity amplitudes

In the following we present the results for the LO predictions to the Drell–Yan processes (2.5) where the corresponding Feynman diagram is shown in Fig. 2.2. For the calculation of the LO and all real-emission amplitudes we employ the Weyl–van-der-Waerden (WvdW) formalism which is summarized in Appendix A.2, and all relevant Feynman rules for this work are collected in Appendix A.3. Before proceeding with the calculation, we first give a general remark on the restrictions on the helicity configurations associated with the fermions: In the massless limit, the helicity is directly related to the chirality of the fermion and is therefore a conserved quantity, since all gauge couplings leave the chirality of the particle untouched.¹ As a consequence, the helicity of the external fermions is uniquely determined by the chiral couplings $C_{V\bar{f}f'}^{\tau_f}$ of the V boson to the fermions. The Feynman rule for the $V\bar{f}f'$ vertex can be found in Table A.4 and the explicit expressions of the non-vanishing flavour combinations and chiralities of the coupling

¹ This can be easily seen in the WvdW spinor formalism from the fact that a fermion line always involves an odd number of chirality matrices (arising from the $V\bar{f}f'$ -vertex and the fermion propagator), which only contain non-vanishing entries in the off-diagonal components in the case of massless fermions.

constants $C_{V\bar{f}f'}^{\tau_f}$ are given by

$$C_{\gamma\bar{f}f}^{\pm} = -Q_f, \quad (2.6a)$$

$$C_{Z\bar{f}f}^{\pm} = -g_f^{\pm}, \quad g_f^+ = -\frac{s_w}{c_w}Q_f, \quad g_f^- = \frac{I_{w,f}^3 - s_w^2 Q_f}{s_w c_w}, \quad (2.6b)$$

$$C_{W^+u_i d_j}^- = \frac{1}{\sqrt{2}s_w}V_{ij}, \quad C_{W^-d_i u_j}^- = \frac{1}{\sqrt{2}s_w}V_{ji}^*, \quad C_{W^+\bar{\nu}_\ell \ell}^- = C_{W^-\bar{\ell} \nu_\ell}^- = \frac{1}{\sqrt{2}s_w}. \quad (2.6c)$$

We therefore use the signs τ_q, τ_ℓ appearing in the chiral couplings of the quarks $C_{V\bar{q}_a q_b}^{\tau_q}$ and the leptons $C_{V\bar{\ell}_1 \ell_2}^{\tau_\ell}$, respectively, to determine the helicity configuration of the external fermions according to

$$C_{V\bar{f}_i f_j}^{\tau_f} \Leftrightarrow \begin{cases} \sigma_i = \begin{cases} -\frac{1}{2} \tau_f, & \text{for an incoming } \bar{f}_i, \\ +\frac{1}{2} \tau_f, & \text{for an outgoing } f_i, \end{cases} \\ \sigma_j = \begin{cases} +\frac{1}{2} \tau_f, & \text{for an incoming } f_j, \\ -\frac{1}{2} \tau_f, & \text{for an outgoing } \bar{f}_j. \end{cases} \end{cases} \quad (2.7)$$

This helicity assignment will be implicitly assumed in all formulae of the helicity amplitudes presented in this work.

For the calculation of the LO amplitudes we consider the generic V -boson exchange diagram of the process $\bar{q}_a q_b \rightarrow \ell_1 \bar{\ell}_2$ shown in Fig. 2.2 and denote the corresponding colour-stripped amplitude by $\mathcal{A}_{0,V}^{\bar{q}_a q_b \rightarrow \ell_1 \bar{\ell}_2}$, where the bottom label “ V ” indicates the gauge boson that is exchanged between the quark and lepton lines. The matrix elements for the three processes given in Eq. (2.5) can then be constructed from this generic amplitude as follows,

$$\mathcal{M}_0^{\bar{d}_i u_j \rightarrow \nu_\ell \ell^+} \left(\begin{bmatrix} p_a \\ \sigma_a \\ c_a \end{bmatrix}, \begin{bmatrix} p_b \\ \sigma_b \\ c_b \end{bmatrix}; \begin{bmatrix} k_1 \\ \sigma_1 \end{bmatrix}, \begin{bmatrix} k_2 \\ \sigma_2 \end{bmatrix} \right) = \delta_{c_a c_b} \mathcal{A}_{0,\tau_q \tau_\ell}^{\bar{d}_i u_j \rightarrow \nu_\ell \ell^+}(p_a, p_b; k_1, k_2), \quad (2.8a)$$

$$\mathcal{M}_0^{\bar{u}_i d_j \rightarrow \ell^- \bar{\nu}_\ell} \left(\begin{bmatrix} p_a \\ \sigma_a \\ c_a \end{bmatrix}, \begin{bmatrix} p_b \\ \sigma_b \\ c_b \end{bmatrix}; \begin{bmatrix} k_1 \\ \sigma_1 \end{bmatrix}, \begin{bmatrix} k_2 \\ \sigma_2 \end{bmatrix} \right) = \delta_{c_a c_b} \mathcal{A}_{0,\tau_q \tau_\ell}^{\bar{u}_i d_j \rightarrow \ell^- \bar{\nu}_\ell}(p_a, p_b; k_1, k_2), \quad (2.8b)$$

$$\begin{aligned} \mathcal{M}_0^{\bar{q} q \rightarrow \ell^- \ell^+} \left(\begin{bmatrix} p_a \\ \sigma_a \\ c_a \end{bmatrix}, \begin{bmatrix} p_b \\ \sigma_b \\ c_b \end{bmatrix}; \begin{bmatrix} k_1 \\ \sigma_1 \end{bmatrix}, \begin{bmatrix} k_2 \\ \sigma_2 \end{bmatrix} \right) \\ = \delta_{c_a c_b} \left(\mathcal{A}_{0,\tau_q \tau_\ell}^{\bar{q} q \rightarrow \ell^- \ell^+}(p_a, p_b; k_1, k_2) + \mathcal{A}_{0,\tau_q \tau_\ell}^{\bar{q} q \rightarrow \ell^- \ell^+}(p_a, p_b; k_1, k_2) \right), \end{aligned} \quad (2.8c)$$

where the neutral-current process receives contributions from two diagrams associated with the exchange of a Z boson and a photon. The order of the arguments in the amplitudes in Eq. (2.2) corresponds to the order of the particles in the process labels and the three components of the vectors appearing as arguments on the l.h.s. denote the momentum, helicity, and colour quantum number, respectively. The colour-stripped amplitude \mathcal{A} carries as index the chiral coupling structure given by τ_q and τ_ℓ . As mentioned above, it is implicitly assumed that the helicity configuration of the fermions σ_f is determined through the sign of τ_f as defined in Eq. (2.7) and that all remaining configurations give a vanishing contribution, i.e. only the configurations satisfying $\sigma_b = -\sigma_a = \tau_q/2$ and $\sigma_1 = -\sigma_2 = \tau_\ell/2$ with $\tau_q, \tau_\ell = \pm 1$ contribute.

The colour-stripped amplitude can be further written in the following form,

$$i\mathbb{A}_{V0,\tau_q\tau_\ell}^{\bar{q}_a q_b \rightarrow \ell_1 \bar{\ell}_2}(p_a, p_b; k_1, k_2) = \frac{2i e^2}{s_{12} - \mu_V^2} C_{V\bar{q}_a q_b}^{\tau_q} C_{V\bar{\ell}_1 \ell_2}^{\tau_\ell} \mathbb{A}_0^{\tau_q \tau_\ell}(p_a, p_b; k_1, k_2), \quad (2.9)$$

where the presence of a resonant particle requires the introduction of a finite decay width as discussed in Sect. 1.2 and $\mathbb{A}_0^{\tau_q \tau_\ell}$ are called the “standard matrix elements”. The helicity structure of all external particles is encoded in $\mathbb{A}_0^{\tau_q \tau_\ell}$ and they are explicitly given by

$$\begin{aligned} \mathbb{A}_0^{--}(p_a, p_b; k_1, k_2) &= \langle p_b k_2 \rangle^* \langle p_a k_1 \rangle, \\ \mathbb{A}_0^{-+}(p_a, p_b; k_1, k_2) &= \langle p_b k_1 \rangle^* \langle p_a k_2 \rangle, \\ \mathbb{A}_0^{++}(p_a, p_b; k_1, k_2) &= \mathcal{P} \left\{ \mathbb{A}_0^{--}(p_a, p_b; k_1, k_2) \right\}, \\ \mathbb{A}_0^{+-}(p_a, p_b; k_1, k_2) &= \mathcal{P} \left\{ \mathbb{A}_0^{-+}(p_a, p_b; k_1, k_2) \right\}, \end{aligned} \quad (2.10)$$

where the last two helicity configurations are obtained from the former two by the application of the modified parity transformation \mathcal{P} defined in Eq. (A.46).² Owing to the simple $2 \rightarrow 2$ kinematics of the LO process, the Dirac structures can be further written as follows,

$$\mathbb{A}^{\pm\pm} = 2t_{a1}, \quad \mathbb{A}^{\pm\mp} = 2t_{a2}, \quad (2.11)$$

up to irrelevant complex phases.

2.2. Survey of NLO corrections

In this section we give an overview on the technical aspects that are involved in the calculation of NLO cross-section predictions. The hadronic cross section for proton–proton collisions at NLO is given by the following convolution formula, cf. Eq. (1.96),

$$\begin{aligned} \sigma_{\text{pp}}^{\text{NLO}}(P_A, P_B) &= \sum_{a,b} \int_0^1 dx_a \int_0^1 dx_b f_{a|p}^{\text{NLO}}(x_a, \mu_F^2) f_{b|p}^{\text{NLO}}(x_b, \mu_F^2) \\ &\times \left[\hat{\sigma}_{ab}^0(p_a, p_b) + \hat{\sigma}_{ab}^{\text{NLO}}(p_a, p_b; \mu_F^2) \right], \end{aligned} \quad (2.12)$$

where the momenta of the partons entering the hard-scattering reaction are given by $p_a = x_a P_A$ and $p_b = x_b P_B$, respectively. The partonic LO cross sections $\hat{\sigma}_{ab}^0$ are obtained from the Born amplitude \mathcal{M}_0 via Eq. (A.49) and were explicitly given in Eq. (2.8) for the different Drell–Yan processes (2.5). At NLO, several ingredients enter into the calculation of the hard-scattering cross section $\hat{\sigma}_{ab}^{\text{NLO}}$: Firstly, the one-loop virtual corrections denoted by $d\sigma^V$, where we assume that the counterterm contributions are included, so that all UV divergences are properly cancelled within $d\sigma^V$ after renormalization. Secondly, the real-emission corrections $d\sigma^R$, which are obtained by considering all processes with an additional particle in the final state that contribute to the observable under consideration. In particular, these corrections include all contributions that lead to degenerate states with respect to the non-radiating process in the unresolved soft and/or collinear configurations. They are integrated over the phase space with an additional final-state

² The complex gauge-boson mass μ_V must be left untouched in the complex conjugation that is involved in the parity transformation \mathcal{P} .

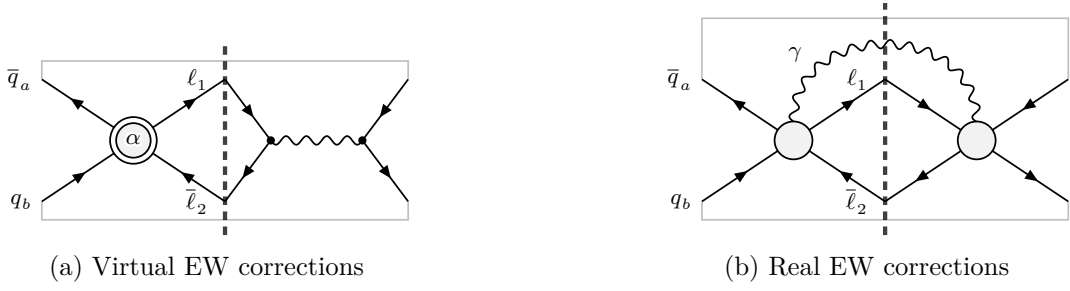


Figure 2.3.: Generic interference diagrams for the various contributions to the NLO corrections of $\mathcal{O}(\alpha_s)$, with blobs representing all relevant tree structures. The blob with “ α ” inside represents one-loop corrections of $\mathcal{O}(\alpha)$.

particle and moreover, new initial-state configurations (ab), or “channels”, may become available at this order which did not contribute at LO. Lastly, one further requires the inclusion of the collinear counterterm $d\sigma^C$, which implements the PDF redefinition from the LO to the NLO PDFs, $f_{a|A}^{(0)}(x) \rightarrow f_{a|A}^{\text{NLO}}(x, \mu_F^2)$, as described in Sect. 1.4 and further introduces the dependence on the factorization scale μ_F into $\hat{\sigma}_{ab}^{\text{NLO}}$.

As was discussed in Sect. 1.3, in general, the calculation of higher-order corrections involving massless particles leads to the occurrence of IR singularities. They cancel between the real-emission bremsstrahlung corrections $d\sigma^R$ and the one-loop virtual corrections $d\sigma^V$ for sufficiently inclusive observables by virtue of the KLN theorem. In the case of hadron–hadron collisions, however, the requirement of inclusiveness is only fulfilled for the soft singularities and the collinear singularities associated with the final state. In case of initial-state collinear singularities the degenerate states are not treated inclusively and consequently, the KLN theorem is not applicable. As explained in Sect. 1.4, the initial-state collinear singularities are process independent and can be absorbed into a redefinition of the PDFs, which is technically accomplished by the introduction of the collinear counterterm $d\sigma^C$. In summary, the hard-scattering cross section at NLO can be schematically written as

$$\hat{\sigma}_{ab}^{\text{NLO}} = \int_{n+1} d\sigma_{ab}^R + \int_n d\sigma_{ab}^V + \int_n d\sigma_{ab}^C, \quad (2.13)$$

where the symbol \int_m denotes the integration over the m -particle phase space and the additional convolution/summation in $d\sigma^C$ (see. Eqs. (1.98) and (1.103)) is suppressed in the notation. Each term on the r.h.s. of Eq. (2.13) is separately divergent, however, all singularities cancel in the sum as described above. Although this solves the problem of IR singularities on a formal ground, in practice, the cancellation is far from trivial, since the individual contributions are each defined on a different phase space. Moreover, the divergences in the real corrections are implicitly hidden in the phase-space integration, whereas the singularities associated with the virtual corrections and the collinear counterterm are made explicit using regulators. The cancellation of the IR singularities therefore requires the analytic control (using regulators) of the divergences in the phase-space integration of the real corrections. On the other hand, a flexible numerical approach is desirable for the phase-space integration in form of a fully differential cross-section prediction which is not restricted to a certain setup or observable. To allow for a stable numerical integration, a careful treatment of IR singularities is required. Essentially two approaches exist to accomplish the analytic cancellation of all IR singularities without

sacrificing the flexibility of a numerical phase-space integration: the subtraction formalism, and the phase-space slicing method. Both methods are used in our calculations and will be briefly motivated in the following.

The *phase-space slicing* method isolates the singular parts of the phase space by the introduction of a set of slicing parameters. The integration over the singular regions of phase space associated with the unresolved particle can be carried out analytically using regulators by exploiting the factorization properties of the real-radiation cross section $d\sigma^R$ and the phase-space measure $d\Phi_{n+1}$ in the soft and/or collinear approximations. In this way, the singularities in the real correction are made explicit and can be cancelled analytically against the respective divergences in $d\sigma^V$ and $d\sigma^C$. The remaining phase-space integration can be safely performed numerically without regulators. A trade-off in the slicing method is the introduction of the “arbitrary” cut parameters for the isolation of the singular regions: These parameters should not be chosen too large in order not to jeopardize the validity of the approximations that are used in the analytical integration, but on the other hand, should not be chosen too small in order to guarantee a stable numerical evaluation. In practice, the slicing parameters need to be varied over a range in order to identify a plateau where both requirements are met. Further details of the slicing method that is used in this work can be found in Appendix C.

The *subtraction* method accomplishes the cancellation of IR singularities by a clever rearrangement of the divergences by subtracting and adding back a suitably chosen auxiliary term $d\sigma^A$ as follows,

$$\hat{\sigma}_{ab}^{\text{NLO}} = \int_{n+1} \left[d\sigma_{ab}^R - d\sigma_{ab}^A \right] + \int_n \left[d\sigma_{ab}^V + d\sigma_{ab}^C + \int_1 d\sigma_{ab}^A \right]. \quad (2.14)$$

The subtraction term mimics the real corrections in all its singular regions and therefore acts as a local counterterm so that the integration of the first term in the r.h.s. of Eq. (2.14) can be performed numerically without regulators. Furthermore, the subtraction term is constructed in a manner that allows for the analytical integration over the singular one-particle subspace, effectively making the singularities contained in $d\sigma^R$ explicit. As a result, all singularities in the second term of Eq. (2.14) can be cancelled analytically and the integration can be again performed numerically without regulators. The so-called dipole subtraction formalism provides a general algorithm for the construction of $d\sigma^A$, which will be discussed in the next chapter.

The dipole subtraction formalism

The purpose of this chapter is to give a more detailed review of the dipole subtraction formalism which was briefly motivated in Sect. 2.2 and to present the extension of this framework to decay kinematics which has been developed in the context of this work. We restrict the presentation of the dipole subtraction formalism to the case of QED corrections and will use dimensional regularization for the treatment of IR singularities. For a detailed discussion of the formalism for the case of QCD corrections we refer to Refs. [129, 149].

The dipole subtraction formalism has been continuously extended since its original formulation in Ref. [129], which was restricted to the computation of NLO QCD radiative corrections involving only massless partons, to cover all possible cases that are relevant in scattering processes: In Ref. [133] the dipole formalism was developed for the calculation of NLO QED corrections where the emission of photons from both massless and massive fermions was considered. The extension of the algorithm for NLO QCD calculations to the case with massive partons has been worked out in Refs. [149, 150]. The treatment of non-collinear-safe observables in QED corrections was presented in Ref. [134] where the formalism was further extended to cover the various fermion–photon splittings that were not considered in Ref. [133].

For the case of decay processes, subtraction terms were constructed in Ref. [151] for NLO QCD corrections to the radiative decay of the top quark with massless partons in the final state. These subtraction terms have been derived based on the results of Ref. [152] and were constructed in such a way that they integrate into the dipole subtraction formalism. Although the discussion in Ref. [151] was restricted to the case of the top quark, this does not pose a serious limitation since the top quark is the only strongly interacting particle in the SM that decays before hadronization. Furthermore, since the soft singularities associated with the decaying particle are independent of its spin (see Eq. (1.89)), the subtraction terms given there should in principle be also applicable to the decay of any strongly interacting particle, with the restriction that only massless partons appear in the final state.

So far, no general algorithm exists for the calculation of NLO QED corrections to decay processes using the dipole subtraction formalism. Within this work we have filled this gap by explicitly constructing such a process-independent subtraction term considering both massless and massive final-state fermions, and further, worked out its extension to the treatment of non-collinear-safe observables.

In Sect. 3.1 we set up our conventions and notation and discuss the general features of the dipole subtraction formalism and its extension to non-collinear-safe observables. Section 3.2 presents the formalism for photon radiation off massless fermions following the conventions of Ref. [133], however, employing dimensional regularization for the treatment of IR singularities. In Sect. 3.3 we give the relevant dipole formulae that are required for the calculation of radiative corrections involving a massive final-state particle. Finally, Sect. 3.4 covers the dipoles that have been developed in the context of this work for the treatment of decay processes.

3.1. Conventions and general remarks

Before proceeding with the discussion of the general features of the dipole subtraction formalism we first establish our notation and conventions that are employed throughout this chapter and in the rest of this work, which essentially follow Ref. [133]. The indices I, J will be used to denote any charged external particle, while the indices a, b will be only used for incoming and i, j only for outgoing particles. The relative charge and the mass of particle I are denoted by Q_I and m_I , and the sign factor $\eta_I = \pm 1$ is defined in the same manner as in Sect. 1.3.2. If not stated otherwise, all phase-space volumes are considered in d dimensions as defined in Eq. (1.44). We introduce the shorthand notation

$$d\Phi_n \equiv d\phi(k_1, \dots, k_n; p_a + p_b), \quad (3.1)$$

and denote the collection of all momenta of the corresponding process simply by Φ_n .

The main idea of the subtraction formalism can be summarised in the following formula,

$$\int d\Phi_{n+\gamma} \sum_{\lambda_\gamma} |\mathcal{M}_R^\gamma|^2 = \int d\Phi_{n+\gamma} \left(\sum_{\lambda_\gamma} |\mathcal{M}_R^\gamma|^2 - |\mathcal{M}_{\text{sub}}|^2 \right) + \int d\tilde{\Phi}_n \otimes \left(\int [dk] |\mathcal{M}_{\text{sub}}|^2 \right), \quad (3.2)$$

where \mathcal{M}_R^γ denotes the transition amplitude of the bremsstrahlung process, $[dk]$ the photon phase space which is obtained by factoring out the n -particle sub-space associated with the non-radiating process, as will be discussed in more detail later. The auxiliary term \mathcal{M}_{sub} is specifically tailored to act as a local counterterm to the real-emission corrections. More precisely, we require the subtraction term $|\mathcal{M}_{\text{sub}}|^2$ to point-wise mimic the real-emission contributions in all its singular limits, i.e. to fulfil the following properties,

$$|\mathcal{M}_{\text{sub}}|^2 \sim \sum_{\lambda_\gamma} |\mathcal{M}_R^\gamma|^2, \quad \text{for } k \rightarrow 0 \quad \text{or } p_i \cdot k \rightarrow 0 \quad \text{or } p_a \cdot k \rightarrow 0. \quad (3.3)$$

The explicit expressions for the respective limits can be found in Eqs. (1.89) and (1.91). The property (3.3) ensures that the first term on the r.h.s. of Eq. (3.2) is free of IR singularities. As a result, the integration over the full real-emission phase space $d\Phi_{n+\gamma}$ can be performed without regulators (in our case the dimensionality of space-time d) which makes it suitable for the evaluation using numerical methods. The singularities originally contained in the real-emission corrections are now fully encapsulated in the second term of Eq. (3.2) which is constructed in such a way to allow for a direct analytical integration of the singular contributions. To this end, the real-emission phase space is factorized into the singular sub-space given by the photonic part $[dk]$ and the remaining phase space integration $d\tilde{\Phi}_n$ associated with the non-radiative process. Here, the symbol “ \otimes ” indicates that this phase-space factorization may contain additional convolutions and summations. Performing the analytical integration over $[dk]$ results in an expression where the singularities are explicitly regularized according to the regularization scheme that is employed. These divergences cancel against the respective singularities appearing in the virtual corrections and the collinear counterterms by virtue of the KLN theorem and factorization. The remaining integration $d\tilde{\Phi}_n$ is free of singularities and can be evaluated numerically.

As shown in Sect. 1.3.2, the real-emission corrections $\sum_{\lambda_\gamma} |\mathcal{M}_R^\gamma|^2$ exhibit a factorization property in the singular limits where the singular behaviour can be described in a process-

independent manner and can be split off from the squared amplitude of the corresponding non-radiating process. The dipole subtraction formalism is constructed in such a way to exploit these factorization properties by partitioning the subtraction term $|\mathcal{M}_{\text{sub}}|^2$ into so-called *dipoles* $|\mathcal{M}_{\text{sub},IJ}|^2$ according to

$$\begin{aligned} |\mathcal{M}_{\text{sub}}(\Phi_{n+\gamma})|^2 &= \sum_{\substack{I,J \\ I \neq J}} |\mathcal{M}_{\text{sub},IJ}(\Phi_{n+\gamma})|^2 \\ &= -4\pi\mu^{2\epsilon}\alpha \sum_{\substack{I,J \\ I \neq J}} \eta_I Q_I \eta_J Q_J g_{IJ}^{(\text{sub})}(p_I, p_J, k) \left| \mathcal{M}_0(\tilde{\Phi}_{n,IJ}) \right|^2, \end{aligned} \quad (3.4)$$

where I and J are called the *emitter* and *spectator* particles, respectively. Each dipole contribution incorporates the collinear singular structure associated with the emitter I . The soft singularities, where all collinear regions overlap, are disentangled according to the second line of Eq. (1.89) and distributed to the individual dipole contributions. Taking advantage of the factorization property of the IR singularities, the dipole terms can be further written as a product of the auxiliary functions $g_{IJ}^{(\text{sub})}$ and the squared matrix element of the non-radiating process $|\mathcal{M}_0|^2$. The former are universal functions that encapsulate the singularity structure and are thus independent of the process under consideration. They can therefore be integrated analytically over the singular photon phase space once and for all. The associated squared matrix element $|\mathcal{M}_0|^2$ is evaluated on the n -particle phase space $\tilde{\Phi}_{n,IJ}$ that remains after the isolation of the singular one-particle sub-space $[dk]$ associated with the photon. These *dipole mappings* are required to reproduce the appropriate kinematic configuration in the singular regions but are otherwise arbitrary and can be chosen differently for each dipole as indicated by the additional label “ $_{IJ}$ ”. This freedom can be exploited to simplify the later analytical integration over $[dk]$. Nonetheless, a property common to all dipole mappings is that they respect exact momentum conservation as well as all mass-shell conditions. To summarise, we demand the following asymptotic behaviour for the subtraction functions $g_{IJ}^{(\text{sub})}$,

$$g_{IJ}^{(\text{sub})}(p_I, p_J, k) \underset{k \rightarrow 0}{\sim} \frac{1}{p_I \cdot k} \left[\frac{2(p_I \cdot p_J)}{p_I \cdot k + p_J \cdot k} - \frac{m_I^2}{p_I \cdot k} \right], \quad (3.5a)$$

$$g_{iJ}^{(\text{sub})}(p_i, p_J, k) \underset{p_i \cdot k \rightarrow 0}{\sim} \frac{1}{p_i \cdot k} \frac{1}{Q_i^2} \hat{P}_{\text{QED}}^{ff}(z_i), \quad z_i = \frac{p_i^0}{p_i^0 + k^0}, \quad (3.5b)$$

$$g_{aJ}^{(\text{sub})}(p_a, p_J, k) \underset{p_a \cdot k \rightarrow 0}{\sim} \frac{1}{x_a(p_a \cdot k)} \frac{1}{Q_a^2} \hat{P}_{\text{QED}}^{ff}(x_a), \quad x_a = \frac{p_a^0 - k^0}{p_a^0}, \quad (3.5c)$$

and the dipole mappings,

$$k \rightarrow 0 : \quad \tilde{p}_I^{(IJ)} \rightarrow p_I, \quad (3.6a)$$

$$p_i \cdot k \rightarrow 0 : \quad \tilde{p}_I^{(iJ)} \rightarrow p_i + k, \quad (3.6b)$$

$$p_a \cdot k \rightarrow 0 : \quad \tilde{p}_I^{(aJ)} \rightarrow p_a - k, \quad (3.6c)$$

where $\tilde{p}_I^{(IJ)}$ denotes the momentum of the emitter in $\tilde{\Phi}_{n,IJ}$ and the momenta of all remaining particles $\{\tilde{k}_n\}$, including the spectator, must approach the corresponding momenta of the real-emission kinematics $\{k_n\}$. Using the properties given in Eqs. (3.5) and (3.6), one can verify

that the subtraction term as constructed in Eq. (3.4) satisfies the requirements of Eq. (3.3).

One aspect that was not addressed so far concerns the definition of the observables, which was not made explicit in the formulae given Eqs. (3.2) and (3.4) in order to focus on the general features. The ability to carry out the analytical integration over the photonic part of the phase space $[dk]$ critically relies on the fact that the observable definition does not depend on the photon momentum k in the subtraction terms. More explicitly, this implies that all observables must be computed from the kinematics given by the respective dipole phase space $\tilde{\Phi}_{n,IJ}$. The first term in Eq. (3.2) is therefore given in the dipole subtraction formalism by the following expression

$$\int d\Phi_{n+\gamma} \left\{ \sum_{\lambda_\gamma} |\mathcal{M}_R^\gamma(\Phi_{n+\gamma})|^2 \Theta_{\text{cut}}(\Phi_{n+\gamma}) - \sum_{\substack{I,J \\ I \neq J}} |\mathcal{M}_{\text{sub},IJ}(\Phi_{n+\gamma})|^2 \Theta_{\text{cut}}(\tilde{\Phi}_{n,IJ}) \right\}, \quad (3.7)$$

where we have made explicit the dependence on the observable by a generic function Θ_{cut} which is equal to one if the considered kinematic configuration passes all selection criteria and zero otherwise.¹ In order not to jeopardize the cancellation of the subtraction formalism as described above, only so-called *IR-safe* observables may be considered which satisfy the properties

$$k \rightarrow 0 : \quad \Theta_{\text{cut}}(p_1, \dots, p_n, k) \rightarrow \Theta_{\text{cut}}(p_1, \dots, p_n), \quad (3.8a)$$

$$p_i \cdot k \rightarrow 0 : \quad \Theta_{\text{cut}}(p_1, \dots, p_i, \dots, p_n, k) \rightarrow \Theta_{\text{cut}}(p_1, \dots, p_i + k, \dots, p_n), \quad (3.8b)$$

$$p_a \cdot k \rightarrow 0 : \quad \Theta_{\text{cut}}(p_1, \dots, p_n, k; p_a) \rightarrow \Theta_{\text{cut}}(p_1, \dots, p_n; p_a - k), \quad (3.8c)$$

in the kinematic degenerate configurations given by the respective limits of Eq. (3.6). In particular, this requires some recombination procedure that assigns a collinearly emitted photon back to the charged fermion. The algorithm employed in our calculation is described in Sect. 4.5.2 together with a summary of our calculational setup. Such a recombination procedure also conforms to the experimental situation for electrons in the final state, where both electrons and photons are detected in the electromagnetic calorimeter and therefore a collinear electron-photon system cannot be distinguished. In case of muons, however, a separation is made possible since the muons are detected separately from the photons in the muon chambers located further outside in the detector. Describing such an experimental setup requires the extension of the dipole subtraction formalism to the case of non-collinear-safe observables which will be reviewed in the following.

Extension to non-collinear safe observables

Before proceeding with the discussion of non-collinear-safe observables, it is first important to note that for a truly massive fermion there exists no collinear singularity associated with it, since its physical mass m_f acts as a natural cut-off in this case. However, if the typical scales in the process are much larger than m_f , retaining the full mass dependence will introduce large scale ratios which may lead to numerical instabilities in the phase-space integration and, moreover, unnecessarily complicates the calculation of the matrix elements and slows down their evaluation. In such cases it is preferable to consider the massless limit $m_f \rightarrow 0$ of the radiating particle. As described in Sect. 1.3.2, such a limit leads to the occurrence of collinear singularities which in

¹ We keep this cut function very generic, for instance, it can also represent the bin boundaries in a histogram of a kinematic distribution.

this case should be regarded as an artefact of the calculation. However, such singularities cancel by virtue of the KLN theorem if only IR-safe observables (3.8) are considered.

The extension to non-collinear-safe observables relaxes the requirement of IR safety and allows for a non-inclusive treatment of collinear configurations in the final state. More precisely, if a photon is collinearly radiated off a final-state fermion, $f \rightarrow f\gamma$, such a energetically degenerate configuration will *not* be treated as one quasi-particle (as it is done for instance by a photon recombination algorithm), but it is assumed that the momentum of the fermion after the splitting is directly accessible. As a consequence, the requirements of the KLN theorem are not satisfied and the corrections will contain uncanceled collinear singularities which manifest themselves by contributions that are enhanced by logarithms of the small fermion mass, $\alpha \ln(m_f)$. Due to the aforementioned complications that arise from keeping the light fermion mass m_f non-zero in all parts of the calculation, it is desirable to isolate the logarithmically enhanced contributions analytically, so that m_f can be set to zero in the remaining parts of the calculation. Such a prescription was developed in Ref. [134] and we briefly outline the formalism presented there and the modifications that it induces within the dipole subtraction formalism in the following.

Since a non-collinear-safe observable is sensitive to the details of the collinear splitting, the subtraction formalism described by Eq. (3.7) is no longer IR finite. The problem arises from the fact that in the collinear limit of Eq. (3.6b) it is no longer guaranteed that $\Theta_{\text{cut}}(\tilde{\Phi}_{n,iJ})$ approaches $\Theta_{\text{cut}}(\Phi_{n+\gamma})$ so that the point-wise cancellation of the singularities is jeopardized. The local cancellation of IR singularities in Eq. (3.7) can be restored by exploiting the information on the collinear splitting, more explicitly, on the variable z_i defined in Eq. (3.5b) which describes the energy distribution between the fermion and the photon. As we will see explicitly in the formulae for the individual dipoles given later, the dipole mapping involving a final-state particle i and an arbitrary spectator J defines the variable z_{iJ} which behaves as $z_{iJ} \rightarrow z_i$ in the respective collinear regions of phase space. Thus, treating the corresponding n -particle event $\tilde{\Phi}_{n,iJ}$ as an $(n+1)$ -particle event with a collinear fermion–photon pair carrying the respective momenta $p_i = z_{iJ} \tilde{p}_i$ and $k = (1 - z_{iJ}) \tilde{p}_i$, ensures that the two integrands approach each other in the collinear limits, so that a local cancellation is guaranteed. Denoting all final-state particles for which a non-collinear-safe observable definition is employed by the index \hat{i} , we therefore must modify all dipole terms where \hat{i} appears as an emitter particle according to,

$$\int d\Phi_{n+\gamma} \left\{ \sum_{\lambda_\gamma} |\mathcal{M}_R^\gamma(\Phi_{n+\gamma})|^2 \Theta_{\text{cut}}(\Phi_{n+\gamma}) - \sum_{\substack{I,J \\ I \neq \hat{i}, J \neq I}} |\mathcal{M}_{\text{sub},IJ}(\Phi_{n+\gamma})|^2 \Theta_{\text{cut}}(\tilde{\Phi}_{n,IJ}) \right. \\ \left. - \sum_{\substack{\hat{i},J \\ J \neq \hat{i}}} |\mathcal{M}_{\text{sub},\hat{i}J}(\Phi_{n+\gamma})|^2 \Theta_{\text{cut}}(\tilde{\Phi}_{n,\hat{i}J} \mid p_{\hat{i}} = z_{\hat{i}J} \tilde{p}_{\hat{i}}, k = (1 - z_{\hat{i}J}) \tilde{p}_{\hat{i}}) \right\}. \quad (3.9)$$

Since Θ_{cut} now depends on the photon momentum through the variable z_{iJ} , the full analytical integration over the photonic part of the phase space $[dk]$ as described in the collinear-safe case above is no longer possible. To this end, we consider one dipole contribution appearing in the second line of Eq. (3.9) and isolate the soft singularity at $z_{iJ} = 1$ using the plus

prescription (A.16),

$$\begin{aligned}
& \int d\Phi_{n+\gamma} \left| \mathcal{M}_{\text{sub},\hat{i}J}(\Phi_{n+\gamma}) \right|^2 \Theta_{\text{cut}} \left(\tilde{\Phi}_{n,\hat{i}J} \mid p_i = z_{iJ} \tilde{p}_i, k = (1 - z_{iJ}) \tilde{p}_i \right) \\
&= \int d\Phi_{n+\gamma} \left| \mathcal{M}_{\text{sub},\hat{i}J}(\Phi_{n+\gamma}) \right|^2 \Theta_{\text{cut}} \left(\tilde{\Phi}_{n,\hat{i}J} \right) \\
&+ \int d\Phi_{n+\gamma} \left| \mathcal{M}_{\text{sub},\hat{i}J}(\Phi_{n+\gamma}) \right|^2 \\
&\times \underbrace{\left[\Theta_{\text{cut}} \left(\tilde{\Phi}_{n,\hat{i}J} \mid p_i = z_{iJ} \tilde{p}_i, k = (1 - z_{iJ}) \tilde{p}_i \right) - \Theta_{\text{cut}} \left(\tilde{\Phi}_{n,\hat{i}J} \right) \right]}_{\equiv \Delta\Theta_{\text{cut}} \left(\tilde{\Phi}_{n,\hat{i}J} \mid z_{iJ} \right)}. \tag{3.10}
\end{aligned}$$

The first term on the r.h.s. of Eq. (3.10) exactly corresponds to the case of collinear-safe observables considered before, i.e. the extension to non-collinear-safe observables amounts to an extra contribution given by the second term. In particular, for any observables that is independent of the variable z_{iJ} , the second term vanishes due to $\Delta\Theta_{\text{cut}}(z_{iJ}) \equiv 0$ and the original expression for collinear-safe observables is recovered. Moreover, this encapsulates the logarithmic dependence on the fermion masses into the new contributions, so that it allows us to use dimensional regularization with exactly massless fermions in the calculation of the collinear-safe parts.

3.2. The dipole subtraction formalism for photon radiation off massless fermions

The dipole subtraction formalism for the general case of photon radiation off massive or massless fermions has been worked out in detail in Ref. [133]. All IR singularities in Ref. [133] are consistently regularized using finite masses, i.e. by introducing a small photon mass m_γ for the soft singularities and retaining the divergent logarithms $\ln(m_f)$ in the limit of small fermion masses. In this work, however, we consistently employ the method of dimensional regularization for the treatment of all singularities that arise in our calculation and therefore, the results given in Ref. [133] cannot be directly applied. To this end, we derived the corresponding formulae in dimensional regularization by converting the results given in Ref. [129] for the case of QCD corrections involving massless quarks by replacing the colour factors with the respective electric charges. However, it is crucial to exactly reproduce the conventions used in Ref. [133] in order to stay compatible with the extension to non-collinear safe observables given in Ref. [134]. This required a further rearrangement of finite contributions and the explicit integration of the subtraction function in the case of a final-state emitter-spectator pair. In the following, we give all relevant formulae for the dipole subtraction formalism for exactly massless fermions using dimensional regularization where the different cases are illustrated in Fig. 3.1 in terms of schematic diagrams.

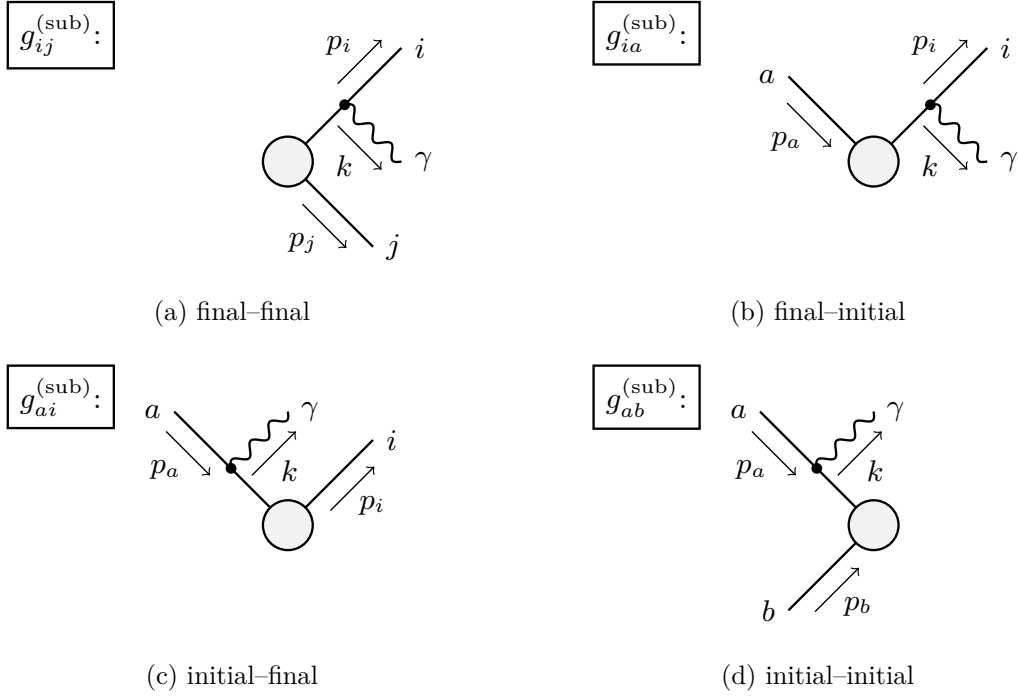


Figure 3.1.: QED dipoles for massless fermions and all possible emitter-spectator combinations.

3.2.1. Final-state emitter and final-state spectator

The phase-space parametrisation $\tilde{\Phi}_{n,ij}$ for the case with a final-state emitter i and a final-state spectator j (see Fig. 3.1(a)) is chosen as

$$\tilde{p}_i^\mu = p_i^\mu + k^\mu - \frac{y_{ij}}{1 - y_{ij}} p_j^\mu, \quad \tilde{p}_j^\mu = \frac{1}{1 - y_{ij}} p_j^\mu, \quad (3.11)$$

where the dipole variables y_{ij} and z_{ij} are given by

$$y_{ij} = \frac{p_i \cdot k}{p_i \cdot p_j + p_i \cdot k + p_j \cdot k}, \quad z_{ij} = \frac{p_i \cdot p_j}{p_i \cdot p_j + p_j \cdot k}. \quad (3.12)$$

Momentum conservation and on-shell relations are retained exactly, which is a property common to all dipoles. The associated dipole function $g_{ij}^{(\text{sub})}$ is defined by

$$g_{ij}^{(\text{sub})}(p_i, p_j, k) = \frac{1}{p_i \cdot k} \frac{1}{1 - y_{ij}} \left[\frac{2}{1 - z_{ij}(1 - y_{ij})} - (1 + z_{ij}) - \epsilon(1 - z_{ij}) \right], \quad (3.13)$$

and differs from the approach used in Ref. [129] by an additional factor of $1/(1 - y_{ij})$. As already stated above, reproducing the convention used in Ref. [133] is desirable so that the results given in Ref. [134] for non-collinear-safe observables can be used without modification. This required the explicit analytical integration of $g_{ij}^{(\text{sub})}$ as given in Eq. (3.13) over the singular one-particle

sub-space $[dk]$ associated with the photon² and the resulting integrated dipole term can be written in the following form

$$\int d\Phi_{n+\gamma} |\mathcal{M}_{\text{sub},ij}(\Phi_{n+\gamma})|^2 = -\frac{\alpha}{2\pi} \eta_i Q_i \eta_j Q_j \int d\tilde{\Phi}_n G_{ij}^{(\text{sub})}(\tilde{\Phi}_n) |\mathcal{M}_0(\tilde{\Phi}_n)|^2. \quad (3.14)$$

The different invariant phase-space measures are given by

$$d\Phi_{n+\gamma} \equiv d\phi(k_1, \dots, k_n, k; Q), \quad d\tilde{\Phi}_n \equiv d\phi(\tilde{k}_1, \dots, \tilde{k}_n; Q) \quad (3.15)$$

i.e. they are defined for the *same* total incoming momentum $Q = p_i + p_j + k = \tilde{p}_i + \tilde{p}_j$. The singular function $G_{ij}^{(\text{sub})}$ explicitly reads,

$$\begin{aligned} G_{ij}^{(\text{sub})}(\tilde{\Phi}_n) = & \frac{c_\epsilon}{\epsilon^2} + \frac{c_\epsilon}{\epsilon} \left[\frac{3}{2} + \ln \left(\frac{\mu^2}{2\tilde{p}_i \cdot \tilde{p}_j} \right) \right] \\ & + \frac{1}{2} \ln^2 \left(\frac{\mu^2}{2\tilde{p}_i \cdot \tilde{p}_j} \right) + \frac{3}{2} \ln \left(\frac{\mu^2}{2\tilde{p}_i \cdot \tilde{p}_j} \right) - \frac{\pi^2}{3} + \frac{7}{2} + \mathcal{O}(\epsilon). \end{aligned} \quad (3.16)$$

Non-collinear-safe observables

The subtraction function $g_{ij}^{(\text{sub})}$ given in Eq. (3.13) was chosen in such a way to ensure the compatibility with the formulae given in Ref. [134] and we will only quote the final result for completeness. The extra term that needs to be added in the case of non-collinear-safe observables can be written as a convolution over the energy fraction $z = z_{ij}$ carried away by the fermion after the collinear splitting $f \rightarrow f\gamma$,

$$\begin{aligned} & \int d\Phi_{n+\gamma} |\mathcal{M}_{\text{sub},ij}(\Phi_{n+\gamma})|^2 \Delta\Theta_{\text{cut}}(\tilde{\Phi}_{n,ij} | z_{ij}) \\ &= -\frac{\alpha}{2\pi} \eta_i Q_i \eta_j Q_j \int d\tilde{\Phi}_n |\mathcal{M}_0(\tilde{\Phi}_n)|^2 \\ & \quad \times \int_0^1 dz \left[\bar{\mathcal{G}}_{ij}^{(\text{sub})}(\tilde{\Phi}_n, z) \right]_+ \Theta_{\text{cut}}(\tilde{\Phi}_n | p_i = z\tilde{p}_i, k = (1-z)\tilde{p}_i), \end{aligned} \quad (3.17)$$

where the plus-distribution $[\dots]_+$ is defined in Eq. (A.16). The function $\bar{\mathcal{G}}_{ij}^{(\text{sub})}$ is given by

$$\bar{\mathcal{G}}_{ij}^{(\text{sub})}(\tilde{\Phi}_n, z) = \frac{1+z^2}{1-z} \left[\ln \left(\frac{2\tilde{p}_i \cdot \tilde{p}_j}{m_i^2} \right) + \ln(z) - 1 \right] + (1+z) \ln(1-z) + (1-z), \quad (3.18)$$

which contains the explicit dependence on the light emitter mass m_i . Note that the dependence of the final result on the physical mass of the fermion requires the use of mass regularization, which differs from our default choice of dimensional regularization.

3.2.2. Final-state emitter and initial-state spectator and vice versa

The case of a final-state emitter with an initial-state spectator (Fig. 3.1(b)) and the situation with the reversed roles (Fig. 3.1(c)) both employ the same phase-space parametrisation chosen

² Alternatively, the results given in Ref. [130] can be used for a conversion between the two regularization schemes.

as follows

$$\tilde{p}_a^\mu = x_{ia} p_a^\mu, \quad \tilde{p}_i^\mu = p_i^\mu + k^\mu - (1 - x_{ia}) p_a^\mu. \quad (3.19)$$

The dipole variables x_{ia} and z_{ia} are defined by

$$x_{ia} = \frac{p_a \cdot p_i + p_a \cdot k - p_i \cdot k}{p_a \cdot p_i + p_a \cdot k}, \quad z_{ia} = \frac{p_a \cdot p_i}{p_a \cdot p_i + p_a \cdot k}, \quad (3.20)$$

and the respective subtraction functions read

$$g_{ia}^{(\text{sub})}(p_i, p_a, k) = \frac{1}{p_i \cdot k} \frac{1}{x_{ia}} \left[\frac{2}{2 - z_{ia} - x_{ia}} - 1 - z_{ia} - \epsilon(1 - z_{ia}) \right], \quad (3.21a)$$

$$g_{ai}^{(\text{sub})}(p_a, p_i, k) = \frac{1}{p_a \cdot k} \frac{1}{x_{ia}} \left[\frac{2}{2 - x_{ia} - z_{ia}} - 1 - x_{ia} - \epsilon(1 - x_{ia}) \right]. \quad (3.21b)$$

Since the momentum of the incoming fermion a is modified through the mapping (3.19), the phase-space factorization now involves an additional convolution over the momentum fraction $x = x_{ia}$. The soft singularity at the endpoint $x = 1$ can be isolated using the plus prescription (A.16), and the integrated dipoles take the form

$$\begin{aligned} & \int d\Phi_{n+\gamma} \left| \mathcal{M}_{\text{sub}, ff'}(\Phi_{n+\gamma}) \right|^2 \\ &= -\frac{\alpha}{2\pi} \eta_i Q_i \eta_a Q_a \left\{ \int d\tilde{\Phi}_n G_{ff'}^{(\text{sub})}(\tilde{\Phi}_n) \left| \mathcal{M}_0(\tilde{\Phi}_n) \right|^2 \right. \\ & \quad \left. + \int_0^1 dx \int d\tilde{\Phi}_n (\tilde{p}_a = xp_a, 2\tilde{p}_i \cdot \tilde{p}_a) \frac{1}{x} \left[\mathcal{G}_{ff'}^{(\text{sub})}(\tilde{\Phi}_n, x) \right]_+ \left| \mathcal{M}_0(\tilde{\Phi}_n) \right|^2 \right\}, \end{aligned} \quad (3.22)$$

where we have introduced the labels f and f' to denote the indices i and a in both orders (3.25). Here, the invariant phase-space measures are defined as

$$\begin{aligned} d\Phi_{n+\gamma} &\equiv d\phi(k_1, \dots, k_n, k; p_a + Q) \\ d\tilde{\Phi}_n (\tilde{p}_a = xp_a, 2\tilde{p}_i \cdot \tilde{p}_a) &\equiv d\phi(\tilde{k}_1, \dots, \tilde{k}_n; xp_a + Q), \end{aligned} \quad (3.23)$$

i.e. the total incoming momentum on the r.h.s. is *reduced* according to $p_a \rightarrow xp_a = \tilde{p}_a$, and the second argument in the corresponding phase-space measure indicates the invariant that is kept fixed in the convolution over x . For $x = 1$ Eq. (3.23) reduces to Eq. (3.15), which corresponds the phase-space measure associated with the endpoint contribution $G_{ff'}^{(\text{sub})}$.

The distributions $\mathcal{G}_{ff'}^{(\text{sub})}$ that are obtained from the two subtraction functions in Eqs. (3.21) explicitly read

$$\mathcal{G}_{ia}^{(\text{sub})}(\tilde{\Phi}_n, x) = \frac{1}{1-x} \left[2 \ln \left(\frac{2-x}{1-x} \right) - \frac{3}{2} \right], \quad (3.24a)$$

$$\begin{aligned} \mathcal{G}_{ai}^{(\text{sub})}(\tilde{\Phi}_n, x) &= - \left[\frac{c_\epsilon}{\epsilon} + \ln \left(\frac{\mu^2}{2\tilde{p}_a \cdot \tilde{p}_i} \right) + \ln(x) \right] \left(\frac{1-x^2}{1-x} \right) - \frac{4}{1-x} \ln \left(\frac{1}{1-x} \right) \\ &\quad - \frac{2}{1-x} \ln(2-x) + (1-x) - (1+x) \ln(1-x) + \mathcal{O}(\epsilon), \end{aligned} \quad (3.24b)$$

with the respective endpoint contributions $G_{ff'}^{(\text{sub})}$ given by

$$G_{ia}^{(\text{sub})}(\tilde{\Phi}_n) = \frac{c_\epsilon}{\epsilon^2} + \frac{c_\epsilon}{\epsilon} \left[\frac{3}{2} + \ln \left(\frac{\mu^2}{2\tilde{p}_i \cdot \tilde{p}_a} \right) \right] + \frac{1}{2} \ln^2 \left(\frac{\mu^2}{2\tilde{p}_i \cdot \tilde{p}_a} \right) + \frac{3}{2} \ln \left(\frac{\mu^2}{2\tilde{p}_i \cdot \tilde{p}_a} \right) - \frac{\pi^2}{2} + \frac{7}{2} + \mathcal{O}(\epsilon), \quad (3.25a)$$

$$G_{ai}^{(\text{sub})}(\tilde{\Phi}_n) = \frac{c_\epsilon}{\epsilon^2} + \frac{c_\epsilon}{\epsilon} \left[\frac{3}{2} + \ln \left(\frac{\mu^2}{2\tilde{p}_a \cdot \tilde{p}_i} \right) \right] + \frac{1}{2} \ln^2 \left(\frac{\mu^2}{2\tilde{p}_a \cdot \tilde{p}_i} \right) + \frac{3}{2} \ln \left(\frac{\mu^2}{2\tilde{p}_a \cdot \tilde{p}_i} \right) + \frac{\pi^2}{6} + 1 + \mathcal{O}(\epsilon). \quad (3.25b)$$

Non-collinear-safe observables

Only the case with a final-state emitter requires a modification of the subtraction formalism in the real-emission contributions according to Eq. (3.9) which leads to an extra term for the integrated counterpart which is given by, cf. Eq. (3.10),

$$\begin{aligned} & \int d\Phi_{n+\gamma} |\mathcal{M}_{\text{sub},ia}(\Phi_{n+\gamma})|^2 \Delta\Theta_{\text{cut}}(\tilde{\Phi}_{n,ia} | z_{ia}) \\ &= -\frac{\alpha}{2\pi} \eta_i Q_i \eta_a Q_a \int_0^1 dx \int d\tilde{\Phi}_n (\tilde{p}_a = xp_a, 2\tilde{p}_i \cdot \tilde{p}_a) |\mathcal{M}_0(\tilde{\Phi}_n)|^2 \\ & \quad \times \int_0^1 dz \frac{1}{x} \left\{ [\bar{\mathcal{G}}_{ia}^{(\text{sub})}(\tilde{\Phi}_n, z)]_+ \delta(1-x) + [\bar{g}_{ia}^{(\text{sub})}(x, z)]_+^{(x,z)} \right\} \\ & \quad \times \Theta_{\text{cut}}(\tilde{\Phi}_n | p_i = z\tilde{p}_i, k = (1-z)\tilde{p}_i). \end{aligned} \quad (3.26)$$

The functions $\bar{\mathcal{G}}_{ia}^{(\text{sub})}$ and $\bar{g}_{ia}^{(\text{sub})}$ explicitly read

$$\begin{aligned} \bar{\mathcal{G}}_{ia}^{(\text{sub})}(\tilde{\Phi}_n, z) &= \frac{1+z^2}{1-z} \left[\ln \left(\frac{2\tilde{p}_i \cdot \tilde{p}_a}{m_i^2} \right) + \ln(x) + \ln(z) - 1 \right] \\ & \quad - \frac{2}{1-z} \ln(2-z) + (1+z) \ln(1-z) + (1-z), \end{aligned} \quad (3.27)$$

$$\bar{g}_{ia}^{(\text{sub})}(x, z) = \frac{1}{1-x} \left(\frac{2}{2-x-z} - 1 - z \right). \quad (3.28)$$

Here, the generalisation of the plus distribution for the case of two variables is defined as

$$\begin{aligned} & \int_0^1 dx \int_0^1 dz [g(x, z)]_+^{(x,z)} f(x, z) \\ & \equiv \int_0^1 dx \int_0^1 dz g(x, z) [f(x, z) - f(1, z) - f(x, 1) + f(1, 1)]. \end{aligned} \quad (3.29)$$

3.2.3. Initial-state emitter and initial-state spectator

For the case where both emitter and spectator are initial-state particles (see Fig. 3.1(d)), their momenta are mapped to the dipole kinematics as follows

$$\tilde{p}_a^\mu = x_{ab} p_a^\mu, \quad \tilde{p}_b^\mu = p_b^\mu, \quad (3.30)$$

with the dipole variable x_{ab} defined by

$$x_{ab} = \frac{p_a \cdot p_b - p_a \cdot k - p_b \cdot k}{p_a \cdot p_b}. \quad (3.31)$$

Since the spectator's momentum p_b is kept fixed, the recoil of the photon must be absorbed by the remaining particles involved in the process. To this end, the auxiliary momenta P_{ab}^μ and \tilde{P}_{ab}^μ are introduced,

$$P_{ab}^\mu = p_a^\mu + p_b^\mu - k^\mu, \quad \tilde{P}_{ab}^\mu = \tilde{p}_a^\mu + p_b^\mu, \quad P_{ab}^2 = \tilde{P}_{ab}^2, \quad (3.32)$$

in order to define the Lorentz transformation that affects all final-state momenta k_j^μ ,

$$\tilde{k}_j^\mu = \Lambda^\mu{}_\nu k_j^\nu, \quad \Lambda^\mu{}_\nu = g^\mu{}_\nu - \frac{(P_{ab} + \tilde{P}_{ab})^\mu (P_{ab} + \tilde{P}_{ab})_\nu}{P_{ab}^2 + P_{ab} \cdot \tilde{P}_{ab}} + \frac{2\tilde{P}_{ab}^\mu P_{ab,\nu}}{P_{ab}^2}, \quad (3.33)$$

including also the momenta of neutral particles that are otherwise not involved in the dipole formalism. The subtraction function $g_{ab}^{(\text{sub})}$ is given by

$$g_{ab}^{(\text{sub})}(p_a, p_b, k) = \frac{1}{p_a \cdot k} \frac{1}{x_{ab}} \left[\frac{2}{1 - x_{ab}} - (1 + x_{ab}) - \epsilon(1 - x_{ab}) \right], \quad (3.34)$$

and the integration over the photonic part of the phase space involves a convolution over the variable $x = x_{ab}$ similar to the case discussed in the previous section and can be written in the following form

$$\begin{aligned} & \int d\Phi_{n+\gamma} |\mathcal{M}_{\text{sub},ab}(\Phi_{n+\gamma})|^2 \\ &= -\frac{\alpha}{2\pi} \eta_a Q_a \eta_b Q_b \left\{ \int d\tilde{\Phi}_n G_{ab}^{(\text{sub})}(\tilde{\Phi}_n) |\mathcal{M}_0(\tilde{\Phi}_n)|^2 \right. \\ & \quad \left. + \int_0^1 dx \int d\tilde{\Phi}_n (\tilde{p}_a = x p_a, 2\tilde{p}_a \cdot \tilde{p}_b/x) \frac{1}{x} [\mathcal{G}_{ab}^{(\text{sub})}(\tilde{\Phi}_n, x)]_+ |\mathcal{M}_0(\tilde{\Phi}_n)|^2 \right\}. \quad (3.35) \end{aligned}$$

The phase-space measures appearing on the r.h.s. of Eq. (3.35) are defined in Eqs. (3.23) and (3.15), and the kinematic invariant that is kept fixed during the convolution over x is chosen as $2\tilde{p}_a \cdot \tilde{p}_b/x = 2p_a \cdot p_b = \hat{s}$ and corresponds to the squared partonic centre-of-mass energy. The function $\mathcal{G}_{ab}^{(\text{sub})}$ is given by

$$\mathcal{G}_{ab}^{(\text{sub})}(\tilde{\Phi}_n, x) = - \left[\frac{c_\epsilon}{\epsilon} + \ln \left(\frac{\mu^2}{2\tilde{p}_a \cdot \tilde{p}_b} \right) + \ln(x) \right] \left(\frac{1 - x^2}{1 - x} \right)$$

$$-\frac{4}{1-x} \ln\left(\frac{1}{1-x}\right) - 2(1+x) \ln(1-x) + (1-x) + \mathcal{O}(\epsilon), \quad (3.36)$$

and the endpoint contribution reads

$$\begin{aligned} G_{ab}^{(\text{sub})}(\tilde{\Phi}_n) &= \frac{c_\epsilon}{\epsilon^2} + \frac{c_\epsilon}{\epsilon} \left[\frac{3}{2} + \ln\left(\frac{\mu^2}{2\tilde{p}_a \cdot \tilde{p}_b}\right) \right] \\ &+ \frac{1}{2} \ln^2\left(\frac{\mu^2}{2\tilde{p}_a \cdot \tilde{p}_b}\right) + \frac{3}{2} \ln\left(\frac{\mu^2}{2\tilde{p}_a \cdot \tilde{p}_b}\right) - \frac{\pi^2}{3} + 4 + \mathcal{O}(\epsilon). \end{aligned} \quad (3.37)$$

3.3. The dipole subtraction formalism for the production of massive particles

In the previous section we have considered the case of photon radiation off massless fermions which is sufficient for the calculation of the NLO EW $\mathcal{O}(\alpha)$ corrections to the Drell–Yan processes. When applying the pole approximation (see Chap. 4), however, we also require the NLO corrections to the on-shell vector-boson production and the subsequent decay sub-processes individually. As a consequence, for the charged-current Drell–Yan process additional dipoles are needed which consider a massive final-state particle (production) and a massive initial-state particle (decay). In this section we will give the formulae for the dipoles that involve a charged massive particle in the final state which can be found in Refs. [133, 134, 149].

The production process relevant in this work only involves at most one final-state charged particle, and as such, the combination involving a final-state emitter with a final-state spectator need not be considered here. As a result, only two additional dipoles are needed in the calculation of the production process, given by the case of a final-state massive emitter with an initial-state spectator and vice versa. They correspond to the schematic diagrams of the subtraction functions shown in Figs. 3.1(b) and 3.1(c) where the final-state particle i now corresponds to a massive particle. Since no massless (light) final-state charged particle is involved in this case, these dipoles remain unaffected by a transition to non-collinear safe observables. We follow the approach of Ref. [149] and employ the formulas that are obtained by a simple replacement of the colour charges with the electric charges in the results given there. Note that we use the results derived for massive fermions in our calculation for the production of a W boson. However, this does not pose a problem since only soft singularities occur which are independent of the spin of the particle. The so-called *quasi-collinear limits* [130, 149] where the mass of the final-state particle becomes very small compared to the hard scale need not be considered here, since in our case the maximal scale of the production process is given by the W-boson mass.

The phase-space parametrization remains identical to the case of a massless emitter given in Eq. (3.19) and the subtraction functions are given by

$$g_{ia}^{(\text{sub})}(p_i, p_a, k) = \frac{1}{p_i \cdot k} \frac{1}{x_{ia}} \left[\frac{2}{2 - x_{ia} - z_{ia}} - 1 - z_{ia} - \frac{m_i^2}{p_i \cdot k} - \epsilon(1 - z_{ia}) \right], \quad (3.38a)$$

$$g_{ai}^{(\text{sub})}(p_a, p_i, k) = \frac{1}{p_a \cdot k} \frac{1}{x_{ia}} \left[\frac{2}{2 - x_{ia} - z_{ia}} - 1 - x_{ia} - \epsilon(1 - x_{ia}) \right]. \quad (3.38b)$$

The rescaled dimensionless mass is defined by

$$\mu_i = \frac{m_i^2}{2\tilde{p}_i \cdot p_a} = x_{ia} \frac{m_i^2}{2\tilde{p}_i \cdot \tilde{p}_a}, \quad (3.39)$$

and the integral of the subtraction functions $g_{ff'}^{(\text{sub})}$ over the photonic phase can be written in a form analogous to the massless case (3.22),

$$\begin{aligned} & \int d\Phi_{n+\gamma} \left| \mathcal{M}_{\text{sub},ff'}(\Phi_{n+\gamma}) \right|^2 \\ &= -\frac{\alpha}{2\pi} \eta_f Q_f \eta_{f'} Q_{f'} \left\{ \int d\tilde{\Phi}_n G_{ff'}^{(\text{sub})}(\tilde{\Phi}_n) \left| \mathcal{M}_0(\tilde{\Phi}_n) \right|^2 \right. \\ & \quad \left. + \int_0^1 dx \int d\tilde{\Phi}_n (\tilde{p}_a = xp_a, 2\tilde{p}_i \cdot \tilde{p}_a/x) \frac{1}{x} \left[\mathcal{G}_{ff'}^{(\text{sub})}(\tilde{\Phi}_n, x) \right]_+ \left| \mathcal{M}_0(\tilde{\Phi}_n) \right|^2 \right\}, \quad (3.40) \end{aligned}$$

where the phase-space measure appearing on the r.h.s. are defined in Eqs. (3.23) and (3.15). Note that the kinematic invariant that is kept fixed during the convolution over x corresponds to keeping μ_i fixed and differs from the massless case and the corresponding approach in Ref. [133]. The choice of which invariant is kept fixed in the x integration has an impact that goes beyond a simple variable substitution in the final result, but differs by IR-finite contributions in a non-trivial manner, as discussed in detail in Appendix B of Ref. [149]. The distributions $\mathcal{G}_{ff'}^{(\text{sub})}$ are given by

$$\begin{aligned} \left[\mathcal{G}_{ia}^{(\text{sub})}(\tilde{\Phi}_n, x) \right]_+ &= \left(\frac{1-x}{2(1-x+\mu_i^2)^2} - \frac{2}{1-x} \left[1 + \ln(1-x+\mu_i^2) \right] \right)_+ \\ & \quad + \left(\frac{2}{1-x} \right)_+ \ln(2+\mu_i^2-x), \quad (3.41a) \end{aligned}$$

$$\begin{aligned} \left[\mathcal{G}_{ai}^{(\text{sub})}(\tilde{\Phi}_n, x) \right]_+ &= - \left[\frac{c_\epsilon}{\epsilon} + \ln \left(\frac{\mu^2}{2\tilde{p}_i \cdot \tilde{p}_a} \right) + \ln(x) \right] \left(\frac{1+x^2}{1-x} \right)_+ - (1+x) \ln(1-x) \\ & \quad - (1+x) \ln \left(\frac{1-x}{1-x+\mu_i^2} \right) + 2 \left(\frac{1}{1-x} \right)_+ \ln \left(\frac{2-x}{2-x+\mu_i^2} \right) \\ & \quad + \left(\frac{4}{1-x} \ln(1-x) \right)_+ - \frac{2}{1-x} \ln(2-x) + (1-x) + \mathcal{O}(\epsilon), \quad (3.41b) \end{aligned}$$

where the plus prescription $[\dots]_+$ on the l.h.s. is merely a symbolic notation to indicate that these expressions contain plus distributions but not that they are themselves a plus distribution. Finally, the endpoint parts $G_{ff'}^{(\text{sub})}$ are given by

$$\begin{aligned} G_{ia}^{(\text{sub})}(\tilde{\Phi}_n) &= \left[\frac{c_\epsilon}{\epsilon} + \ln \left(\frac{\mu^2}{2\tilde{p}_i \cdot \tilde{p}_a} \right) \right] \left[1 + \ln \left(\frac{\mu_i^2}{1+\mu_i^2} \right) \right] - 4 \text{Li}_2(-\mu_i^2) \\ & \quad + \frac{1}{2} \ln^2(1+\mu_i^2) - \frac{1}{2} \ln^2(\mu_i^2) - 2 \ln(1+\mu_i^2) \ln(\mu_i^2) \\ & \quad + \frac{1}{2} \ln(1+\mu_i^2) + \frac{1}{2} \ln(\mu_i^2) - \frac{2\pi^2}{3} + \frac{3}{2} + \frac{\mu_i^2}{2(1+\mu_i^2)} + \mathcal{O}(\epsilon), \quad (3.42a) \end{aligned}$$

$$\begin{aligned}
G_{ai}^{(\text{sub})}(\tilde{\Phi}_n) = & \frac{c_\epsilon}{\epsilon^2} + \left[\frac{c_\epsilon}{\epsilon} + \ln \left(\frac{\mu^2}{2\tilde{p}_i \cdot \tilde{p}_a} \right) \right] \left[\frac{3}{2} + \ln \left(\frac{\mu^2}{2\tilde{p}_i \cdot \tilde{p}_a} \right) + \ln(1 + \mu_i^2) \right] \\
& + 2 \text{Li}_2 \left(\frac{1}{1 + \mu_i^2} \right) - \frac{1}{2} \ln^2 \left(\frac{\mu^2}{2\tilde{p}_i \cdot \tilde{p}_a} \right) + \frac{1}{2} \ln^2(1 + \mu_i^2) - \frac{\pi^2}{3} + \mathcal{O}(\epsilon). \quad (3.42b)
\end{aligned}$$

3.4. The dipole subtraction formalism for particle decays

As pointed out in the introduction to this chapter, so far, no general algorithm exists in the literature for the calculation of NLO QED corrections to decay processes within the dipole subtraction formalism. We present the construction of such a general algorithm in this section which is organized as follows: In Sect. 3.4.1 we give a brief overview on the construction and the properties of the subtraction functions for particle decays. Although not explicitly needed in this work, we present the results for the decay process involving massive final-state fermions in Sect. 3.4.2 and briefly comment on the special case of light fermion masses which corresponds to the situation where the collinear singularities are regularized using small fermion masses. The corresponding results in dimensional regularisation with massless fermions are given in Sect. 3.4.3, which is the relevant case for this work. Finally, the extension to non-collinear-safe observables is discussed in Sect. 3.4.4.

3.4.1. General properties

A rigorous extension in the spirit of the dipole subtraction formalism for the decay process would require the construction of two new subtraction terms: First, a dipole where the decaying particle a is considered the emitter, $g_{ai}^{(\text{sub})}$, and second, where a acts as the spectator $g_{ia}^{(\text{sub})}$. Further demanding the asymptotic behaviour given in Eqs. (3.5) would then ensure the proper point-wise cancellation in all singular regions of phase space. However, it is possible to exploit a feature that is unique to the decay process, which is given by the fact that the decaying particle has always a non-vanishing mass which even represents the maximal scale of the decay process and, as such, will never be considered in the small-mass limit. As a consequence, there are no collinear singularities associated with the initial-state particle a which allows for the term $g_{ai}^{(\text{sub})}$ to be absorbed into the subtraction function $g_{ia}^{(\text{sub})}$. We denote the combined subtraction function by $d_{ia}^{(\text{sub})}$ which is illustrated in Fig. 3.2 in terms of the two schematic diagrams that would be associated with $g_{ai}^{(\text{sub})}$ and $g_{ia}^{(\text{sub})}$. Such a combined treatment reduces the number of dipoles that need to be computed separately and speeds up the numerical evaluation and, moreover, allows part of the calculation to be taken over from the case with a final-state emitter and spectator, as will become apparent in the explicit construction of $d_{ia}^{(\text{sub})}$ described below. Due to the combined treatment, the asymptotic behaviour of the subtraction function $d_{ia}^{(\text{sub})}$ differs from those of $g^{(\text{sub})}$ given in Eq. (3.5a) in the soft limit and explicitly reads

$$d_{ia}^{(\text{sub})}(p_i, p_a, k) \underset{k \rightarrow 0}{\sim} \frac{2p_i \cdot p_a}{(p_i \cdot k)(p_a \cdot k)} - \frac{m_i^2}{(p_i \cdot k)^2} - \frac{m_a^2}{(p_a \cdot k)^2}. \quad (3.43)$$

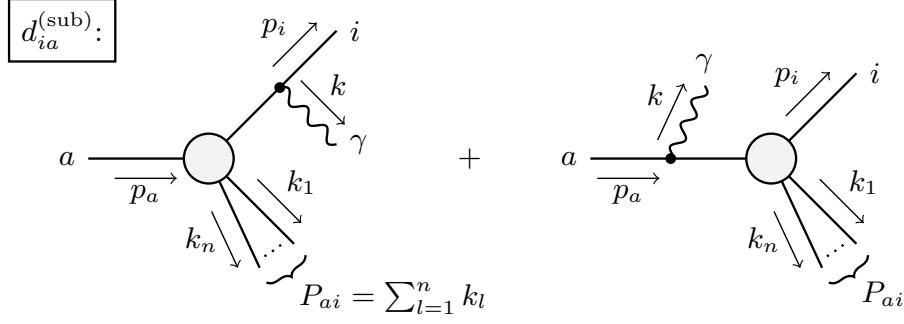


Figure 3.2.: Schematic diagrams illustrating the subtraction function $d_{ia}^{(\text{sub})}$ for the decay of a particle a and a charged final-state particle i . The decay dipole merges the two configurations associated with photon radiation from the final state (left) and initial state (right) into one subtraction term.

In the limit of small fermion masses $m_i \rightarrow 0$ the asymptotic form in the collinear region is required to be

$$d_{ia}^{(\text{sub})}(p_i, p_a, k) \underset{p_i \cdot k \rightarrow 0}{\sim} \frac{1}{p_i \cdot k} \left[\left(\frac{1 + z_i^2}{1 - z_i} \right) - \frac{m_i^2}{p_i \cdot k} \right], \quad z_i = \frac{p_i^0}{p_i^0 + k^0}, \quad (3.44)$$

where the small mass m_i is used as the regulator of the collinear singularity. In case the collinear singularities are regularized using dimensional regularisation, the asymptotic behaviour in the collinear limit is instead given by, cf. Eqs. (3.44) and (3.5b),

$$d_{ia}^{(\text{sub})}(p_i, p_a, k) \underset{p_i \cdot k \rightarrow 0}{\sim} \frac{1}{p_i \cdot k} \left[\left(\frac{1 + z_i^2}{1 - z_i} \right) - \epsilon (1 - z_i) \right]. \quad (3.45)$$

The subtraction term $|\mathcal{M}_{\text{sub}}|^2$ in the dipole subtraction formalism is then given by the following expression in the case of decay processes, cf. Eq. (3.4),

$$\begin{aligned} |\mathcal{M}_{\text{sub}}(\Phi_{n+\gamma})|^2 &= \sum_i |\mathcal{M}_{\text{sub},ia}(\Phi_{n+\gamma})|^2 + \sum_{\substack{i,j \\ i \neq j}} |\mathcal{M}_{\text{sub},ij}(\Phi_{n+\gamma})|^2 \\ &= -4\pi\mu^{2\epsilon}\alpha \sum_i \eta_i Q_i \left\{ \eta_a Q_a d_{ia}^{(\text{sub})}(p_i, p_a, k) \left| \mathcal{M}_0(\tilde{\Phi}_{n,ia}) \right|^2 \right. \\ &\quad \left. + \sum_{\substack{j \\ j \neq i}} \eta_j Q_j g_{ij}^{(\text{sub})}(p_i, p_j, k) \left| \mathcal{M}_0(\tilde{\Phi}_{n,ij}) \right|^2 \right\}, \end{aligned} \quad (3.46)$$

where the summation over the indices i, j extends over all charged particles in the final-state, a denotes the decaying particle, and $g_{ij}^{(\text{sub})}$ are the known subtraction functions of the dipoles with a final-state emitter–spectator pair. Using the above properties of $d_{ia}^{(\text{sub})}$ and of $g_{ij}^{(\text{sub})}$ given in Eq. (3.5) one can verify that the requirement of Eq. (3.3) is correctly satisfied.

3.4.2. Subtraction function for massive final-state fermions

In the following we present the construction of the subtraction function $d_{ia}^{(\text{sub})}$ for the decay of a particle a of mass m_a with a massive final-state fermion i of mass m_i . The special case of light fermions can be obtained by a systematic expansion in m_i and is given at the end of this section. The corresponding results using dimensional regularization and exactly massless fermions is covered in the next section.

In the construction of the modified momenta $\tilde{\Phi}_{n,ai}$ for the decay dipole it is convenient to keep the four-momentum of the decaying particle a fixed. Similar to the initial–initial dipole discussed in Sect. 3.2.3, keeping the momentum of either the spectator or emitter fixed requires the deformation of all remaining momenta k_l via a Lorentz transformation. Such a transformation is necessary in order to compensate the recoil induced by the radiated photon so that four-momentum conservation and all mass-shell conditions are retained. To this end, we define the auxiliary momentum P_{ia}^μ of the “recoiling system”, see Fig. 3.2,

$$P_{ia}^\mu = p_a^\mu - p_i^\mu - k^\mu = \sum_{l=1}^n k_l^\mu, \quad (3.47)$$

which absorbs the recoil of the radiated photon through the transformation

$$\tilde{P}_{ia}^\mu = \frac{\sqrt{\lambda_{ia}}}{\sqrt{\lambda(1, \mu_i^2 + \frac{2p_i \cdot k}{m_a^2}, \mu_{ia}^2)}} \left(P_{ia}^\mu - \frac{P_{ia} \cdot p_a}{m_a^2} p_a^\mu \right) + \frac{1}{2} (1 + \mu_{ia}^2 - \mu_i^2) p_a^\mu, \quad (3.48)$$

where

$$\lambda_{ia} = \lambda(1, \mu_i^2, \mu_{ia}^2), \quad (3.49)$$

and $\lambda(x, y, z)$ denotes the Källén function defined in Eq. (A.14). The dimensionless rescaled masses are defined by

$$\mu_i^2 = \frac{m_i^2}{m_a^2}, \quad \mu_{ia}^2 = \frac{P_{ia}^2}{m_a^2}, \quad \bar{\mu}^2 \equiv 1 - \mu_i^2 - \mu_{ia}^2, \quad (3.50)$$

and stay invariant under the dipole mapping ($P_{ia}^2 = \tilde{P}_{ia}^2$). The transformation of the momenta then explicitly reads

$$\tilde{p}_a^\mu = p_a^\mu, \quad \tilde{p}_i^\mu = p_i^\mu - \tilde{P}_{ia}^\mu, \quad \tilde{k}_l^\mu = \Lambda^\mu{}_\nu k_l^\nu, \quad (3.51)$$

where k_l denotes the momenta of all remaining particles of the decay process, including all neutral particles. The Lorentz transformation $\Lambda^\mu{}_\nu$ can be expressed in terms of the momenta P_{ia}^μ and \tilde{P}_{ia}^μ as follows, cf. Eq. (3.33),

$$\Lambda^\mu{}_\nu = g^\mu{}_\nu - \frac{(P_{ia} + \tilde{P}_{ia})^\mu (P_{ia} + \tilde{P}_{ia})_\nu}{P_{ia}^2 + P_{ia} \cdot \tilde{P}_{ia}} + \frac{2\tilde{P}_{ia}^\mu P_{ia,\nu}}{P_{ia}^2}. \quad (3.52)$$

This phase-space parametrisation is identical to the one used in the case of a final-state emitter with a final-state spectator, where particle i plays the role of the emitter and the recoiling system the role of the spectator of mass $m^2 = P_{ij}^2$.

Further, using the same dipole variables as defined in Eq. (3.12),

$$y_{ia} = \frac{p_i \cdot k}{p_i \cdot k + p_i \cdot P_{ia} + P_{ia} \cdot k} = \frac{p_i \cdot k}{p_a \cdot p_i + p_a \cdot k - p_i \cdot k - m_i^2}, \quad (3.53)$$

$$z_{ia} = \frac{p_i \cdot P_{ia}}{p_i \cdot P_{ia} + P_{ia} \cdot k} = \frac{p_a \cdot p_i - m_i^2 - p_i \cdot k}{p_a \cdot p_i - m_i^2 + p_a \cdot k - 2p_i \cdot k} = 1 - z_\gamma, \quad (3.54)$$

we construct the subtraction function $d_{ia}^{(\text{sub})}$ as follows,

$$d_{ia}^{(\text{sub})}(p_i, p_a, k) = \frac{1}{(p_i \cdot k) R_{ia}(y_{ia})} \left[\frac{2}{1 - z_{ia}(1 - y_{ia})} \left(1 + \frac{2\mu_i^2}{\bar{\mu}^2} \right) - 1 - z_{ia} - \frac{m_i^2}{p_i \cdot k} \right] - \frac{1}{m_a^2 \bar{\mu}^4 R_{ia}(y_{ia})} \frac{4}{[1 - z_{ia}(1 - y_{ia})]^2}, \quad (3.55)$$

where we have defined the auxiliary function R_{ia} ,

$$R_{ia}(y_{ia}) = \frac{\sqrt{[2\mu_{ia}^2 + \bar{\mu}^2(1 - y_{ia})]^2 - 4\mu_{ia}^2}}{\sqrt{\lambda_{ia}}}. \quad (3.56)$$

The first line in Eq. (3.55) is almost identical to the subtraction function $g_{ij}^{(\text{sub})}$ given in Eq. (4.4) of Ref [133] with the only difference being the additional factor of $(1 + 2\mu_i^2/\bar{\mu}^2)$ multiplying the first term inside the square brackets. This additional factor is introduced in order to obtain the correct asymptotic behaviour in the soft limit (3.43), however, without interfering with the collinear limit (3.44) which is already correctly reproduced by $g_{ij}^{(\text{sub})}$. The second line in Eq. (3.55) is obtained by writing the last term in Eq. (3.44) in terms of the dipole variables, where an additional factor $1/R_{ia}(y_{ia})$ was included for convenience which, however, has no impact in the soft limit.

The phase-space factorisation can be found in Ref. [133, 149] and reads

$$d\phi(p_i, k, P_{ia}; p_a) = d\phi(\tilde{p}_i, \tilde{P}_{ia}; p_a) [dk(\tilde{p}_i, \tilde{P}_{ia})], \quad (3.57)$$

where the photonic part of the phase space can be parametrised in terms of the dipole variables y_{ia} and $z_{ia} = (1 - z_\gamma)$,

$$[dk(\tilde{p}_i, \tilde{P}_{ia})] = \frac{1}{4} (2\pi)^{-3+2\epsilon} (m_a^2)^{1-\epsilon} (\bar{\mu}^2)^{2-2\epsilon} (\sqrt{\lambda_{ia}})^{-1+2\epsilon} \int d^{d-3}\Omega \times \int_0^{y^+} dy_{ia} (1 - y_{ia})^{1-2\epsilon} (\mu_i^2 + \bar{\mu}^2 y_{ia})^{-\epsilon} \times \int_{z_{\gamma,-}(y_{ia})}^{z_{\gamma,+}(y_{ia})} dz_\gamma [z_{\gamma,+}(y_{ia}) - z_\gamma]^{-\epsilon} [z_\gamma - z_{\gamma,-}(y_{ia})]^{-\epsilon}, \quad (3.58)$$

with the integration boundaries given by

$$y^+ = 1 - \frac{2\mu_{ia}(1 - \mu_{ia})}{\bar{\mu}}, \quad z_{\gamma,\pm}(y_{ia}) = \frac{\bar{\mu}^2 y_{ia}}{2(\mu_i^2 + \bar{\mu}^2 y_{ia})} \left(1 \pm \frac{\sqrt{\lambda_{ia}} R_{ia}(y_{ia})}{\bar{\mu}^2 (1 - y_{ia})} \right). \quad (3.59)$$

The analytic integration of the subtraction function over the photonic part of the phase space

gives rise to the integrated counterpart denoted by $D_{ia}^{(\text{sub})}$, which we decompose into three contributions according to

$$\begin{aligned} D_{ia}^{(\text{sub})}(\tilde{\Phi}_n) &= 8\pi^2 \mu^{2\epsilon} \int [dk(\tilde{p}_i, \tilde{P}_{ia})] d_{ia}^{(\text{sub})}(p_i, p_a, k) \\ &\equiv D_{ia}^{(\text{eik})}(\tilde{\Phi}_n) + D_{ia}^{(\text{coll})}(\tilde{\Phi}_n) + D_{ia}^{(\text{eik}')}(\tilde{\Phi}_n), \end{aligned} \quad (3.60)$$

with

$$D_{ia}^{(\text{eik})}(\tilde{\Phi}_n) = \int [dk(\tilde{p}_i, \tilde{P}_{ia})] \frac{16\pi^2 \mu^{2\epsilon}}{(p_i \cdot k) R_{ia}(y_{ia})} \frac{1 + 2\mu_i^2/\bar{\mu}^2}{1 - z_{ij}(1 - y_{ij})}, \quad (3.61a)$$

$$D_{ia}^{(\text{coll})}(\tilde{\Phi}_n) = \int [dk(\tilde{p}_i, \tilde{P}_{ia})] \frac{-8\pi^2 \mu^{2\epsilon}}{(p_i \cdot k) R_{ia}(y_{ia})} \left[1 + z_{ia} + \frac{m_i^2}{p_i \cdot k} \right], \quad (3.61b)$$

$$D_{ia}^{(\text{eik}')}(\tilde{\Phi}_n) = \int [dk(\tilde{p}_i, \tilde{P}_{ia})] \frac{-32\pi^2 \mu^{2\epsilon}}{m_a^2 \bar{\mu}^4 R_{ia}(y_{ia})} \frac{1}{[1 - z_{ia}(1 - y_{ia})]^2}. \quad (3.61c)$$

Since the additional factor $(1 + 2\mu_i^2/\bar{\mu}^2)$ appearing in $D_{ia}^{(\text{eik})}$ is invariant under the phase-space mapping (3.51), it can be pulled out from the integration over $[dk]$. As a consequence, both $D_{ia}^{(\text{eik})}$ and $D_{ia}^{(\text{coll})}$ can be directly read off from the corresponding result for the case with a massive final-state emitter and spectator given in Ref. [133],

$$\begin{aligned} D_{ia}^{(\text{eik})}(\tilde{\Phi}_n) &= \frac{\bar{\mu}^2 + 2\mu_i^2}{\sqrt{\lambda_{ia}}} \left\{ \left[\frac{c_\epsilon}{\epsilon} + \ln \left(\frac{\mu^2}{m_a^2} \right) \right] \ln(a_1) + \ln(a_1) \ln \left(\frac{\mu_{ia}^2}{\lambda_{ia} a_2} \right) + 2 \text{Li}_2(a_1) \right. \\ &\quad \left. + 4 \text{Li}_2 \left(-\sqrt{\frac{a_2}{a_1}} \right) - 4 \text{Li}_2(-\sqrt{a_1 a_2}) + \frac{1}{2} \ln^2(a_1) - \frac{\pi^2}{3} + \mathcal{O}(\epsilon) \right\}, \end{aligned} \quad (3.62)$$

$$D_{ia}^{(\text{coll})}(\tilde{\Phi}_n) = \frac{c_\epsilon}{\epsilon} + \ln \left(\frac{\mu^2}{m_a^2} \right) - \ln(\mu_i^2) + 3 \ln(a_3) - 2 \ln(1 - a_3^2) + \frac{a_3^2}{2} + \frac{3}{2} + \mathcal{O}(\epsilon), \quad (3.63)$$

with the abbreviations

$$a_1 = \frac{\bar{\mu}^2 + 2\mu_i^2 - \sqrt{\lambda_{ia}}}{\bar{\mu}^2 + 2\mu_i^2 + \sqrt{\lambda_{ia}}}, \quad a_2 = \frac{\bar{\mu}^2 - \sqrt{\lambda_{ia}}}{\bar{\mu}^2 + \sqrt{\lambda_{ia}}}, \quad a_3 = \frac{\mu_i}{1 - \mu_{ia}}. \quad (3.64)$$

Here, the soft singularity regularised with an infinitesimal photon mass m_γ in Ref. [133] was converted to the corresponding expression using dimensional regularisation according to the replacement

$$\ln \left(\frac{m_\gamma^2}{Q^2} \right) \xrightarrow{\text{dimensional regularization}} \frac{c_\epsilon}{\epsilon} + \ln \left(\frac{\mu^2}{Q^2} \right) + \mathcal{O}(\epsilon). \quad (3.65)$$

Finally, the last contribution $D_{ia}^{(\text{eik}')}$ defined in Eq. (3.61c) represents a genuinely new contribution and its analytical integration will briefly be sketched in the following. First, using Eq. (3.58) and performing the substitution

$$\bar{z} = [z_{\gamma,+}(y_{ia}) - z_\gamma] \frac{1 - y_{ia}}{y_{ia}} \frac{\mu_i^2 + \bar{\mu}^2 y_{ia}}{\sqrt{\lambda_{ia}} R_{ia}(y_{ia})}, \quad (3.66)$$

Eq. (3.61c) can be written as follows,

$$D_{ia}^{(\text{eik}')}(\tilde{\Phi}_n) = -8 \frac{1}{\Gamma(1-\epsilon)} \left(\frac{4\pi\mu^2}{m_a^2} \right)^\epsilon (\bar{\mu}^2)^{-2\epsilon} \int_0^1 d\bar{z} (1-\bar{z})^{-\epsilon} (\bar{z})^{-\epsilon} \\ \times \int_0^{y_+} dy_{ia} y_{ia}^{-1-2\epsilon} \frac{(\mu_i^2 + \bar{\mu}^2 y_{ia})^{1+\epsilon} [R_{ia}(y_{ia})]^{-2\epsilon}}{[2\mu_i^2 + \bar{\mu}^2(1+y_{ia}) + \sqrt{\lambda_{ia}} R_{ia}(y_{ia}) (1-2\bar{z})]^2}. \quad (3.67)$$

The only IR singularity is of soft nature and arises from the integration region where y_{ia} tends to zero. The singularity can be therefore isolated by splitting the y range into two pieces as described in Appendix C.1 of Ref. [133]:

$$(a) \quad 0 < y < \Delta y \ll 1,$$

$$(b) \quad \Delta y < y < y_+ < 1.$$

First, in the integration over region (a), the parameter y can be set to zero in all non-singular contributions in $\mathcal{O}(\Delta y)$ owing to the choice $0 < \Delta y \ll 1$ and we obtain

$$D_{ia}^{(\text{eik}')}(\tilde{\Phi}_n)|_{(a)} = -8 \frac{1}{\Gamma(1-\epsilon)} \left(\frac{4\pi\mu^2}{m_a^2} \right)^\epsilon (\bar{\mu}^2)^{-2\epsilon} (\mu_i^2)^{1+\epsilon} \\ \times \int_0^1 d\bar{z} \frac{(1-\bar{z})^{-\epsilon} (\bar{z})^{-\epsilon}}{[\bar{\mu}^2 + 2\mu_i^2 + \sqrt{\lambda_{ia}} (1-2\bar{z})]^2} \int_0^{\Delta y} dy_{ia} y_{ia}^{-1-2\epsilon} \\ = \frac{c_\epsilon}{\epsilon} + \ln \left(\frac{\mu^2}{m_a^2} \right) - 2 \ln(\Delta y) + 2 \ln \left(\frac{\mu_i}{\bar{\mu}^2} \right) - \frac{\bar{\mu}^2 + 2\mu_i^2}{\sqrt{\lambda_{ia}}} \ln(a_1). \quad (3.68)$$

Second, the integration over region (b) does not contain any singularities and thus, no regulator is required and we set $\epsilon = 0$ to obtain

$$D_{ia}^{(\text{eik}')}(\tilde{\Phi}_n)|_{(b)} = -8 \int_{\Delta y}^{y_+} \frac{dy_{ia}}{y_{ia}} (\mu_i^2 + \bar{\mu}^2 y_{ia}) \\ \times \int_0^1 \frac{d\bar{z}}{[2\mu_i^2 + \bar{\mu}^2(1+y_{ia}) + \sqrt{\lambda_{ia}} R_{ia}(y_{ia}) (1-2\bar{z})]^2} \\ = -2 \int_{\Delta y}^{y_+} \frac{dy_{ia}}{y_{ia}} \\ = -2 \ln \left(1 - \frac{2\mu_{ia}(1-\mu_{ia})}{\bar{\mu}^2} \right) + 2 \ln(\Delta y). \quad (3.69)$$

Adding the two contributions, the dependence on the arbitrary parameter Δy cancels, and we arrive at the final result for the contribution of Eq. (3.61c)

$$D_{ia}^{(\text{eik}')}(\tilde{\Phi}_n) = D_{ia}^{(\text{eik}')}(\tilde{\Phi}_n)|_{(a)} + D_{ia}^{(\text{eik}')}(\tilde{\Phi}_n)|_{(b)} \\ = \frac{c_\epsilon}{\epsilon} + \ln \left(\frac{\mu^2}{m_a^2} \right) + 2 \ln \left(\frac{\mu_i}{\bar{\mu}^2} \right) \\ - 2 \ln \left(1 - \frac{2\mu_{ia}(1-\mu_{ia})}{\bar{\mu}^2} \right) - \frac{2\mu_i^2 + \bar{\mu}^2}{\sqrt{\lambda_{ia}}} \ln(a_1) + \mathcal{O}(\epsilon). \quad (3.70)$$

Collecting all partial results, the integrated decay dipole can be written in the form

$$\int d\Phi_{n+\gamma} |\mathcal{M}_{\text{sub},ia}(\Phi_{n+\gamma})|^2 = -\frac{\alpha}{2\pi} \eta_i Q_i \eta_a Q_a \int d\tilde{\Phi}_n D_{ia}^{(\text{sub})}(\tilde{\Phi}_n) |\mathcal{M}_0(\tilde{\Phi}_n)|^2, \quad (3.71)$$

with

$$\begin{aligned} D_{ia}^{(\text{sub})}(\tilde{\Phi}_n) &= D_{ia}^{(\text{eik})}(\tilde{\Phi}_n) + D_{ia}^{(\text{coll})}(\tilde{\Phi}_n) + D_{ia}^{(\text{eik}')}(\tilde{\Phi}_n) \\ &= \left[\frac{c_\epsilon}{\epsilon} + \ln \left(\frac{\mu^2}{m_a^2} \right) \right] \left[2 + \frac{\bar{\mu}^2 + 2\mu_i^2}{\sqrt{\lambda_{ia}}} \ln(a_1) \right] + 3 \ln(a_3) - 2 \ln(1 - a_3^2) \\ &\quad - 2 \ln(\bar{\mu}^2) - 2 \ln \left(1 - \frac{2\mu_{ia}(1 - \mu_{ia})}{\bar{\mu}^2} \right) + \frac{a_3^2}{2} + \frac{3}{2} \\ &\quad + \frac{\bar{\mu}^2 + 2\mu_i^2}{\sqrt{\lambda_{ia}}} \left\{ 2 \text{Li}_2(a_1) + 4 \text{Li}_2 \left(-\sqrt{\frac{a_2}{a_1}} \right) - 4 \text{Li}_2(-\sqrt{a_1 a_2}) \right. \\ &\quad \left. + \frac{1}{2} \ln^2(a_1) + \ln(a_1) \ln \left(\frac{\mu_{ia}^2}{\lambda_{ia} a_2} \right) - \ln(a_1) - \frac{\pi^2}{3} + \mathcal{O}(\epsilon) \right\}, \end{aligned} \quad (3.72)$$

and the abbreviations a_i given in Eq. (3.64).

Special case of light fermions

The subtraction function $d_{ia}^{(\text{sub})}$ given in Eq. (3.55) is already defined in such a way to correctly reproduce the asymptotic form in the collinear limit as demanded in Eq. (3.44) for the special case of small fermion masses $m_i \rightarrow 0$. The corresponding expression for the integrated dipole is obtained by expanding Eq. (3.72) in m_i and only retaining the logarithmic divergent terms,

$$\begin{aligned} D_{ia}^{(\text{sub})}(\tilde{\Phi}_n) &= \left[\frac{c_\epsilon}{\epsilon} + \ln \left(\frac{\mu^2}{m_a^2} \right) \right] \left[2 + \ln(\mu_i^2) - 2 \ln(\bar{\mu}^2) \right] \\ &\quad + 4 \text{Li}_2(-\mu_{ia}) - \frac{1}{2} \ln^2(\mu_i^2) + 2 \ln^2(\bar{\mu}^2) - 2 \ln \left(\frac{1 - \mu_{ia}}{1 + \mu_{ia}} \right) \\ &\quad - 3 \ln(1 - \mu_{ia}) + \frac{1}{2} \ln(\mu_i^2) - \frac{\pi^2}{3} + \frac{3}{2} + \mathcal{O}(\epsilon). \end{aligned} \quad (3.73)$$

The result using full mass regularization also for the soft singularities is then given by the reverse application of the replacement (3.65). The corresponding result with exactly massless fermions and the collinear singularities regularized using dimensional regularisation is discussed in the next section.

3.4.3. Subtraction function for massless final-state fermions

In the case where fermion masses are set to zero and the collinear singularities are regularised using dimensional regularisation, the asymptotic behaviour in the collinear limit is given by

Eq. (3.45) and the subtraction function is defined as

$$d_{ia}^{(\text{sub})}(p_i, p_a, k) = \frac{1}{R_{ia}(y_{ia})} \left\{ \frac{1}{p_i \cdot k} \left[\frac{2}{1 - z_{ia}(1 - y_{ia})} - 1 - z_{ia} - \epsilon(1 - z_{ia}) \right] - \frac{4}{m_a^2(1 - \mu_{ia}^2)^2} \frac{1}{[1 - z_{ia}(1 - y_{ia})]^2} \right\}. \quad (3.74)$$

For a massless final-state fermion ($m_i \equiv 0$), the photonic part of the phase space (3.58) simplifies as follows

$$[dk(\tilde{p}_i, \tilde{P}_{ia})] = \frac{1}{16\pi^2} \frac{(4\pi)^\epsilon}{\Gamma(1 - \epsilon)} [m_a^2(1 - \mu_{ia}^2)]^{1-\epsilon} \int_0^{y^+} dy_{ia} (1 - y_{ia})^{1-2\epsilon} y_{ia}^{-\epsilon} \times \int_{z_-(y_{ia})}^{z_+(y_{ia})} dz_{ia} [z_+(y_{ia}) - z_{ia}]^{-\epsilon} [z_{ia} - z_-(y_{ia})]^{-\epsilon}, \quad (3.75)$$

with the integration boundaries given by

$$y^+ = \frac{1 - \mu_{ia}}{1 + \mu_{ia}}, \quad z_{\pm}(y_{ia}) = \frac{1}{2} \left(1 \pm \frac{R(y_{ia})}{1 - y_{ia}} \right). \quad (3.76)$$

Performing the analogous decomposition of $D_{ia}^{(\text{sub})}$ as in Eq. (3.60), we obtain

$$\begin{aligned} D_{ia}^{(\text{eik})}(\tilde{\Phi}_n) &= \int [dk(\tilde{p}_i, \tilde{P}_{ia})] \frac{16\pi^2 \mu^{2\epsilon}}{(p_i \cdot k) R_{ia}(y_{ia})} \frac{1}{1 - z_{ij}(1 - y_{ij})}, \\ &= \frac{c_\epsilon}{\epsilon^2} + \frac{c_\epsilon}{\epsilon} \left[\ln \left(\frac{\mu^2}{m_a^2} \right) - 2 \ln(1 - \mu_{ia}^2) \right] + 4 \text{Li}_2(-\mu_{ia}) \\ &\quad + \frac{1}{2} \left[\ln \left(\frac{\mu^2}{m_a^2} \right) - 2 \ln(1 - \mu_{ia}^2) \right]^2 - \frac{\pi^2}{3} + \mathcal{O}(\epsilon), \end{aligned} \quad (3.77a)$$

$$\begin{aligned} D_{ia}^{(\text{coll})}(\tilde{\Phi}_n) &= \int [dk(\tilde{p}_i, \tilde{P}_{ia})] \frac{-8\pi^2 \mu^{2\epsilon}}{(p_i \cdot k) R_{ia}(y_{ia})} [1 + z_{ia} + \epsilon(1 - z_{ia})] \\ &= \frac{3}{2} \left[\frac{c_\epsilon}{\epsilon} + \ln \left(\frac{\mu^2}{m_a^2} \right) \right] - 3 \ln(1 - \mu_{ia}) + \frac{7}{2} - 6 \frac{\mu_{ia}^2}{1 - \mu_{ia}^2} + \mathcal{O}(\epsilon), \end{aligned} \quad (3.77b)$$

$$\begin{aligned} D_{ia}^{(\text{eik}')}(\tilde{\Phi}_n) &= \int [dk(\tilde{p}_i, \tilde{P}_{ia})] \frac{-32\pi^2 \mu^{2\epsilon}}{m_a^2 \bar{\mu}^4 R_{ia}(y_{ia})} \frac{1}{[1 - z_{ia}(1 - y_{ia})]^2} \\ &= \frac{1}{\epsilon} + \ln \left(\frac{\mu^2}{m_a^2} \right) - 2 \ln \left(\frac{1 - \mu_{ia}}{1 + \mu_{ia}} \right) + \mathcal{O}(\epsilon). \end{aligned} \quad (3.77c)$$

The term $D_{ia}^{(\text{eik}')}$ can be inferred from Eq. (3.70) by taking the limit $\mu_i \rightarrow 0$, which was found to be in agreement with the result obtained by a separate direct calculation. The final result for the integrated decay dipole $D_{ia}^{(\text{sub})}$ in dimensional regularisation then reads

$$D_{ia}^{(\text{sub})}(\tilde{\Phi}_n) = \frac{c_\epsilon}{\epsilon^2} + \frac{c_\epsilon}{\epsilon} \left[\frac{5}{2} + \ln \left(\frac{\mu^2}{m_a^2} \right) - 2 \ln(1 - \mu_{ia}^2) \right]$$

$$\begin{aligned}
& + 4 \operatorname{Li}_2(-\mu_{ia}) + \frac{1}{2} \left[\frac{5}{2} + \ln \left(\frac{\mu^2}{m_a^2} \right) - 2 \ln(1 - \mu_{ia}^2) \right]^2 \\
& + 7 \ln(1 + \mu_{ia}) - \frac{\pi^2}{3} + \frac{3}{8} - 6 \frac{\mu_{ia}^2}{1 - \mu_{ia}^2} + \mathcal{O}(\epsilon).
\end{aligned} \tag{3.78}$$

Alternatively, this result can be obtained from Eq. (3.73) by performing a transition between the regularization schemes using the results of Ref. [130].

3.4.4. Extension to non-collinear-safe observables

The extension to non-collinear-safe observables is only relevant in the case of a light fermion mass m_i . Since the observable explicitly depends on the collinear splitting of the fermion into a fermion–photon pair described by the variable $z \equiv z_{ia}$, the integration over z cannot be performed analytically. Therefore, the order of integration in the variables y_{ia} and z_γ in the photonic phase-space (3.58) needs to be interchanged, and the integration in the collinear-splitting variable $z_{ia} = (1 - z_\gamma)$ is left open for a later numerical evaluation.

The final result can be brought into the following form,

$$\begin{aligned}
& \int d\Phi_{n+\gamma} |\mathcal{M}_{\text{sub},ia}(\Phi_{n+\gamma})|^2 \Delta\Theta_{\text{cut}}(\tilde{\Phi}_{n,ia} | z_{ia}) \\
& = -\frac{\alpha}{2\pi} \eta_i Q_i \eta_j Q_j \int d\tilde{\Phi}_n |\mathcal{M}_0(\tilde{\Phi}_n)|^2 \\
& \quad \times \int_0^1 dz \left[\bar{\mathcal{D}}_{ia}^{(\text{sub})}(\tilde{\Phi}_n, z) \right]_+ \Theta_{\text{cut}}(\tilde{\Phi}_n | p_i = z \tilde{p}_i, k = (1 - z) \tilde{p}_i),
\end{aligned} \tag{3.79}$$

where the function $\bar{\mathcal{D}}_{ia}^{(\text{sub})}$ is obtained after carrying out the analytical integration over the dipole variable y_{ia} . We decompose $\bar{\mathcal{D}}_{ia}^{(\text{sub})}$ into three contributions as in Eq. (3.60) and the parts associated with $\bar{\mathcal{D}}_{ia}^{(\text{eik})}$ and $\bar{\mathcal{D}}_{ia}^{(\text{coll})}$ can be directly taken over from the case of a final-state emitter and spectator,

$$\begin{aligned}
& \bar{\mathcal{D}}_{ia}^{(\text{eik})}(\tilde{\Phi}_n, z) + \bar{\mathcal{D}}_{ia}^{(\text{coll})}(\tilde{\Phi}_n, z) \\
& = -\left(\frac{1+z^2}{1-z} \right) \ln \left(\frac{\mu_i^2}{z(1-\mu_{ia}^2)} [1 - \eta(z)] \right) + (1+z) \ln(1-z) - \frac{2z}{1-z} \\
& \quad + (1+z) \ln \left(1 + \frac{\bar{\mu}_{ia}^2}{\eta(z)} \right) - \frac{2}{(1-z)\sigma(z)} \left\{ \ln \left(1 + \frac{\eta(z)[1 - z\eta(z)]}{\bar{\mu}_{ia}^2(1-z)} \right) \right. \\
& \quad \left. - 2 \ln \left(1 - \frac{2z\eta(z)}{1 + \sigma(z)} \right) + \sigma(z) \ln \left(\frac{\bar{\mu}_{ia}^2}{\eta(z)} (1-z) \right) \right\},
\end{aligned} \tag{3.80}$$

as given in Ref. [134] with

$$\eta(z) = \begin{cases} [1 - y_+(z)] z & \text{for } z < \frac{1}{2}, \\ [1 - y_+(z)] (1 - z) & \text{for } \frac{1}{2} < z. \end{cases}, \quad \sigma(z) = \sqrt{1 + 4\bar{\mu}_{ia}^2 z(1-z)}. \tag{3.81}$$

The remaining term $\bar{\mathcal{D}}_{ia}^{(\text{eik}')}$ is IR finite, since all soft singularities were isolated via the plus prescription as described in Eq. (3.10) and the mass divergences are fully contained in Eq. (3.80).

We can therefore perform the integration of this part without regulators ($\epsilon = 0$, $m_i = 0$) and, using the phase-space parametrisation given in Appendix A of [134], we arrive at the following expression

$$\bar{\mathcal{D}}_{ia}^{(\text{eik}')}(\tilde{\Phi}_n, z) = -\frac{2}{(1 - \mu_{ia}^2)} \int_0^{y_+(z)} dy_{ia} \frac{(1 - y_{ia})}{R_{ia}(y_{ia})} \frac{1}{[1 - z_{ia}(1 - y_{ia})]^2}, \quad (3.82)$$

where the upper integration boundary is given by

$$y_+(z) = \left[\xi(z) + 1 + \sqrt{\xi(z)[\xi(z) + 2]} \right]^{-1}, \quad \xi(z) = \frac{\mu_{ia}^2}{2(1 - \mu_{ia}^2)z(1 - z)}. \quad (3.83)$$

Performing the substitution $x(y) = 1 - y_{ia} - R_{ia}(y_{ia})$ and further introducing the abbreviation $\bar{\mu}_{ia}^2 = \frac{\mu_{ia}^2}{1 - \mu_{ia}^2}$, we obtain

$$\bar{\mathcal{D}}_{ia}^{(\text{eik}')}(\tilde{\Phi}_n, z) = -\frac{2}{(1 - \mu_{ia}^2)} \int_0^{2\eta(z)} dx \frac{x^2 + 4\bar{\mu}_{ia}^2}{[-zx^2 + 2x + 4\bar{\mu}_{ia}^2(1 - z)]^2}. \quad (3.84)$$

The roots of the quadratic form appearing in the denominator of the integrand in Eq. (3.84) are determined as $x_{1,2} = (1 \pm \sigma(z))/2$ and performing the substitution $a(x) = 1 - xz$ we obtain

$$\begin{aligned} \bar{\mathcal{D}}_{ia}^{(\text{eik}')}(\tilde{\Phi}_n, z) &= \frac{4}{z(1 - \mu_{ia}^2)} \int_{1-2z\eta(z)}^1 da \left\{ \frac{1}{[\sigma(z) - a][\sigma(z) + a]} - \frac{2(1 - a + 2\bar{\mu}_{ia}^2 z)}{[\sigma(z) - a]^2[\sigma(z) + a]^2} \right\} \\ &= \frac{2}{z(1 - \mu_{ia}^2)} \int_{1-2z\eta(z)}^1 da \left\{ \frac{1}{\sigma(z)} \left[\frac{1}{[\sigma(z) - a]} + \frac{1}{[\sigma(z) + a]} \right] \left[1 - \frac{1 + 2\bar{\mu}_{ia}^2 z}{\sigma(z)^2} \right] \right. \\ &\quad \left. - \frac{1 + 2\bar{\mu}_{ia}^2 z - \sigma(z)}{\sigma(z)^2} \frac{1}{[\sigma(z) - a]^2} - \frac{1 + 2\bar{\mu}_{ia}^2 z + \sigma(z)}{\sigma(z)^2} \frac{1}{[\sigma(z) + a]^2} \right\} \\ &= \frac{2}{(1 - \mu_{ia}^2)\sigma(z)^2} \left\{ \frac{2\bar{\mu}_{ia}^2(1 - 2z)}{\sigma(z)} \ln \left(\frac{2\bar{\mu}_{ia}^2(1 - z) + \eta(z)[1 + \sigma(z)]}{2\bar{\mu}_{ia}^2(1 - z) + \eta(z)[1 - \sigma(z)]} \right) \right. \\ &\quad \left. - \frac{1}{1 - z} - \frac{1}{1 - z[1 - y_+(z)]} \left(\bar{\mu}_{ia}^2 + \eta(z) - \frac{\bar{\mu}_{ia}^2(1 + \bar{\mu}_{ia}^2)}{\bar{\mu}_{ia}^2 + \eta(z)} \right) \right\}. \end{aligned} \quad (3.85)$$

As the final result we can write the extra term

$$\begin{aligned} &\int d\Phi_{n+\gamma} |\mathcal{M}_{\text{sub},ia}(\Phi_{n+\gamma})|^2 \Delta\Theta_{\text{cut}}(\tilde{\Phi}_{n,ia} | z_{ia}) \\ &= -\frac{\alpha}{2\pi} \eta_i Q_i \eta_j Q_j \int d\tilde{\Phi}_n |\mathcal{M}_0(\tilde{\Phi}_n)|^2 \\ &\quad \times \int_0^1 dz \left[\bar{\mathcal{D}}_{ia}^{(\text{sub})}(\tilde{\Phi}_n, z) \right]_+ \Theta_{\text{cut}}(\tilde{\Phi}_n | p_i = z\tilde{p}_i, k = (1 - z)\tilde{p}_i) \end{aligned} \quad (3.86)$$

where the function $\bar{\mathcal{D}}_{ia}^{(\text{sub})}$ reads

$$\bar{\mathcal{D}}_{ia}^{(\text{sub})}(z) = \bar{\mathcal{D}}_{ia}^{(\text{eik})}(z) + \bar{\mathcal{D}}_{ia}^{(\text{coll})}(z) + \bar{\mathcal{D}}_{ia}^{(\text{eik}')}(\tilde{\Phi}_n, z)$$

$$\begin{aligned}
&= - \left(\frac{1+z^2}{1-z} \right) \ln \left(\frac{\mu_i^2}{z(1-\mu_{ia}^2)} [1-\eta(z)] \right) + (1+z) \ln(1-z) - \frac{2z}{1-z} \\
&\quad + (1+z) \ln \left(1 + \frac{\bar{\mu}_{ia}^2}{\eta(z)} \right) - \frac{2}{(1-z)\sigma(z)} \left\{ \ln \left(1 + \frac{\eta(z)[1-z\eta(z)]}{\bar{\mu}_{ia}^2(1-z)} \right) \right. \\
&\quad \left. - 2 \ln \left(1 - \frac{2z\eta(z)}{1+\sigma(z)} \right) + \sigma(z) \ln \left(\frac{\bar{\mu}_{ia}^2}{\eta(z)} (1-z) \right) \right\} \\
&\quad + \frac{2}{(1-\mu_{ia}^2)\sigma(z)^2} \left\{ \frac{2\bar{\mu}_{ia}^2(1-2z)}{\sigma(z)} \ln \left(\frac{2\bar{\mu}_{ia}^2(1-z) + \eta(z)[1+\sigma(z)]}{2\bar{\mu}_{ia}^2(1-z) + \eta(z)[1-\sigma(z)]} \right) \right. \\
&\quad \left. - \frac{1}{1-z} - \frac{1}{1-z[1-y_+(z)]} \left(\bar{\mu}_{ia}^2 + \eta(z) - \frac{\bar{\mu}_{ia}^2(1+\bar{\mu}_{ia}^2)}{\bar{\mu}_{ia}^2 + \eta(z)} \right) \right\}. \tag{3.87}
\end{aligned}$$

Pole expansion of the NLO $\mathcal{O}(\alpha)$ corrections to Drell–Yan processes

In this chapter we discuss the computation of the NLO EW corrections to the processes in Eqs. (2.5) in the vicinity of an intermediate vector-boson resonance, $(k_1 + k_2)^2 \approx M_V^2$ (see Fig. 2.2 for the leading-order diagram). We classify and calculate the corrections to the cross section that are enhanced by resonance factors

$$\left[p_V^2 - M_V^2 + iM_V\Gamma_V \right]^{-1} \sim \mathcal{O}\left(\frac{1}{M_V\Gamma_V}\right), \quad p_V^2 - M_V^2 = \mathcal{O}(M_V\Gamma_V) \quad (4.1)$$

where $p_V = k_1 + k_2$ and Γ_V is the decay width of the vector-boson resonance. The exact NLO EW corrections to the processes (2.5) are known [34–45], but we discuss the pole expansion in some detail in order to introduce the concept employed in the computation of the $\mathcal{O}(\alpha_s\alpha)$ corrections in Part II and in order to establish the numerical accuracy of the PA. This PA is based on the leading term in the expansion of all cross-section contributions about the vector-boson resonance.

After describing the general concept of the PA in Sect. 4.1, which classifies the corrections into the so-called factorizable and non-factorizable corrections, we present the calculation of the respective contributions in Sect. 4.2. The cancellation of IR singularities will be discussed in Sect. 4.3, where we provide the final result in a form suitable for numerical evaluation. Section 4.4 briefly reviews the calculation and the results for the NLO QCD corrections, which are needed as building block at $\mathcal{O}(\alpha_s\alpha)$ later. In Sect. 4.5 we compare the numerical results of the PA to the full NLO result, revealing agreement at the level of fractions of 1% in the resonance regions. We, therefore, can expect an approximation of the full $\mathcal{O}(\alpha_s\alpha)$ corrections by the PA at the level of $\sim 0.1\%$, which is more than sufficient for phenomenology. The results presented in this chapter have been published to a large extent in Ref. [87].

4.1. Concept of the pole expansion

The general idea [119, 153] of a PA for any Feynman diagram with a single resonance is the systematic isolation of all parts that are enhanced by a resonance factor (4.1). For W production different variants of PAs have been suggested and discussed at NLO already in Refs. [37, 154, 155]. For the virtual corrections we follow the PA approach of Ref. [37]. In that reference the real-emission corrections were evaluated on the basis of the full amplitudes without further approximations. After a proper cancellation of IR singularities between the real and virtual corrections, the PA was then applied only to the finite remainder of the virtual corrections. In order to be able to calculate and discuss the different contributions of factorizable (production and decay) and non-factorizable corrections separately, a consistent application of the PA also

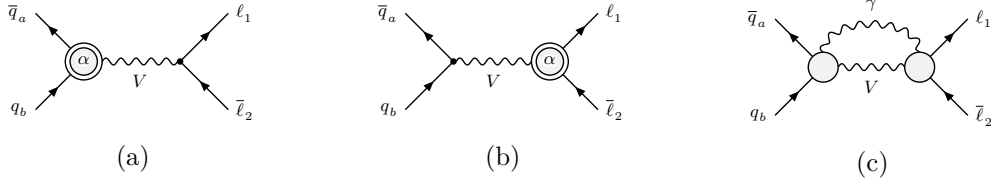


Figure 4.1.: Generic diagrams for the EW virtual NLO factorizable corrections to production (a) and decay (b), as well as for virtual non-factorizable corrections (c), where the empty blobs stand for all relevant tree structures and the ones with “ α ” inside for one-loop corrections of $\mathcal{O}(\alpha)$.

in the real corrections is required. Here, we follow Ref. [156] for the pole expansion for the real corrections in order to prepare for the extension to the mixed QCD–EW corrections. We do not apply the PA to the LO cross section, which is kept without approximation.

Schematically, each transition amplitude for the processes (2.3) has the form

$$\mathcal{M} = \frac{W(p_V^2)}{p_V^2 - M_V^2 + \Sigma(p_V^2)} + N(p_V^2), \quad (4.2)$$

with functions W and N describing resonant and non-resonant parts, respectively, and Σ denoting the self-energy of V . The resonant contributions of \mathcal{M} are isolated in a gauge-invariant way as follows,

$$\mathcal{M} = \frac{W(\mu_V^2)}{p_V^2 - \mu_V^2} \frac{1}{1 + \Sigma'(\mu_V^2)} + \left[\frac{W(p_V^2)}{p_V^2 - M_V^2 + \Sigma(p_V^2)} - \frac{W(\mu_V^2)}{p_V^2 - \mu_V^2} \frac{1}{1 + \Sigma'(\mu_V^2)} \right] + N(p_V^2), \quad (4.3)$$

where

$$\mu_V^2 = M_V^2 - iM_V\Gamma_V \quad (4.4)$$

is the gauge-invariant location of the propagator pole in the complex p_V^2 plane [118, 157, 158]. Equation (4.3) can serve as a basis for the gauge-invariant introduction of the finite decay width in the resonance propagator, thereby defining the so-called *pole scheme*. In this scheme the term in square brackets is perturbatively expanded in the coupling α including terms up to $\mathcal{O}(\alpha)$, while the full p_V^2 dependence is kept. An application of this scheme to Z-boson production is, e.g., described in Ref. [45] in detail.

The PA for the amplitude results from the r.h.s. of Eq. (4.3) upon neglecting the last, non-resonant term and asymptotically expanding the term in square brackets in p_V^2 about the point $p_V^2 = \mu_V^2$, where only the leading, resonant term of the expansion is kept. The first term on the r.h.s. of (4.3) defines the so-called *factorizable* corrections in which on-shell production and decay amplitudes for V are linked by the off-shell propagator; these contributions are illustrated by diagrams (a) and (b) of Fig. 4.1. The term on the r.h.s. of Eq. (4.3) in square brackets contains the so-called *non-factorizable* corrections which receive resonant contributions from all diagrams where the limit $p_V^2 \rightarrow \mu_V^2$ in $W(p_V^2)$ or $\Sigma'(p_V^2)$ would lead to (infrared) singularities. At NLO, this happens if a soft photon of energy $E_\gamma \lesssim \Gamma_V$ is exchanged among the production process, the decay part, and the intermediate V bosons; a generic loop diagram is shown in Fig. 4.1(c). Figure 4.2 shows the real-photon emission counterparts of the one-loop corrections displayed in Fig 4.1.

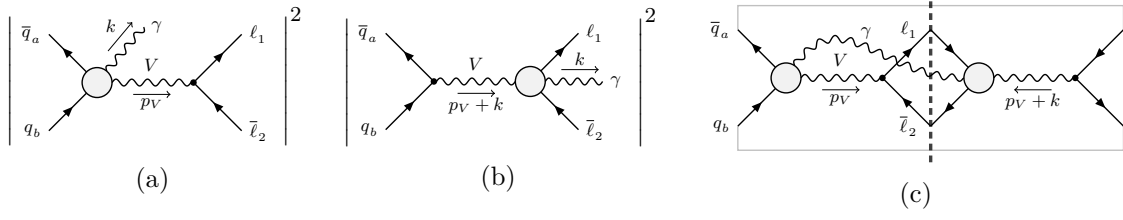


Figure 4.2.: Generic diagrams for the real photonic NLO factorizable corrections to production (a) and decay (a), as well as for real non-factorizable corrections (a), where the blobs stand for all relevant tree structures.

4.2. Calculation of the $\mathcal{O}(\alpha)$ corrections in the pole approximation

4.2.1. Virtual corrections

In this section we discuss the virtual NLO EW corrections to the processes (2.5). After briefly reviewing the structure of the full NLO EW results, we move on to consider the calculation of the corrections in the PA in more detail.

Full NLO EW results

The exact NLO EW corrections to the processes (2.5) are known [34–45] and were implemented independently into our Monte Carlo program using the complex-mass scheme [159, 160] for the treatment of the unstable intermediate gauge boson. In case of the charged-current processes, the virtual corrections can be expressed in terms of a correction factor δ^{virt} multiplying the Born amplitude,

$$\delta \mathcal{M}_{\text{Vew}}^{\bar{d}_i u_j \rightarrow \nu_\ell \ell^+} = \delta^{\text{virt}} \mathcal{M}_0^{\bar{d}_i u_j \rightarrow \nu_\ell \ell^+}, \quad (4.5)$$

with δ^{virt} defined in Eq. (2.10) of Ref. [37]. For the neutral-current process the virtual corrections do not factorize completely from the Born amplitude due to the additional dependence of the corrections on the chiral coupling structure. Using the definition of the form factors $f_{q\bar{q},\text{phot}}^{\text{virt},\tau_q\tau_\ell}$ and $f_{q\bar{q},\text{weak}}^{\text{virt},\tau_q\tau_\ell}$ given in Eqs. (3.4) and (3.26) of Ref. [45], the virtual corrections to the neutral-current process can be written in the following form,

$$\delta \mathcal{M}_{\text{Vew}}^{\bar{q}q \rightarrow \ell^- \ell^+} = \left(f_{q\bar{q},\text{phot}}^{\text{virt},\tau_q\tau_\ell} + f_{q\bar{q},\text{weak}}^{\text{virt},\tau_q\tau_\ell} \right) \mathbb{A}_0^{\tau_q\tau_\ell}, \quad (4.6)$$

with the standard matrix element $\mathbb{A}_0^{\tau_q\tau_\ell}$ given in Eq. (2.10).

The NLO EW corrections in the PA

The *factorizable* virtual corrections are defined as the product of the on-shell matrix elements of V -boson production and decay times the off-shell V -boson propagator, as illustrated in

Figs. 4.1(a,b),

$$\begin{aligned} \delta\mathcal{M}_{V_{\text{ew}},\text{fact}}^{\bar{q}_a q_b \rightarrow \ell_1 \bar{\ell}_2} &= \sum_{\lambda_V} \frac{\delta\mathcal{M}_{V_{\text{ew}}}^{\bar{q}_a q_b \rightarrow V}(\lambda_V) \mathcal{M}_0^{V \rightarrow \ell_1 \bar{\ell}_2}(\lambda_V) + \mathcal{M}_0^{\bar{q}_a q_b \rightarrow V}(\lambda_V) \delta\mathcal{M}_{V_{\text{ew}}}^{V \rightarrow \ell_1 \bar{\ell}_2}(\lambda_V)}{p_V^2 - \mu_V^2} \\ &\equiv \delta\mathcal{M}_{V_{\text{ew}},\text{prod}}^{\bar{q}_a q_b \rightarrow \ell_1 \bar{\ell}_2} + \delta\mathcal{M}_{V_{\text{ew}},\text{dec}}^{\bar{q}_a q_b \rightarrow \ell_1 \bar{\ell}_2}, \end{aligned} \quad (4.7)$$

where the sum over the physical polarization states λ_V of the vector boson V encodes the proper spin correlation. Here \mathcal{M}_0 and $\delta\mathcal{M}_{V_{\text{ew}}}$ denote tree-level and EW one-loop amplitudes, respectively, and the two amplitudes defined in the last step correspond to the two terms appearing in the numerator. Care has to be taken that the sub-amplitudes appearing on either side of the V resonance are evaluated for on-shell V bosons, otherwise gauge invariance cannot be guaranteed. For the $\mathcal{O}(\alpha)$ approximation, the use of the problematic complex value $p_V^2 = \mu_V^2$ in the on-shell condition of the sub-amplitudes is not necessary, so that we have set $p_V^2 = M_V^2$ in the numerator of the first term of Eq. (4.3) in order to obtain Eq. (4.7). Similarly, the conventional on-shell renormalization scheme (see Sect. 1.1.2) can be used where the real part of the residue of the propagator is normalized to one at $p_V^2 = M_V^2$. Furthermore, the gauge-boson width Γ_V can be set to zero in the self-energy in the $\mathcal{O}(\alpha)$ approximation, so that the residue correction $(1 + \Sigma')^{-1}$ in Eq. (4.3) reduces to one in the on-shell renormalization scheme and does not appear in Eq. (4.7). The factorizable corrections to the production and decay sub-processes are therefore given by the virtual corrections to the $V\bar{q}_a q$ and $V\bar{\ell}_1 \ell_2$ vertices, respectively. The one-loop amplitudes defined in the last line of Eq. (4.7) can be written in the following form,

$$\delta\mathcal{M}_{V_{\text{ew}},\text{prod}}^{\bar{q}_a q_b \rightarrow \ell_1 \bar{\ell}_2} = \delta_{c_a c_b} \hat{F}_{V\bar{q}_a q_b}^{\tau_q}(M_V^2) \mathcal{A}_{V0,\tau_q\tau_\ell}^{\bar{q}_a q_b \rightarrow \ell_1 \bar{\ell}_2} \equiv \delta_{V_{\text{ew}}(\tau_q)}^{\text{prod}} \mathcal{M}_{0,\text{PA}}^{\bar{q}_a q_b \rightarrow \ell_1 \bar{\ell}_2}, \quad (4.8a)$$

$$\delta\mathcal{M}_{V_{\text{ew}},\text{dec}}^{\bar{q}_a q_b \rightarrow \ell_1 \bar{\ell}_2} = \delta_{c_a c_b} \hat{F}_{V\bar{\ell}_1 \ell_2}^{\tau_\ell}(M_V^2) \mathcal{A}_{V0,\tau_q\tau_\ell}^{\bar{q}_a q_b \rightarrow \ell_1 \bar{\ell}_2} \equiv \delta_{V_{\text{ew}}(\tau_\ell)}^{\text{dec}} \mathcal{M}_{0,\text{PA}}^{\bar{q}_a q_b \rightarrow \ell_1 \bar{\ell}_2}, \quad (4.8b)$$

where $\hat{F}_{V\bar{f}f'}^\tau$ denotes the renormalized $\mathcal{O}(\alpha)$ form factor to the $V\bar{f}f'$ vertex which is evaluated at its on-shell point, $p_V^2 = M_V^2$. The explicit expressions for $\hat{F}_{V\bar{f}f'}^\tau$ are given in Appendix B.2 for $V = W, Z$, and the one-loop sub-graphs that appear inside the blobs of the generic Feynman diagrams of Figs. 4.1(a,b) are shown in Fig. B.3 for the charged-current and in Figs. B.4 and B.5 for the neutral-current processes. The subscript PA on the lower-order matrix element in Eq. (4.8) indicates that the non-resonant photon-exchange diagrams are not included in case of the neutral-current Drell–Yan process, i.e. the second term in Eq. (2.8c) is omitted. We have further introduced the short hand notation $\delta_{V_{\text{ew}}(\tau_q)}^{\text{prod}}$ and $\delta_{V_{\text{ew}}(\tau_\ell)}^{\text{dec}}$ for the factorizable virtual corrections to the production and decay vertices, respectively, and indicate the additional dependence on the chiral coupling structure by the additional labels $\tau_{q/\ell}$. As already mentioned above, the amplitudes \mathcal{M}_0 and $\delta\mathcal{M}_{V_{\text{ew}}}$ in Eq. (4.7) must be evaluated for on-shell V bosons and therefore, also the amplitude $\mathcal{M}_{0,\text{PA}}$ appearing on the r.h.s. of Eqs. (4.8) must be evaluated with on-shell kinematics, except for the gauge-boson momentum in the resonant propagator which is kept off shell. The *on-shell projection* $p_V^2 \rightarrow M_V^2$ has to be defined carefully and is not unique, because the phase space is parametrized by more than one variable. Different variants may lead to results that differ within the intrinsic uncertainty of the PA, which is of $\mathcal{O}(\alpha/\pi \times \Gamma_V/M_V)$ in the resonance region when applied to $\mathcal{O}(\alpha)$ corrections. Despite this freedom in the choice of the specific on-shell projection, care has to be taken that virtual and real corrections still match properly in the (soft and collinear) infrared limits in order to guarantee the cancellation of the

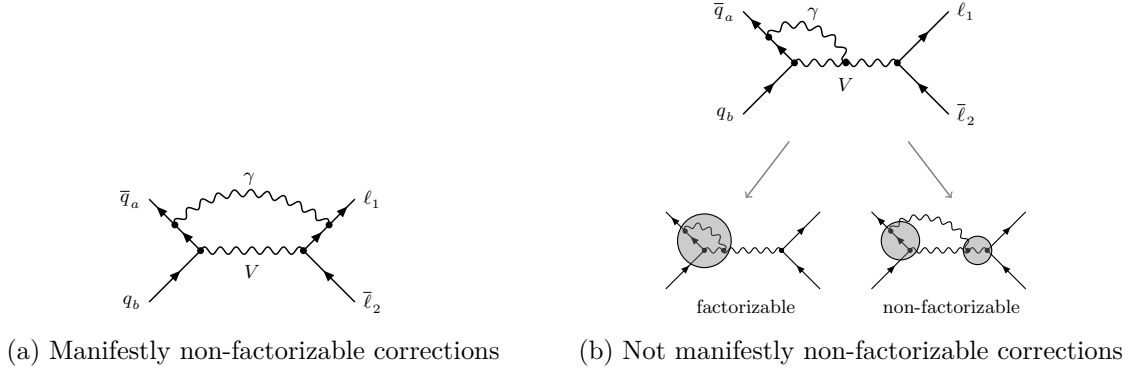


Figure 4.3.: Example diagrams illustrating the manifestly non-factorizable corrections (a), and contributions that contain both, factorizable and non-factorizable corrections (b).

corresponding singularities.

The *non-factorizable* corrections involve contributions for which the production and decay sub-processes do not proceed independently and is illustrated in Fig. 4.1(c) for the case of virtual corrections. The manifestly non-factorizable corrections, for instance given by the diagram in Fig. 4.3(a), do not contain an explicit propagator factor $(p_V^2 - \mu_V^2)^{-1}$ before the loop integration. As shown in Ref. [156] by power-counting arguments, a resonant contribution of such diagrams is connected to the soft-photon exchange between the production and decay sub-processes and involves IR singularities, while the exchange of massive particles (such as Z bosons) or highly-energetic photons between production and decay leads to non-resonant corrections only. Diagrams with photons coupled to the intermediate vector boson V contribute to both the factorizable and non-factorizable corrections. The factorizable part of those diagrams is obtained upon setting the vector-boson momentum p_V on its mass shell in the loop containing the photon. This attributes this contribution either to on-shell production or on-shell decay of the V boson, which are already contained in the correction factors $\delta_{V_{ew}}^{\text{prod}}(\tau_q)$ and $\delta_{V_{ew}}^{\text{dec}}(\tau_\ell)$ defined in Eqs. (4.8). The difference between the full amplitude of diagrams like Fig. 4.3(b) and its factorizable part (4.7) defines their non-factorizable contributions, which result from the fact that setting p_V on shell in the loop creates artificial soft singularities,

$$\delta\mathcal{M}_{V_{ew},nf}^{\bar{q}_a q_b \rightarrow \ell_1 \bar{\ell}_2} = \left\{ \delta\mathcal{M}_{V_{ew}}^{\bar{q}_a q_b \rightarrow \ell_1 \bar{\ell}_2} - \delta\mathcal{M}_{V_{ew},\text{fact}}^{\bar{q}_a q_b \rightarrow \ell_1 \bar{\ell}_2} \right\}_{p_V^2 \rightarrow M_V^2}. \quad (4.9)$$

In fact the whole non-factorizable part receives only resonant contributions from soft-photon exchange and entirely results from the non-commutativity of the on-shell and soft-photon limits. The explicit evaluation of the non-factorizable corrections proceeds by applying the so-called “extended soft-photon approximation” (ESPA). It differs from the usual soft-photon approximation by keeping the exact dependence on the photon momentum q in propagators intact where $q \rightarrow 0$ would lead to further singularities, but setting $q = 0$ in all other regular factors. The complex mass μ_V is used in the gauge-boson propagators throughout, but the limits $p_V^2, \mu_V^2 \rightarrow M_V^2$ are taken whenever they do not lead to divergences. In particular, the soft photon momentum cannot be neglected in the resonant gauge-boson propagators since the scalar product $(p_V \cdot q)$ is of the same order as the virtuality $(p_V^2 - \mu_V^2) \sim M_V \Gamma_V$. In the numerators, all photon momenta are negligible, reducing the occurrence of loop integrals to scalar

integrals only. For the not manifestly non-factorizable corrections, e.g. given by the diagram in Fig. 4.3(b), the scalar integrals appearing in those corrections are expanded around the resonance ($p_V^2 \approx M_V^2$). This allows to identify and cancel the factorizable contributions in the difference of Eq. (4.9) and further isolates the remaining resonant non-factorizable contributions. The expansion of the scalar integrals was performed using the Mellin–Barnes method as described in Appendix B.1.1, and the explicit expressions of the loop integrals relevant for the calculation of the non-factorizable corrections in this work are summarized in Appendix B.1.2. The non-factorizable corrections factorize from the lower-order amplitude, as a direct consequence of the property of the corrections in the soft limit,

$$\delta \mathcal{M}_{V_{\text{ew,nf}}}^{\bar{q}_a q_b \rightarrow \ell_1 \bar{\ell}_2} = \delta_{V_{\text{ew,nf}}}^{\bar{q}_a q_b \rightarrow \ell_1 \bar{\ell}_2} \mathcal{M}_{0,\text{PA}}^{\bar{q}_a q_b \rightarrow \ell_1 \bar{\ell}_2}. \quad (4.10)$$

All one-loop diagrams that enter into the calculation of the correction factor $\delta_{V_{\text{ew,nf}}}^{\bar{q}_a q_b \rightarrow \ell_1 \bar{\ell}_2}$ are given in Eq. (B.37) together with the intermediate result expressed in terms of scalar integrals. Equation (B.37) can be further simplified to the following expression,

$$\begin{aligned} \delta_{V_{\text{ew,nf}}}^{\bar{q}_a q_b \rightarrow \ell_1 \bar{\ell}_2} = & -\frac{\alpha}{2\pi} \sum_{\substack{i=a,b \\ f=1,2}} \eta_i Q_i \eta_f Q_f \left\{ 2 + \text{Li}_2 \left(1 + \frac{M_V^2}{t_{if}} \right) \right. \\ & \left. + \left[\frac{c_\epsilon}{\epsilon} - 2 \ln \left(\frac{\mu_V^2 - s_{12}}{\mu M_V} \right) \right] \left[1 - \ln \left(\frac{M_V^2}{-t_{if}} \right) \right] \right\}, \end{aligned} \quad (4.11)$$

where $s_{12} = (k_1 + k_2)^2$, $t_{if} = (p_i - k_f)^2$, and $\eta_i = 1$ for incoming particles and outgoing antiparticles and $\eta_i = -1$ for incoming antiparticles and outgoing particles as defined in Sect. 1.3.2. For W production this result was already given in Ref. [37]. Note that all collinear singularities cancel in the non-factorizable corrections and only a soft singularity remains. In case of neutral-current processes, all terms in Eq. (4.11) that do not depend on the indices i or f vanish due to charge conservation,

$$Q_{V=Z} = \sum_{i=a,b} \eta_i Q_i = - \sum_{f=1,2} \eta_f Q_f = 0. \quad (4.12)$$

4.2.2. Real corrections

This section describes the calculation of the real-emission corrections given by the process $\bar{q}_a q_b \rightarrow \ell_1 \bar{\ell}_2 \gamma$ with an additional photon in the final state. The corresponding Feynman graphs are shown in Fig. 4.4 and can be classified into the diagrams where the photon is emitted from the incoming quarks (a), the final-state leptons (c), and in the case of the charged-current process also from the intermediate gauge boson (b). The photon-induced processes $\gamma q_b \rightarrow \ell_1 \bar{\ell}_2 q_a$, $\gamma \bar{q}_a \rightarrow \ell_1 \bar{\ell}_2 \bar{q}_b$, which appear in $\mathcal{O}(\alpha)$ as well, are not considered here. As discussed in Refs. [42, 44, 45] they deliver only small corrections at $\mathcal{O}(\alpha)$ especially in the resonance region. Therefore their contributions in $\mathcal{O}(\alpha_s \alpha)$ can be safely neglected. Moreover, applying a PA would not lead to any simplification here. In particular, the photon-induced processes do not contribute to the non-factorizable corrections.

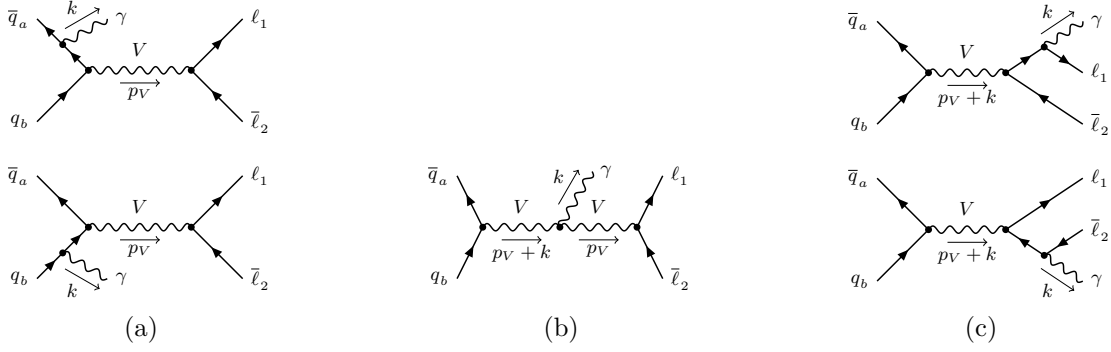


Figure 4.4.: The three sets of Feynman diagrams that contribute to the real-emission process $\bar{q}_a q_b \rightarrow \ell_1 \bar{\ell}_2 \gamma$. The photon can be attached to the quark line (a), the lepton line (c), and in the case of the charged-current processes also to the intermediate W boson (b). The momentum p_V of the intermediate vector boson V is given by $p_V = p_a + p_b - k = -k_1 + k_2$.

Full NLO EW results

In direct analogy to the calculation of the LO amplitude presented in Sect. 2.1, we define the colour-stripped amplitude $\mathcal{A}_{V\text{Rew},\tau_q\tau_\ell\lambda}^{\bar{q}_a q_b \rightarrow \ell_1 \bar{\ell}_2 \gamma}$ for the sum of the five diagrams shown in Fig. 4.4. The matrix elements of the bremsstrahlung corrections to the processes (2.5) are then constructed in the same manner as in the LO case (2.8),

$$\mathcal{M}_{\text{Rew}}^{\bar{d}_i u_j \rightarrow \nu_\ell \ell^+ \gamma} \left(\begin{bmatrix} p_a \\ \sigma_a \\ c_a \end{bmatrix}, \begin{bmatrix} p_b \\ \sigma_b \\ c_b \end{bmatrix}; \begin{bmatrix} k_1 \\ \sigma_1 \end{bmatrix}, \begin{bmatrix} k_2 \\ \sigma_2 \end{bmatrix}, \begin{bmatrix} k \\ \lambda \end{bmatrix} \right) = \delta_{c_a c_b} \mathcal{A}_{V\text{Rew},\tau_q\tau_\ell\lambda}^{\bar{q}_a q_b \rightarrow \ell_1 \bar{\ell}_2 \gamma}(p_a, p_b; k_1, k_2, k), \quad (4.13a)$$

$$\mathcal{M}_{\text{Rew}}^{\bar{u}_i d_j \rightarrow \ell^- \bar{\nu}_\ell \gamma} \left(\begin{bmatrix} p_a \\ \sigma_a \\ c_a \end{bmatrix}, \begin{bmatrix} p_b \\ \sigma_b \\ c_b \end{bmatrix}; \begin{bmatrix} k_1 \\ \sigma_1 \end{bmatrix}, \begin{bmatrix} k_2 \\ \sigma_2 \end{bmatrix}, \begin{bmatrix} k \\ \lambda \end{bmatrix} \right) = \delta_{c_a c_b} \mathcal{A}_{V\text{Rew},\tau_q\tau_\ell\lambda}^{\bar{u}_i d_j \rightarrow \ell^- \bar{\nu}_\ell \gamma}(p_a, p_b; k_1, k_2, k), \quad (4.13b)$$

$$\begin{aligned} \mathcal{M}_{\text{Rew}}^{\bar{q} q \rightarrow \ell^- \ell^+ \gamma} \left(\begin{bmatrix} p_a \\ \sigma_a \\ c_a \end{bmatrix}, \begin{bmatrix} p_b \\ \sigma_b \\ c_b \end{bmatrix}; \begin{bmatrix} k_1 \\ \sigma_1 \end{bmatrix}, \begin{bmatrix} k_2 \\ \sigma_2 \end{bmatrix}, \begin{bmatrix} k \\ \lambda \end{bmatrix} \right) \\ = \delta_{c_a c_b} \left(\mathcal{A}_{Z\text{Rew},\tau_q\tau_\ell\lambda}^{\bar{q} q \rightarrow \ell^- \ell^+ \gamma}(p_a, p_b; k_1, k_2, k) + \mathcal{A}_{\gamma\text{Rew},\tau_q\tau_\ell\lambda}^{\bar{q} q \rightarrow \ell^- \ell^+ \gamma}(p_a, p_b; k_1, k_2, k) \right), \end{aligned} \quad (4.13c)$$

using the notation and conventions introduced in Sect. 2.1, and λ denoting the helicity of the photon. Only the spin configuration satisfying Eq. (2.7) gives a non-vanishing contribution, and the colour-stripped amplitude can be further written in the following form,

$$\begin{aligned} i \mathcal{A}_{V\text{Rew},\tau_q\tau_\ell\lambda}^{\bar{q}_a q_b \rightarrow \ell_1 \bar{\ell}_2 \gamma}(p_a, p_b; k_1, k_2, k) \\ = 2\sqrt{2} i e^3 C_{V\bar{q}_a q_b}^{\tau_q} C_{V\bar{\ell}_1 \ell_2}^{\tau_\ell} \\ \times \left(\underbrace{\frac{Q_a (k \cdot p_b) + Q_b (k \cdot p_a)}{k \cdot (p_a + p_b)}}_{\xrightarrow{\text{NC}} Q_q, \text{ for } Q_a = Q_b \equiv Q_q} \frac{\mathcal{A}_{\text{prod}}^{\tau_q \tau_\ell \lambda}(p_a, p_b; k_1, k_2, k)}{s_{12} - \mu_V^2} \right) \end{aligned}$$

$$+ \underbrace{\frac{Q_1(k \cdot k_2) + Q_2(k \cdot k_1)}{k \cdot (k_1 + k_2)}}_{\xrightarrow{\text{NC}} Q_\ell, \text{ for } Q_1 = Q_2 \equiv Q_\ell} \frac{\mathbb{A}_{\text{dec}}^{\tau_q \tau_\ell \lambda}(p_a, p_b; k_1, k_2, k)}{s_{12\gamma} - \mu_V^2} \Big) \quad (4.14)$$

with $s_{12\gamma} = (k_1 + k_2 + k)^2$. In the case of the neutral-current (NC) process, Eq. (4.14) further simplifies due to the identical charges of the quarks and the leptons, respectively. The standard matrix elements $\mathbb{A}_{\text{prod}}^{\tau_q \tau_\ell \lambda}$ and $\mathbb{A}_{\text{dec}}^{\tau_q \tau_\ell \lambda}$ associated with the two resonance structures are related to each other via a simple interchange of momenta and helicities of the quarks with those of the leptons given by,

$$\mathbb{A}_{\text{prod}}^{\tau_q \tau_\ell \lambda}(p_a, p_b; k_1, k_2, k) = \mathbb{A}_{\text{dec}}^{\tau_q \tau_\ell \lambda}(p_a, p_b; k_1, k_2, k) \Big|_{\substack{q_a \leftrightarrow \ell_1 \\ q_b \leftrightarrow \ell_2}} = \mathbb{A}_{\text{dec}}^{\tau_\ell \tau_q \lambda}(k_1, k_2; p_a, p_b, k). \quad (4.15)$$

The explicit expressions for $\mathbb{A}_{\text{dec}}^{\tau_q \tau_\ell \lambda}$ and the different helicity configurations are given by

$$\begin{aligned} \mathbb{A}_{\text{dec}}^{+++}(p_a, p_b; k_1, k_2, k) &= \frac{\langle p_a p_b \rangle^*}{\langle k k_1 \rangle \langle k k_2 \rangle} (\langle p_b k_2 \rangle)^2, \\ \mathbb{A}_{\text{dec}}^{+-+}(p_a, p_b; k_1, k_2, k) &= -\frac{\langle p_a p_b \rangle^*}{\langle k k_1 \rangle \langle k k_2 \rangle} (\langle p_b k_1 \rangle)^2, \\ \mathbb{A}_{\text{dec}}^{-++}(p_a, p_b; k_1, k_2, k) &= -\frac{\langle p_a p_b \rangle^*}{\langle k k_1 \rangle \langle k k_2 \rangle} (\langle p_a k_2 \rangle)^2, \\ \mathbb{A}_{\text{dec}}^{--+}(p_a, p_b; k_1, k_2, k) &= \frac{\langle p_a p_b \rangle^*}{\langle k k_1 \rangle \langle k k_2 \rangle} (\langle p_a k_1 \rangle)^2, \\ \mathbb{A}_{\text{dec}}^{\tau_q \tau_\ell -}(p_a, p_b; k_1, k_2, k) &= \mathcal{P} \left\{ \mathbb{A}_{\text{dec}}^{(-\tau_q)(-\tau_\ell)+}(p_a, p_b; k_1, k_2, k) \right\}, \end{aligned} \quad (4.16)$$

where the modified parity operation \mathcal{P} used in the last line is defined in Eq. (A.46).

The NLO EW corrections in the PA

In the previous section we have already encountered the subtlety in the separation of the factorizable from the non-factorizable virtual corrections in the case where the virtual photon is attached to the internal V propagator. The real corrections involve the additional complication that photon emission off a V propagator leads to two V -boson resonances in phase space which overlap if the photon is not very hard, i.e. for $E_\gamma = k^0 \lesssim \Gamma_V$. To disentangle the two adjacent resonance factors, the following identity can be applied to the diagram shown in Fig. 4.4(b),

$$\frac{1}{(p_V + k)^2 - \mu_V^2} \cdot \frac{1}{p_V^2 - \mu_V^2} = \frac{1}{2p_V \cdot k} \left[\frac{1}{p_V^2 - \mu_V^2} - \frac{1}{(p_V + k)^2 - \mu_V^2} \right], \quad (4.17)$$

In fact identity (4.17) was already used in the derivation of Eq. (4.14) in order to identify the two standard matrix elements associated with the two resonance structures, which were

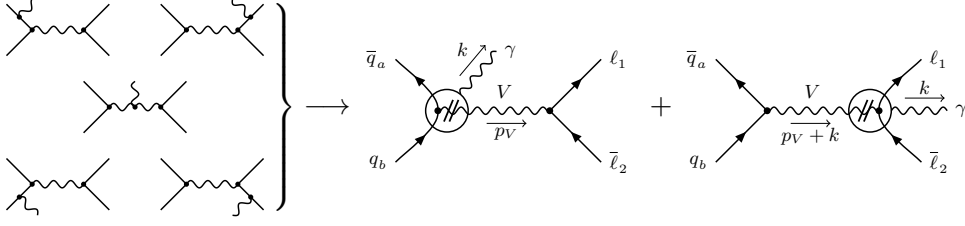


Figure 4.5.: Real-emission diagrams divided into initial-state and final-state contributions, where the compact diagrammatic notation defined in Eq. (4.19) is used. Double lines on the V propagator indicate on-shellness.

already labelled as “prod” and “dec” in anticipation of the calculation in the PA. Note that the factor $2p_V \cdot k$ in Eq. (4.17) resembles a propagator denominator for an on-shell V boson, e.g. $2p_V \cdot k = (p_V + k)^2 - \mu_V^2$ for $p_V^2 = \mu_V^2$ and $k^2 = 0$. The double slash on a propagator line indicates which momentum is set on its mass shell in the rest of the diagram (but not on the slashed line itself). Similar to the virtual corrections, the use of the real on-shell conditions $p_V^2 = M_V^2$ and $(p_V + k)^2 = M_V^2$ in the $\mathcal{O}(\alpha)$ corrections is possible in $\mathcal{O}(\alpha)$ precision. We will employ this in the following to avoid the unnecessary complication by complex momenta.

Figure 4.5 illustrates the decomposition that is obtained by applying identity (4.17) to the real-emission diagrams (see Fig. 4.4). We define the two corresponding colour-stripped amplitudes as follows,

$$i\mathcal{A}_{V\text{Rew},\tau_q\tau_\ell\lambda}^{\bar{q}_a q_b \rightarrow \ell_1 \bar{\ell}_2 \gamma} \equiv i\mathcal{A}_{V\text{prod},\tau_q\tau_\ell\lambda}^{\bar{q}_a q_b \rightarrow \ell_1 \bar{\ell}_2 \gamma} + i\mathcal{A}_{V\text{dec},\tau_q\tau_\ell\lambda}^{\bar{q}_a q_b \rightarrow \ell_1 \bar{\ell}_2 \gamma}, \quad (4.18)$$

which are identified with the two terms appearing inside the parenthesis on the r.h.s. of Eq. (4.14). We have further introduced a compact diagrammatic notation, where a particle attached to a circle represents all diagrams where the particle is attached in all possible ways to the encircled sub-diagram. Furthermore, the double-line at the V propagator inside the circle indicates that the V boson should be considered on shell inside the blob,

$$\text{Diagram with blob and double-slash } V \text{ propagator} = \text{Diagram 1} + \text{Diagram 2} + \text{Diagram 3}, \quad (4.19)$$

where the last diagram corresponds to the contribution coming from the first term on the r.h.s. of Eq. (4.17).

The *factorizable* real corrections consist of the two separately gauge-invariant parts induced by photon emission during the V production or V decay ($V = W^\pm, Z$). The respective squared amplitudes $|\mathcal{M}_{\text{Rew,prod}}^{\bar{q}_a q_b \rightarrow \ell_1 \bar{\ell}_2 \gamma}|^2$ and $|\mathcal{M}_{\text{Rew,dec}}^{\bar{q}_a q_b \rightarrow \ell_1 \bar{\ell}_2 \gamma}|^2$ are derived from the on-shell matrix elements for vector-boson production with an additional photon emitted from the initial or final state,

$$\mathcal{M}_{\text{Rew,prod}}^{\bar{q}_a q_b \rightarrow \ell_1 \bar{\ell}_2 \gamma} = \sum_{\lambda_V} \frac{\mathcal{M}_{\text{Rew}}^{\bar{q}_a q_b \rightarrow V \gamma}(\lambda_V) \mathcal{M}_0^{V \rightarrow \ell_1 \bar{\ell}_2}(\lambda_V)}{p_V^2 - \mu_V^2} = \delta_{c_a c_b} \mathcal{A}_{V\text{prod}}^{\bar{q}_a q_b \rightarrow \ell_1 \bar{\ell}_2 \gamma}, \quad (4.20a)$$

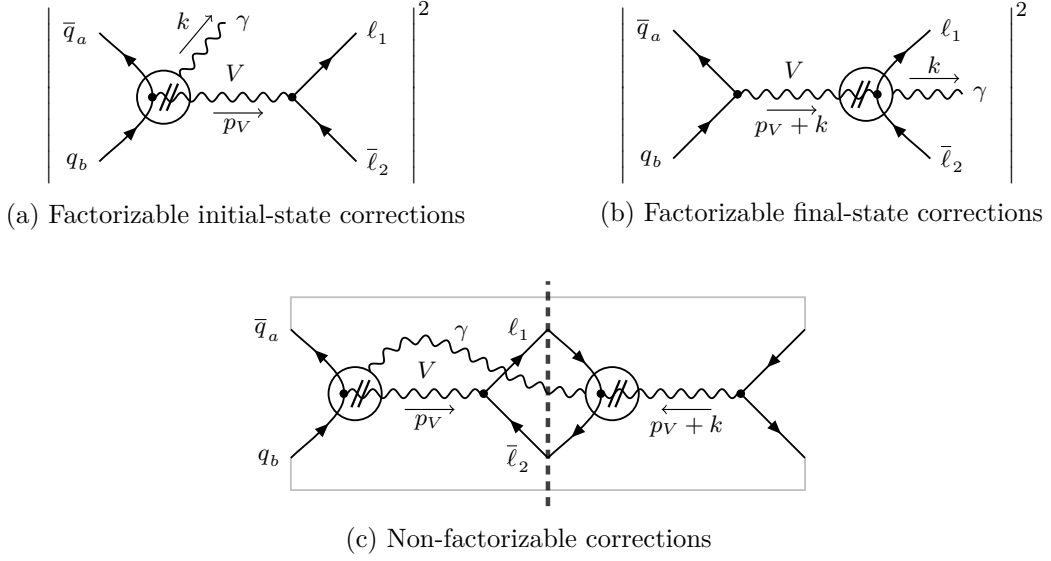


Figure 4.6.: Factorizable real photonic corrections to production (a) and decay (b), as well as non-factorizable real photonic corrections (c).

$$\mathcal{M}_{\text{Rew,dec}}^{\bar{q}_a q_b \rightarrow \ell_1 \bar{\ell}_2 \gamma} = \sum_{\lambda_V} \frac{\mathcal{M}_0^{\bar{q}_a q_b \rightarrow V}(\lambda_V) \mathcal{M}_{\text{Rew}}^{V \rightarrow \ell_1 \bar{\ell}_2 \gamma}(\lambda_V)}{(p_V + k)^2 - \mu_V^2} = \delta_{c_a c_b} \mathcal{A}_{V,\text{dec}}^{\bar{q}_a q_b \rightarrow \ell_1 \bar{\ell}_2 \gamma}, \quad (4.20b)$$

as illustrated in Figs. 4.6(a,b). Similarly to the virtual case, a projection of the kinematics onto the on-shell phase space is necessary to render the sub-amplitudes gauge invariant, while retaining the full off-shell kinematics in the resonant gauge-boson propagator. Note that for the real corrections, however, two different projections of the V momentum $p_V = k_1 + k_2$ are required, with $p_V^2 \rightarrow M_V^2$ and $(p_V + k)^2 \rightarrow M_V^2$, for the corrections to the decay and the production sub-processes, respectively.

The *non-factorizable* corrections emerge from the interference terms illustrated in Fig. 4.6(c). This definition is analogous to the virtual case, where the non-factorizable corrections are defined through the difference of the full squared matrix element and the factorizable corrections. For hard-photon emission the two V propagators of the interference term shown in Fig. 4.6(c) are widely separated and do not overlap, so that no resonant contribution results. Thus, only the soft-photon region $k^0 \lesssim \Gamma_V$ is relevant for resonant corrections, where the ESPA can be applied. The real non-factorizable corrections then can be written as a correction to the Born cross section,

$$\left| \mathcal{M}_{\text{Rew}}^{\bar{q}_a q_b \rightarrow \ell_1 \bar{\ell}_2 \gamma} \right|_{\text{nf}}^2 = \delta_{\text{Rew,nf}}^{\bar{q}_a q_b \rightarrow \ell_1 \bar{\ell}_2 \gamma} \left| \mathcal{M}_{0,\text{PA}}^{\bar{q}_a q_b \rightarrow \ell_1 \bar{\ell}_2 \gamma} \right|^2 \quad (4.21)$$

with

$$\delta_{\text{Rew,nf}}^{\bar{q}_a q_b \rightarrow \ell_1 \bar{\ell}_2 \gamma} = -2 \text{Re} \left\{ \mathcal{J}_{\text{prod},\mu}(p_a, p_b, p_a + p_b) (\mathcal{J}_{\text{dec}}^\mu(k_1, k_2))^* \right\}. \quad (4.22)$$

The emission of the photon is described by the following modified eikonal currents [156],

$$\mathcal{J}_{\text{prod}}^\mu(p_a, p_b, p_V) = e \left[Q_a \frac{p_a^\mu}{p_a \cdot k} - Q_b \frac{p_b^\mu}{p_b \cdot k} - (Q_a - Q_b) \frac{p_V^\mu}{p_V \cdot k} \right], \quad (4.23a)$$

$$\begin{aligned} \mathcal{J}_{\text{dec}}^\mu(k_1, k_2) = e & \left[Q_1 \frac{k_1^\mu}{k_1 \cdot k} - Q_2 \frac{k_2^\mu}{k_2 \cdot k} - (Q_1 - Q_2) \frac{k_1^\mu + k_2^\mu}{(k_1 + k_2) \cdot k} \right] \\ & \times \frac{(k_1 + k_2)^2 - \mu_V^2}{(k_1 + k_2 + k)^2 - \mu_V^2}, \end{aligned} \quad (4.23b)$$

where the ratio of propagators in Eq. (4.23b) is required to restore the correct momenta in the V propagators of the interference term shown in Fig. 4.6(c).

4.3. Complete result for the NLO EW corrections in the pole approximation

In the previous section we have presented the calculation of the virtual and real EW $\mathcal{O}(\alpha)$ corrections to the Drell–Yan processes (2.5) in the PA. The complete results for the cross section prediction is obtained by integrating the different contributions over the respective phase spaces.

However, as was described in Sect. 2.2, the actual numerical evaluation of the corrections further requires a careful isolation of soft and/or collinear singularities that arise in these higher-order corrections. To this end, we employ the dipole subtraction approach for photon radiation described in Chap. 3 for the calculation of the factorizable corrections and the phase-space slicing method for the non-factorizable corrections. The choice of the phase-space slicing method for the latter contribution is motivated by the fact that only soft singularities arise in the non-factorizable corrections. In this special case, the slicing method becomes particularly simple, in contrast to the subtraction formalism which would have resulted in an unnecessarily cumbersome implementation. In the following, we explicitly give the final results of the different corrections in the PA where all IR singularities are treated using the respective methods and which are suitable for a numerical evaluation.

4.3.1. The factorizable corrections to the production

The factorizable corrections to the production sub-process comprise the virtual corrections (4.8a), the bremsstrahlung corrections (4.20a), and further requires the inclusion of the collinear counterterm (1.103) in order to absorb residual initial-state collinear divergences into the NLO PDFs,

$$\begin{aligned} \hat{\sigma}_{\bar{q}_a q_b, \text{prod}}^{\text{NLO}_{\text{ew}}} &= \iint_{2+\gamma} d\sigma_{\bar{q}_a q_b, \text{prod}}^{\text{R}_{\text{ew}}} + \int_2 d\sigma_{\bar{q}_a q_b, \text{prod}}^{\text{V}_{\text{ew}}} + \int_2 d\sigma_{\bar{q}_a q_b}^{\text{C}_{\text{ew}}}, \\ &= \iint_{2+\gamma} d\sigma_{\bar{q}_a q_b, \text{prod}}^{\text{R}_{\text{ew}}} + \int_2 2 \text{Re} \left\{ \delta_{\text{V}_{\text{ew}}(\tau_q)}^{\text{prod}} \right\} d\sigma_{\bar{q}_a q_b, \text{PA}}^0 + \int_2 d\sigma_{\bar{q}_a q_b}^{\text{C}_{\text{ew}}}. \end{aligned} \quad (4.24)$$

Applying the dipole subtraction formalism described in Chap. 3 to Eq. (4.24), we obtain the final result for the factorizable final-state corrections

$$\begin{aligned}
\hat{\sigma}_{\bar{q}_a q_b, \text{prod}}^{\text{NLO}_{\text{ew}}} = & \iint_{2+\gamma} \left\{ d\sigma_{\bar{q}_a q_b, \text{prod}}^{\text{R}_{\text{ew}}} + 4\pi\alpha \sum_{\substack{I,J \\ I \neq J}} \eta_I Q_I \eta_J Q_J g_{IJ}^{(\text{sub})} d\sigma_{\bar{q}_a q_b, \text{PA}}^0(\tilde{\Phi}_{2,IJ}) \right\} \\
& + \int_2 \left[2 \text{Re} \left\{ \delta_{V_{\text{ew}}(\tau_q)}^{\text{prod}} \right\} - \frac{\alpha}{2\pi} \sum_{\substack{I,J \\ I \neq J}} \eta_I Q_I \eta_J Q_J G_{IJ}^{(\text{sub})} \right] d\sigma_{\bar{q}_a q_b, \text{PA}}^0 \\
& + \frac{\alpha}{2\pi} Q_{q_a} \sum_{J=\bar{q}_b, V} \int_0^1 dx \int_2 d\sigma_{\bar{q}_a q_b, \text{PA}}^0(xp_a, p_b) \frac{1}{x} \left[\mathcal{G}_{\bar{q}_a J}^{(\text{sub})}(x) \right]_+ \\
& - \frac{\alpha}{2\pi} Q_{q_b} \sum_{J=\bar{q}_a, V} \int_0^1 dx \int_2 d\sigma_{\bar{q}_a q_b, \text{PA}}^0(p_a, xp_b) \frac{1}{x} \left[\mathcal{G}_{q_b J}^{(\text{sub})}(x) \right]_+ \\
& + \int_2 d\sigma_{\bar{q}_a q_b}^{\text{C}_{\text{ew}}}, \tag{4.25}
\end{aligned}$$

where the sum over the emitter I and spectator J extends over the particles of the production sub-process, i.e. $I, J = \bar{q}_a, q_b, V$. Note that no photon emission from the final-state leptons is part of these corrections and thus, no singularity arises from collinear photon–lepton configurations. As a result, using a non-collinear-safe observable definition requires no further modification of Eq. (4.25).

4.3.2. The factorizable corrections to the decay

In contrast to the initial-state corrections discussed above, no photon emission from the incoming quarks is part of the corrections to the decay sub-process. Therefore, no collinear counterterm is required and the factorizable corrections to the decay sub-process is thus given by the following two terms,

$$\begin{aligned}
\hat{\sigma}_{\bar{q}_a q_b, \text{dec}}^{\text{NLO}_{\text{ew}}} = & \iint_{2+\gamma} d\sigma_{\bar{q}_a q_b, \text{dec}}^{\text{R}_{\text{ew}}} + \int_2 d\sigma_{\bar{q}_a q_b, \text{dec}}^{\text{V}_{\text{ew}}} \\
= & \iint_{2+\gamma} d\sigma_{\bar{q}_a q_b, \text{dec}}^{\text{R}_{\text{ew}}} + \int_2 2 \text{Re} \left\{ \delta_{V_{\text{ew}}(\tau_\ell)}^{\text{dec}} \right\} d\sigma_{\bar{q}_a q_b, \text{PA}}^0. \tag{4.26}
\end{aligned}$$

Applying the dipole subtraction formalism for decay processes as defined in Eq. (3.46), Eq. (4.26) can be written in the following form,

$$\begin{aligned}
\hat{\sigma}_{\bar{q}_a q_b, \text{dec}}^{\text{NLO}_{\text{ew}}} = & \iint_{2+\gamma} \left\{ d\sigma_{\text{dec}}^{\text{R}_{\text{ew}}} - \sum_{\substack{I,J \\ I \neq J}} d\sigma_{\bar{q}_a q_b, \text{PA}}^0 \otimes dV_{\text{dip}, IJ}^{\text{ew}} \right\} \\
& + \int_2 \left[2 \text{Re} \left\{ \delta_{V_{\text{ew}}(\tau_\ell)}^{\text{dec}} \right\} + I^{\text{ew}} \right] d\sigma_{\bar{q}_a q_b, \text{PA}}^0, \tag{4.27}
\end{aligned}$$

where the sum in the first line extends over all emitter–spectator pairs (I, J) of the particles in the decay sub-process given by $\ell_1, \bar{\ell}_2$, and V . Furthermore, we have introduced the short hand

notation

$$dV_{\text{dip},IJ}^{\text{ew}} = 4\pi\alpha \eta_I Q_I \eta_J Q_J \begin{cases} d_{IV}^{(\text{sub})}, & \text{for } (I \neq V) \wedge (J = V), \\ g_{IJ}^{(\text{sub})}, & \text{for } (I \neq V) \wedge (J = \ell_1, \bar{\ell}_2), \\ 0, & \text{for } I = V, \end{cases} \quad (4.28)$$

and denote the integrated counterpart of the dipoles by I^{ew} in order to make the formalism more transparent in Eq. (4.27). The sum of the dipole contributions is explicitly given by

$$\begin{aligned} \sum_{\substack{I,J \\ I \neq J}} d\sigma_{\bar{q}_a q_b, \text{PA}}^0 \otimes dV_{\text{dip},IJ}^{\text{ew}} &= -4\pi\alpha Q_{\ell_1} \left\{ (Q_{\ell_1} - Q_{\ell_2}) d_{\ell_1 V}^{(\text{sub})} d\sigma_{\bar{q}_a q_b, \text{PA}}^0(\tilde{\Phi}_{2,\ell_1 V}) \right. \\ &\quad \left. + Q_{\ell_2} g_{\ell_1 \bar{\ell}_2}^{(\text{sub})} d\sigma_{\bar{q}_a q_b, \text{PA}}^0(\tilde{\Phi}_{2,\ell_1 \bar{\ell}_2}) \right\} + (\ell_1 \leftrightarrow \bar{\ell}_2) \end{aligned} \quad (4.29)$$

and the corresponding integrated counterpart reads

$$I^{\text{ew}} = \frac{\alpha}{2\pi} Q_{\ell_1} \left[(Q_{\ell_1} - Q_{\ell_2}) D_{\ell_1 V}^{(\text{sub})} + Q_{\ell_2} G_{\ell_1 \bar{\ell}_2}^{(\text{sub})} \right] + (\ell_1 \leftrightarrow \bar{\ell}_2), \quad (4.30)$$

where $(\ell_1 \leftrightarrow \bar{\ell}_2)$ denotes the expression that is obtained by interchanging all labels $\ell_1 \leftrightarrow \bar{\ell}_2$ in the term that precedes it.

Non-collinear-safe observables

In case a non-collinear-safe observable definition with respect to the leptons $\hat{i} = \ell_1, \bar{\ell}_2$ is used, the subtracted dipole terms (4.29) must be modified according to (see Eq. (3.9)),

$$d\sigma_{\bar{q}_a q_b, \text{PA}}^0(\tilde{\Phi}_{2,\hat{i}J}) \longrightarrow d\sigma_{\bar{q}_a q_b, \text{PA}}^0(\tilde{\Phi}_{2,\hat{i}J}) \Theta_{\text{cut}} \left(\tilde{\Phi}_{2,\hat{i}J} \mid k_{\hat{i}} = z_{\hat{i}J} \tilde{k}_{\hat{i}}, k = (1 - z_{\hat{i}J}) \tilde{k}_{\hat{i}} \right). \quad (4.31)$$

This results in an additional convolution term that needs to be added to Eq. (4.27) and which we denote by

$$\tilde{\sigma}_{\bar{q}_a q_b, \text{dec}}^{\bar{\text{R}}_{\text{ew}}} \equiv \int_2 d\sigma_{\bar{q}_a q_b, \text{PA}}^0 \int_0^1 dz \left[\bar{\mathcal{I}}^{\text{ew}}(z) \right]_+, \quad (4.32)$$

with

$$\begin{aligned} \bar{\mathcal{I}}^{\text{ew}}(z) &= \frac{\alpha}{2\pi} Q_{\ell_1} \left[(Q_{\ell_1} - Q_{\ell_2}) \bar{\mathcal{D}}_{\ell_1 V}^{(\text{sub})}(z) + Q_{\ell_2} \bar{\mathcal{G}}_{\ell_1 \bar{\ell}_2}^{(\text{sub})}(z) \right] \\ &\quad \times \Theta_{\text{cut}} \left(\tilde{\Phi}_2 \mid k_{\ell_1} = z \tilde{k}_{\ell_1}, k = (1 - z) \tilde{k}_{\ell_1} \right) + (\ell_1 \leftrightarrow \bar{\ell}_2). \end{aligned} \quad (4.33)$$

4.3.3. The non-factorizable corrections

The actual phase-space integration of $|\mathcal{M}_{\text{R}_{\text{ew}}}^{\bar{q}_a q_b \rightarrow \ell_1 \bar{\ell}_2 \gamma}|_{\text{nf}}^2$ in Eq. (4.21) can be performed in two different ways, which are equally good in PA accuracy. One possibility, is to evaluate the

phase-space integral

$$\int d\Phi_{\ell_1 \ell_2 \gamma} = \int \frac{d^3 \mathbf{k}_1}{2k_1^0 (2\pi)^3} \int \frac{d^3 \mathbf{k}_2}{2k_2^0 (2\pi)^3} \int \frac{d^3 \mathbf{k}}{2k^0 (2\pi)^3} (2\pi)^4 \delta(p_a + p_b - k_1 - k_2 - k) \Big|_{\substack{k^0=|\mathbf{k}|, \\ k_i^0=|\mathbf{k}_i|}} \quad (4.34)$$

without any approximation. Within the PA, however, the photon momentum k can be neglected in the δ function, i.e. the phase space can be factorized according to

$$\int d\Phi_{\ell_1 \ell_2 \gamma} \rightarrow \int d\hat{\Phi}_{\ell_1 \ell_2 \gamma} = \int d\Phi_{\ell_1 \ell_2} \int \frac{d^3 \mathbf{k}}{2k^0 (2\pi)^3} \Big|_{k^0=|\mathbf{k}|}, \quad (4.35)$$

leading to some technical simplifications. Note that the upper limit of k_{\max}^0 of the photon energy k^0 is not fixed by the process kinematics any more. Reasonable values for k_{\max}^0 cover the whole range of photons with $k^0 \lesssim \Gamma_V$, without introducing artificially large scales. Although the introduction of k_{\max}^0 even cuts off an artificially created UV singularity at $k^0 \rightarrow \infty$, it only enters suppressed non-resonant terms that are beyond PA accuracy. In practice, we set k_{\max}^0 to some value within $(10 - 20) \times \Gamma_V$. We have checked that both variants of integrating the non-factorizable corrections yield identical results with an accuracy below the 0.1% level.

Similarly to the virtual non-factorizable correction, collinear singularities cancel when the non-factorizable corrections are integrated over the photon phase space, while a soft singularity remains. Here we regularize this singularity using soft slicing. The integral over the photon momentum is split into two contributions according to $E_\gamma < \Delta E$ and $E_\gamma > \Delta E$, where $E_\gamma = k^0$ denotes the energy of the photon in the partonic centre-of-mass frame. The cutoff has to be chosen much smaller than any relevant scale of the process, i.e. $\Delta E \ll \Gamma_V$. The cross section with NLO non-factorizable corrections can then be written in the form

$$\hat{\sigma}_{\text{nf}}^{\text{NLO}_{\text{ew}}} = \iint_{2+\gamma} d\sigma_{\text{nf}}^{\text{R}_{\text{ew}}} + \int_2 d\sigma_{\text{nf}}^{\text{V}_{\text{ew}}} = \iint_{\substack{2+\gamma \\ E_\gamma > \Delta E}} d\sigma_{\text{nf}}^{\text{R}_{\text{ew}}} + \iint_{\substack{2+\gamma \\ E_\gamma < \Delta E}} d\sigma_{\text{nf}}^{\text{R}_{\text{ew}}} + \int_2 d\sigma_{\text{nf}}^{\text{V}_{\text{ew}}}. \quad (4.36)$$

Below the cutoff ($E_\gamma < \Delta E$), the photon momentum can be also neglected in the resonant V propagators, so that the ratio of propagators in the decay current (4.23b) cancels and the ESPA reduces to the usual eikonal approximation. The resulting integrals can be performed analytically,

$$\begin{aligned} \delta_{\text{soft}}^{\bar{q}_a q_b \rightarrow \ell_1 \bar{\ell}_2}(\Delta E) &= -\mu^{2\epsilon} \int_{|\mathbf{k}| < \Delta E} \frac{d^{d-1} \mathbf{k}}{(2\pi)^{d-1} 2k^0} 2 \text{Re} \{ \mathcal{J}_{\text{prod}, \mu} (\mathcal{J}_{\text{dec}}^\mu)^* \} \Big|_{k^0=|\mathbf{k}|} \\ &= \frac{\alpha}{\pi} \sum_{\substack{i=a,b \\ f=1,2}} \eta_i Q_i \eta_f Q_f \left\{ 2 + \text{Li}_2 \left(1 + \frac{M_V^2}{t_{if}} \right) \right. \\ &\quad \left. + \left[\frac{c_\epsilon}{\epsilon} - 2 \ln \left(\frac{2\Delta E}{\mu} \right) \right] \left[1 - \ln \left(\frac{M_V^2}{-t_{if}} \right) \right] \right\}, \end{aligned} \quad (4.37)$$

and the explicit expressions for the soft integrals that are needed in this work are collected in Appendix C,

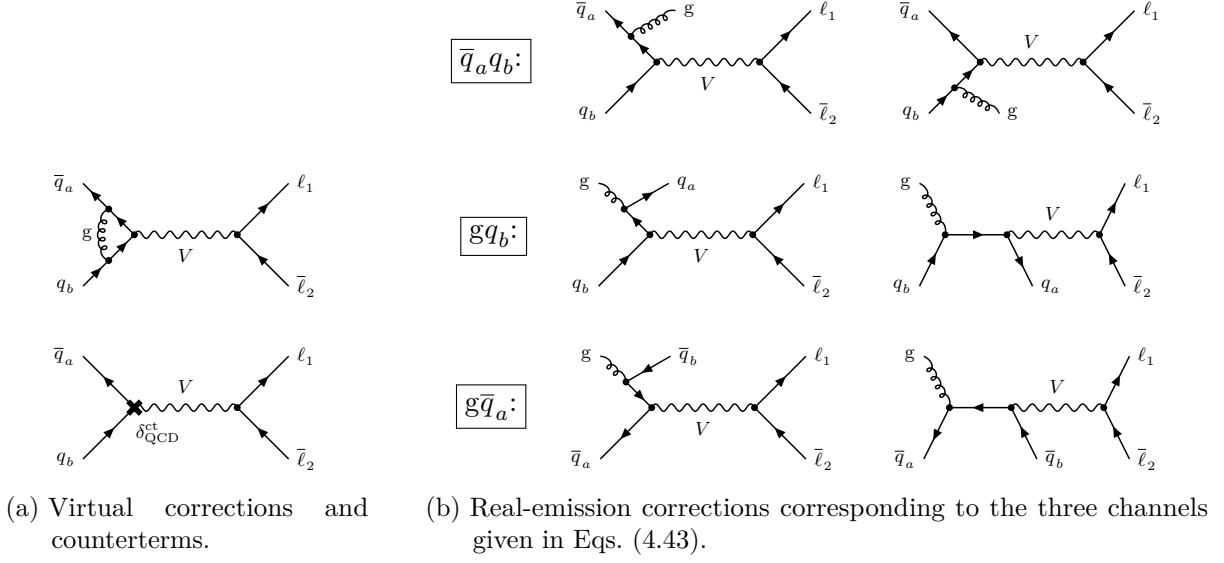


Figure 4.7.: The Feynman diagrams of the NLO QCD corrections divided into the virtual corrections with the counterterm contributions (a) and the real-emission corrections (b).

We then obtain our final form for the non-factorizable corrections to the cross section

$$\hat{\sigma}_{\text{nf}}^{\text{NLO}_{\text{ew}}} = \iint_{\substack{2+\gamma \\ E_\gamma > \Delta E}} d\sigma_{\text{PA}}^0 \delta_{\text{R}_{\text{ew,nf}}}^{\bar{q}_a q_b \rightarrow \ell_1 \bar{\ell}_2 \gamma} + \int_2 d\sigma_{\text{PA}}^0 \left[2 \text{Re} \left\{ \delta_{\text{V}_{\text{ew,nf}}}^{\bar{q}_a q_b \rightarrow \ell_1 \bar{\ell}_2} \right\} + \delta_{\text{soft}}^{\bar{q}_a q_b \rightarrow \ell_1 \bar{\ell}_2}(\Delta E) \right], \quad (4.38)$$

where the subscript PA in the leading-order cross section indicates the omission of non-resonant diagrams. The poles in ϵ cancel between the virtual non-factorizable corrections and the integrated soft slicing terms. The remaining integral over the real-photon phase space with the cutoff $E_\gamma > \Delta E$ can be safely evaluated numerically.

4.4. QCD corrections

Since the NLO QCD corrections to process (2.3) will also appear as building blocks in the calculation of $\mathcal{O}(\alpha_s \alpha)$ corrections in Part II, we here review their calculation and recite the well-known results. The virtual QCD corrections to vector-boson production cross sections comprise the one-loop diagram and counterterm contribution shown in Fig. 4.7(a) and can be written in terms of a correction factor $\delta_{\text{V}_s}^{V \bar{q}_a q_b}$ multiplying the Born cross section

$$d\sigma_{\bar{q}_a q_b}^{\text{V}_s} = 2 \text{Re} \left\{ \delta_{\text{V}_s}^{V \bar{q}_a q_b}(s_{ab}) \right\} d\sigma_{\bar{q}_a q_b}^0. \quad (4.39)$$

The correction factor can be obtained from the photonic vertex corrections given in Eq. (B.29) via the replacement $\alpha Q_f^2 \rightarrow \alpha_s C_F$ and is explicitly given by

$$\delta_{V_s}^{V\bar{q}_a q_b}(s_{ab}) = -\frac{\alpha_s}{2\pi} C_F \left\{ \frac{c_\epsilon}{\epsilon^2} + \frac{c_\epsilon}{\epsilon} \left[\ln \left(\frac{\mu^2}{-s_{ab} - i0} \right) + \frac{3}{2} \right] + \frac{1}{2} \ln^2 \left(\frac{\mu^2}{-s_{ab} - i0} \right) + \frac{3}{2} \ln \left(\frac{\mu^2}{-s_{ab} - i0} \right) - \frac{\pi^2}{6} + 4 \right\}, \quad (4.40)$$

with $s_{ab} = (p_a + p_b)^2$. The real-emission amplitudes are obtained from the photonic bremsstrahlung corrections (4.13) through a similar replacement and can be written in the following form,

$$\mathcal{M}_{R_s}^{\bar{d}_i u_j \rightarrow \nu_\ell \ell^+ g} \left(\left[\begin{smallmatrix} p_a \\ \sigma_a \\ c_a \end{smallmatrix} \right], \left[\begin{smallmatrix} p_b \\ \sigma_b \\ c_b \end{smallmatrix} \right]; \left[\begin{smallmatrix} k_1 \\ \sigma_1 \end{smallmatrix} \right], \left[\begin{smallmatrix} k_2 \\ \sigma_2 \end{smallmatrix} \right], \left[\begin{smallmatrix} k_g \\ \lambda_g \\ a \end{smallmatrix} \right] \right) = t_{c_a c_b}^a \mathcal{A}_{W_{R_s}, \tau_q \tau_\ell \lambda_g}^{\bar{q}_a q_b \rightarrow \ell_1 \bar{\ell}_2 g}(p_a, p_b; k_1, k_2, k_g), \quad (4.41a)$$

$$\mathcal{M}_{R_s}^{\bar{u}_i d_j \rightarrow \ell^- \bar{\nu}_\ell g} \left(\left[\begin{smallmatrix} p_a \\ \sigma_a \\ c_a \end{smallmatrix} \right], \left[\begin{smallmatrix} p_b \\ \sigma_b \\ c_b \end{smallmatrix} \right]; \left[\begin{smallmatrix} k_1 \\ \sigma_1 \end{smallmatrix} \right], \left[\begin{smallmatrix} k_2 \\ \sigma_2 \end{smallmatrix} \right], \left[\begin{smallmatrix} k_g \\ \lambda_g \\ a \end{smallmatrix} \right] \right) = t_{c_a c_b}^a \mathcal{A}_{W_{R_s}, \tau_q \tau_\ell \lambda_g}^{\bar{u}_i d_j \rightarrow \ell^- \bar{\nu}_\ell g}(p_a, p_b; k_1, k_2, k_g), \quad (4.41b)$$

$$\begin{aligned} \mathcal{M}_{R_s}^{\bar{q} q \rightarrow \ell^- \ell^+ g} \left(\left[\begin{smallmatrix} p_a \\ \sigma_a \\ c_a \end{smallmatrix} \right], \left[\begin{smallmatrix} p_b \\ \sigma_b \\ c_b \end{smallmatrix} \right]; \left[\begin{smallmatrix} k_1 \\ \sigma_1 \end{smallmatrix} \right], \left[\begin{smallmatrix} k_2 \\ \sigma_2 \end{smallmatrix} \right], \left[\begin{smallmatrix} k_g \\ \lambda_g \\ a \end{smallmatrix} \right] \right) \\ = t_{c_a c_b}^a \left(\mathcal{A}_{Z_{R_s}, \tau_q \tau_\ell \lambda_g}^{\bar{q} q \rightarrow \ell^- \ell^+ g}(p_a, p_b; k_1, k_2, k_g) + \mathcal{A}_{\gamma_{R_s}, \tau_q \tau_\ell \lambda_g}^{\bar{q} q \rightarrow \ell^- \ell^+ g}(p_a, p_b; k_1, k_2, k_g) \right), \end{aligned} \quad (4.41c)$$

where the colour-stripped amplitude is given by

$$i \mathcal{A}_{V_{R_s}, \tau_q \tau_\ell \lambda_g}^{\bar{q}_a q_b \rightarrow \ell_1 \bar{\ell}_2 g}(p_a, p_b; k_1, k_2, k_g) = \frac{2\sqrt{2} i e^2 g_s}{s_{12} - \mu_V^2} C_{V\bar{q}_a q_b}^{\tau_q} C_{V\bar{\ell}_1 \ell_2}^{\tau_\ell} \mathbb{A}_{\text{prod}}^{\tau_q \tau_\ell \lambda_g}(p_a, p_b; k_1, k_2, k_g), \quad (4.42)$$

with $\mathbb{A}_{\text{prod}}^{\tau_q \tau_\ell \lambda}$ defined in Eq. (4.15). In addition to the quark–anti-quark induced processes, new gluon-induced channels become available in the real-correction contributions as shown in Fig. 4.7(b):

$$\bar{q}_a(p_a) + q_b(p_b) \rightarrow \ell_1(k_1) + \bar{\ell}_2(k_2) + g(k_g), \quad (4.43a)$$

$$g(p_g) + q_b(p_b) \rightarrow \ell_1(k_1) + \bar{\ell}_2(k_2) + q_a(k_a), \quad (4.43b)$$

$$g(p_g) + \bar{q}_a(p_a) \rightarrow \ell_1(k_1) + \bar{\ell}_2(k_2) + \bar{q}_b(k_b). \quad (4.43c)$$

The matrix elements of the gluon-induced channels can be obtained using the crossing transformation \mathcal{X} defined in Eq. (A.45),

$$\mathcal{M}_{R_s}^{g q_b \rightarrow \ell_1 \bar{\ell}_2 q_a} = \mathcal{X} \left[\begin{smallmatrix} \bar{q}_a(p_a) \rightarrow q_a(k_a) \\ g(k_g) \leftarrow g(p_g) \end{smallmatrix} \right] \left\{ \mathcal{M}_{R_s}^{\bar{q}_a q_b \rightarrow \ell_1 \bar{\ell}_2 g} \right\}, \quad (4.44a)$$

$$\mathcal{M}_{R_s}^{g \bar{q}_a \rightarrow \ell_1 \bar{\ell}_2 \bar{q}_b} = \mathcal{X} \left[\begin{smallmatrix} q_b(p_b) \rightarrow \bar{q}_b(k_b) \\ g(k_g) \leftarrow g(p_g) \end{smallmatrix} \right] \left\{ \mathcal{M}_{R_s}^{\bar{q}_a q_b \rightarrow \ell_1 \bar{\ell}_2 g} \right\}. \quad (4.44b)$$

To regularize the phase-space integral of the real corrections we employ the dipole subtraction formalism described in Ref. [129]. In this framework, the hard partonic cross section can be schematically written as

$$\hat{\sigma}^{\text{NLO}_s} = \int_3 d\sigma^{\text{R}_s} + \int_2 d\sigma^{\text{V}_s} + \int_2 d\sigma^{\text{C}_s}$$

$$\begin{aligned}
&= \int_3 \left[\left(d\sigma^{\text{R}_s} \right)_{\epsilon=0} - \left(\sum_{\substack{\text{QCD} \\ \text{dipoles}}} d\sigma^0 \otimes dV_{\text{dip}} \right)_{\epsilon=0} \right] \\
&+ \int_2 \left[d\sigma^{\text{V}_s} + d\sigma^0 \otimes \mathbf{I} \right]_{\epsilon=0} + \int_0^1 dx \int_2 \left[d\sigma^0 \otimes (\mathbf{K} + \mathbf{P}) \right]_{\epsilon=0}, \tag{4.45}
\end{aligned}$$

where \otimes encodes the possible colour and helicity correlations between $d\sigma^0$ and the dipole operators (dV_{dip} , \mathbf{I} , \mathbf{K} , and \mathbf{P}), and the integration over x corresponds to a convolution over the momentum fraction carried away by collinear parton emission of the initial state. The insertion operators \mathbf{I} , \mathbf{K} , and \mathbf{P} emerge from the collinear counterterm and the integrated dipoles. More details and the explicit expressions for these insertion operators can be found in Ref. [129]. Using this formalism, the contributions of the virtual corrections, Eq. (4.39), and the real-correction sub-processes in Eq. (4.43) to the partonic NLO QCD cross section read

$$\begin{aligned}
\hat{\sigma}_{\bar{q}_a q_b}^{\text{NLO}_s}(p_a, p_b) &= \int_3 \left[d\sigma_{\bar{q}_a q_b}^{\text{R}_s}(p_a, p_b) \right. \\
&\quad \left. - d\sigma_{\bar{q}_a q_b}^0(\tilde{\Phi}_{2,(\bar{q}_a g)q_b}) \otimes dV_{\text{dip}}^{\bar{q}_a, \bar{q}_a} - d\sigma_{\bar{q}_a q_b}^0(\tilde{\Phi}_{2,(q_b g)\bar{q}_a}) \otimes dV_{\text{dip}}^{q_b, q_b} \right] \\
&+ \int_2 \left[d\sigma_{\bar{q}_a q_b}^{\text{V}_s}(p_a, p_b) + d\sigma_{\bar{q}_a q_b}^0(p_a, p_b) \otimes \mathbf{I} \right] \\
&+ \int_0^1 dx \int_2 d\sigma_{\bar{q}_a q_b}^0(xp_a, p_b) \otimes (\mathbf{K} + \mathbf{P})^{\bar{q}_a, \bar{q}_a} \\
&+ \int_0^1 dx \int_2 d\sigma_{\bar{q}_a q_b}^0(p_a, xp_b) \otimes (\mathbf{K} + \mathbf{P})^{q_b, q_b}, \tag{4.46a}
\end{aligned}$$

$$\begin{aligned}
\hat{\sigma}_{g q_b}^{\text{NLO}_s}(p_g, p_b) &= \int_3 \left[d\sigma_{g q_b}^{\text{R}_s}(p_g, p_b) - d\sigma_{g q_b}^0(\tilde{\Phi}_{2,(g \bar{q}_a)q_b}) \otimes dV_{\text{dip}}^{g, \bar{q}_a} \right] \\
&+ \int_0^1 dx \int_2 d\sigma_{g q_b}^0(xp_g, p_b) \otimes (\mathbf{K} + \mathbf{P})^{g, \bar{q}_a}, \tag{4.46b}
\end{aligned}$$

and an analogous expression for the gluon–anti-quark induced channel. The dipole phase space $\tilde{\Phi}_{n,(ai)b}(\tilde{p}_{ai}^\mu, \tilde{p}_b; \tilde{k}_1, \tilde{k}_2)$ is constructed from the real-emission phase space $\Phi_{n+1}(p_a, p_b; k_1, k_2, k_i)$ as follows,

$$\tilde{p}_{ai}^\mu = x_{i,ab} p_a^\mu, \quad x_{i,ab} = \frac{p_a \cdot p_b - k_i \cdot p_a - k_i \cdot p_b}{p_a \cdot p_b}, \tag{4.47a}$$

$$\tilde{p}_b^\mu = p_b^\mu, \quad \tilde{k}_j^\mu = \Lambda^\mu{}_\nu k_j^\nu \quad (j = 1, 2), \tag{4.47b}$$

where k_i is the momentum of the additional gluon or (anti-)quark in the final state. This dipole mapping is identical to the analogous case in the QED dipole subtraction formalism given in Eqs. (3.30) and (3.33). Note that the dipole kinematics corresponds to a collinear splitting of an initial-state parton $ai(p_a) \rightarrow a(x_{i,ab}p_a) + i((1 - x_{i,ab})p_a)$ with $i = g, q, \bar{q}$ and that its partonic rest frame for the momentum $\tilde{p}_{ai} + \tilde{p}_b$ is Lorentz boosted along the beam axis with respect to the rest frame of the real-emission kinematics with the momentum $p_a + p_b$.

4.5. Numerical results at NLO

In this section we present the numerical results for the NLO corrections to the Drell–Yan process at the LHC for a centre-of-mass energy of $\sqrt{s} = 14$ TeV, where we restrict ourselves to the discussion of the two specific processes

$$p + p \rightarrow W^+ \rightarrow \nu_\mu + \mu^+, \quad (4.48)$$

$$p + p \rightarrow Z (\gamma^*) \rightarrow \mu^- + \mu^+, \quad (4.49)$$

with muons in the final state. Note that a proper description of the experimental detection of electrons requires a recombination procedure to be present which treats collinear photon–electron configurations inclusively. In this case, the results are free of collinear singularities and as such, independent of the finite lepton mass that is introduced as a regulator. As a consequence, the corrections become independent of the lepton flavour and the results denoted as “dressed leptons” below, are equally valid for electrons in the final state. Further details on the recombination algorithm used in our calculation are given in Sect. 4.5.2. We further compare the results obtained by the full NLO EW calculation with those obtained by applying the PA as described in the previous sections.

4.5.1. Input parameters and setup

For the numerical evaluation we use the following set of input parameters¹

$$\begin{aligned} G_\mu &= 1.166\,378\,7 \times 10^{-5} \text{ GeV}^{-2}, & \alpha_s(M_Z) &= 0.119, \\ M_W^{\text{OS}} &= 80.385 \text{ GeV}, & \Gamma_W^{\text{OS}} &= 2.085 \text{ GeV}, \\ M_Z^{\text{OS}} &= 91.1876 \text{ GeV}, & \Gamma_Z^{\text{OS}} &= 2.4952 \text{ GeV}, \\ M_H &= 125.9 \text{ GeV}, & m_t &= 173.07 \text{ GeV}, \end{aligned} \quad (4.50)$$

which essentially follow Ref. [123]. As explained in Sect. 1.1.3, we employ the G_μ scheme, where the electroweak coupling constant is derived from the Fermi constant via the relation

$$\alpha_{G_\mu} = \frac{\sqrt{2}}{\pi} G_\mu M_W^2 \left(1 - \frac{M_W^2}{M_Z^2} \right), \quad (4.51)$$

which avoids large logarithms of the light fermion masses induced by the running of the coupling constant $\alpha(Q^2)$ from the Thomson limit ($Q^2 = 0$) to the electroweak scale ($Q^2 \sim M_Z^2$). The masses of the light quark flavours (u, d, c, s, b) and of the leptons are neglected throughout, with the only exception in case of non-collinear-safe observables, where the final-state collinear singularity is regularized by the finite physical mass of the muon,

$$m_\mu = 105.658\,369 \text{ MeV}. \quad (4.52)$$

¹Note that we take the experimental values of the W- and Z-boson widths as input parameters instead of calculating the decay widths in the respective order.

The on-shell masses and widths of the gauge bosons in Eq. (4.50) are converted to the corresponding pole masses and widths via the relation given in Eq. (1.85),

$$M_V = \frac{M_V^{\text{OS}}}{c_V}, \quad \Gamma_V = \frac{\Gamma_V^{\text{OS}}}{c_V}, \quad c_V = \sqrt{1 + \left(\frac{\Gamma_V^{\text{OS}}}{M_V^{\text{OS}}} \right)^2}. \quad (4.53)$$

The CKM matrix is chosen diagonal in the third generation, and the mixing between the first two generations is parametrized by the following values for the entries of the quark-mixing matrix,

$$|V_{ud}| = |V_{cs}| = 0.974, \quad |V_{cd}| = |V_{us}| 0.227. \quad (4.54)$$

For the PDFs we consistently use the NNPDF2.3 sets [143], where the NLO corrections are evaluated using the NNPDF2.3QED NLO set [142], which also includes $\mathcal{O}(\alpha)$ corrections. The value of the strong coupling $\alpha_s(M_Z)$ quoted in Eq. (4.50) is dictated by the choice of these PDF sets. The renormalization and factorization scales are set equal, with a fixed value given by the respective gauge-boson mass,

$$\mu_R = \mu_F \equiv \mu = M_V, \quad (4.55)$$

of the process under consideration.

4.5.2. Phase-space cuts and event selection

For the experimental identification of the Drell–Yan process we impose the following cuts on the charged leptons

$$p_{T,\ell^\pm} > 25 \text{ GeV}, \quad |\eta_{\ell^\pm}| < 2.5, \quad (4.56)$$

and additionally

$$E_T^{\text{miss}} > 25 \text{ GeV}, \quad (4.57)$$

which is only relevant in case of the charged-current process. For the neutral-current process we further require the cut on the invariant mass of the lepton pair

$$M_{\ell^+\ell^-} > 50 \text{ GeV}, \quad (4.58)$$

in order to avoid the photon pole at $M_{\ell^+\ell^-} \rightarrow 0$.

The event selection described so far is not collinear safe with respect to the emission of photons from the charged leptons and will in general lead to corrections that involve large logarithms of the small lepton mass. While the experimental isolation of a collinear lepton–photon configuration is feasible in case of muons (“bare muons”), for electrons such collinear configurations need to be treated inclusively, as can be achieved by a so-called photon recombination. The photon-recombination procedure that we apply for a collinear-safe observable definition proceeds as follows:

1. Photons close to the beam with a rapidity $|\eta_\gamma| > 3$ are treated as beam remnants and are not further considered in the event selection.

2. For the photons that pass the first step, the angular distance to the charged leptons $R_{\ell^\pm\gamma} = \sqrt{(\eta_{\ell^\pm} - \eta_\gamma)^2 + (\phi_{\ell^\pm} - \phi_\gamma)^2}$ is computed, where ϕ denotes the azimuth angle in the transverse plane. If the distance between the photon and the closest lepton is smaller than $R_{\ell^\pm\gamma} < 0.1$, the photon is recombined with the lepton by adding the respective four-momenta $\ell^\pm(k_i) + \gamma(k) \rightarrow \ell^\pm(k_i + k)$.
3. Finally, the event selection cuts from Eqs. (4.56)–(4.58) are applied on the resulting event kinematics.

A similar recombination algorithm was also used in Ref. [37] for the charged-current and in Ref. [45] for the neutral-current process.

4.5.3. Results

In the following, we present the numerical results for Drell–Yan-like W^+ and Z production at the LHC at a centre-of-mass energy of $\sqrt{s} = 14$ TeV. We denote the full LO cross section (2.2) by σ_{pp}^{LO} and define the relative QCD corrections with respect to the LO prediction via

$$\sigma_{pp}^{\text{NLO}_s} = \sigma_{pp}^0 + \Delta\sigma_{pp}^{\text{NLO}_s} \equiv \sigma_{pp}^{\text{LO}} \times (1 + \delta_{\alpha_s}), \quad \delta_{\alpha_s} = \frac{\sigma_{pp}^0 - \sigma_{pp}^{\text{LO}} + \Delta\sigma_{pp}^{\text{NLO}_s}}{\sigma_{pp}^{\text{LO}}} \quad (4.59)$$

where the contributions σ_{pp}^0 and $\Delta\sigma_{pp}^{\text{NLO}_s}$ result from the respective terms inside the square brackets on the r.h.s. of Eq. (2.12), i.e. σ_{pp}^0 denotes the LO cross section evaluated with NLO PDFs and $\Delta\sigma_{pp}^{\text{NLO}_s}$ corresponds to the genuine $\mathcal{O}(\alpha_s)$ corrections in the NLO prediction given by the convolution of the hard-scattering amplitude $\hat{\sigma}_{ab}^{\text{NLO}_s}$ with the respective NLO PDFs. The standard QCD K factor is related to the correction factor via $K^{\text{NLO}_s} = 1 + \delta_{\alpha_s}$. The relative EW correction is always derived from the ratio of the NLO EW contribution $\Delta\sigma_{pp}^{\text{NLO}_{\text{ew}}}$ with respect to the LO contribution σ_{pp}^0 according to

$$\delta_{\alpha_{\text{ew}}} \equiv \frac{\Delta\sigma_{pp}^{\text{NLO}_{\text{ew}}}}{\sigma_{pp}^0}, \quad (4.60)$$

so that the EW correction factors are practically independent of the PDFs. The results for bare muons and dressed leptons will be distinguished by an additional label $\delta_\alpha^{\text{bare}}$ and $\delta_\alpha^{\gamma\text{-rec.}}$, respectively. An ansatz for the mixed QCD–EW corrections $\sigma_{pp,\text{naive fact}}^{\text{NNLO}_{s\otimes\text{ew}}}$ based on the naive factorization of QCD and EW corrections then reads,

$$\sigma_{pp,\text{naive fact}}^{\text{NNLO}_{s\otimes\text{ew}}} = \sigma_{pp}^{\text{NLO}_s} (1 + \delta_{\alpha_{\text{ew}}}) = \sigma_{pp}^{\text{LO}} (1 + \delta_{\alpha_s}) (1 + \delta_{\alpha_{\text{ew}}}). \quad (4.61)$$

To illustrate the structure and quality of the PA applied to the EW corrections, we study two crucial observables for W^+ production at the LHC: the transverse-mass $M_{T,\nu\ell}$ and the transverse-lepton-momentum $p_{T,\ell}$ distribution, which are shown in Fig. 4.8. The transverse mass is defined as

$$M_{T,\nu\ell} = \sqrt{2 p_{T,\ell} E_T^{\text{miss}} (1 - \cos \phi_{\nu\ell})}, \quad (4.62)$$

where $\phi_{\nu\ell}$ denotes the angle between the lepton and the missing momentum in the transverse plane. The uppermost plots in Fig. 4.8 show the absolute predictions which exhibit the well-

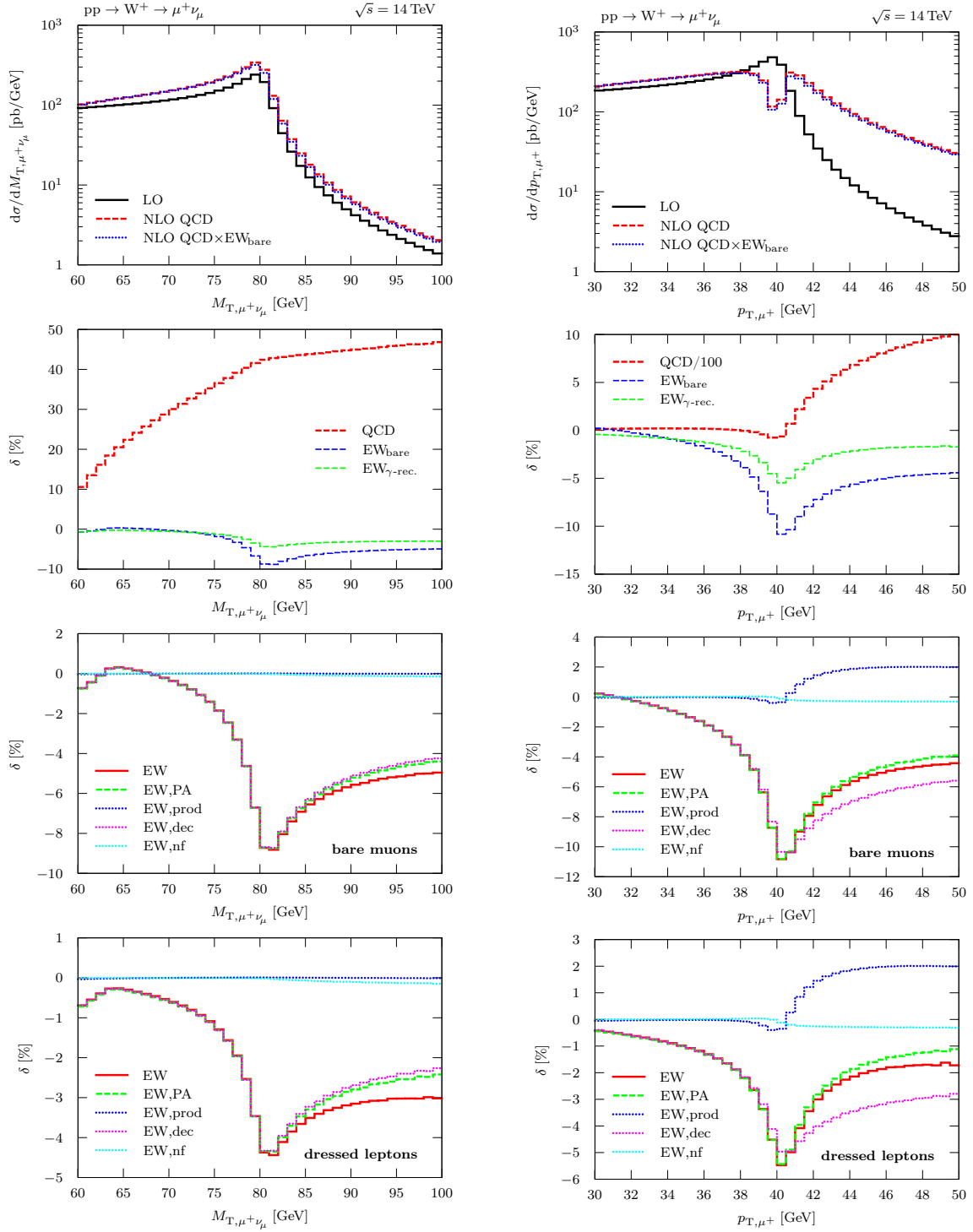


Figure 4.8.: Distributions in the transverse-mass (left) and transverse-lepton-momentum (right) for W^+ production at the LHC, with the upper plot showing the absolute distributions, the plots in the second row the full relative NLO QCD and EW corrections, and the lower two plots the relative NLO EW corrections in PA for bare and dressed leptons broken up into their factorizable and non-factorizable parts.

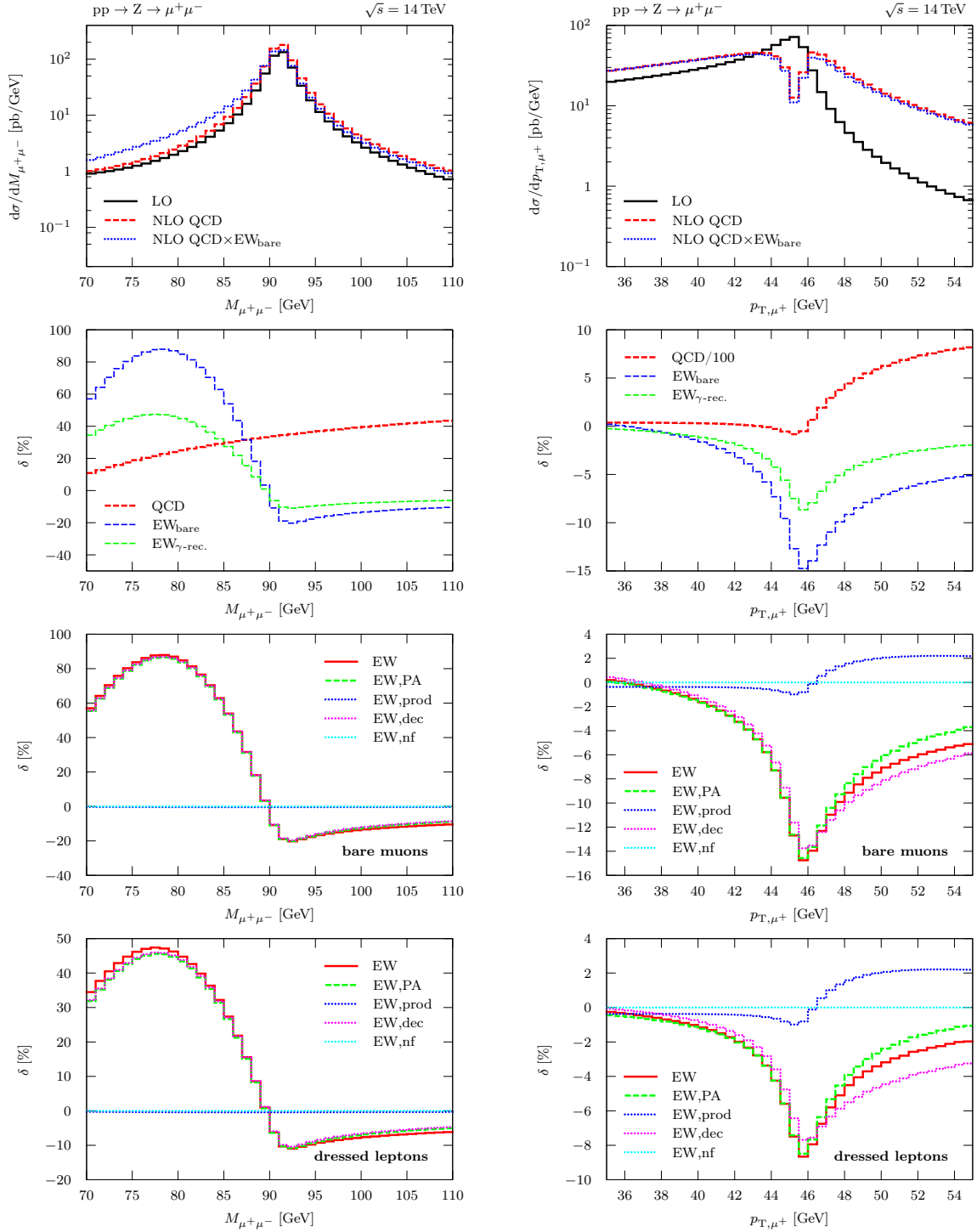


Figure 4.9.: Distributions in the invariant-mass (left) and transverse-lepton-momentum (right) for Z production at the LHC, with the upper plot showing the absolute distributions, the middle plots the full relative NLO QCD and EW corrections, and the lower plots the relative NLO EW corrections in PA broken up into their factorizable and non-factorizable parts.

known Jacobian peaks at $M_{T,\nu\ell} \approx M_W$ and $p_{T,\ell} \approx M_W/2$, respectively, which play a central role in the measurement of the W-boson mass M_W at hadron colliders. In addition to the LO result, these plots include the NLO QCD predictions and the curve obtained by assuming naive factorization according to Eq. (4.61) for the case of bare muons. A more detailed discussion of the corrections obtained by the naive factorization ansatz will be given in Part. II, where it will be compared against the corrections obtained from a PA. The panels in the second row of Fig. 4.8 show the relative QCD and EW corrections defined in Eqs. (4.59) and (4.60), respectively. Note that the QCD correction factor is rescaled in some distributions. It can be seen that the EW corrections significantly distort the distributions and shift the peak position. For bare muons, the corrections around the threshold amount to $\approx -9\%$ in the $M_{T,\nu\ell}$ and $\approx -11\%$ in the $p_{T,\ell}$ distributions. The results obtained by photon recombination give rise to corrections that are typically reduced by a factor of two compared to the respective corrections for “bare muons”. While the QCD corrections are moderate for the $M_{T,\nu\ell}$ distribution, they become extremely large above the Jacobian peak in the $p_{T,\ell}$ distribution. This effect is induced by the recoil of the W boson against the hard jet in the QCD real-emission corrections which feeds events with resonant W bosons into the range with $p_{T,\ell} > M_W/2$ in contrast to the situation at LO where resonant W production is restricted to $p_{T,\ell} < M_W/2$. Furthermore, a large dip is observed in the $p_{T,\ell}$ distribution of the NLO QCD prediction around the threshold $p_{T,\ell} \approx M_W/2$, which represents the transition region between W and W + jet production. This artefact indicates that a fixed-order QCD prediction is insufficient to properly describe the cross section in this region and that careful QCD resummation is required. Indeed, theoretical predictions obtained by matching the QCD corrections to a parton-shower such as the results shown in Ref. [65] do not display this dip but show a smooth behaviour in the threshold region. Such a matching procedure is, however, beyond the scope of this thesis.

In order to assess the quality of the PA, in the lower two panels of Fig. 4.8 we perform a comparison of the results obtained using the PA against the full NLO EW corrections for both bare muons and dressed leptons. We also break down the result of the PA further into factorizable corrections to the production/decay sub-processes and into the non-factorizable contributions. The accuracy of the PA near the resonance is excellent, of the order of some 0.1%. Above the Jacobian peaks, the difference to the full EW correction grows to the percent level. The PA remains accurate below the peaks where the distributions are still dominated by resonant W production. Turning to the relative importance of the different contributions in the PA, it is seen that the impact of the non-factorizable corrections is suppressed to the 0.1% level and, thus, phenomenologically negligible. The factorizable initial-state corrections are also very small for the case of the $M_{T,\nu\ell}$ spectrum and for the $p_{T,\ell}$ distribution below the peaks. In the latter case, the relative correction with respect to the LO prediction becomes more sizeable above threshold, however, it should be taken into account that the EW corrections to the $p_{T,\ell}$ distribution are overwhelmed by the QCD corrections in this region. Thus, the relevant part of the NLO EW corrections near the threshold almost entirely results from the factorizable final-state corrections, where the bulk originates from collinear final-state radiation from the charged leptons.

Figure 4.9 shows the respective results for the lepton-invariant-mass ($M_{\ell\ell}$) and transverse-lepton-momentum ($p_{T,\ell}$) distributions in case of the neutral-current Drell–Yan process. The invariant-mass spectrum shows much larger EW corrections than the other distributions, which is a well known effect of photonic final-state corrections that shift the peak location to lower values. At maximum, the corrections amount to $\approx 90\%$ for bare muons and to $\approx 50\%$ for the case with photon recombination. The corrections to the transverse-momentum distribution are similar in

shape to the charged-current case discussed above. The PA works well for the invariant-mass range considered in the plot and is again completely dominated by the final-state factorizable corrections. Due to the additional charged lepton in the final-state, the EW corrections to the neutral-current Drell–Yan process are larger compared to the corrections for the charged-current case.

Part II.

Pole expansion for the mixed
QCD–electroweak $\mathcal{O}(\alpha_s\alpha)$ corrections

Concept of the pole expansion and classification of contributions

In the framework of the PA, the radiative corrections to the Drell–Yan process (2.3) decompose into separate well-defined parts given by the factorizable corrections to W/Z production and decay sub-processes and the non-factorizable corrections which link production and decay by soft-photon exchange. For the case of NLO EW corrections this classification is illustrated in Fig. 4.1 for the virtual corrections. Each part of the factorizable and non-factorizable corrections consists of the virtual one-loop and real-emission corrections as shown in Fig. 2.3 in terms of generic interference diagrams, which comprise the two ingredients that enter a NLO calculation. The calculation of the NLO EW corrections in the PA was presented in the previous chapter in great detail. The transition to NNLO corrections at $\mathcal{O}(\alpha_s\alpha)$ increases the complexity in both these respects: Firstly, the different ingredients that enter into the NNLO calculation now range from the double-virtual two-loop corrections up to double-real-emission corrections with two additional particles in the final state. Secondly, the structure of the individual corrections that are identified after the application of the PA become more involved, in particular, with respect to the treatment of overlapping IR singularities between the QCD and EW corrections. Although having only colour-neutral particles in the final state mostly confines the QCD corrections to the production sub-process, the different types of factorizable corrections increases to three distinct contributions at $\mathcal{O}(\alpha_s\alpha)$.

The purpose of this chapter is to give an overview of the different ingredients that enter into the calculation of the NNLO $\mathcal{O}(\alpha_s\alpha)$ corrections to the Drell–Yan process (2.3) in general, and to set up the PA at this order. Furthermore, it is intended to serve as a reference for the reader in the explicit calculations that are presented in Chap. 6 and 7. Section 5.1 categorizes the different types of corrections that arise in NNLO corrections and sketches the strategy for the application of the PA for the individual parts. In Sect. 5.2 we outline the structure of the pole expansion and classify the different contributions to the PA.

5.1. Survey of NNLO corrections

In this section we categorize the different ingredients that enter into the full calculation of the NNLO $\mathcal{O}(\alpha_s\alpha)$ corrections to the process (2.3). The four types of contributions are illustrated in Fig. 5.1 in terms of generic interference diagrams. A similar set of diagrams will be shown in the explicit calculation of the two PA contributions presented in Chap. 6 and 7 in order to further specify the structure of the respective corrections.

- (a) **Double-virtual corrections:** The double-virtual corrections of $\mathcal{O}(\alpha_s\alpha)$ are shown in Fig. 5.1(a) and may be further divided into two types: Firstly, the two-loop corrections

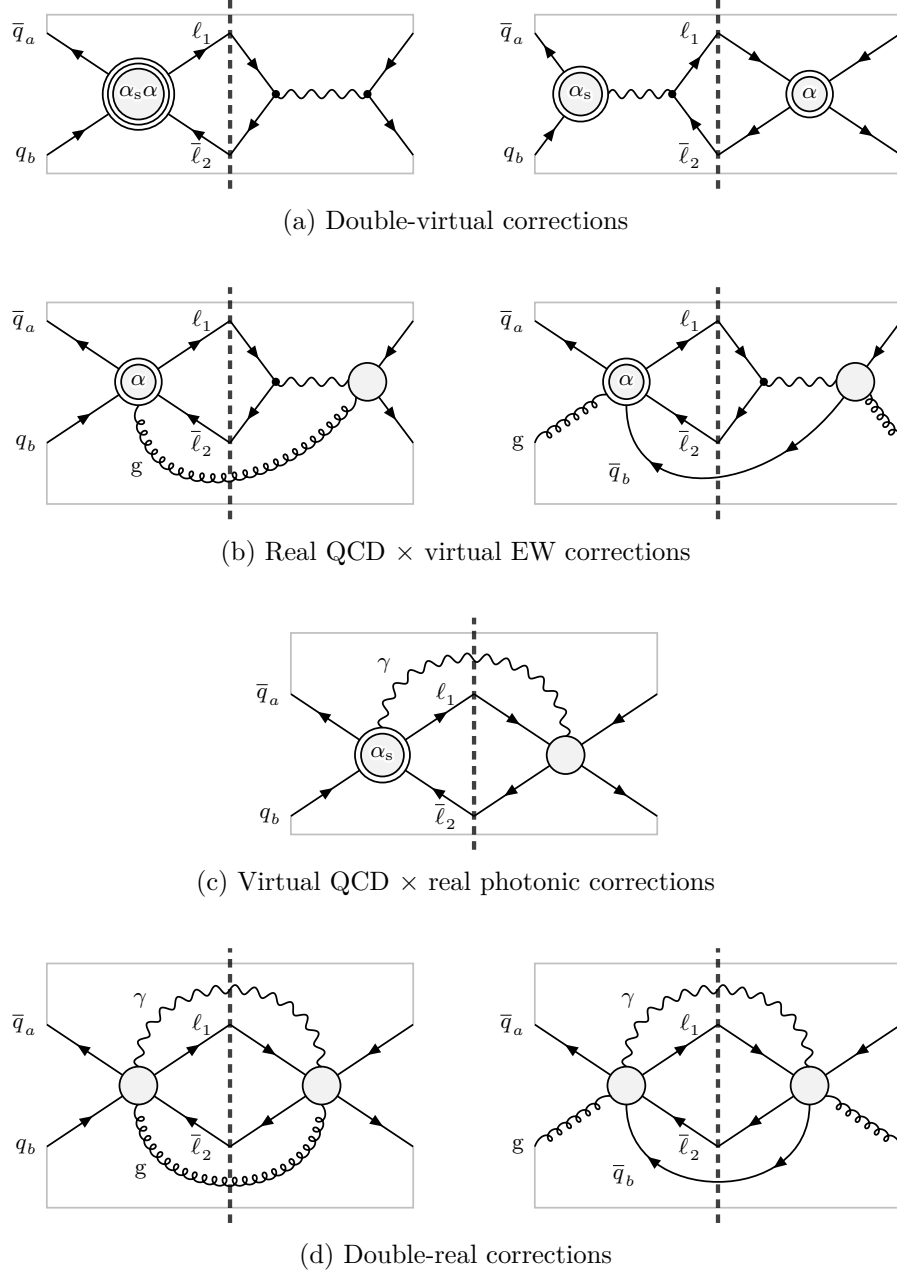


Figure 5.1.: Interference diagrams for the various contributions to the NNLO corrections of $\mathcal{O}(\alpha_s\alpha)$, with blobs representing all relevant tree structures. The blobs with “ α ” and “ α_s ” inside represent one-loop corrections of $\mathcal{O}(\alpha)$ and $\mathcal{O}(\alpha_s)$, respectively. The two-loop corrections of $\mathcal{O}(\alpha_s\alpha)$ is represented by the blob with “ $\alpha_s\alpha$ ” inside. For comparison, the generic interference graphs for the NLO EW case can be found in Fig. 2.3.

to the hard process (2.3) which interfere with the Born amplitude (left diagram), and secondly, the interferences of one-loop amplitudes of $\mathcal{O}(\alpha_s)$ and $\mathcal{O}(\alpha)$ (right diagram). The former comprise two-loop corrections for which no complete analytical is known so far, however, the application of the PA leads to significant simplifications which is discussed in more detail in the explicit calculations presented in Chap. 6 and 7 below. The latter contributions are given by the product of one-loop QCD and EW corrections, which we have already encountered in the NLO calculations discussed in Chap. 4. Note, however, that the product of two one-loop amplitudes will, in general, lead to an increased divergence behaviour with poles up to $\frac{1}{\epsilon^4}$.¹ As a consequence, the one-loop results are in principle required in an expansion up to $\mathcal{O}(\epsilon^2)$ in order to obtain all finite contributions. In the calculation of corrections in the PA discussed in this work, however, the results of the NLO calculation given up to $\mathcal{O}(\epsilon^0)$ turn out to be sufficient owing to the factorized form of their IR singularity structure as we illustrate in more detail in the discussion of the cancellation of IR singularities in the respective calculations.

(b) **Real QCD \times virtual EW corrections:** This type of corrections involves the virtual $\mathcal{O}(\alpha)$ corrections to the dilepton plus jet production channels which we have considered previously for the real $\mathcal{O}(\alpha_s)$ QCD corrections in Eq. (4.43). The interference diagrams for the $\bar{q}q$ and $\bar{q}g$ channels are shown in Fig. 5.1(b) and the remaining qg channel is obtained from the latter by reversing the fermion arrow on the quark line. The application of the PA for these contributions exactly corresponds to the PA applied to the virtual NLO EW corrections to dilepton plus jet production and, therefore, their calculation proceeds in the same manner as described in Sect. 4.2.1. The kinematics of the additional parton in the final state is treated exactly.

(c) **Virtual QCD \times real photonic corrections:** These corrections mainly consist of virtual $\mathcal{O}(\alpha_s)$ corrections to dilepton plus photon production,

$$\bar{q}_a(p_a) + q_b(p_b) \rightarrow \ell_1(k_1) + \bar{\ell}_2(k_2) + \gamma(k). \quad (5.1)$$

Of course, there are also contributions from the crossed channels with photons in the initial state, but owing to their smallness already at NLO (i.e. without QCD corrections) their impact is certainly negligible at $\mathcal{O}(\alpha_s\alpha)$. The generic interference diagram to process (5.1) is shown in Fig. 5.1(c). In order to work out a PA for the photonic bremsstrahlung correction (5.1), we proceed exactly as described for the pure $\mathcal{O}(\alpha)$ case in Sect. 4.2.2, however, with the difference that each contribution to squared matrix elements now contains a QCD loop of $\mathcal{O}(\alpha_s)$. As a consequence, overlapping IR singularities between the QCD and EW corrections arise, which require a careful treatment.

(d) **Double-real corrections:** The double-real $\mathcal{O}(\alpha_s\alpha)$ corrections consist of the tree-level amplitudes to dilepton production in association with a photon and a jet, which receive

¹ This can be seen, for instance, from the fact that both the QCD and photonic corrections to the $V\bar{f}f'$ vertex contain IR poles of $\frac{1}{\epsilon^2}$ which are given in Eqs. (4.40) and (B.29), respectively.

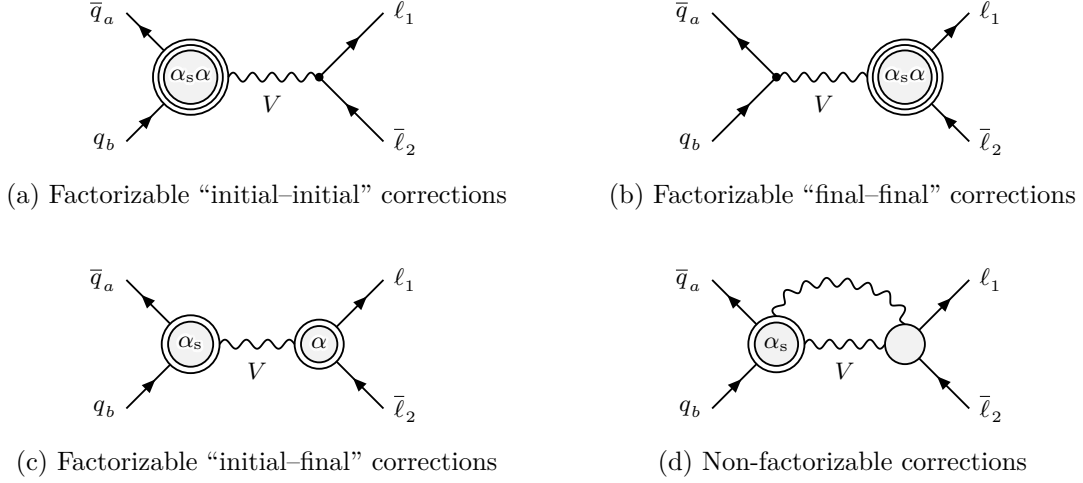


Figure 5.2.: The four types of contributions to the mixed QCD–electroweak corrections in the PA illustrated in terms of generic two-loop amplitudes.

contributions from the following partonic channels:

$$\bar{q}_a(p_a) + q_b(p_b) \rightarrow \ell_1(k_1) + \bar{\ell}_2(k_2) + g(k_g) + \gamma(k), \quad (5.2a)$$

$$g(p_g) + q_b(p_b) \rightarrow \ell_1(k_1) + \bar{\ell}_2(k_2) + q_a(k_a) + \gamma(k), \quad (5.2b)$$

$$g(p_g) + \bar{q}_a(p_a) \rightarrow \ell_1(k_1) + \bar{\ell}_2(k_2) + \bar{q}_b(k_b) + \gamma(k). \quad (5.2c)$$

As in the (virtual QCD) \times (real photonic) corrections, we neglect contributions from crossed channels with photons in the initial state. The generic interference diagrams for the $\bar{q}q$ and $\bar{q}g$ channels are shown in Fig. 5.1(d). The PA for the double-real corrections (5.2) is again constructed as in the pure $\mathcal{O}(\alpha)$ case discussed in Sect. 4.2.2 and is equivalent to the PA applied to the photonic bremsstrahlung corrections to dilepton plus jet production. The additional feature is the presence of an additional final-state parton whose kinematics will be treated exactly.

5.2. Classification of corrections in the pole approximation

As in the NLO EW corrections discussed in Chap. 4 our aim is to calculate the leading corrections in the PA, i.e. the expansion around the resonance pole $p_V^2 \approx M_V^2$. We have already briefly sketched the strategy of the calculation for the different parts that enter into the $\mathcal{O}(\alpha_s \alpha)$ corrections in the previous section. In this section we classify the corrections at this order in terms of the different contributions that can be identified in the PA. Figure 5.2 shows a generic two-loop Feynman graph for each of these contributions which can be divided into three distinct factorizable and the non-factorizable corrections. In the following we describe the general features of the individual PA contributions and estimate their numerical impact to the full $\mathcal{O}(\alpha_s \alpha)$ corrections.

- (a) Factorizable corrections of the type “initial–initial”, i.e. two-loop $\mathcal{O}(\alpha_s \alpha)$ corrections to W/Z production (see Fig. 5.2(a)) and corresponding real-emission and interference parts. From the analysis of the corresponding $\mathcal{O}(\alpha)$ contributions we do not expect very significant

corrections from this part, in particular, in distributions that are insensitive to initial-state radiation effects, such as the transverse-mass and lepton-invariant-mass distributions in the case of W and Z production, respectively. The transverse-lepton-momentum distribution, on the other hand, is sensitive to initial-state recoil effects and the corrections that arise from this part are expected to be more sizeable for this observable. Note, however, that the transverse-lepton-momentum distribution is overwhelmed by large QCD corrections above the threshold for $V + \text{jet}$ production and furthermore, that a fixed-order calculation is insufficient to properly describe this observable around the Jacobian peak as we discussed in Sect. 4.5. Furthermore, the initial–initial contribution involves some additional uncertainty, since no fully adapted set of parton distributions including $\mathcal{O}(\alpha_s\alpha)$ corrections is available. All the more it is important to consistently isolate this contribution—as the pole approximation does—from the rest of the corrections, in order to properly assess its uncertainty.

- (b) Factorizable corrections of the type “final–final”, i.e. two-loop $\mathcal{O}(\alpha_s\alpha)$ corrections to the leptonic W/Z decays as illustrated in Fig. 5.2(b). Such corrections are entirely furnished by virtual contributions from two-loop counterterms and therefore have no contributions from the real-emission corrections of the types shown in Figs. 5.1(b-d). They will be small in size and will not have any visible effect on the shape of distributions, and thus are expected to be phenomenologically insignificant.
- (c) Factorizable corrections of the type “initial–final”, i.e. $\mathcal{O}(\alpha_s)$ corrections to W/Z production in combination with $\mathcal{O}(\alpha)$ corrections to the leptonic W/Z decays. The generic two-loop diagram for this case is shown in Fig. 5.2(c). The factorizable initial–final corrections comprise reducible contributions of the type (one-loop) \times (one-loop) on the virtual side, mixed virtual/real contributions induced by one-loop graphs with single real photon or gluon emission, and double-real contributions with photon and gluon emission. The largest effect at the $\mathcal{O}(\alpha_s\alpha)$ is to be expected from this part, because these reducible contributions combine large QCD corrections to the production with large electroweak corrections to the W/Z decay. The leading part of collinear final-state photon radiation is known to factorize from the QCD-corrected cross section, but only a proper evaluation of these initial–final corrections can reveal to which accuracy simplified factorization approaches hold. The explicit calculation of this contribution is presented in Chap. 7.
- (d) Non-factorizable corrections with QCD corrections to the production and soft-photon exchange between production and decay (see Fig. 5.2(d)). These corrections comprise the most delicate contribution to the PA. Although the non-factorizable corrections are already strongly suppressed in $\mathcal{O}(\alpha)$, such a suppression cannot be safely predicted in advance because of a conceivable enhancement due to QCD recoil effects. Moreover, a new feature arises at $\mathcal{O}(\alpha_s\alpha)$ which was not present at NLO, which constitutes the soft-photon exchange between two final-state particles. Such contributions emerge from the gluon-induced real-QCD emission diagrams as illustrated in the right plots of Figs. 5.1(b,d). Here, the final-state quark is associated with the production sub-process of the V boson and a non-factorizable contribution is given by, e.g. the exchange of a soft photon between the final-state quark and one of the charged leptons. It is therefore important to assess the impact of these corrections and the explicit calculation of this contribution is presented in Chap. 6.

The non-factorizable $\mathcal{O}(\alpha_s\alpha)$ corrections

In this chapter we present the calculation of the non-factorizable corrections of the NNLO $\mathcal{O}(\alpha_s\alpha)$ corrections to the Drell–Yan process (2.3). The results presented in this chapter are the basis of Ref. [87], where the results have been published to a large extent. Section 6.1 describes the calculation of the different contributions to the non-factorizable corrections and in Sect. 6.2 we combine these building blocks into a master formula suitable for numerical evaluation and discuss our treatment of IR singularities. The numerical results are presented in Sect. 6.3.

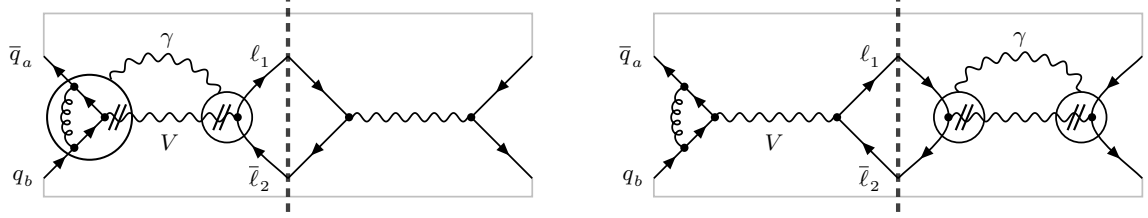
6.1. Calculation of the non-factorizable corrections

In this section we calculate the various contributions to the non-factorizable corrections of $\mathcal{O}(\alpha_s\alpha)$, which are diagrammatically characterized in Fig. 6.1. The calculation makes use of factorization properties of the virtual and real photonic parts of the non-factorizable $\mathcal{O}(\alpha_s\alpha)$ corrections, which result from the soft nature of the effect. Extending the arguments given in the classic paper [131] of Yennie, Frautschi and Suura (YFS), we show in Sect. 6.1.1 that this factorization of the photonic factors even holds to any order in the strong coupling α_s . In the remainder of this section we use this insight to show that both the virtual and real-photon corrections can be written as correction factors to squared matrix elements containing gluon loops or external gluons, i.e. the necessary building blocks are obtained from tree-level and one-loop calculations. We have verified this statement by an explicit diagrammatic calculation as discussed in Sect. 6.1.2 for the example of the double-virtual corrections.

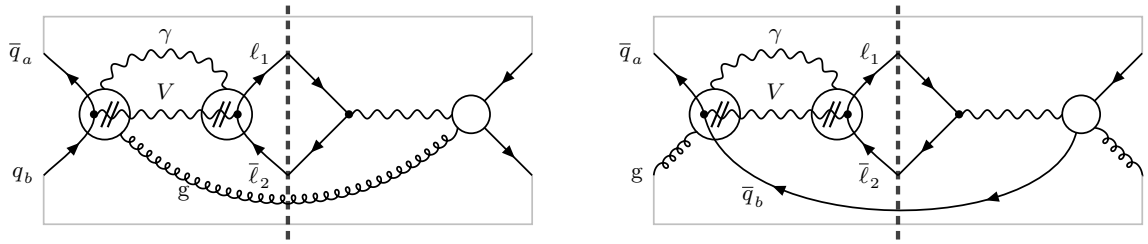
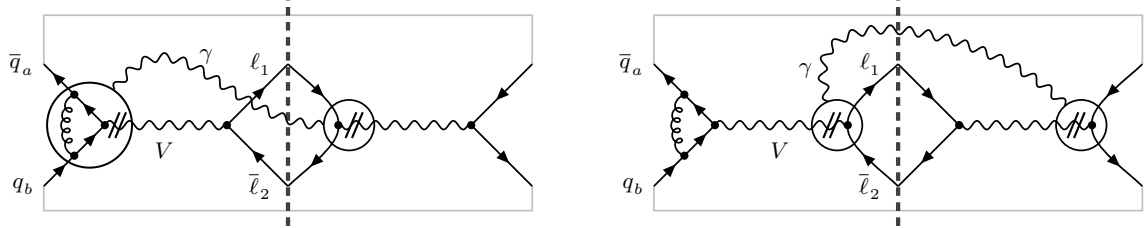
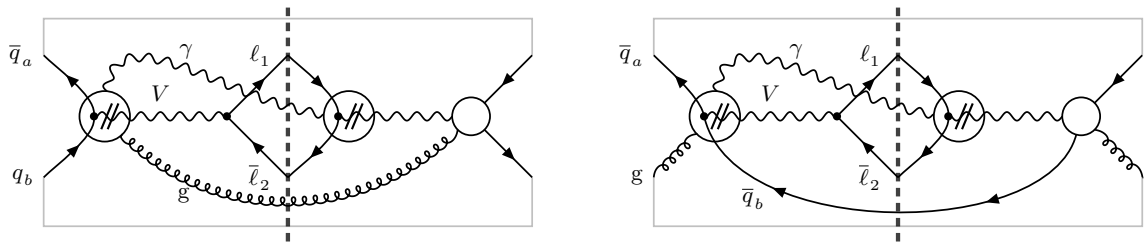
6.1.1. Soft-photon radiation off a quark line—the YFS approach

Before entering the calculation of the non-factorizable corrections of $\mathcal{O}(\alpha_s\alpha)$, it is useful to discuss the general pattern of soft-photon radiation off a quark line with arbitrary gluon emission or exchange. In this investigation we closely follow the appendix of Ref. [131], where the analogous situation is considered in pure QED. An alternative formulation based on Ward identities of vertex functions was given in Ref. [87]. The starting point of our discussion is an arbitrary QCD diagram with any number of real or virtual quarks and gluons, for instance given by the sample Feynman graph shown in Fig. 6.2. We consider all diagrams that are obtained by attaching one end of an additional soft photon into this diagram in all possible ways, where we do not further specify whether the photon is virtual or real. In case of a virtual photon the argument presented in the following can be applied independently for the other end of the photon line that attaches to a different quark line.¹

¹The case where a virtual photon is emitted and reabsorbed from the *same* quark line without a hard interaction in between is not considered here. This case does not occur in the calculation of the non-factorizable corrections where the photon always has to link the production and decay of an unstable particle.



(a) Non-factorizable double-virtual corrections

(b) Non-factorizable real QCD \times virtual EW corrections(c) Non-factorizable virtual QCD \times real photonic corrections

(d) Non-factorizable double-real corrections

Figure 6.1.: Interference diagrams for the various contributions to the non-factorizable corrections of $\mathcal{O}(\alpha_s\alpha)$, with blobs representing all relevant tree structures. The encircled QCD loop diagrams with a photon attached stand for all possibilities to couple the photon to the quark line and the gauge boson V , see Eq. (4.19).

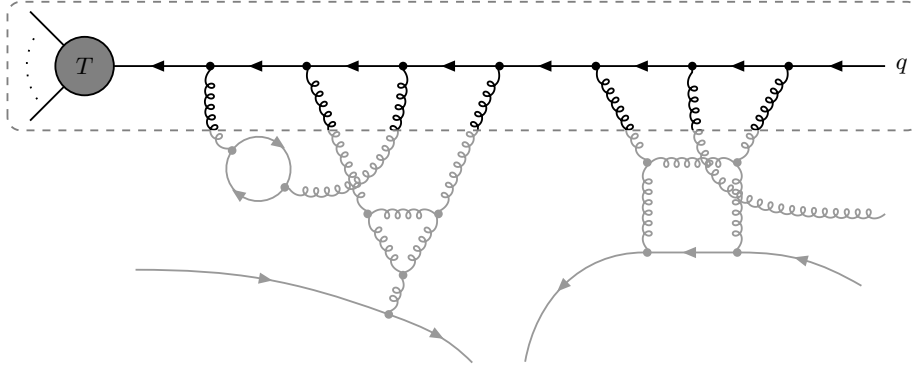


Figure 6.2.: An arbitrary QCD diagram containing a sub-graph with an external quark line terminating at a hard interaction represented by the T -blob.

The insertion of the photon can either occur along a quark line that runs through the diagram connecting two external legs or at an internal propagator of a closed quark loop. For the latter case the argument presented in Ref. [131] can be directly generalized, where we observe that taking the derivative with respect to the loop momentum running along the fermion loop yields the set of diagrams obtained by attaching a photon with zero momentum to the original closed quark line in all possible ways. As a consequence, the attachment of a soft photon along a quark loop vanishes since it leads to an integral of a total derivative and therefore will not be further considered in the following. For a quark line that is connected to an external leg we restrict our discussion to the case where the quark participates in a hard scattering as illustrated by the sub-graph encircled by the dashed box in Fig. 6.2, where the T -blob represents the hard interaction. This special case is used in the application of the results of this section to the Drell–Yan process, where all non-QCD interactions associated with the production and decay of the gauge boson can be “hidden” inside the T -blob, so that the assumption to have a pure QCD diagram as the starting point can be relaxed. The generalisation to the case without an identified hard interaction is straight-forward and proceeds by applying the argument presented in the following from both ends of the fermion line.

We therefore consider the following sub-graph with an incoming external quark line² with n gluon attachments with momenta q_i (treated as incoming by convention) before the hard scattering sub-process represented by the T -blob,

$$\begin{aligned}
 T_0 &\equiv \text{Diagram with } T \text{-blob and } n \text{ gluon attachments } q_1, \dots, q_n \text{ to a quark line with momenta } p_n, \dots, p_1, q \\
 &= T(p_n) \frac{i}{\not{p}_n} \check{\Gamma}^{\bar{q}qg \dots g}(-p_n, p, q_n, \dots, q_1) u(p) \equiv \text{Diagram with } T \text{-blob and } \check{\Gamma} \text{-blob}
 \end{aligned} \tag{6.1}$$

Here p_k denotes the momentum flowing through the quark propagator after the k -th gluon

²The proof is analogous for incoming anti-quarks or outgoing (anti-)quarks.

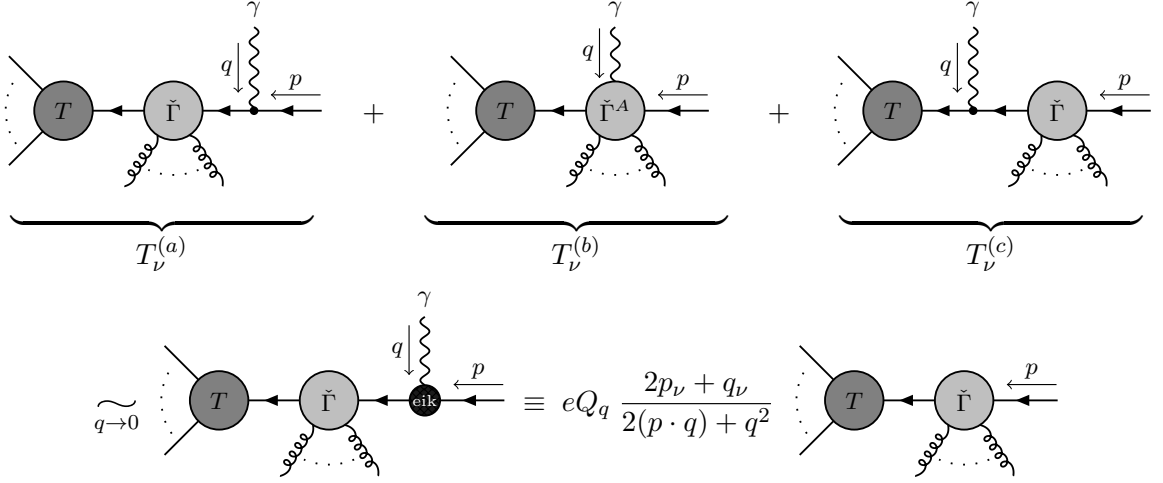


Figure 6.3.: Diagrammatical result of result Eq. (6.17), with the vertex labelled by “eik” denoting the eikonal approximation given explicitly in the right-hand diagram on the last line.

attachment,

$$p_k = p + Q_k, \quad Q_k = \sum_{i=1}^k q_i. \quad (6.2)$$

In the last line of Eq. (6.1) we introduced the matrix $\check{\Gamma}^{\bar{q}qg \cdots g}$ which corresponds to a quark line where n gluons are attached with an ordered assignment that follows the direction of the fermion arrow. Note that the Lorentz and colour indices are suppressed in the notation for clarity. In case of one single gluon $\check{\Gamma}$ is given by the expression for the anti-quark–quark–gluon vertex

$$\check{\Gamma}^{\bar{q}qg}(\bar{p}, p) = -ig_s t_{cc}^a \gamma_\mu, \quad (6.3)$$

where μ and a are the open Lorentz and colour indices of the gluon, respectively, and c (\bar{c}) the colour index of the (anti-)quark. The general case with n gluon attachments is obtained by recursively joining n such vertices with $(n-1)$ quark propagators

$$\check{\Gamma}^{\bar{q}q \overbrace{g \cdots g}^n}(\bar{p}, p, q_n, \dots, q_1) = \check{\Gamma}^{\bar{q}q \overbrace{g \cdots g}^{n-1}}(\bar{p}, p_1, q_n, \dots, q_2) \frac{i}{\not{p}_1} \check{\Gamma}^{\bar{q}qg}(-p_1, p, q_1), \quad (6.4)$$

where we have also included the dependence on the gluon momenta q_i for definiteness.

The sum over all diagrams that are obtained by inserting one end of a soft photon with momentum q along the quark line in the diagram of Eq. (6.1) in all possible ways can be classified into three different contributions (see first line in Fig. 6.3): The attachment at the external end of the quark line (a), at a propagator inside the matrix $\check{\Gamma}^{\bar{q}qg \cdots g}$ (b), and at the propagator joining $\check{\Gamma}^{\bar{q}qg \cdots g}$ and the remaining hard scattering described by $T(p_n + q)$ (c),

$$T_\nu^{(a)} = T(p_n + q) \frac{i}{\not{p}_n + \not{q}} \check{\Gamma}^{\bar{q}qg \cdots g}(-p_n - q, p + q) \frac{i}{\not{p} + \not{q}} (-ie Q_q \gamma_\nu) u(p), \quad (6.5a)$$

$$T_\nu^{(b)} = T(p_n + q) \frac{i}{\not{p}_n + \not{q}} \check{\Gamma}_\nu^{A\bar{q}qg\cdots g}(q, -p_n - q, p + q) u(p), \quad (6.5b)$$

$$T_\nu^{(c)} = T(p_n + q) \frac{i}{\not{p}_n + \not{q}} (-ieQ_q \gamma_\nu) \frac{i}{\not{p}_n} \check{\Gamma}^{\bar{q}qg\cdots g}(-p_n - q, p + q) u(p). \quad (6.5c)$$

The matrix $\check{\Gamma}_\nu^{A\bar{q}qg\cdots g}$ in Eq. (6.5b) is obtained by summing over the $(n - 1)$ possible insertions of the photon at the internal quark propagators of $\check{\Gamma}^{\bar{q}qg\cdots g}$,

$$\begin{aligned} \check{\Gamma}_\mu^{A\bar{q}q\overbrace{g\cdots g}^n}(q, -p_n - q, p) &= \sum_{i=1}^{n-1} \overbrace{\check{\Gamma}^{\bar{q}q\overbrace{g\cdots g}^{n-i}}(-p_n - q, p_i + q)} \frac{i}{\not{p}_i + \not{q}} (-ieQ_q \gamma_\mu) \frac{i}{\not{p}_i} \check{\Gamma}^{\bar{q}q\overbrace{g\cdots g}^i}(-p_i, p). \end{aligned} \quad (6.6)$$

The diagram illustrates the summation over photon insertions at internal quark propagators. It shows a horizontal quark line with momentum p entering from the right and $-p_n - q$ exiting to the left. There are n gluon insertions (represented by curly lines) along the quark chain, with momenta q_1, q_2, \dots, q_n entering from below. A photon (represented by a wavy line) is inserted at the i -th internal quark propagator with momentum q entering from above. The diagram is labeled with equation (6.6).

With the aim to extract the leading singular behaviour in the soft limit ($q \rightarrow 0$), we manipulate the diagram with the photon attachment at the external leg as follows,

$$\begin{aligned} T_\nu^{(a)} &= T(p_n) \frac{i}{\not{p}_n + \not{q}} \check{\Gamma}^{\bar{q}qg\cdots g}(-p_n - q, p + q) \frac{(\not{p} + \not{q})\gamma_\nu}{2(p \cdot q) + q^2} u(p) eQ_q \\ &\underset{q \rightarrow 0}{\sim} T(p_n) \frac{i}{\not{p}_n + \not{q}} \check{\Gamma}^{\bar{q}qg\cdots g}(-p_n - q, p + q) u(p) eQ_q \frac{2p_\nu + q_\nu}{2(p \cdot q) + q^2}, \end{aligned} \quad (6.7)$$

where the Dirac equation for massless fermions ($\not{p}u(p) = 0$) was used in the last step. Here we have omitted the photon momentum inside $T(p_n + q) \underset{q \rightarrow 0}{\sim} T(p_n)$, which is allowed by definition of the hard interaction. However, setting $q = 0$ in the remaining terms of Eq. (6.7) is not feasible beyond NLO, as the difference with respect to such an omission can be just as divergent as the leading singular contribution due to potentially overlapping IR singularities. In order to disentangle the dependence on the photon momentum q we successively apply the propagator identity

$$\frac{i}{\not{p}_k + \not{q}} = \frac{i}{\not{p}_k} - \frac{i}{\not{p}_k + \not{q}} (-i\not{q}) \frac{i}{\not{p}_k} \quad (6.8)$$

to the internal propagators of $\check{\Gamma}^{\bar{q}qg\cdots g}(-p_n - q, p + q)$ and obtain

$$\begin{aligned} \check{\Gamma}^{\bar{q}q\overbrace{g\cdots g}^n}(-p_n - q, p + q) &\stackrel{(6.4)}{=} \check{\Gamma}^{\bar{q}q\overbrace{g\cdots g}^{n-1}}(-p_n - q, p_1 + q) \frac{i}{\not{p}_1 + \not{q}} \check{\Gamma}^{\bar{q}qg}(-p_1, p) \\ &\stackrel{(6.8)}{=} \check{\Gamma}^{\bar{q}q\overbrace{g\cdots g}^{n-2}}(-p_n - q, p_2 + q) \frac{i}{\not{p}_2 + \not{q}} \check{\Gamma}^{\bar{q}qg}(-p_2, p) \\ &\quad - \check{\Gamma}^{\bar{q}q\overbrace{g\cdots g}^{n-1}}(-p_n - q, p_1 + q) \frac{i}{\not{p}_1 + \not{q}} (-i\not{q}) \frac{i}{\not{p}_1} \check{\Gamma}^{\bar{q}qg}(-p_1, p) \end{aligned}$$

$$\begin{aligned}
& \vdots \\
& = \check{\Gamma}^{\bar{q}q\overbrace{\cdots g}^n}(-p_n, p) - \frac{q^\mu}{eQ_q} \check{\Gamma}_\mu^{A\bar{q}q\overbrace{\cdots g}^n}(q, -p_n - q, p).
\end{aligned} \tag{6.9}$$

Equation (6.9) can be viewed as a QED Ward identity that relates $q^\mu \check{\Gamma}_\mu^{A\bar{q}q\cdots g}$ to the difference of two matrices $\check{\Gamma}^{\bar{q}q\cdots g}$ that are shifted by the photon momentum. In a final step, identity (6.8) is applied to the remaining propagator between $\check{\Gamma}^{\bar{q}q\cdots g}$ and the T -blob and Eq. (6.7) can be written as

$$\begin{aligned}
T_\nu^{(a)} & \underset{q \rightarrow 0}{\sim} eQ_q \frac{2p_\nu + q_\nu}{2(p \cdot q) + q^2} T_0 \\
& - q^\mu \frac{2p_\nu + q_\nu}{2(p \cdot q) + q^2} T(p_n) \frac{i}{\not{p}_n + \not{q}} \\
& \times \left[(-ieQ_q \gamma_\mu) \frac{i}{\not{p}_n} \check{\Gamma}^{\bar{q}q\cdots g}(-p_n, p) + \check{\Gamma}_\mu^{A\bar{q}q\cdots g}(q, -p_n - q, p) \right] u(p).
\end{aligned} \tag{6.10}$$

The two terms inside the square bracket show a striking resemblance to the contributions $T_\nu^{(c)}$ and $T_\nu^{(b)}$, respectively, and can be incorporated by a modified coupling structure of the photon to quarks. Gathering all contributions of Eq. (6.5), we write

$$T_\nu^{(a)} + T_\nu^{(b)} + T_\nu^{(c)} \underset{q \rightarrow 0}{\sim} eQ_q \frac{2p_\nu + q_\nu}{2(p \cdot q) + q^2} T_0 + T_\nu^{(\text{int})}, \tag{6.11}$$

where we have introduced the expression

$$T_\nu^{(\text{int})} = T(p_n) \frac{i}{\not{p}_n + \not{q}} \left[(-ieQ_q \gamma_\mu) \frac{i}{\not{p}_n} \check{\Gamma}^{\bar{q}q\cdots g}(-p_n, p) + \check{\Gamma}_\mu^{A\bar{q}q\cdots g}(q, -p_n - q, p) \right] u(p) G^\mu{}_\nu, \tag{6.12}$$

with

$$G^\mu{}_\nu = \delta^\mu{}_\nu - q^\mu \frac{2p_\nu + q_\nu}{2(p \cdot q) + q^2}. \tag{6.13}$$

As in the pure QED case [131] we obtain the result that soft-photon emission from external lines is described by an eikonal factor times the lower-order matrix element, while soft-photon emission from internal lines is described by the replacement $\gamma_\nu \rightarrow \gamma_\mu G^\mu{}_\nu$ in the photon–anti-fermion–fermion vertices.

The attachment of the photon to the quark chain after the momentum flow p_k is described by the replacement

$$\frac{1}{\not{p}_k} \longrightarrow \frac{1}{\not{p}_k + \not{q}} \gamma_\mu G^\mu{}_\nu \frac{1}{\not{p}_k} \stackrel{(6.2)}{=} \frac{1}{\not{p} + \not{Q}_k + \not{q}} \gamma_\mu G^\mu{}_\nu \frac{1}{\not{p} + \not{Q}_k}, \tag{6.14}$$

in the lower-order matrix element T_0 and the appropriate momentum shift $p_l \rightarrow p_l + q$ in the propagators with $l > k$. We observe that in the case where q and Q_k become *simultaneously* soft, this substitution amounts to the replacement of one small denominator by two, potentially worsening the IR-singular behaviour compared to that of T_0 . Hard momenta Q_k , on the other hand, do not lead to singularities and constitute sub-leading contributions that need not be

considered further.

In order to study the potentially problematic case where q and Q_k in Eq. (6.14) become simultaneously soft, we first rewrite the r.h.s. of Eq. (6.14) as follows,

$$\begin{aligned} & \frac{\not{p} + \not{Q}_k + \not{q}}{q^2 + 2q \cdot (p + Q_k) + 2p \cdot Q_k + Q_k^2} \gamma_\mu G^\mu{}_\nu \frac{\not{p} + \not{Q}_k}{2p \cdot Q_k + Q_k^2} \\ &= \frac{1}{q^2 + 2q \cdot (p + Q_k) + 2p \cdot Q_k + Q_k^2} \left\{ \not{p}, \gamma_\mu G^\mu{}_\nu \right\} \not{p} \frac{1}{2p \cdot Q_k + Q_k^2} + \dots, \end{aligned} \quad (6.15)$$

where the on-shell condition $p^2 = 0$ for massless quarks was used and the ellipsis collects all sub-leading contributions that originate from the soft momenta q and Q_k in the numerators of the propagators. Upon closer inspection of the anti-commutator, it can be seen to vanish in the soft-photon limit,

$$\left\{ \not{p}, \gamma_\mu G^\mu{}_\nu \right\} = 2p_\mu G^\mu{}_\nu = -q_\nu + q^2 \frac{2p_\nu + q_\nu}{2(p \cdot q) + q^2} = -q_\mu G^\mu{}_\nu \underset{q \rightarrow 0}{\sim} 0. \quad (6.16)$$

Focussing on the double-soft limit $q \rightarrow \lambda q$, $Q_k \rightarrow \lambda Q_k$ of Eq. (6.15), we observe that the scaling behaviour of the right-hand side of Eq. (6.14) is not λ^{-2} as naively estimated, but rather only λ^{-1} , which is of the same order as the $Q_k \sim 0$ limit of the sub-amplitude T_0 without soft-photon insertion. Therefore, the term $T^{(\text{int})}$ in Eq. (6.11) is suppressed by one power of λ compared to the eikonal term (describing emission from external lines) in the soft-photon limit $q \rightarrow 0$.

We arrive at the final result of this section which states that the sum of the three contributions in Eq. (6.5) simplifies as follows:

$$T_\nu^{(a)} + T_\nu^{(b)} + T_\nu^{(c)} \underset{q \rightarrow 0}{\sim} eQ_q \frac{2p_\nu + q_\nu}{2(p \cdot q) + q^2} T_0, \quad (6.17)$$

independently of the gluon momenta q_i flowing into the quark line which can be hard or soft. This formula will be extensively employed in the following sections in the calculation of the non-factorizable corrections.

6.1.2. Double-virtual corrections

The double-virtual non-factorizable corrections consist of two different contributions, which are illustrated in Fig. 6.1(a) by interference diagrams: First, the $\mathcal{O}(\alpha_s \alpha)$ corrections to the $\bar{q}_a q_b \rightarrow \ell_1 \bar{\ell}_2$ amplitude, which interfere with the Born diagram (the left diagram in Fig. 6.1(a)), and second, the interference between two one-loop-corrected amplitudes with corrections of $\mathcal{O}(\alpha_s)$ and $\mathcal{O}(\alpha)$, respectively,

$$\begin{aligned} |\mathcal{M}_{\bar{q}_a q_b \rightarrow \ell_1 \bar{\ell}_2}|^2 \Big|_{\text{nf}}^{\text{V}_s \otimes \text{V}_{\text{ew}}} &= 2 \text{Re} \left\{ \delta \mathcal{M}_{\text{V}_s \otimes \text{V}_{\text{ew}}, \text{nf}}^{\bar{q}_a q_b \rightarrow \ell_1 \bar{\ell}_2} \left(\mathcal{M}_{0, \text{PA}}^{\bar{q}_a q_b \rightarrow \ell_1 \bar{\ell}_2} \right)^* \right\} \\ &+ 2 \text{Re} \left\{ \delta \mathcal{M}_{\text{V}_{\text{ew}}, \text{nf}}^{\bar{q}_a q_b \rightarrow \ell_1 \bar{\ell}_2} \left(\delta \mathcal{M}_{\text{V}_s, \text{PA}}^{\bar{q}_a q_b \rightarrow \ell_1 \bar{\ell}_2} \right)^* \right\}. \end{aligned} \quad (6.18)$$

The latter correction is shown in the right-hand diagram in Fig. 6.1(a). It can be directly

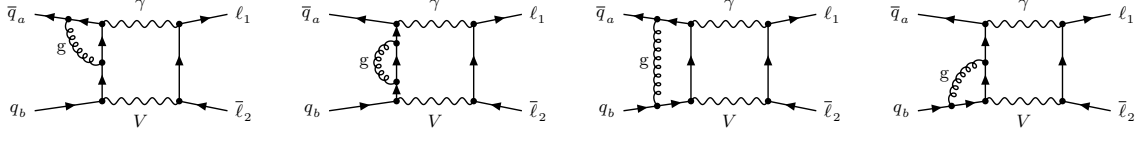


Figure 6.4.: Example diagrams for the non-factorizable double-virtual corrections.

obtained from the results of Sect. 4 and reads

$$\begin{aligned} & \text{Re} \left\{ \delta \mathcal{M}_{V_{\text{ew}}, \text{nf}}^{\bar{q}_a q_b \rightarrow \ell_1 \bar{\ell}_2} \left(\delta \mathcal{M}_{V_s, \text{PA}}^{\bar{q}_a q_b \rightarrow \ell_1 \bar{\ell}_2} \right)^* \right\} \\ &= \text{Re} \left\{ \delta_{V_{\text{ew}}, \text{nf}}^{\bar{q}_a q_b \rightarrow \ell_1 \bar{\ell}_2} \left(\delta_{V_s}^{V \bar{q}_a q_b} \right)^* \right\} \left| \mathcal{M}_{0, \text{PA}}^{\bar{q}_a q_b \rightarrow \ell_1 \bar{\ell}_2} \right|^2. \end{aligned} \quad (6.19)$$

The expressions for $\delta_{V_{\text{ew}}, \text{nf}}^{\bar{q}_a q_b \rightarrow \ell_1 \bar{\ell}_2}$ and $\delta_{V_s}^{V \bar{q}_a q_b}$ are given in Eqs. (4.11) and (4.40), respectively.

The non-factorizable part of the two-loop correction $\delta \mathcal{M}_{V_s \otimes V_{\text{ew}}, \text{nf}}^{\bar{q}_a q_b \rightarrow \ell_1 \bar{\ell}_2}$ in Eq. (6.18) is defined in analogy to the NLO case discussed in Sect. 4.2.1. The contributing two-loop diagrams can be obtained from the NLO diagrams of Fig. 4.3 by attaching a virtual gluon in all possible ways to the quark line. For the example of the initial–final state interference diagram of Fig. 4.3(a), the resulting diagrams are displayed in Fig. 6.4. As at NLO, there are diagrams containing only non-factorizable contributions as well as diagrams possessing both factorizable and non-factorizable parts. For the latter type of diagrams the non-factorizable part is defined via the generalization of Eq. (4.9),

$$\delta \mathcal{M}_{V_s \otimes V_{\text{ew}}, \text{nf}}^{\bar{q}_a q_b \rightarrow \ell_1 \bar{\ell}_2} = \left\{ \delta \mathcal{M}_{V_s \otimes V_{\text{ew}}}^{\bar{q}_a q_b \rightarrow \ell_1 \bar{\ell}_2} - \delta \mathcal{M}_{V_s \otimes V_{\text{ew}}, \text{fact}}^{\bar{q}_a q_b \rightarrow \ell_1 \bar{\ell}_2} \right\}_{p_V^2 \rightarrow M_V^2}. \quad (6.20)$$

A complication compared to the NLO calculation originates from the possibility of overlapping QCD and soft-photon corrections, as in the first and third diagram of Fig. 6.4. After non-trivial cancellations, which are discussed in detail below, the two-loop corrections factorize from the Born amplitude,

$$\delta \mathcal{M}_{V_s \otimes V_{\text{ew}}, \text{nf}}^{\bar{q}_a q_b \rightarrow \ell_1 \bar{\ell}_2} = \delta_{V_{\text{ew}}, \text{nf}}^{\bar{q}_a q_b \rightarrow \ell_1 \bar{\ell}_2} \delta_{V_s}^{V \bar{q}_a q_b} \mathcal{M}_{0, \text{PA}}^{\bar{q}_a q_b \rightarrow \ell_1 \bar{\ell}_2}, \quad (6.21)$$

with identical correction factors as in Eq. (6.19) above. The final result of the double-virtual corrections to the cross section then reads

$$\begin{aligned} d\sigma_{\bar{q}_a q_b, \text{nf}}^{V_s \otimes V_{\text{ew}}} &= 2 \left[\text{Re} \left\{ \delta_{V_{\text{ew}}, \text{nf}}^{\bar{q}_a q_b \rightarrow \ell_1 \bar{\ell}_2} \left(\delta_{V_s}^{V \bar{q}_a q_b} \right)^* \right\} + \text{Re} \left\{ \delta_{V_{\text{ew}}, \text{nf}}^{\bar{q}_a q_b \rightarrow \ell_1 \bar{\ell}_2} \delta_{V_s}^{V \bar{q}_a q_b} \right\} \right] d\sigma_{\bar{q}_a q_b, \text{PA}}^0 \\ &= 4 \text{Re} \left\{ \delta_{V_{\text{ew}}, \text{nf}}^{\bar{q}_a q_b \rightarrow \ell_1 \bar{\ell}_2} \right\} \text{Re} \left\{ \delta_{V_s}^{V \bar{q}_a q_b} \right\} d\sigma_{\bar{q}_a q_b, \text{PA}}^0. \end{aligned} \quad (6.22)$$

We still have to fill the gap of proving Eq. (6.21), a task that we have attacked in two different ways:³ First, using the results from the YFS approach of Sect. 6.1.1 and second, evaluating the non-factorizable parts of the two-loop diagrams directly using the Mellin–Barnes technique.

³ A third calculation was performed using effective-field-theory techniques, which is discussed in Ref. [87].

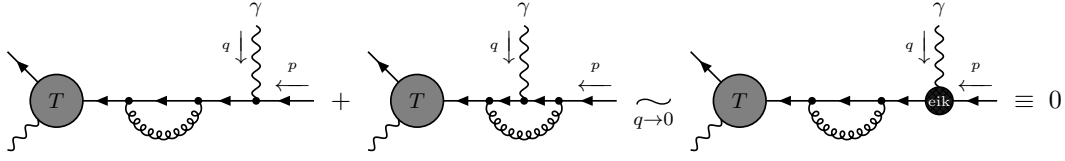
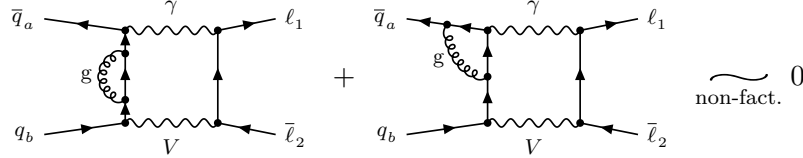


Figure 6.5.: Application of Eq. (6.17) to self-energy diagrams.

Figure 6.6.: Cancellation of diagrams in the non-factorizable double-virtual QCD \times EW corrections due to the identity (6.23) illustrated in Fig. 6.5.

YFS argument

In order to prove the factorization of the two-loop corrections into a product of one-loop factors in Eq. (6.21) we deduce two results from Eq. (6.17). Firstly, we consider the situation in which the $\check{\Gamma}$ blocks in Eqs. (6.5) and (6.17) (see also Fig. 6.3) do not involve external gluons, but only one internal QCD loop, i.e. the $\check{\Gamma}$'s are proportional to α_s , counting powers of α_s only. Owing to our on-shell wave-function renormalization of the external quark field the $T^{(c)}$ part is absent, i.e. $T^{(c)} = 0$, and likewise the whole r.h.s. of Eq. (6.17). The parts $T^{(a)}$ and $T^{(b)}$, however, are non-vanishing and, thus, cancel in the sum as shown in Fig. 6.5. The respective $\check{\Gamma}$ functions of $T^{(a)}$ and $T^{(b)}$ are given by the one-loop quark self-energy factor $i\Sigma^q$ and by the quark-photon vertex function $\Gamma^{A\bar{q}q}$, so that Eq. (6.17) turns into the identity

$$T(p + Q + q) \frac{i}{\not{p} + \not{q}} \left\{ i\Sigma^q(p + q) \frac{i}{\not{p} + \not{q}} (-ieQ_q \gamma_\nu) + \Gamma_\nu^{A\bar{q}q}(q, -p - q, p) \right\} u(p) \underset{q \rightarrow 0}{\simeq} 0. \quad (6.23)$$

Furthermore, since the identity is also valid for the case where the soft photon is virtual, the photon can as well be connected to one of the other charged-particle lines entering the hard function T . Applied to the non-factorizable double-virtual corrections, this leads to the cancellation of all diagrams involving a QCD correction to the quark-photon vertex against diagrams with a QCD self-energy correction to an internal quark line. In the example diagrams from Fig. 6.4 this leads to the cancellation of the two diagrams shown in Fig. 6.6.

As the second application of Eq. (6.17), we take the truncated Green function $\check{\Gamma}$ to be the tree-level quark-gluon vertex. In this case the term $T^{(b)}$ in Eq. (6.17) vanishes since there is no tree-level gluon-photon-anti-quark-quark vertex. As discussed above, the emitted gluon can be connected to the hard sub-process by a loop so that we obtain the identity shown in Fig. 6.7. In the application to the double-virtual non-factorizable corrections, the resulting identity shows that the sum of the diagrams involving a QCD correction to the (off-shell) V -boson-anti-quark-quark vertex and box-type diagrams simplifies to diagrams with a one-loop QCD vertex with on-shell quarks and anti-quarks inserted into the one-loop non-factorizable corrections. This simplification is illustrated in Fig. 6.8.

The remaining non-factorizable double-virtual corrections can be obtained from the example

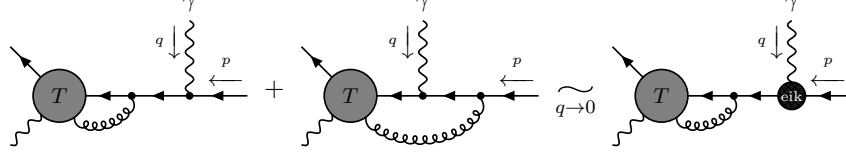
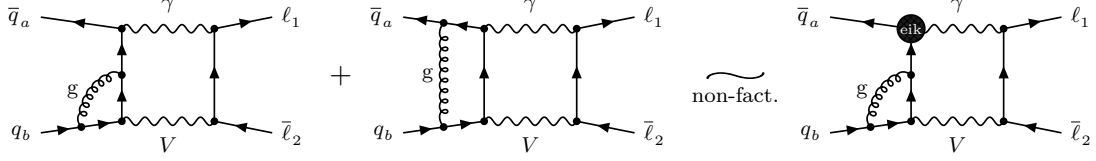


Figure 6.7.: Application of Eq. (6.17) to vertex diagrams.

Figure 6.8.: Simplification of diagrams in the non-factorizable double-virtual QCD \times EW corrections.

diagrams in Fig. 6.4 by moving the photon from the lepton line to the antilepton or V -boson lines, and by attaching it to the incoming quark instead of the anti-quark line. In all diagrams, the two identities in Figs. 6.5 and 6.7 can be applied in an analogous way. As a result, the sum of all diagrams where the V boson is attached directly to the QCD loop is represented in PA by the NLO diagrams for the non-factorizable corrections without gluon exchange times the QCD correction factor (4.40) for the on-shell $V\bar{q}_a q_b$ vertex, while all other diagrams where V is not attached to the QCD loop cancel each other. This establishes the identity in Eq. (6.21).

Mellin–Barnes calculation

In this calculation of the non-factorizable contributions, the resonance-enhanced terms are extracted from the double-virtual corrections on a diagram-by-diagram basis by means of the Mellin–Barnes technique describes in Appendix B.1.1. For manifestly non-factorizable diagrams, following an analogous power-counting argument as presented in Ref. [156], a one-to-one correspondence can be established between the resonant non-factorizable contributions and the terms that diverge linearly for soft photon momenta in the on-shell limit ($p_V^2 = M_V^2$). In the case where the virtual photon is attached to the intermediate gauge-boson propagator, i.e. diagrams that contain both factorizable and non-factorizable parts, Eq. (6.20) defines the gauge-invariant prescription to extract the non-factorizable contributions. Here, all terms that are not IR singular in the on-shell limit with respect to the photon momentum cancel in the difference. In summary, the non-factorizable corrections receive contributions only from the soft-photon region of the loop integrals. As a consequence, only scalar two-loop integrals appear in the final result of the non-factorizable corrections. They are evaluated using the Mellin–Barnes method, which can be employed to perform a systematic expansion in powers of $\frac{p_V^2 - \mu_V^2}{M_V^2}$, where only the leading contribution is needed for the resonance-enhanced non-factorizable corrections. In the following we present the explicit calculation of the two diagrams shown in Fig. 6.6 and demonstrate their cancellation. To this end, we denote the contributions of the two diagrams to

the two-loop matrix element by

$$\mathcal{M}^{(a)} \equiv \quad , \quad \mathcal{M}^{(b)} \equiv \quad . \quad (6.24)$$

The resonant contributions of the two-loop diagrams arise from a soft photon momentum q . The correspondence between the non-factorizable corrections and the leading linear IR singularity in the photon momentum at the on-shell point ($p_V^2 = M_V^2$) allows for the extraction of the relevant resonant contribution before evaluating the two-loop integrals. To this end, we perform the standard tensor reduction of the internal “QCD sub-loop” and by a simple power-counting argument identify all terms that do not contribute to the linear IR singularity and, therefore, can be omitted in the calculation of the non-factorizable corrections. Applying this procedure leads to *scalar* master integrals only, since all terms involving additional factors of the photon momentum in the numerator are less singular and can be neglected. Only retaining these leading singular terms, i.e. applying the ESPA, the second two-loop diagram in Eq. (6.24) reduces to a correction factor multiplying the Born matrix element,

$$\mathcal{M}^{(b)} \sim \frac{C_{\text{F}} \alpha_s}{4\pi} \frac{Q_a Q_1 \alpha}{2\pi} \mathcal{M}_0 (1 - \epsilon) (-t_{a1}) (\mu_V^2 - s_{12}) I(s_{12}, t_{a1}), \quad (6.25)$$

where the scalar two-loop integral is given by the expression

$$I(s_{12}, t_{a1}) = \quad (6.26)$$

$$= \left[\frac{(2\pi\mu)^{2\epsilon}}{i\pi^2} \right]^2 \int \frac{d^d q}{q^2 (q + p_a)^2 [(q + p_a + p_b)^2 - \mu_V^2] (q + k_1)^2} \int \frac{d^d q'}{q'^2 (q' + q + p_a)^2}$$

$$= (4\pi\mu^2)^{2\epsilon} \frac{\Gamma(\epsilon) \Gamma(1 - \epsilon)^2 \Gamma(2 + 2\epsilon)}{\Gamma(1 + \epsilon) \Gamma(2 - 2\epsilon)}$$

$$\times \int_0^1 d^4 x \delta\left(1 - \sum_{i=1}^4 x_i\right) x_1^\epsilon \left[x_1 x_3 (-t_{a1}) + x_2 x_4 (\mu_V^2 - s_{12}) + (1 - x_2) x_4 M_V^2 \right]^{-2-2\epsilon},$$

and all external momenta p_i, k_i correspond to on-shell massless particles $p_i^2 = k_i^2 = 0$. In the last step the integration over the two-loop momenta q and q' was performed after introducing the Feynman parameters x_i and the term $(\mu_V^2 - s_{12})$ was extracted in the anticipation of the expansion we apply in the next step.

The integration over the four Feynman parameters x_i can be performed at the expense of

introducing two Mellin–Barnes integrals,

$$\begin{aligned}
I(s_{12}, t_{a1}) = & \frac{1}{M_V^4} \left(\frac{4\pi\mu^2}{M_V^2} \right)^{2\epsilon} \frac{\Gamma(\epsilon) \Gamma(1-\epsilon)^2}{\Gamma(1+\epsilon) \Gamma(2-2\epsilon) \Gamma(-3\epsilon)} \\
& \frac{1}{(2\pi i)^2} \int_{-i\infty}^{+i\infty} d^2 z \left(\frac{\mu_V^2 - s_{12}}{M_V^2} \right)^{z_1} \left(\frac{-t_{a1}}{M_V^2} \right)^{z_2} \Gamma(2+2\epsilon+z_1+z_2) \Gamma(1+z_1) \\
& \Gamma(-1-3\epsilon-z_1) \Gamma(-z_1) \frac{\Gamma(1+z_2) \Gamma(1+\epsilon+z_2) \Gamma(-1-2\epsilon-z_2) \Gamma(-z_2)}{\Gamma(1-\epsilon+z_2)},
\end{aligned} \tag{6.27}$$

where the integration contour of the complex variable z_i is taken to the right of the “left poles” $\Gamma(\dots + z_i)$ and left of the “right poles” $\Gamma(\dots - z_i)$. Closing the integration contour of z_1 to the right and collecting the residues of the poles in z_1 allows us to perform a systematic expansion in powers of $\frac{\mu_V^2 - s_{12}}{M_V^2}$. The leading term emerges from the residue at $z_1 = (-1 - 3\epsilon)$, whereas all further contributions are not enhanced by resonant propagator factors and can therefore be neglected in the PA,

$$\begin{aligned}
I(s_{12}, t_{a1}) \sim & \frac{1}{M_V^4} \left(\frac{4\pi\mu^2}{M_V^2} \right)^{2\epsilon} \frac{\Gamma(\epsilon) \Gamma(1-\epsilon)^2 \Gamma(1+3\epsilon)}{\Gamma(1+\epsilon) \Gamma(2-2\epsilon)} \left(\frac{\mu_V^2 - s_{12}}{M_V^2} \right)^{-1-3\epsilon} \\
& \frac{1}{(2\pi i)} \int_{-i\infty}^{+i\infty} dz \left(\frac{-t_{a1}}{M_V^2} \right)^z \Gamma(1+\epsilon+z) \Gamma(1+z) \Gamma(-1-2\epsilon-z) \Gamma(-z).
\end{aligned} \tag{6.28}$$

The second Mellin–Barnes integral can be performed in the usual manner by first extracting the divergent terms in ϵ , which correspond to the residues of the poles that pinch the integration contour in the limit $\epsilon \rightarrow 0$, and then performing an expansion in ϵ for the finite remainder. The final result for the scalar two-loop integral reads

$$\begin{aligned}
I(s_{12}, t_{a1}) = & \frac{\Gamma(1+\epsilon)^2}{(\mu_V^2 - s_{12})(-t_{a1})} \left(\frac{\mu_V^2 - s_{12}}{M_V^2} \right)^{-3\epsilon} \left(\frac{4\pi\mu^2}{-t_{a1}} \right)^{2\epsilon} \left\{ \frac{1}{2\epsilon^3} + \frac{1}{\epsilon^2} \right. \\
& + \frac{1}{\epsilon} \left[2 + \frac{5\pi^2}{12} + \text{Li}_2\left(1 + \frac{t_{a1}}{M_V^2}\right) \right] + 2 \text{Li}_3\left(\frac{-t_{a1}}{M_V^2}\right) + \text{Li}_3\left(1 + \frac{t_{a1}}{M_V^2}\right) \\
& - 2 \ln\left(\frac{-t_{a1}}{M_V^2}\right) \left[\frac{\pi^2}{6} - \text{Li}_2\left(1 + \frac{t_{a1}}{M_V^2}\right) \right] + \ln^2\left(\frac{-t_{a1}}{M_V^2}\right) \ln\left(1 + \frac{t_{a1}}{M_V^2}\right) \\
& \left. - 6\zeta(3) + \frac{5\pi^2}{6} + 2 \text{Li}_2\left(1 + \frac{t_{a1}}{M_V^2}\right) + 4 + \mathcal{O}(\epsilon) + \mathcal{O}(s_{12} - \mu_V^2) \right\}.
\end{aligned} \tag{6.29}$$

The calculation of the other two-loop amplitude $\mathcal{M}^{(a)}$ in Eq. (6.24) containing the quark self-energy insertion proceeds along the same lines as discussed above. Applying the tensor reduction to the internal QCD sub-loop generates a term $(\not{q} + \not{p}_a)$ in the numerator which cancels one of the internal quark propagators. The resulting loop structure of the denominators corresponds to the two-loop master integral (6.26). Keeping only the leading singular parts in

the photon momentum, i.e. neglecting all photon momenta q in the numerators, we obtain

$$\mathcal{M}^{(a)} \sim -\frac{C_F \alpha_s}{4\pi} \frac{Q_a Q_1 \alpha}{2\pi} \mathcal{M}_0 (1 - \epsilon) (-t_{a1}) (\mu_V^2 - s_{12}) I(s_{12}, t_{a1}), \quad (6.30)$$

where the correction factor multiplying the Born amplitude involves the same scalar master integral $I(s_{12}, t_{a1})$ as in the case $\mathcal{M}^{(b)}$ and, furthermore, only differs by a global sign. Thus the non-factorizable contributions of the two diagrams of Eq. (6.24) cancel exactly, which was to be shown.

These cancellations can already be seen after performing the integral over the gluon momentum, i.e. before integrating over the photon momentum, so that the result directly extends to diagrams where the soft photon is attached to the intermediate V boson or the $\bar{\ell}_2$ final-state lepton, and to real soft-photon emission. We have also explicitly verified the identity shown in Fig. 6.8 using this method which involves the same soft-photon loop integral after integrating out the gluon sub-loop.

6.1.3. Real QCD \times virtual EW corrections

The (real QCD) \times (virtual EW) corrections are given by the virtual $\mathcal{O}(\alpha)$ corrections to dilepton plus jet production, with the three production channels of Eq. (4.43). The diagrams contributing to the non-factorizable part of these corrections are the same as those for the virtual non-factorizable corrections to V -boson production and decay in association with a jet. Two generic interference diagrams are shown in Fig. 6.1(b) for the quark–anti-quark induced (left-hand diagram) and gluon–quark induced (right-hand diagram) channels. The calculation proceeds in an analogous manner as presented in Sect. 4.2.1 for the case of V production, but becomes more involved due to the additional external particle. Furthermore, a new feature comes into play for the gluon-induced processes, where the photon exchange between two final-state particles enters the calculation. Considering for example the $\bar{q}q$ initial state, the non-factorizable corrections are defined in analogy to Eq. (4.9) by the difference of the full diagrams and the factorizable contributions in the limit where the vector boson is on shell,

$$\delta \mathcal{M}_{\text{Vew,nf}}^{\bar{q}_a q_b \rightarrow \ell_1 \bar{\ell}_2 g} = \left\{ \delta \mathcal{M}_{\text{Vew}}^{\bar{q}_a q_b \rightarrow \ell_1 \bar{\ell}_2 g} - \delta \mathcal{M}_{\text{Vew,fact}}^{\bar{q}_a q_b \rightarrow \ell_1 \bar{\ell}_2 g} \right\}_{p_V^2 \rightarrow M_V^2}. \quad (6.31)$$

Note that we will make no assumption on the momentum k_g of the real gluon, in particular it is not assumed to be soft. Therefore in the (real QCD) \times (virtual EW) case the resonance expansion is performed for

$$p_V^2 = (k_1 + k_2)^2 = s_{ab} - 2(p_a + p_b) \cdot k_g \approx M_V^2, \quad (6.32)$$

with $s_{ab} = (p_a + p_b)^2$. The definition of the non-factorizable corrections for the gq - and $g\bar{q}$ -initiated channels is analogous. As in the NLO case, only soft-photon exchange delivers resonant contributions, so that the YFS arguments of Sect. 6.1.1 apply. Since these arguments work equally well for real and virtual gluons, the same reasoning made explicit in the double-virtual case of the previous section implies that the virtual non-factorizable photonic corrections factorize from the real QCD amplitude. As an example, the analogue of the identity from Fig. 6.7 for real-gluon emission is shown in Fig. 6.9, and the application to the non-factorizable corrections is illustrated in Fig. 6.10 for a set of example diagrams.

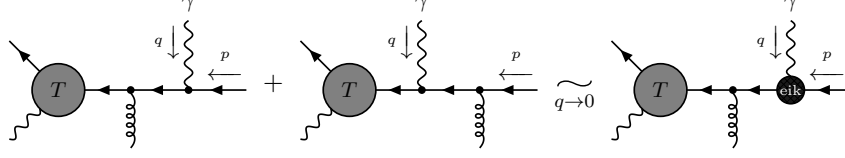
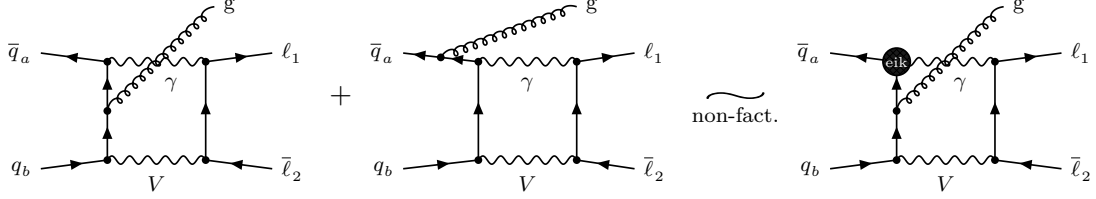


Figure 6.9.: Application of Eq. (6.17) to gluon-emission diagrams.

Figure 6.10.: Example diagrams for the (real QCD) \times (virtual EW) non-factorizable initial-final corrections. The application of the identity of Fig. 6.9 shows that the resonance expansion of the sum of the diagrams is equal to the one-loop non-factorizable initial-final soft correction to the process $\bar{q}_a q_b \rightarrow \ell_1 \bar{\ell}_2 g$ as indicated by the last diagram.

We obtain the final result

$$d\sigma_{\bar{q}_a q_b, \text{nf}}^{\text{Rs} \otimes \text{Vew}} = 2 \text{Re} \left\{ \delta_{\text{Vew}, \text{nf}}^{\bar{q}_a q_b \rightarrow \ell_1 \bar{\ell}_2 g} \right\} d\sigma_{\bar{q}_a q_b, \text{PA}}^{\text{Rs}}, \quad (6.33a)$$

$$d\sigma_{g q_b, \text{nf}}^{\text{Rs} \otimes \text{Vew}} = 2 \text{Re} \left\{ \delta_{\text{Vew}, \text{nf}}^{g q_b \rightarrow \ell_1 \bar{\ell}_2 q_a} \right\} d\sigma_{g q_b, \text{PA}}^{\text{Rs}}, \quad (6.33b)$$

$$d\sigma_{g \bar{q}_a, \text{nf}}^{\text{Rs} \otimes \text{Vew}} = 2 \text{Re} \left\{ \delta_{\text{Vew}, \text{nf}}^{g \bar{q}_a \rightarrow \ell_1 \bar{\ell}_2 \bar{q}_b} \right\} d\sigma_{g \bar{q}_a, \text{PA}}^{\text{Rs}}, \quad (6.33c)$$

where the tree-level cross sections $d\sigma_{\text{PA}}^{\text{Rs}}$ result from the real NLO QCD corrections in Eqs. (4.45) and (4.46) upon neglecting non-resonant contributions, i.e. the photon-exchange diagrams in the neutral-current process. The virtual correction factors have been computed by directly evaluating the difference of the one-loop integrals and the intermediate result in terms of scalar integrals together with the contributing Feynman diagrams are given in Eq. (B.38). The explicit results for each channel are given by

$$\begin{aligned} \delta_{\text{Vew}, \text{nf}}^{\bar{q}_a q_b \rightarrow \ell_1 \bar{\ell}_2 g} = & -\frac{\alpha}{2\pi} \sum_{\substack{ii'=ab,ba \\ f=1,2}} \eta_i Q_i \eta_f Q_f \left\{ 2 + \text{Li}_2 \left(1 + \frac{M_V^2 - t_{i'g}}{t_{if}} \right) \right. \\ & \left. + \left[\frac{c_\epsilon}{\epsilon} - 2 \ln \left(\frac{\mu_V^2 - s_{12}}{\mu M_V} \right) \right] \left[1 - \ln \left(\frac{M_V^2 - t_{i'g}}{-t_{if}} \right) \right] \right\}, \end{aligned} \quad (6.34a)$$

$$\delta_{\text{Vew}, \text{nf}}^{g q_b \rightarrow \ell_1 \bar{\ell}_2 q_a} = -\frac{\alpha}{2\pi} \sum_{f=1,2} \eta_f Q_f \left\{ \left[\frac{c_\epsilon}{\epsilon} - 2 \ln \left(\frac{\mu_V^2 - s_{12}}{\mu M_V} \right) \right] \right\}$$

$$\begin{aligned}
& \times \left[(Q_b - Q_a) - Q_b \ln \left(\frac{M_V^2 - t_{ga}}{-t_{bf}} \right) + Q_a \ln \left(\frac{s_{gb} - M_V^2}{s_{af}} \right) \right] \\
& + 2(Q_b - Q_a) + Q_b \text{Li}_2 \left(1 + \frac{M_V^2 - t_{ga}}{t_{bf}} \right) - Q_a \text{Li}_2 \left(1 - \frac{s_{gb} - M_V^2}{s_{af}} \right) \Big\},
\end{aligned} \tag{6.34b}$$

$$\delta_{\text{Vew,nf}}^{\bar{q}_a q_b \rightarrow \ell_1 \bar{\ell}_2 \bar{q}_b} = -\delta_{\text{Vew,nf}}^{\bar{q}_a q_b \rightarrow \ell_1 \bar{\ell}_2 q_a} \Big|_{a \leftrightarrow b}. \tag{6.34c}$$

In the limits of soft and/or collinear gluons, these correction factors can be related to the one in Eq. (4.11) for the hard process without the additional QCD radiation,

$$\delta_{\text{Vew,nf}}^{\bar{q}_a q_b \rightarrow \ell_1 \bar{\ell}_2 g}(p_a, p_b, k_1, k_2, k_g) \xrightarrow{k_g \text{ soft}} \delta_{\text{Vew,nf}}^{\bar{q}_a q_b \rightarrow \ell_1 \bar{\ell}_2}(p_a, p_b, k_1, k_2), \tag{6.35a}$$

$$\delta_{\text{Vew,nf}}^{\bar{q}_a q_b \rightarrow \ell_1 \bar{\ell}_2 g}(p_a, p_b, k_1, k_2, k_g) \xrightarrow{k_g \rightarrow (1-x)p_a} \delta_{\text{Vew,nf}}^{\bar{q}_a q_b \rightarrow \ell_1 \bar{\ell}_2}(xp_a, p_b, k_1, k_2), \tag{6.35b}$$

$$\delta_{\text{Vew,nf}}^{\bar{q}_a q_b \rightarrow \ell_1 \bar{\ell}_2 g}(p_a, p_b, k_1, k_2, k_g) \xrightarrow{k_g \rightarrow (1-x)p_b} \delta_{\text{Vew,nf}}^{\bar{q}_a q_b \rightarrow \ell_1 \bar{\ell}_2}(p_a, xp_b, k_1, k_2), \tag{6.35c}$$

$$\delta_{\text{Vew,nf}}^{g \bar{q}_a q_b \rightarrow \ell_1 \bar{\ell}_2 q_a}(p_g, p_b, k_1, k_2, k_a) \xrightarrow{k_a \rightarrow (1-x)p_g} \delta_{\text{Vew,nf}}^{\bar{q}_a q_b \rightarrow \ell_1 \bar{\ell}_2}(xp_g, p_b, k_1, k_2), \tag{6.35d}$$

$$\delta_{\text{Vew,nf}}^{g \bar{q}_a q_b \rightarrow \ell_1 \bar{\ell}_2 \bar{q}_b}(p_g, p_a, k_1, k_2, k_b) \xrightarrow{k_b \rightarrow (1-x)p_g} \delta_{\text{Vew,nf}}^{\bar{q}_a q_b \rightarrow \ell_1 \bar{\ell}_2}(p_a, xp_g, k_1, k_2). \tag{6.35e}$$

These properties are crucial in the cancellation of IR singularities, as will be discussed in more detail in Sect. 6.2.

6.1.4. Virtual QCD \times real photonic corrections

The non-factorizable (virtual QCD) \times (real photonic) corrections are constructed from the one-loop QCD amplitude for dilepton plus photon production (5.1) by an extension of the method used at NLO in Sect. 4.2.2. We split photon emission from the V -boson line into initial- and final-state radiation parts via the partial fractioning (4.17). The non-factorizable corrections arise from the interference of diagrams with initial-state radiation with those with final-state radiation. The contributing diagrams are obtained by attaching a virtual gluon in all possible ways to the quark line in the NLO real non-factorizable corrections in Fig. 4.6(c). The two possible contributions are illustrated in Fig. 6.1(c) in terms of interference diagrams. Again, a resonance enhancement only occurs if the momentum of the real photon is soft. The contributions of the form of the right-hand diagram are already factorized into the virtual QCD corrections to V -boson production and the final-initial real-photonic corrections. In contrast, the contributions shown in the left-hand diagram involve the virtual QCD corrections to V -boson plus photon production. The contributing diagrams are obtained from those for the double-virtual corrections (cf. Fig. 6.4) by turning the virtual photon into a real photon by detaching it from the final-state lepton line.

The fastest way to calculate the latter contributions is again to make use of the YFS arguments described in Sect. 6.1.1, where we did not specify whether the soft photon with momentum q is virtual or real. This is true, in particular, for the identities shown in Figs. 6.5 and 6.7 used in the derivation using the YFS method of Sect. 6.1.2 for the double-virtual case. In the same way as for the double-virtual corrections, these simplifications imply that the (virtual QCD) \times (real photonic) initial-state corrections to the matrix element factorize into the QCD

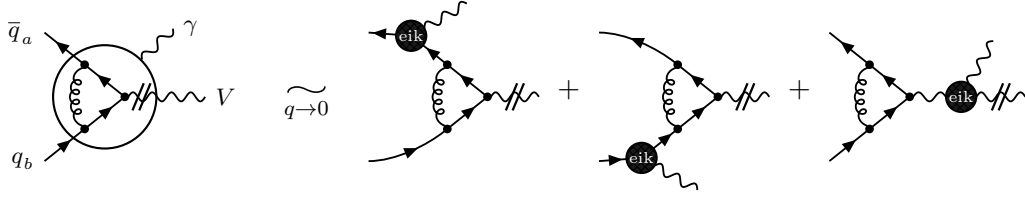


Figure 6.11.: Simplifications of the (virtual QCD) \times (real photonic initial-state) corrections appearing in the left-hand diagram of Fig. 6.1(c) as a result of the YFS identities of Figs. 6.5 and 6.7.

on-shell vertex corrections $\delta_{V_s}^{V\bar{q}aq_b}$ of Eq. (4.40) and the eikonal current $\mathcal{J}_{\text{prod}}$ of Eq. (4.22). This result is illustrated diagrammatically in Fig. 6.11. The same result is obtained using the Feynman-diagrammatic approach of Sect. 6.1.2, since the cancellations of the diagrams in Figs. 6.5 and 6.7 can be observed already after performing the integral over the gluon loop momentum and holds both for real or virtual soft photons.

The result for the complete (virtual QCD) \times (real photonic) non-factorizable corrections, thus, is

$$d\sigma_{\bar{q}aq_b, \text{nf}}^{V_s \otimes \text{R}_{\text{ew}}} = \delta_{\text{R}_{\text{ew}}, \text{nf}}^{\bar{q}aq_b \rightarrow \ell_1 \bar{\ell}_2 \gamma} d\sigma_{\bar{q}aq_b, \text{PA}}^{V_s} = \delta_{\text{R}_{\text{ew}}, \text{nf}}^{\bar{q}aq_b \rightarrow \ell_1 \bar{\ell}_2 \gamma} 2 \text{Re} \left\{ \delta_{V_s}^{V\bar{q}aq_b} \right\} d\sigma_{\bar{q}aq_b, \text{PA}}^0, \quad (6.36)$$

with the real-photon correction factor (4.22). The soft-photon factor required for the regularization of the soft singularities using the slicing method is identical to the one at NLO and given in Eq. (4.37).

6.1.5. Double-real corrections

The non-factorizable double-real corrections are calculated by applying the construction of Sect. 4.2.2 to the three partonic channels (5.2) for dilepton production in association with a jet and a photon. As for the (real QCD) \times (virtual EW) corrections the kinematics of the extra final-state QCD parton will be treated exactly so that the resonance condition is given by Eq. (6.32) for the case of the sub-process $\bar{q}aq_b \rightarrow \ell_1 \bar{\ell}_2 g \gamma$, and analogous expressions for the other two gluon-induced sub-processes. The non-factorizable contributions are again given by the interference of diagrams with soft-photon emission from the production and decay stages of the vector boson. Diagrams for the quark–anti-quark and quark–gluon initial states are shown in Fig. 6.1(d). Note that for the channels with an initial-state gluon, photon radiation from the production sub-process is not limited to initial-state radiation because of photon emission off the final-state quark or anti-quark.

The YFS arguments of Sect. 6.1.1 prove that the non-factorizable real photonic corrections, which are induced by soft photons with $E_\gamma \lesssim \Gamma_V$ only, factorize from the respective squared amplitudes of the processes (4.43) with external (hard or soft) partons. The squared matrix elements for the double-real corrections,

$$\left| \mathcal{M}_{\text{R}_s \otimes \text{R}_{\text{ew}}}^{\bar{q}aq_b \rightarrow \ell_1 \bar{\ell}_2 \gamma g} \right|_{\text{nf}}^2 = \delta_{\text{R}_{\text{ew}}, \text{nf}}^{\bar{q}aq_b \rightarrow \ell_1 \bar{\ell}_2 \gamma g} \left| \mathcal{M}_{\text{R}_s, \text{PA}}^{\bar{q}aq_b \rightarrow \ell_1 \bar{\ell}_2 g} \right|^2, \quad (6.37a)$$

$$\left| \mathcal{M}_{\text{R}_s \otimes \text{R}_{\text{ew}}}^{gq_b \rightarrow \ell_1 \bar{\ell}_2 \gamma q_a} \right|_{\text{nf}}^2 = \delta_{\text{R}_{\text{ew}}, \text{nf}}^{gq_b \rightarrow \ell_1 \bar{\ell}_2 \gamma q_a} \left| \mathcal{M}_{\text{R}_s, \text{PA}}^{gq_b \rightarrow \ell_1 \bar{\ell}_2 q_a} \right|^2, \quad (6.37b)$$

$$\left| \mathcal{M}_{\text{R}_s \otimes \text{R}_{\text{ew}}}^{g\bar{q}_a \rightarrow \ell_1 \bar{\ell}_2 \gamma \bar{q}_b} \right|_{\text{nf}}^2 = \delta_{\text{R}_{\text{ew}}, \text{nf}}^{g\bar{q}_a \rightarrow \ell_1 \bar{\ell}_2 \gamma \bar{q}_b} \left| \mathcal{M}_{\text{R}_s, \text{PA}}^{g\bar{q}_a \rightarrow \ell_1 \bar{\ell}_2 \gamma \bar{q}_b} \right|^2, \quad (6.37c)$$

are, thus, given by the ones for the tree matrix elements with an additional final-state parton, multiplied by the correction factors

$$\delta_{\text{R}_{\text{ew}}, \text{nf}}^{\bar{q}_a q_b \rightarrow \ell_1 \bar{\ell}_2 \gamma g} = -2 \text{Re} \left\{ \mathcal{J}_{\text{prod}}^\mu(p_a, p_b, p_a + p_b - k_g) (\mathcal{J}_{\text{dec}, \mu}(k_1, k_2))^* \right\}, \quad (6.38a)$$

$$\delta_{\text{R}_{\text{ew}}, \text{nf}}^{g q_b \rightarrow \ell_1 \bar{\ell}_2 \gamma q_a} = -2 \text{Re} \left\{ \mathcal{J}_{\text{prod}}^\mu(-k_a, p_b, p_g + p_b - k_a) (\mathcal{J}_{\text{dec}, \mu}(k_1, k_2))^* \right\}, \quad (6.38b)$$

$$\delta_{\text{R}_{\text{ew}}, \text{nf}}^{g \bar{q}_a \rightarrow \ell_1 \bar{\ell}_2 \gamma \bar{q}_b} = -2 \text{Re} \left\{ \mathcal{J}_{\text{prod}}^\mu(p_a, -k_b, p_g + p_a - k_b) (\mathcal{J}_{\text{dec}, \mu}(k_1, k_2))^* \right\}, \quad (6.38c)$$

for the non-factorizable real photonic corrections, which are derived from the modified eikonal currents (4.23). The difference between the three versions of $\mathcal{J}_{\text{prod}}^\mu$ in Eq. (6.38) lies only in the momentum insertions; the first two arguments of $\mathcal{J}_{\text{prod}}^\mu$ refer to the momenta of the photon-radiating (anti-)quark legs, the third to the resonant internal V boson which takes care of the momentum loss induced by parton emission before the resonance. Note that the gluon momentum (but not the soft photon momentum) now enters momentum conservation, i.e. $p_a + p_b = k_1 + k_2 + k_g$ for process (5.2a), etc., in the evaluation of $\delta_{\text{R}_{\text{ew}}, \text{nf}}^{\dots}$ via Eq. (6.38).

As already done at NLO, we regularize the soft-photon singularity by applying a slicing cut $\Delta E \ll \Gamma_V$ on the photon energy. Soft photons obeying $\Delta E < E_\gamma \lesssim \Gamma_V \ll M_V$ are included in the integration of $\delta_{\text{R}_{\text{ew}}, \text{nf}}^{\dots}$ in Eq. (6.38), and extremely soft photons with $E_\gamma < \Delta E$ are included via eikonal integrals based on the usual soft-photon asymptotics as given in Eq. (4.37) for the NLO case. Here we have to generalize this result to take into account the hard-gluon kinematics and the possibility to have gluons in the initial state. Using the results of Appendix C, the following soft factors are obtained

$$\begin{aligned} \delta_{\text{soft}}^{\bar{q}_a q_b \rightarrow \ell_1 \bar{\ell}_2 g} &= \frac{\alpha}{\pi} \sum_{\substack{ii'=ab,ba \\ ff'=12,21}} \eta_i Q_i \eta_f Q_f \left\{ \left[\frac{c_\epsilon}{\epsilon} - 2 \ln \left(\frac{2\Delta E}{\mu} \right) \right] \left[1 - \ln \left(\frac{M_V^2 - t_{i'g}}{-t_{if}} \right) \right] \right. \\ &\quad + \frac{s_{ab} + M_V^2}{s_{ab} - M_V^2} \ln \left(\frac{s_{ab}}{M_V^2} \right) - \frac{1}{2} \ln^2 \left(\frac{s_{ab}}{M_V^2} \right) - \text{Li}_2 \left(-\frac{s_{gf}}{M_V^2} \right) - \text{Li}_2 \left(\frac{s_{gf'}}{s_{ab}} \right) \\ &\quad \left. + \text{Li}_2 \left(-\frac{t_{i'f}}{t_{if}} \right) - \text{Li}_2 \left(\frac{t_{ig}}{s_{ab} + t_{ig}} \right) - \text{Li}_2 \left(\frac{-t_{i'g}}{M_V^2 - t_{i'g}} \right) \right\}, \end{aligned} \quad (6.39a)$$

$$\begin{aligned} \delta_{\text{soft}}^{g q_b \rightarrow \ell_1 \bar{\ell}_2 q_a} &= \frac{\alpha}{\pi} \sum_{ff'=12,21} \eta_f Q_f \left\{ \left[\frac{c_\epsilon}{\epsilon} - 2 \ln \left(\frac{2\Delta E}{\mu} \right) \right] \right. \\ &\quad \times \left[Q_b - Q_a - Q_b \ln \left(\frac{M_V^2 - t_{ga}}{-t_{bf}} \right) + Q_a \ln \left(\frac{s_{gb} - M_V^2}{s_{af}} \right) \right] \\ &\quad + (Q_b - Q_a) \left[\frac{s_{gb} + M_V^2}{s_{gb} - M_V^2} \ln \left(\frac{s_{gb}}{M_V^2} \right) - \text{Li}_2 \left(-\frac{s_{af}}{M_V^2} \right) - \text{Li}_2 \left(\frac{s_{af'}}{s_{gb}} \right) \right] \\ &\quad \left. + Q_b \left[\text{Li}_2 \left(-\frac{t_{gf}}{t_{bf}} \right) - \text{Li}_2 \left(\frac{t_{ba}}{s_{gb} + t_{ba}} \right) - \text{Li}_2 \left(\frac{-t_{ga}}{M_V^2 - t_{ga}} \right) - \frac{1}{2} \ln^2 \left(\frac{s_{gb}}{M_V^2} \right) \right] \right\} \end{aligned}$$

$$-Q_a \left[\text{Li}_2 \left(-\frac{M_V^2}{s_{gb}} \frac{s_{af'}}{s_{af}} \right) + \text{Li}_2 \left(1 - \frac{s_{gb}}{M_V^2} \right) \right] \Bigg\}, \quad (6.39b)$$

$$\delta_{\text{soft}}^{g\bar{q}_a \rightarrow \ell_1 \bar{\ell}_2 \bar{q}_b} = -\delta_{\text{soft}}^{gq_b \rightarrow \ell_1 \bar{\ell}_2 q_a} \Big|_{a \leftrightarrow b}, \quad (6.39c)$$

where $s_{ii'} = (p_i + p_{i'})^2$ and $t_{if} = (p_i - k_f)^2$. In the soft-gluon limit, the correction factors reduce to the respective case without the gluon emission from Sect. 4.2.2,

$$\delta_{\text{soft}}^{g\bar{q}_a q_b \rightarrow \ell_1 \bar{\ell}_2 g}(p_a, p_b, k_1, k_2, k_g) \xrightarrow{k_g \text{ soft}} \delta_{\text{soft}}^{g\bar{q}_a q_b \rightarrow \ell_1 \bar{\ell}_2}(p_a, p_b, k_1, k_2). \quad (6.40a)$$

In the limits of collinear quark–gluon splittings in the initial states, the frame dependence of the slicing factors becomes apparent, and we obtain

$$\delta_{\text{soft}}^{g\bar{q}_a q_b \rightarrow \ell_1 \bar{\ell}_2 g}(p_a, p_b, k_1, k_2, k_g) \xrightarrow{k_g \rightarrow (1-x)p_a} \delta_{\text{soft}, \Lambda_z(x,1)}^{g\bar{q}_a q_b \rightarrow \ell_1 \bar{\ell}_2}(xp_a, p_b, k_1, k_2), \quad (6.40b)$$

$$\delta_{\text{soft}}^{g\bar{q}_a q_b \rightarrow \ell_1 \bar{\ell}_2 g}(p_a, p_b, k_1, k_2, k_g) \xrightarrow{k_g \rightarrow (1-x)p_b} \delta_{\text{soft}, \Lambda_z(1,x)}^{g\bar{q}_a q_b \rightarrow \ell_1 \bar{\ell}_2}(p_a, xp_b, k_1, k_2), \quad (6.40c)$$

$$\delta_{\text{soft}}^{gq_b \rightarrow \ell_1 \bar{\ell}_2 q_a}(p_g, p_b, k_1, k_2, k_a) \xrightarrow{k_a \rightarrow (1-x)p_g} \delta_{\text{soft}, \Lambda_z(x,1)}^{g\bar{q}_a q_b \rightarrow \ell_1 \bar{\ell}_2}(xp_g, p_b, k_1, k_2), \quad (6.40d)$$

$$\delta_{\text{soft}}^{g\bar{q}_a \rightarrow \ell_1 \bar{\ell}_2 \bar{q}_b}(p_g, p_a, k_1, k_2, k_b) \xrightarrow{k_b \rightarrow (1-x)p_g} \delta_{\text{soft}, \Lambda_z(1,x)}^{g\bar{q}_a q_b \rightarrow \ell_1 \bar{\ell}_2}(p_a, xp_g, k_1, k_2). \quad (6.40e)$$

The generic factor $\delta_{\text{soft}, \Lambda_z(z_a, z_b)}^{g\bar{q}_a q_b \rightarrow \ell_1 \bar{\ell}_2}(p_a, p_b, k_1, k_2)$ is the slicing factor obtained for the process $\bar{q}_a q_b \rightarrow \ell_1 \bar{\ell}_2$, evaluated not in the partonic centre-of-mass frame (given by the rest frame of the momentum $p_a + p_b$), but in the rest frame of the momentum $\frac{p_a}{z_a} + \frac{p_b}{z_b}$, which is Lorentz boosted along the beam axis

$$\begin{aligned} & \delta_{\text{soft}, \Lambda_z(z_a, z_b)}^{g\bar{q}_a q_b \rightarrow \ell_1 \bar{\ell}_2}(p_a, p_b, k_1, k_2) \\ &= \frac{\alpha}{\pi} \sum_{\substack{ii'=ab,ba \\ f=1,2}} \eta_i Q_i \eta_f Q_f \left\{ \left[\frac{c_\epsilon}{\epsilon} - 2 \ln \left(\frac{2\Delta E}{\mu} \right) \right] \left[1 - \ln \left(\frac{M_V^2}{-t_{if}} \right) \right] \right. \\ & \quad + \frac{z_a + z_b}{z_a - z_b} \ln \left(\frac{z_a}{z_b} \right) + \text{Li}_2 \left(-\frac{z_i}{z_{i'}} \frac{t_{i'f}}{t_{if}} \right) + \text{Li}_2 \left(1 - \frac{z_{i'}}{z_i} \right) \\ & \quad \left. - \text{Li}_2 \left(\left(1 - \frac{z_{i'}}{z_i} \right) \frac{-t_{if}}{M_V^2} \right) - \text{Li}_2 \left(\left(1 - \frac{z_i}{z_{i'}} \right) \frac{-t_{i'f}}{M_V^2} \right) \right\}. \end{aligned} \quad (6.41)$$

For the proper cancellation of the overlapping (QCD) \times (photonic) IR singularities, these correction factors are employed in the context of the dipole subtraction formalism.

6.2. Complete result for the non-factorizable corrections

The non-factorizable corrections to the cross section are obtained by integrating the different contributions calculated in Sect. 6.1 over the respective phase spaces,

$$\hat{\sigma}_{\text{nf}}^{\text{NNLO}_{\text{s} \otimes \text{ew}}} = \int_2 d\sigma_{\text{nf}}^{\text{V}_s \otimes \text{V}_{\text{ew}}} + \int_3 d\sigma_{\text{nf}}^{\text{R}_s \otimes \text{V}_{\text{ew}}} + \int_2 d\sigma_{\text{nf}}^{\text{C}_s \otimes \text{V}_{\text{ew}}}$$

$$\begin{aligned}
& + \iint_{2+\gamma} d\sigma_{\text{nf}}^{V_s \otimes R_{\text{ew}}} + \iint_{3+\gamma} d\sigma_{\text{nf}}^{R_s \otimes R_{\text{ew}}} + \iint_{2+\gamma} d\sigma_{\text{nf}}^{C_s \otimes R_{\text{ew}}} \\
& = \int_2 d\sigma_{\text{PA}}^{V_s} 2 \operatorname{Re} \left\{ \delta_{V_{\text{ew},\text{nf}}}^{2 \rightarrow 2} \right\} + \int_3 d\sigma_{\text{PA}}^{R_s} 2 \operatorname{Re} \left\{ \delta_{V_{\text{ew},\text{nf}}}^{2 \rightarrow 3} \right\} + \int_2 d\sigma_{\text{PA}}^{C_s} 2 \operatorname{Re} \left\{ \delta_{V_{\text{ew},\text{nf}}}^{2 \rightarrow 2} \right\} \\
& + \iint_{2+\gamma} d\sigma_{\text{PA}}^{V_s} \delta_{R_{\text{ew},\text{nf}}}^{2 \rightarrow 2+\gamma} + \iint_{3+\gamma} d\sigma_{\text{PA}}^{R_s} \delta_{R_{\text{ew},\text{nf}}}^{2 \rightarrow 3+\gamma} + \iint_{2+\gamma} d\sigma_{\text{PA}}^{C_s} \delta_{R_{\text{ew},\text{nf}}}^{2 \rightarrow 2+\gamma}. \tag{6.42}
\end{aligned}$$

Here $\delta_{V_{\text{ew},\text{nf}}}^{2 \rightarrow 2}$ is a shorthand for the virtual NLO non-factorizable corrections (4.11), while the factor $\delta_{V_{\text{ew},\text{nf}}}^{2 \rightarrow 3}$ is a generic expression for the virtual non-factorizable corrections to the various real-QCD correction channels given in Eq. (6.33). Similar abbreviations have been introduced for the real non-factorizable corrections. In the first line of Eq. (6.42) a collinear counterterm $d\sigma_{\text{nf}}^{C_s \otimes V_{\text{ew}}}$ has been added to subtract collinear singularities remaining in the sum of the double-virtual and the (real QCD) \times (virtual EW) corrections that are absorbed into the PDFs. The term $d\sigma_{\text{nf}}^{C_s \otimes R_{\text{ew}}}$ plays the same role for the sum of the (virtual QCD) \times (real EW) and the double-real corrections in the second line. Since the non-factorizable EW corrections contain only soft singularities, all collinear singularities are purely of QCD origin. The collinear subtraction term exploits factorization properties in the collinear limits and is therefore universal in the sense that it is constructed as a convolution of the Altarelli–Parisi splitting kernels with the lower-order (in α_s) cross section. Therefore, the results of Sect. 4.2 for the non-factorizable EW corrections can be used to write these collinear counterterms schematically as a product of $d\sigma_{\text{PA}}^{C_s}$, which is obtained from the collinear counterterm appearing in the NLO QCD corrections in Eq. (4.45) upon neglecting non-resonant contributions, and the photonic correction factors $\delta_{V_{\text{ew},\text{nf}}}^{2 \rightarrow 2}$ and $\delta_{R_{\text{ew},\text{nf}}}^{2 \rightarrow 2+\gamma}$, respectively. Each of the six integrals in Eq. (6.42) are separately IR divergent, however, all divergences cancel in the sum. As described for the NLO calculation in Chap. 4, IR singularities from QCD emission are rearranged using the dipole subtraction formalism, while the soft singularities from photon emission are regularized by the slicing method.

We first apply the dipole subtraction formalism to Eq. (6.42) in order to cancel the IR singularities associated with the QCD corrections. For the double-real contribution, we construct the dipole terms in the following way,

$$\iint_{3+\gamma} \left\{ d\sigma_{\text{PA}}^{R_s} \delta_{R_{\text{ew},\text{nf}}}^{2 \rightarrow 3+\gamma} (\Phi_{3+\gamma}) - \sum_{\substack{\text{QCD} \\ \text{dipoles}}} d\sigma_{\text{PA}}^0 \delta_{R_{\text{ew},\text{nf}}}^{2 \rightarrow 2+\gamma} (\tilde{\Phi}_{2+\gamma}) \otimes dV_{\text{dip}} \right\}, \tag{6.43}$$

where the relative correction factors $\delta_{R_{\text{ew},\text{nf}}}^{2 \rightarrow n+\gamma}$ of the non-factorizable photonic corrections match the differential cross sections they are multiplied with. In particular, the correction factor to the dipoles dV_{dip} is consistently evaluated on the respective dipole phase space. In the singular regions, where the additional QCD emission tends towards a soft and/or collinear configuration, the correction factors coincide

$$\delta_{R_{\text{ew},\text{nf}}}^{2 \rightarrow 3+\gamma} \xrightarrow[\text{QCD partons}]{\text{soft and/or collinear}} \delta_{R_{\text{ew},\text{nf}}}^{2 \rightarrow 2+\gamma}, \tag{6.44}$$

and a proper cancellation of divergences is ensured.

Similarly to the double-real case, the dipole terms for the (real QCD) \times (virtual EW) corrections

are constructed as follows,

$$\int_3 \left\{ d\sigma_{\text{PA}}^{\text{Rs}} 2 \text{Re} \left\{ \delta_{\text{Vew,nf}}^{2 \rightarrow 3}(\Phi_3) \right\} - \sum_{\substack{\text{QCD} \\ \text{dipoles}}} d\sigma_{\text{PA}}^0 2 \text{Re} \left\{ \delta_{\text{Vew,nf}}^{2 \rightarrow 2}(\tilde{\Phi}_2) \right\} \otimes dV_{\text{dip}} \right\}. \quad (6.45)$$

The relation between the correction factors $\delta_{\text{Vew,nf}}^{2 \rightarrow 3}$ and $\delta_{\text{Vew,nf}}^{2 \rightarrow 2}$ in the soft and/or collinear limits given in Eq. (6.35) ensures that the cancellation in the singular regions remains unaffected although different correction factors are introduced for the real cross-section and subtraction terms.

As in the NLO QCD case described in Sect. 4.4, the subtraction functions are integrated over the one-parton phase space containing the soft and collinear QCD singularities, leading to the **I**, **K**, and **P** terms. This integration is essentially unchanged in the $\mathcal{O}(\alpha_s\alpha)$ non-factorizable corrections, since the additional $\mathcal{O}(\alpha)$ factors $\delta_{\text{Rew,nf}}^{2 \rightarrow 2+\gamma}$ and $\delta_{\text{Vew,nf}}^{2 \rightarrow 2}$ multiplying the dipoles dV_{dip} in Eqs. (6.43) and (6.45), respectively, do not depend on the singular parton kinematics, but merely appear as constant factors in the singular integrals. Introducing the insertion operators of the dipole subtraction formalism, as described in Sect. 4.4, we obtain

$$\begin{aligned} \hat{\sigma}_{\text{nf}}^{\text{NNLO}_{\text{s} \otimes \text{ew}}} = & \int_2 \left\{ d\sigma_{\text{PA}}^{\text{Vs}} + d\sigma_{\text{PA}}^0 \otimes \mathbf{I} \right\} 2 \text{Re} \left\{ \delta_{\text{Vew,nf}}^{2 \rightarrow 2} \right\} \\ & + \int_3 \left\{ d\sigma_{\text{PA}}^{\text{Rs}} 2 \text{Re} \left\{ \delta_{\text{Vew,nf}}^{2 \rightarrow 3} \right\} - \sum_{\substack{\text{QCD} \\ \text{dipoles}}} d\sigma_{\text{PA}}^0 2 \text{Re} \left\{ \delta_{\text{Vew,nf}}^{2 \rightarrow 2} \right\} \otimes dV_{\text{dip}} \right\} \\ & + \int_0^1 dx \int_2 d\sigma_{\text{PA}}^0 2 \text{Re} \left\{ \delta_{\text{Vew,nf}}^{2 \rightarrow 2} \right\} \otimes (\mathbf{K} + \mathbf{P}) \\ & + \iint \left\{ d\sigma_{\text{PA}}^{\text{Vs}} + d\sigma_{\text{PA}}^0 \otimes \mathbf{I} \right\} \delta_{\text{Rew,nf}}^{2 \rightarrow 2+\gamma} \\ & + \iint \left\{ d\sigma_{\text{PA}}^{\text{Rs}} \delta_{\text{Rew,nf}}^{2 \rightarrow 3+\gamma} - \sum_{\substack{\text{QCD} \\ \text{dipoles}}} d\sigma_{\text{PA}}^0 \delta_{\text{Rew,nf}}^{2 \rightarrow 2+\gamma} \otimes dV_{\text{dip}} \right\} \\ & + \int_0^1 dx \iint d\sigma_{\text{PA}}^0 \delta_{\text{Rew,nf}}^{2 \rightarrow 2+\gamma} \otimes (\mathbf{K} + \mathbf{P}), \end{aligned} \quad (6.46)$$

where we have suppressed the dependence on the phase-space kinematics for the sake of transparency. It is implicitly assumed that all correction factors are evaluated with the same kinematics as the differential cross sections $d\sigma$ in front of them.

All lines of Eq. (6.46) are now individually free of QCD singularities, however, the integrals over the photon phase space in the last three lines still gives rise to soft singularities that cancel against the IR singularities in the virtual photonic corrections in the first three lines. These soft singularities are dealt with using the slicing method as described in Sect. 4.2.2 for the NLO EW case. As a result we are able to arrange the six contributions in Eq. (6.46) into a form where all IR divergences are cancelled in the integrands explicitly,

$$\hat{\sigma}_{\text{nf}}^{\text{NNLO}_{\text{s} \otimes \text{ew}}} = \tilde{\sigma}_{\text{nf}}^{\text{Vs} \otimes \text{Vew}} + \tilde{\sigma}_{\text{nf}}^{\text{Vs} \otimes \text{Rew}} + \tilde{\sigma}_{\text{nf}}^{\text{Rs} \otimes \text{Vew}} + \tilde{\sigma}_{\text{nf}}^{\text{Rs} \otimes \text{Rew}} + \tilde{\sigma}_{\text{nf}}^{\text{Cs} \otimes \text{Vew}} + \tilde{\sigma}_{\text{nf}}^{\text{Cs} \otimes \text{Rew}}, \quad (6.47)$$

where each term is an IR-finite object and its phase-space integration can be performed

numerically in four dimensions. However, individual terms depend on an artificial energy-slicing parameter ΔE that cancels in the sum. Equation (6.47) will be our master formula for the numerical evaluation discussed in Sect. 6.3. In the following we describe the construction of the individual ingredients. In order to discuss some subtle points in the implementation that are not obvious in the compact notation used here, we give the explicit expressions for all contributions for the quark–anti-quark and quark–gluon induced channels in Appendix D.1.

The first two terms in Eq. (6.47) arise from the sum of the double-virtual and the (virtual QCD) \times (real photonic) corrections, including the insertion operators from the dipole formalism. Analogously to the NLO case discussed in the end of Sect. 4.2.2, the integral over the photon momentum with $E_\gamma < \Delta E$ in the real photonic corrections is computed analytically and added to the double-virtual corrections,

$$\tilde{\sigma}_{\text{nf}}^{\text{Vs} \otimes \text{Vew}} = \int_2 \left\{ d\sigma_{\text{PA}}^{\text{Vs}} + d\sigma_{\text{PA}}^0 \otimes \mathbf{I} \right\} \left[2 \operatorname{Re} \left\{ \delta_{\text{Vew,nf}}^{2 \rightarrow 2} \right\} + \delta_{\text{soft}}^{2 \rightarrow 2}(\Delta E) \right], \quad (6.48)$$

$$\tilde{\sigma}_{\text{nf}}^{\text{Vs} \otimes \text{Rew}} = \iint_{\substack{2+\gamma \\ E_\gamma > \Delta E}} \left\{ d\sigma_{\text{PA}}^{\text{Vs}} + d\sigma_{\text{PA}}^0 \otimes \mathbf{I} \right\} \delta_{\text{Rew,nf}}^{2 \rightarrow 2+\gamma}, \quad (6.49)$$

where the integrated soft-photon factor $\delta_{\text{soft}}^{2 \rightarrow 2}$ is the same as at NLO, see Eq. (4.37).

For the contributions involving real QCD corrections, special care must be taken since the procedure of applying a cut on the photon energy depends on the frame of reference. In order not to spoil the cancellation of the IR singularities treated with the subtraction method, the slicing cut on the photon energy in $\tilde{\sigma}_{\text{nf}}^{\text{Rs} \otimes \text{Rew}}$ is applied in the partonic centre-of-mass frame of the $2 \rightarrow 3 + \gamma$ process for both the double-real cross section and the dipole terms. This results in the following expressions for the IR-finite real-gluon contributions to the cross section,

$$\begin{aligned} \tilde{\sigma}_{\text{nf}}^{\text{Rs} \otimes \text{Vew}} &= \int_3 \left\{ d\sigma_{\text{PA}}^{\text{Rs}} \left[2 \operatorname{Re} \left\{ \delta_{\text{Vew,nf}}^{2 \rightarrow 3} \right\} + \delta_{\text{soft}}^{2 \rightarrow 3}(\Delta E) \right] \right. \\ &\quad \left. - \sum_{\substack{\text{QCD} \\ \text{dipoles}}} d\sigma_{\text{PA}}^0 \left[2 \operatorname{Re} \left\{ \delta_{\text{Vew,nf}}^{2 \rightarrow 2} \right\} + \delta_{\text{soft}, \Lambda_z(x_{\text{dip}})}^{2 \rightarrow 2}(\Delta E) \right] \otimes dV_{\text{dip}} \right\}, \end{aligned} \quad (6.50)$$

$$\tilde{\sigma}_{\text{nf}}^{\text{Rs} \otimes \text{Rew}} = \iint_{\substack{3+\gamma \\ E_\gamma > \Delta E}} \left\{ d\sigma_{\text{PA}}^{\text{Rs}} \delta_{\text{Rew,nf}}^{2 \rightarrow 3+\gamma} - \sum_{\substack{\text{QCD} \\ \text{dipoles}}} d\sigma_{\text{PA}}^0 \delta_{\text{Rew,nf}}^{2 \rightarrow 2+\gamma} \otimes dV_{\text{dip}} \right\}, \quad (6.51)$$

using a generic notation $\Lambda_z(x_{\text{dip}})$ for the boost in the soft-photon factor of Eq. (6.41). Note that the dipole kinematics in Eq. (6.51) is boosted along the beam axis, cf. Eq. (4.47). Therefore, the analytical integration over the soft-photon phase space results in the boosted slicing factor $\delta_{\text{soft}, \Lambda_z}^{2 \rightarrow 2}$, given in Eq. (6.41), for the integrated dipole terms appearing in Eq. (6.50). Inspecting the limiting behaviour of $\delta_{\text{soft}}^{2 \rightarrow 3}$ and $\delta_{\text{soft}, \Lambda_z}^{2 \rightarrow 2}$ in the singular limits, as given in Eq. (6.40), one can easily verify that expression (6.50) is IR finite.

Finally, we consider the convolution terms with additional virtual or real EW corrections in the third and sixth line of Eq. (6.46). The cut on the photon energy $E_\gamma > \Delta E$ in the bremsstrahlung contribution is applied in the rest frame of the incoming momenta *before* the collinear splittings, i.e. the rest frame of the momenta $p_a/x + p_b$ or $p_a + p_b/x$, where p_a and p_b denote the momenta entering the hard scattering cross section σ_{PA}^0 . This choice is consistent

with the cut prescription chosen in the the double-real corrections in Eq. (6.51). For the resulting IR-finite contributions to the cross section we obtain

$$\tilde{\sigma}_{\text{nf}}^{\text{C}_s \otimes \text{V}_{\text{ew}}} = \int_0^1 dx \int_2 d\sigma_{\text{PA}}^0 \left[2 \text{Re} \left\{ \delta_{\text{V}_{\text{ew}}, \text{nf}}^{2 \rightarrow 2} \right\} + \delta_{\text{soft}, \Lambda_z(x)}^{2 \rightarrow 2}(\Delta E) \right] \otimes (\mathbf{K} + \mathbf{P}), \quad (6.52)$$

$$\tilde{\sigma}_{\text{nf}}^{\text{C}_s \otimes \text{R}_{\text{ew}}} = \int_0^1 dx \int\!\!\!\int_{\substack{2+\gamma \\ E_\gamma > \Delta E}} d\sigma_{\text{PA}}^0 \delta_{\text{R}_{\text{ew}}, \text{nf}}^{2 \rightarrow 2+\gamma} \otimes (\mathbf{K} + \mathbf{P}). \quad (6.53)$$

6.3. Numerical results for non-factorizable corrections

Figure 6.12 shows our numerical results for the $\mathcal{O}(\alpha_s\alpha)$ non-factorizable corrections to the $M_{\text{T},\nu\ell}$ and $p_{\text{T},\ell}$ distributions for W^+ production at the LHC in terms of relative correction factors ($\delta_{\alpha_s\alpha}^{\text{nf}}$) to the LO prediction. We employ the identical setup as in the NLO calculation which is described in Sect. 4.5. The absolute distributions and the results of the NLO calculation are shown in Fig. 4.8. The contributions induced by virtual photons, indicated by α_{virt} , are IR regularized upon adding the real soft-photon counterpart which accounts for the emission of photons of energy $E_\gamma < \Delta E \ll \Gamma_V$. Correspondingly, the real photonic contributions denoted by α_{real} only consider the emission of photons with $E_\gamma > \Delta E$. Therefore, both contributions, α_{virt} and α_{real} , depend on the unphysical slicing parameter ΔE which cancels in their sum. Note that the photon-energy cut ΔE , which we numerically set to $\Delta E = 10^{-4} \times \sqrt{\hat{s}}/2$, is much smaller than the width Γ_V of the resonating gauge boson. Our results are further broken down into the quark–anti-quark and the gluon-induced channels, denoted by $q\bar{q}$ and qg , receptively.⁴ The individual contributions from virtual and real photons roughly reach the 0.5% level in case of the $M_{\text{T},\nu\ell}$ distribution and even grow to a several percent in the $p_{\text{T},\ell}$ distribution. The relatively large corrections observed in the transverse-momentum distributions above the threshold are induced by the recoil of the W boson against a hard jet in the real QCD corrections which was also observed for the NLO QCD corrections as shown in the plots in the second row of Fig. 4.8. However, in the ΔE -independent sum of all non-factorizable corrections, these contributions cancel almost perfectly leading to a net correction that is way below the 0.1% level and, thus, phenomenologically negligible.

The numerical results of the non-factorizable $\mathcal{O}(\alpha_s\alpha)$ corrections to the neutral-current process are shown in Fig. 6.13, which comprise the relative correction factors to the $M_{\ell\ell}$ and $p_{\text{T},\ell}$ distribution. The respective absolute distributions and results of the NLO calculation are shown in Fig. 4.9. These corrections turn out to be even smaller than in the charged-current case, the individual virtual and real photonic contributions staying below the 0.02% and 0.5% level for the invariant-mass and the transverse-momentum distribution, respectively. The smallness of these corrections can be understood by inspecting the behaviour of the non-factorizable corrections under the interchange of the momenta of the two leptons. For the neutral-current process, the correction factors δ_{nf} are antisymmetric under such an interchange ($k_1 \leftrightarrow k_2$), which can be directly seen from the respective formulas by using $Q_1 = Q_2$ and $\eta_1 = -\eta_2$. This property of δ_{nf} effectively projects out the antisymmetric part of the cross section that they multiply, which is highly suppressed compared to the symmetric part that enters the LO prediction in the normalization. Similar suppression effects were observed in the literature in the comparison of non-factorizable corrections between ZZ [161] and WW [156, 162, 163]

⁴The anti-quark–gluon induced contributions are included in the contributions labelled qg in the figures.

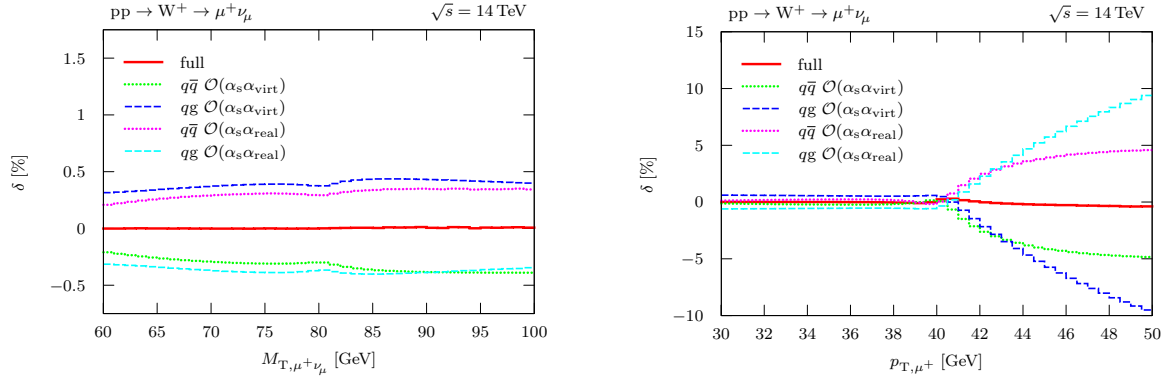


Figure 6.12.: Relative non-factorizable corrections of $\mathcal{O}(\alpha_s \alpha)$ to the distributions in the transverse mass (left) and transverse lepton momentum (right) for W^+ production at the LHC, broken up into contributions of partonic $q\bar{q}/qg$ initial states and virtual/real photonic contributions.

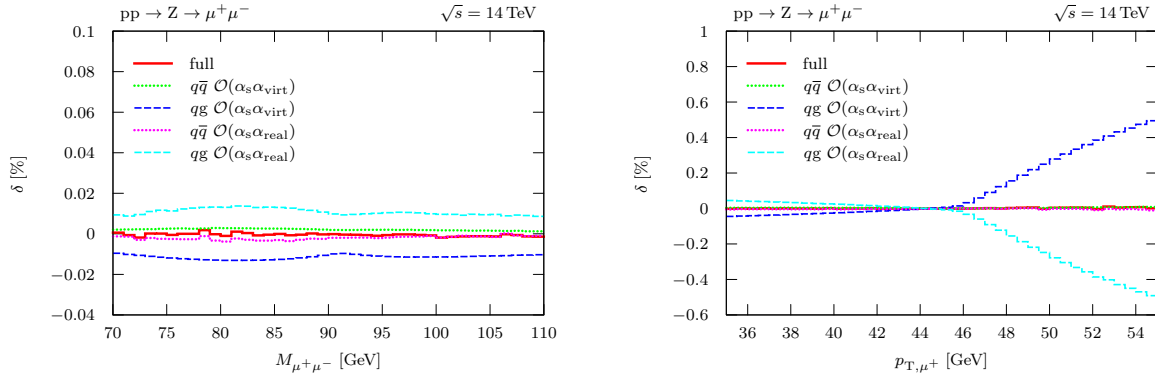


Figure 6.13.: Relative non-factorizable corrections of $\mathcal{O}(\alpha_s \alpha)$ to the distributions in the invariant mass (left) and transverse lepton momentum (right) for Z production at the LHC, broken up into contributions of partonic $q\bar{q}/qg$ initial states and virtual/real photonic contributions.

production. Apart from the overall size, the corrections show a similar behaviour as in the case of W production discussed above, leading to the same conclusion that the mixed QCD–electroweak non-factorizable corrections are phenomenologically negligible.

Of course, one could have speculated on this suppression, since the impact of non-factorizable photonic corrections is already at the level of some 0.1% at NLO. However, the $\mathcal{O}(\alpha_s \alpha)$ corrections mix EW and QCD effects, so that small photonic corrections might have been enhanced by the strong jet recoil effect observed in the $p_{T, \ell}$ distribution (cf. Sect. 4.5.3). This enhancement is seen in the virtual and real corrections separately, but not in their sum. Furthermore, the existence of gluon-induced (qg) channels implies a new feature in the non-factorizable corrections. In the $q\bar{q}$ channels, and thus in the full NLO part of the non-factorizable corrections, the soft-photon exchange proceeds between initial- and final-state particles, whereas in the qg channels at $\mathcal{O}(\alpha_s \alpha)$ the photon is also exchanged between final-state particles. The known suppression mechanisms in non-factorizable corrections work somewhat differently in those cases [164].

The factorizable initial–final $\mathcal{O}(\alpha_s\alpha)$ corrections

In this chapter we present the calculation of the factorizable $\mathcal{O}(\alpha_s\alpha)$ corrections of “initial–final” type. Preliminary numerical results of these corrections were shown in Ref. [89]. In Sect. 7.1 we discuss the calculation of the different ingredients that enter into the NNLO cross section prediction and combine these contributions in Sect. 7.2 into a formula suitable for numerical evaluation where all IR singularities are cancelled explicitly. Finally, in Sect. 7.3 we present the numerical results for the factorizable initial–final corrections and compare them with a naive product ansatz that is obtained by multiplying the the NLO QCD and EW correction factors.

7.1. Calculation of the factorizable initial–final corrections

In this section we calculate the various contributions to the factorizable initial–final corrections of $\mathcal{O}(\alpha_s\alpha)$, which are diagrammatically characterized in Fig. 7.1. Owing to the property that the QCD and EW corrections are confined to the production and the decay sub-processes, respectively, many parts of the calculation of these factorizable corrections will be reducible into the form of a product of (NLO QCD) \times (NLO EW) corrections. This section therefore heavily makes use of results for the NLO building blocks which were discussed in great detail in Chap. 4.

7.1.1. Double-virtual corrections

The double-virtual corrections consist of two different contributions, which are illustrated in Fig. 7.1(a) in terms of interference diagrams: Firstly, the $\mathcal{O}(\alpha_s\alpha)$ corrections to the $\bar{q}_a q_b \rightarrow \ell_1 \bar{\ell}_2$ amplitude that comprise of reducible (one-loop) \times (one-loop) diagrams, which interfere with the Born amplitude; secondly, the interference between two one-loop-corrected amplitudes with corrections of $\mathcal{O}(\alpha_s)$ and $\mathcal{O}(\alpha)$, respectively. As a result, the double-virtual corrections are given by the following expression,

$$\begin{aligned} |\mathcal{M}_{\bar{q}_a q_b \rightarrow \ell_1 \bar{\ell}_2}|^2 \Big|_{\text{prod} \times \text{dec}}^{\text{V}_s \otimes \text{V}_{\text{ew}}} &= 2 \operatorname{Re} \left\{ \delta \mathcal{M}_{\bar{q}_a q_b \rightarrow \ell_1 \bar{\ell}_2}^{\text{V}_s \otimes \text{V}_{\text{ew}, \text{prod} \times \text{dec}}} \left(\mathcal{M}_{0, \text{PA}}^{\bar{q}_a q_b \rightarrow \ell_1 \bar{\ell}_2} \right)^* \right\} \\ &+ 2 \operatorname{Re} \left\{ \delta \mathcal{M}_{\bar{q}_a q_b \rightarrow \ell_1 \bar{\ell}_2}^{\text{V}_{\text{ew}, \text{dec}}} \left(\delta \mathcal{M}_{\bar{q}_a q_b \rightarrow \ell_1 \bar{\ell}_2}^{\text{V}_s, \text{PA}} \right)^* \right\}. \end{aligned} \quad (7.1)$$

Since the $\mathcal{O}(\alpha_s\alpha)$ amplitude does not involve genuine two-loop diagrams, but only consists of products of one-loop sub-amplitudes associated with the production and decay $V\bar{f}f$ vertices, it can be immediately written using the results of the NLO corrections of Chap. 4 as follows,

$$\delta \mathcal{M}_{\bar{q}_a q_b \rightarrow \ell_1 \bar{\ell}_2}^{\text{V}_s \otimes \text{V}_{\text{ew}, \text{prod} \times \text{dec}}} = \delta_{\text{V}_s}^{\text{V}_{\bar{q}_a q_b}} \delta_{\text{V}_{\text{ew}}(\tau_\ell)}^{\text{dec}} \mathcal{M}_{0, \text{PA}}^{\bar{q}_a q_b \rightarrow \ell_1 \bar{\ell}_2}, \quad (7.2)$$

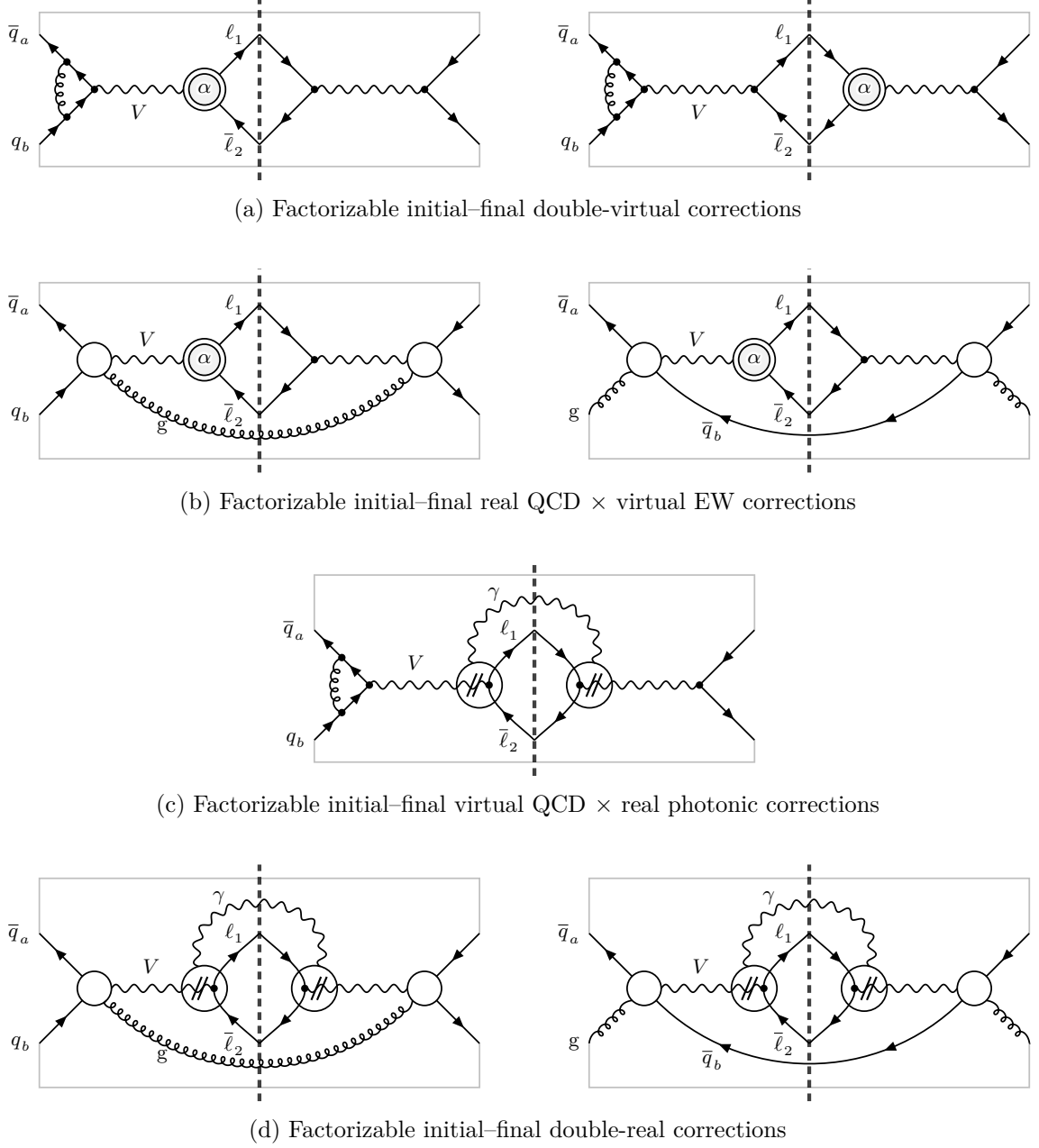


Figure 7.1.: Interference diagrams for the various contributions to the factorizable initial-final corrections of $\mathcal{O}(\alpha_s\alpha)$, with blobs representing all relevant tree structures. The encircled diagrams with a photon attached stand for all possibilities to couple the photon to the fermion line and the gauge boson V , see Eq. (4.19). The blobs with “ α ” inside represent one-loop corrections of $\mathcal{O}(\alpha)$, see Figs. B.3, B.4, and B.5.

where the correction factors $\delta_{V_{ew}(\tau_\ell)}^{\text{dec}}$ and $\delta_{V_s}^{V\bar{q}_a q_b}$ are given in Eqs. (4.8b) and (4.40), respectively. Note the additional label τ_ℓ in $\delta_{V_{ew}(\tau_\ell)}^{\text{dec}}$, which indicates the dependence of the correction factor on the chiral structure of the amplitude, as explained in Sect. 4.2.1. Because both correction factors contain $\frac{1}{\epsilon^2}$ poles, in principle, Eq. (7.2) requires the evaluation of the correction factors up to $\mathcal{O}(\epsilon^2)$ in order to obtain all finite $\mathcal{O}(\epsilon^0)$ terms. However, after applying the subtraction formalism, which we describe in detail in Sect. 7.2, the poles are cancelled before performing the full expansion in ϵ and, thus, the analytic results given in Sect. 4.2 up to order $\mathcal{O}(\epsilon^0)$ are sufficient. Similarly, the corrections shown in the right-hand diagram of Fig. 7.1(a) can also be directly obtained from the results of Sect. 4.2 and read

$$\text{Re} \left\{ \delta \mathcal{M}_{V_{ew}, \text{dec}}^{\bar{q}_a q_b \rightarrow \ell_1 \bar{\ell}_2} \left(\delta \mathcal{M}_{V_s, \text{PA}}^{\bar{q}_a q_b \rightarrow \ell_1 \bar{\ell}_2} \right)^* \right\} = \text{Re} \left\{ \delta_{V_{ew}(\tau_\ell)}^{\text{dec}} \left(\delta_{V_s}^{V\bar{q}_a q_b} \right)^* \right\} \left| \mathcal{M}_{0, \text{PA}}^{\bar{q}_a q_b \rightarrow \ell_1 \bar{\ell}_2} \right|^2, \quad (7.3)$$

with the same correction factors as in Eq. (7.2). As will be discussed in Sect. 7.2, the expansion of the correction factors up to higher powers in ϵ is also not required for these contributions. The final result for the double-virtual corrections to the cross section is therefore given by

$$\begin{aligned} d\sigma_{\bar{q}_a q_b, \text{prod} \times \text{dec}}^{V_s \otimes V_{ew}} &= 2 \left[\text{Re} \left\{ \delta_{V_{ew}(\tau_\ell)}^{\text{dec}} \left(\delta_{V_s}^{V\bar{q}_a q_b} \right)^* \right\} + \text{Re} \left\{ \delta_{V_{ew}(\tau_\ell)}^{\text{dec}} \delta_{V_s}^{V\bar{q}_a q_b} \right\} \right] d\sigma_{\bar{q}_a q_b, \text{PA}}^0 \\ &= 4 \text{Re} \left\{ \delta_{V_{ew}(\tau_\ell)}^{\text{dec}} \right\} \text{Re} \left\{ \delta_{V_s}^{V\bar{q}_a q_b} \right\} d\sigma_{\bar{q}_a q_b, \text{PA}}^0. \end{aligned} \quad (7.4)$$

Note that all terms in Eq. (7.4), in particular the correction factors $\delta_{V_{ew}(\tau_\ell)}^{\text{dec}}$ and $\delta_{V_s}^{V\bar{q}_a q_b}$, must be evaluated for on-shell gauge bosons $p_V^2 = M_V^2$ in order to guarantee gauge invariance. The only exception is the resonant propagator contained in $\sigma_{\bar{q}_a q_b, \text{PA}}^0$ which is evaluated for off-shell kinematics. Similarly to the NLO case discussed in Sect. 4.2.1, there is a freedom in choosing a specific on-shell mapping, since the phase-space parametrization involves more kinematic variables than the virtuality of the gauge boson alone. However, in the singular soft and/or collinear limits, the choice of the mappings in the virtual and real corrections must match properly in order to ensure the correct cancellation of IR singularities.

7.1.2. Real \times virtual corrections

As we have observed in the calculation of the double-virtual corrections in the previous section, the property that the QCD and electroweak corrections are fully contained within their respective production and decay sub-processes essentially reduces the corrections into the form of a product of the two NLO corrections. This property also holds in the corrections of the single-real-emission corrections which are discussed in the following.

Real QCD \times virtual EW corrections

The (real QCD) \times (virtual EW) contributions to the factorizable initial–final corrections are given by the processes of Eqs. (4.43) of $V + \text{jet}$ production with additional virtual corrections to the W/Z decays into leptons as shown in Fig. 7.1(b). For the quark-induced channel the corrections are given by the product of on-shell matrix elements for $V + g$ production and V

decay times the off-shell propagator,

$$\delta\mathcal{M}_{\text{R}_s \otimes \text{V}_{\text{ew}}, \text{prod} \times \text{dec}}^{\bar{q}_a q_b \rightarrow \ell_1 \bar{\ell}_2 g} = \sum_{\lambda_V} \frac{\mathcal{M}_{\text{R}_s}^{\bar{q}_a q_b \rightarrow gV}(\lambda_V) \delta\mathcal{M}_{\text{V}_{\text{ew}}}^{V \rightarrow \ell_1 \bar{\ell}_2}(\lambda_V)}{p_V^2 - \mu_V^2}, \quad (7.5)$$

where the sum over the physical polarization states λ_V of the vector boson V encodes the proper spin correlation. Here \mathcal{M}_{R_s} and $\delta\mathcal{M}_{\text{V}_{\text{ew}}}$ denote QCD real-emission and EW one-loop amplitudes, respectively. The latter can be directly taken over from Eq. (4.8b), which take the form of a correction factor multiplying the tree amplitude for V decay. The tree amplitudes of the production and decay sub-processes can then be reassembled to give the NLO real-emission matrix elements. As a result, we obtain the final result for (real QCD) \times (virtual EW) corrections to the cross section which reads

$$d\sigma_{\bar{q}_a q_b, \text{prod} \times \text{dec}}^{\text{R}_s \otimes \text{V}_{\text{ew}}} = 2 \text{Re} \left\{ \delta_{\text{V}_{\text{ew}}(\tau_\ell)}^{\text{dec}} \right\} d\sigma_{\bar{q}_a q_b, \text{PA}}^{\text{R}_s}, \quad (7.6a)$$

$$d\sigma_{g q_b, \text{prod} \times \text{dec}}^{\text{R}_s \otimes \text{V}_{\text{ew}}} = 2 \text{Re} \left\{ \delta_{\text{V}_{\text{ew}}(\tau_\ell)}^{\text{dec}} \right\} d\sigma_{g q_b, \text{PA}}^{\text{R}_s}, \quad (7.6b)$$

$$d\sigma_{g \bar{q}_a, \text{prod} \times \text{dec}}^{\text{R}_s \otimes \text{V}_{\text{ew}}} = 2 \text{Re} \left\{ \delta_{\text{V}_{\text{ew}}(\tau_\ell)}^{\text{dec}} \right\} d\sigma_{g \bar{q}_a, \text{PA}}^{\text{R}_s}, \quad (7.6c)$$

where $\delta_{\text{V}_{\text{ew}}(\tau_\ell)}^{\text{dec}}$ is defined in (4.8b). The label PA in the real-emission corrections denotes that all non-resonant terms, i.e. the photon-exchange diagrams in case of the neutral-current process, are omitted in the QCD real-emission amplitudes of Eqs. (4.41).

Virtual QCD \times real photonic corrections

The generic interference diagram for the (virtual QCD) \times (real photonic) factorizable corrections of initial–final type is shown in Fig. 7.1(c) and comprise virtual QCD corrections to the process $\bar{q}_a q_b \rightarrow \ell_1 \bar{\ell}_2 \gamma$. The QCD corrections can be immediately written in a factorized form with the correction factor given in Eq. (4.40) since the QCD corrections are completely blind to the details of the process following the production of the V boson and, therefore, unaffected by the additional photon emission which is confined to the decay sub-process. The final result for the (virtual QCD) \times (real photonic) corrections is therefore given by the factorizable real photonic corrections to the decay multiplied with the QCD correction factor $\delta_{\text{V}_s}^{V \bar{q}_a q_b}$,

$$d\sigma_{\bar{q}_a q_b, \text{prod} \times \text{dec}}^{\text{V}_s \otimes \text{R}_{\text{ew}}} = 2 \text{Re} \left\{ \delta_{\text{V}_s}^{V \bar{q}_a q_b} \right\} d\sigma_{\bar{q}_a q_b, \text{dec}}^{\text{R}_{\text{ew}}}, \quad (7.7)$$

where the amplitudes of the factorizable final-state corrections are given in Eq. (4.20b).

7.1.3. Double-real corrections

The double-real emission corrections constitute the only contribution to the factorizable initial–final corrections that do not take the form of a product of NLO QCD and EW corrections and are illustrated in Fig. 7.1(d) in terms of interference diagrams. The calculation of the double-real corrections proceeds along the same lines as the calculation of the real-emission corrections at NLO discussed in Sect. 4.2.2 and we start with the decomposition of the full amplitude $\bar{q}_a q_b \rightarrow \ell_1 \bar{\ell}_2 g \gamma$ into the contributions associated with photon emission from the production and decay sub-processes. To this end, we apply the propagator identity (4.17) to disentangle the



Figure 7.2.: Decomposition of the double-real corrections $\bar{q}_a q_b \rightarrow \ell_1 \bar{\ell}_2 g \gamma$ using the propagator identity in Eq. (4.17) into the contributions where the photon is emitted from the production (a) and the decay (b) sub-processes. The momentum p_V of the intermediate vector boson V is given by $p_V = p_a + p_b - k_g - k = k_1 + k_2$.

two resonance structures contained in the diagrams with a photon attached to the intermediate gauge boson V . Using the diagrammatic notation of Eq. (4.19) the double-real corrections can be divided into the two contributions shown in Fig. 7.2. The factorizable corrections of “initial–final” type are given by the generic diagram of Fig. 7.2(b). We write the corresponding matrix element of the double-real radiation process $\bar{q}_a q_b \rightarrow \ell_1 \bar{\ell}_2 g \gamma$ as follows,

$$i\mathcal{M}_{\text{prod} \times \text{dec}}^{\bar{q}_a q_b \rightarrow \ell_1 \bar{\ell}_2 g \gamma} \left(\begin{bmatrix} p_a \\ \sigma_a \\ c_a \end{bmatrix}, \begin{bmatrix} p_b \\ \sigma_b \\ c_b \end{bmatrix}; \begin{bmatrix} k_1 \\ \sigma_1 \end{bmatrix}, \begin{bmatrix} k_2 \\ \sigma_2 \end{bmatrix}, \begin{bmatrix} k_g \\ \lambda_g \\ a \end{bmatrix}, \begin{bmatrix} k \\ \lambda \end{bmatrix} \right) = 4i e^3 g_s t_{c_a c_b}^a C_{V \bar{q}_a q_b}^{\tau_q} C_{V \ell_1 \bar{\ell}_2}^{\tau_\ell} \\ \times \left(\underbrace{\frac{Q_1(k \cdot k_2) + Q_2(k \cdot k_1)}{k \cdot (k_1 + k_2)}}_{\xrightarrow{\text{NC}} Q_\ell, \text{ for } Q_1 = Q_2 \equiv Q_\ell} \frac{\mathbb{A}_{\text{prod} \times \text{dec}}^{\tau_q \tau_\ell \lambda_g \lambda}(p_a, p_b; k_1, k_2, k_g, k)}{s_{12\gamma} - \mu_V^2} \right), \quad (7.8)$$

with $s_{12\gamma} = (k_1 + k_2 + k)^2$ and using the notation introduced in Sect. 2.1. Note that only the massive gauge bosons must be considered in the PA, i.e. $V = W, Z$. The labels λ_g and λ denote the helicity of the gluon and photon, respectively, and the helicities of the external fermions are determined by relation (2.7) from the signs τ_q and τ_ℓ in the chiral couplings. The respective results for the gluon-induced channels are obtained by applying the crossing transformation defined in Eq. (A.45),

$$\mathcal{M}_{\text{prod} \times \text{dec}}^{g q_b \rightarrow \ell_1 \bar{\ell}_2 q_a \gamma} = \mathcal{X} \left[\begin{array}{c} \bar{q}_a(p_a) \rightarrow q_a(k_a) \\ g(k_g) \leftarrow g(p_g) \end{array} \right] \left\{ \mathcal{M}_{\text{prod} \times \text{dec}}^{\bar{q}_a q_b \rightarrow \ell_1 \bar{\ell}_2 g \gamma} \right\}, \quad (7.9a)$$

$$\mathcal{M}_{\text{prod} \times \text{dec}}^{g \bar{q}_a \rightarrow \ell_1 \bar{\ell}_2 \bar{q}_b \gamma} = \mathcal{X} \left[\begin{array}{c} q_b(p_b) \rightarrow \bar{q}_b(k_b) \\ g(k_g) \leftarrow g(p_g) \end{array} \right] \left\{ \mathcal{M}_{\text{prod} \times \text{dec}}^{\bar{q}_a q_b \rightarrow \ell_1 \bar{\ell}_2 g \gamma} \right\}. \quad (7.9b)$$

The standard matrix elements $\mathbb{A}_{\text{prod} \times \text{dec}}^{\tau_q \tau_\ell \lambda_g \lambda}$ appearing in Eq. (7.8) explicitly read

$$\mathbb{A}_{\text{prod} \times \text{dec}}^{--++}(p_a, p_b; k_1, k_2, k_g, k) = \frac{s_{12\gamma} (\langle p_a k_1 \rangle)^2}{\langle k_g p_a \rangle \langle k_g p_b \rangle \langle k k_1 \rangle \langle k k_2 \rangle},$$

$$\mathbb{A}_{\text{prod} \times \text{dec}}^{++++}(p_a, p_b; k_1, k_2, k_g, k) = \frac{s_{12\gamma} (\langle p_b k_2 \rangle)^2}{\langle k_g p_a \rangle \langle k_g p_b \rangle \langle k k_1 \rangle \langle k k_2 \rangle},$$

$$\mathbb{A}_{\text{prod} \times \text{dec}}^{-+++}(p_a, p_b; k_1, k_2, k_g, k) = -\frac{s_{12\gamma} (\langle p_a k_2 \rangle)^2}{\langle k_g p_a \rangle \langle k_g p_b \rangle \langle k k_1 \rangle \langle k k_2 \rangle},$$

$$\begin{aligned}
\mathbb{A}_{\text{prod} \times \text{dec}}^{+-+-+}(p_a, p_b; k_1, k_2, k_g, k) &= -\frac{s_{12\gamma} (\langle p_b k_1 \rangle)^2}{\langle k_g p_a \rangle \langle k_g p_b \rangle \langle k k_1 \rangle \langle k k_2 \rangle}, \\
\mathbb{A}_{\text{prod} \times \text{dec}}^{----+}(p_a, p_b; k_1, k_2, k_g, k) &= \frac{(\langle p_b | K_2 + K | k_1 \rangle)^2}{\langle k_g p_a \rangle^* \langle k_g p_b \rangle^* \langle k k_1 \rangle \langle k k_2 \rangle}, \\
\mathbb{A}_{\text{prod} \times \text{dec}}^{++-+}(p_a, p_b; k_1, k_2, k_g, k) &= \frac{(\langle p_a | K_1 + K | k_2 \rangle)^2}{\langle k_g p_a \rangle^* \langle k_g p_b \rangle^* \langle k k_1 \rangle \langle k k_2 \rangle}, \\
\mathbb{A}_{\text{prod} \times \text{dec}}^{-++-}(p_a, p_b; k_1, k_2, k_g, k) &= -\frac{(\langle p_b | K_1 + K | k_2 \rangle)^2}{\langle k_g p_a \rangle^* \langle k_g p_b \rangle^* \langle k k_1 \rangle \langle k k_2 \rangle}, \\
\mathbb{A}_{\text{prod} \times \text{dec}}^{+--+}(p_a, p_b; k_1, k_2, k_g, k) &= -\frac{(\langle p_a | K_2 + K | k_1 \rangle)^2}{\langle k_g p_a \rangle^* \langle k_g p_b \rangle^* \langle k k_1 \rangle \langle k k_2 \rangle}, \\
\mathbb{A}_{\text{prod} \times \text{dec}}^{\tau_q \tau_\ell --}(p_a, p_b; k_1, k_2, k_g, k) &= \mathcal{P} \left\{ \mathbb{A}_{\text{prod} \times \text{dec}}^{(-\tau_q)(-\tau_\ell)++}(p_a, p_b; k_1, k_2, k_g, k) \right\}, \\
\mathbb{A}_{\text{prod} \times \text{dec}}^{\tau_q \tau_\ell +-}(p_a, p_b; k_1, k_2, k_g, k) &= \mathcal{P} \left\{ \mathbb{A}_{\text{prod} \times \text{dec}}^{(-\tau_q)(-\tau_\ell)-+}(p_a, p_b; k_1, k_2, k_g, k) \right\},
\end{aligned} \tag{7.10}$$

where we have used the modified parity transformation defined in Eq. (A.46) in the last two lines and introduced the short hand notation $\langle p|Q|k \rangle$ for the spinor product defined as

$$\langle p|Q|k \rangle \equiv p_A Q^{AB} k_B. \tag{7.11}$$

7.2. Complete result for the factorizable initial–final corrections

The factorizable initial–final corrections to the cross section are obtained by integrating the individual contributions of Sect. 7.1 over the respective phase spaces,

$$\begin{aligned}
\hat{\sigma}_{\text{prod} \times \text{dec}}^{\text{NNLO}_{\text{s} \otimes \text{ew}}} &= \int_2 d\sigma_{\text{prod} \times \text{dec}}^{\text{V}_s \otimes \text{V}_{\text{ew}}} + \iint_{2+\gamma} d\sigma_{\text{prod} \times \text{dec}}^{\text{V}_s \otimes \text{R}_{\text{ew}}} + \int_3 d\sigma_{\text{prod} \times \text{dec}}^{\text{R}_s \otimes \text{V}_{\text{ew}}} + \iint_{3+\gamma} d\sigma_{\text{prod} \times \text{dec}}^{\text{R}_s \otimes \text{R}_{\text{ew}}} \\
&\quad + \int_2 d\sigma_{\text{prod} \times \text{dec}}^{\text{C}_s \otimes \text{V}_{\text{ew}}} + \iint_{2+\gamma} d\sigma_{\text{prod} \times \text{dec}}^{\text{C}_s \otimes \text{R}_{\text{ew}}},
\end{aligned} \tag{7.12}$$

where the additional collinear counterterms in the last line were introduced to absorb the collinear singularities associated with the quarks and gluons in the initial state into the NLO PDFs. Note that the EW corrections are completely confined to the decay sub-process, and consequently, no singularities arise from initial-state collinear quark–photon splittings and no corresponding collinear counterterm is introduced. Since the collinear counterterm (1.98) is essentially given by the convolution of the lower-order (in α_s) cross section with the Altarelli–Parisi splitting kernels, the counterterms in the last line of Eq. (7.12) can be obtained by replacing σ^0 in Eq. (1.98) by the respective NLO EW cross sections. This is only feasible if the EW corrections do not introduce additional initial-state collinear singularities, as is the case here. Using the results of the previous section and Chap. 4, we can therefore write

$$\hat{\sigma}_{\text{prod} \times \text{dec}}^{\text{NNLO}_{\text{s} \otimes \text{ew}}} = \int_2 4 \text{Re} \left\{ \delta_{\text{V}_s}^{V \bar{q}_a q_b} \right\} \text{Re} \left\{ \delta_{\text{V}_{\text{ew}}(\tau_\ell)}^{\text{dec}} \right\} d\sigma_{\text{PA}}^0 + \iint_{2+\gamma} 2 \text{Re} \left\{ \delta_{\text{V}_s}^{V \bar{q}_a q_b} \right\} d\sigma_{\text{dec}}^{\text{R}_{\text{ew}}}$$

$$\begin{aligned}
& + \int_3 2 \operatorname{Re} \left\{ \delta_{V_{\text{ew}}(\tau_\ell)}^{\text{dec}} \right\} d\sigma_{\text{PA}}^{\text{R}_s} + \iint_{3+\gamma} d\sigma_{\text{prod} \times \text{dec}}^{\text{R}_s \otimes \text{R}_{\text{ew}}} \\
& + \int_2 2 \operatorname{Re} \left\{ \delta_{V_{\text{ew}}(\tau_\ell)}^{\text{dec}} \right\} d\sigma_{\text{PA}}^{\text{C}_s} + \iint_{2+\gamma} d\sigma_{\text{prod} \times \text{dec}}^{\text{C}_s \otimes \text{R}_{\text{ew}}}.
\end{aligned} \tag{7.13}$$

We first apply the QCD dipole subtraction formalism to Eq. (7.13) in order to cancel the IR singularities associated with the QCD corrections. Using the dipole operators introduced in Sect. 4.4, Eq. (7.13) can be written in the following form,

$$\begin{aligned}
\hat{\sigma}_{\text{prod} \times \text{dec}}^{\text{NNLO}_{\text{s} \otimes \text{ew}}} &= \int_2 2 \operatorname{Re} \left\{ \delta_{V_{\text{ew}}(\tau_\ell)}^{\text{dec}} \right\} d\sigma_{\text{PA}}^0 \otimes \left[2 \operatorname{Re} \left\{ \delta_{V_s}^{V \bar{q}_a q_b} \right\} + \mathbf{I} \right] \\
&+ \iint_{2+\gamma} d\sigma_{\text{dec}}^{\text{R}_{\text{ew}}} \otimes \left[2 \operatorname{Re} \left\{ \delta_{V_s}^{V \bar{q}_a q_b} \right\} + \mathbf{I} \right] \\
&+ \int_3 2 \operatorname{Re} \left\{ \delta_{V_{\text{ew}}(\tau_\ell)}^{\text{dec}} \right\} \left\{ d\sigma_{\text{PA}}^{\text{R}_s} - \sum_{\substack{\text{QCD} \\ \text{dipoles}}} d\sigma_{\text{PA}}^0 \otimes dV_{\text{dip}} \right\} \\
&+ \iint_{3+\gamma} \left\{ d\sigma_{\text{prod} \times \text{dec}}^{\text{R}_s \otimes \text{R}_{\text{ew}}} - \sum_{\substack{\text{QCD} \\ \text{dipoles}}} d\sigma_{\text{dec}}^{\text{R}_{\text{ew}}} \otimes dV_{\text{dip}} \right\} \\
&+ \int_0^1 dx \int_2 2 \operatorname{Re} \left\{ \delta_{V_{\text{ew}}(\tau_\ell)}^{\text{dec}} \right\} d\sigma_{\text{PA}}^0 \otimes (\mathbf{K} + \mathbf{P}) \\
&+ \int_0^1 dx \iint_{2+\gamma} d\sigma_{\text{dec}}^{\text{R}_{\text{ew}}} \otimes (\mathbf{K} + \mathbf{P}),
\end{aligned} \tag{7.14}$$

where \otimes denotes possible additional helicity and colour correlations and it is implicitly assumed that the cross sections multiplying the dipole operators dV_{dip} are evaluated on the respective dipole-mapped phase-space point (4.47a). All lines of Eq. (7.14) are now individually free of QCD singularities, however, remain IR divergent owing to the singularities contained in the EW corrections which still need to be cancelled between the virtual corrections and the corresponding real-photon-emission parts.

The IR singularities associated with the EW corrections are dealt with using the dipole subtraction formalism already used in the calculation of the factorizable corrections at NLO in Sect. 4.3. More explicitly, we use the extension of the formalism to treat decay kinematics as described in detail in Sect. 3.4. As a result we are able to arrange the six contributions in Eq. (7.14) into a form where all IR divergences are cancelled in the integrands explicitly,

$$\hat{\sigma}_{\text{prod} \times \text{dec}}^{\text{NNLO}_{\text{s} \otimes \text{ew}}} = \tilde{\sigma}_{\text{prod} \times \text{dec}}^{\text{V}_s \otimes \text{V}_{\text{ew}}} + \tilde{\sigma}_{\text{prod} \times \text{dec}}^{\text{V}_s \otimes \text{R}_{\text{ew}}} + \tilde{\sigma}_{\text{prod} \times \text{dec}}^{\text{R}_s \otimes \text{V}_{\text{ew}}} + \tilde{\sigma}_{\text{prod} \times \text{dec}}^{\text{R}_s \otimes \text{R}_{\text{ew}}} + \tilde{\sigma}_{\text{prod} \times \text{dec}}^{\text{C}_s \otimes \text{V}_{\text{ew}}} + \tilde{\sigma}_{\text{prod} \times \text{dec}}^{\text{C}_s \otimes \text{R}_{\text{ew}}}, \tag{7.15}$$

where each term is an IR-finite object and its phase-space integration can be performed numerically in four dimensions. Equation (7.15) will be our master formula for the numerical evaluation discussed in Sect. 7.3. In the following we describe the construction of the individual ingredients. In order to discuss some subtle points in the implementation that are not obvious in the compact notation used here, we give the explicit expressions for all contributions for the quark–anti-quark and quark–gluon induced channels in Appendix D.2.

The first two terms in Eq. (7.15) arise from the sum of the double-virtual and the (virtual QCD)×(real-photonic) corrections, including the insertion operators from the QCD dipole formalism, and correspond to the sum of the first two lines in Eq. (7.14). Applying the dipole formalism to rearrange the IR singularities of photonic origin between the virtual and real EW corrections, we obtain the following expressions for the IR-finite virtual QCD contributions to the cross section,

$$\tilde{\sigma}_{\text{prod} \times \text{dec}}^{\text{Vs} \otimes \text{Vew}} = \int_2 \left[2 \text{Re} \left\{ \delta_{\text{Vew}(\tau_\ell)}^{\text{dec}} \right\} + I^{\text{ew}} \right] d\sigma_{\text{PA}}^0 \otimes \left[2 \text{Re} \left\{ \delta_{\text{Vs}}^{V\bar{q}_a q_b} \right\} + \mathbf{I} \right], \quad (7.16)$$

$$\tilde{\sigma}_{\text{prod} \times \text{dec}}^{\text{Vs} \otimes \text{Rew}} = \iint_{2+\gamma} \left\{ d\sigma_{\text{dec}}^{\text{Rew}} - \sum_{\substack{I,J \\ I \neq J}} d\sigma_{\text{PA}}^0 \otimes dV_{\text{dip},IJ}^{\text{ew}} \right\} \otimes \left[2 \text{Re} \left\{ \delta_{\text{Vs}}^{V\bar{q}_a q_b} \right\} + \mathbf{I} \right], \quad (7.17)$$

where we have used the compact notation $dV_{\text{dip}}^{\text{ew}}$ defined in Eq. (4.28) for the QED dipoles and I^{ew} to denote their integrated counterpart. The sum over the emitter–spectator pairs (I, J) in Eq. (7.17) extends over all particles of the decay sub-process, i.e. $I, J = \ell_1, \bar{\ell}_2, V$. The explicit expressions for the sum of the dipole terms and the endpoint contribution I^{ew} are given in Eqs. (4.29) and (4.30), respectively. As was briefly mentioned in the context of the double-virtual corrections in Sect. 7.1.1, we observe that all IR singularities contained in $\delta_{\text{Vs}}^{V\bar{q}_a q_b}$ cancel exactly against the corresponding poles of the \mathbf{I} operator within the second square bracket of Eq. (7.16). Similarly, all singularities in $\delta_{\text{Vew}(\tau_\ell)}^{\text{dec}}$ cancel against the corresponding poles in I^{ew} in the first square bracket of Eq. (7.16). As a consequence, the correction factors $\delta_{\text{Vew}(\tau_\ell)}^{\text{dec}}$ and $\delta_{\text{Vs}}^{V\bar{q}_a q_b}$ need not be evaluated up to $\mathcal{O}(\epsilon^2)$, but the analytic results given in Chap. 4 up to $\mathcal{O}(\epsilon^0)$ are sufficient. Furthermore, note that the relative correction factors $\delta_{\text{Vs}}^{V\bar{q}_a q_b}$ and $\delta_{\text{Vew}(\tau_\ell)}^{\text{dec}}$ are c-numbers, given by the vertex corrections evaluated at the on-shell point $p_V^2 = M_V^2$ and, thus, independent of the phase-space kinematics.¹

The contributions involving real QCD corrections are given by the third and forth term in Eq. (7.15). They are obtained by applying the QED dipole subtraction formalism to the sum of the third and forth line of Eq. (7.14) and result in the following expressions for the IR-finite real-gluon contributions to the cross section,

$$\tilde{\sigma}_{\text{prod} \times \text{dec}}^{\text{Rs} \otimes \text{Vew}} = \int_3 \left[2 \text{Re} \left\{ \delta_{\text{Vew}(\tau_\ell)}^{\text{dec}} \right\} + I^{\text{ew}} \right] \left\{ d\sigma_{\text{PA}}^{\text{Rs}} - \sum_{\substack{\text{QCD} \\ \text{dipoles}}} d\sigma_{\text{PA}}^0 \otimes dV_{\text{dip}} \right\}, \quad (7.18)$$

$$\begin{aligned} \tilde{\sigma}_{\text{prod} \times \text{dec}}^{\text{Rs} \otimes \text{Rew}} = & \iint_{3+\gamma} \left\{ d\sigma_{\text{prod} \times \text{dec}}^{\text{Rs} \otimes \text{Rew}} - \sum_{\substack{\text{QCD} \\ \text{dipoles}}} d\sigma_{\text{dec}}^{\text{Rew}} \otimes dV_{\text{dip}} - \sum_{\substack{I,J \\ I \neq J}} d\sigma_{\text{PA}}^{\text{Rs}} \otimes dV_{\text{dip},IJ}^{\text{ew}} \right. \\ & \left. + \sum_{\substack{\text{QCD} \\ \text{dipoles}}} \sum_{\substack{I,J \\ I \neq J}} d\sigma_{\text{PA}}^0 \otimes dV_{\text{dip}} \otimes dV_{\text{dip},IJ}^{\text{ew}} \right\}, \end{aligned} \quad (7.19)$$

with $I, J = \ell_1, \bar{\ell}_2, V$ and the electroweak dipole functions $dV_{\text{dip}}^{\text{ew}}$ and I^{ew} defined in Eqs. (4.28) and (4.30), respectively. The last term inside the curly brackets of Eq. (7.19) is obtained by multiplying the QCD and QED dipoles to the Born cross section in PA. In particular, this

¹ Note, however, the dependence of $\delta_{\text{Vew}(\tau_\ell)}^{\text{dec}}$ on the chiral coupling in the $V\bar{\ell}_1\ell_2$ vertex.

involves the successive application of two dipole phase-space mappings, which reduces the “3+ γ ” double-real emission kinematics to a two-particle configuration. Owing to the property of the factorizable initial–final corrections where the emissions in the production and decay stages of the V boson proceed independently, the two dipole mappings do not interfere with each other. The order in which they are applied is therefore irrelevant so that the following diagram commutes

$$\begin{array}{ccc}
 & \tilde{\Phi}_{3,IJ} & \\
 \text{QED dipole} \nearrow & & \searrow \text{QCD dipole} \\
 \Phi_{3+\gamma} & & \tilde{\Phi}_{2,IJ}^{(ab)c} \\
 \text{QCD dipole} \searrow & & \nearrow \text{QED dipole} \\
 & \tilde{\Phi}_{2+\gamma,(ab),c} &
 \end{array} \tag{7.20}$$

where (ab) and c denote the emitter-pair and the spectator of the QCD dipoles, respectively. For the case of the quark-induced process, $\bar{q}_a q_b \rightarrow \ell_1 \bar{\ell}_2 g \gamma$, the contributing dipoles are given by (see Eq. (4.46a)): $(ab)c = (\bar{q}_a g) q_b, (q_b g) \bar{q}_a$. We have further denoted the phase-space kinematics obtained by the successive application of both QCD and EW dipole mappings in Eq. (1.37) by $\tilde{\Phi}_{2,IJ}^{(ab)c}$. Related to the commutation property (7.20) is the factorization of the dipole phase space where the two one-particle sub-spaces associated with the two unresolved emissions can be isolated simultaneously. Using the generic notation of Eq. (3.2) for the phase-space factorization, this implies

$$d\Phi_{3+\gamma} = d\tilde{\Phi}_{2+\gamma,(ab),c} \otimes [dk_b] = d\tilde{\Phi}_{3,IJ} [dk] = d\tilde{\Phi}_{2,IJ}^{(ab)c} \otimes [dk_b][dk], \tag{7.21}$$

where the symbol \otimes indicates the additional convolution that arises in the case of the QCD dipoles that involve the initial-state particles. This has the important consequence that the analytic integration over the singular sub-spaces $([dk_b][dk])$ can be carried out in the same manner as it was done at NLO, which allows to reuse the known formulae given in Chap. 3 and Sect. 4.4 without modification. Now that we have addressed the analytic integration of the $\mathcal{O}(\alpha_s \alpha)$ “double-dipoles” given by the last term inside the curly brackets of Eq. (7.19), let us examine the local cancellation of the IR singularities in Eq. (7.19) in more detail. The second term inside the curly brackets of Eq. (7.19) corresponds to the QCD dipoles constructed for the NLO QCD corrections to $V + \gamma$ production. They will therefore act as a local counterterm to the double-real emission cross section $d\sigma^{\text{Rs} \otimes \text{R}_{\text{ew}}}$ in all regions of phase space where the additional QCD radiation becomes unresolved, i.e. soft and/or collinear to the beam. In the phase-space regions where the photon becomes soft and/or collinear to a final-state lepton the third term inside the curly brackets of Eq. (7.19) mimics the singular behaviour of $d\sigma^{\text{Rs} \otimes \text{R}_{\text{ew}}}$ and ensures the cancellation of IR singularities. This subtraction term corresponds to the QED dipoles constructed for the NLO EW corrections to $V + \text{jet}$ production. A subtlety arises in the double-unresolved cases, where the cross sections $d\sigma_{\text{dec}}^{\text{R}_{\text{ew}}}$ and $d\sigma_{\text{PA}}^{\text{Rs}}$ become singular as well, and both subtraction terms above will simultaneously act as a local counterterm, leading to the twofold subtraction of the IR singularities. This disparity in the double-unresolved limits is exactly compensated by the last term inside the curly brackets of Eq. (7.19), which therefore has the opposite sign.

Finally, we consider the convolution terms with additional virtual or real EW corrections given by the last two terms in Eq. (7.15). Since these contributions are essentially given by the lower-order (in α_s) cross sections, convoluted with the dipole operators \mathbf{K} and \mathbf{P} , they pose no additional complications, and the resulting IR-finite contributions to the cross section can be written as

$$\tilde{\sigma}_{\text{prod} \times \text{dec}}^{\text{C}_s \otimes \text{V}_{\text{ew}}} = \int_0^1 dx \int_2 \left[2 \text{Re} \left\{ \delta_{\text{V}_{\text{ew}}(\tau_\ell)}^{\text{dec}} \right\} + I^{\text{ew}} \right] d\sigma_{\text{PA}}^0 \otimes (\mathbf{K} + \mathbf{P}), \quad (7.22)$$

$$\tilde{\sigma}_{\text{prod} \times \text{dec}}^{\text{C}_s \otimes \text{R}_{\text{ew}}} = \int_0^1 dx \iint_{2+\gamma} \left\{ d\sigma_{\text{dec}}^{\text{R}_{\text{ew}}} - \sum_{\substack{I,J \\ I \neq J}} d\sigma_{\text{PA}}^0 \otimes dV_{\text{dip},IJ}^{\text{ew}} \right\} \otimes (\mathbf{K} + \mathbf{P}), \quad (7.23)$$

using the results of Chap. 4. Owing to the Lorentz invariance of the dipole formalism, no special treatment is required in contrast to the case of the non-factorizable corrections discussed in Chap. 6.

So far, we have focussed on the treatment of IR singularities for the case of IR-safe observables which satisfy the properties (3.8). In the remainder of this section we discuss the modifications to Eq. (7.15) that arise in the calculation of non-collinear-safe observables.

Non-collinear-safe observables

The extension to a non-collinear-safe observable with respect to the final-state leptons $\hat{i} = \ell_1, \bar{\ell}_2$ requires a modification to the subtraction terms where \hat{i} enters as the emitter particle as described in Sect. 3.1. To this end, the n -particle kinematics is treated as an $(n+1)$ -particle event with a collinear lepton–photon pair, cf. Eqs. (4.31) and (3.9),

$$d\sigma_{\text{PA}}^0(\tilde{\Phi}_{2,\hat{i}J}) \longrightarrow d\sigma_{\text{PA}}^0(\tilde{\Phi}_{2,\hat{i}J}) \Theta_{\text{cut}}(\tilde{\Phi}_{2,\hat{i}J} \mid k_{\hat{i}} = z_{\hat{i}J} \tilde{k}_{\hat{i}}, k = (1 - z_{\hat{i}J}) \tilde{p}_{\hat{i}}), \quad (7.24a)$$

$$d\sigma_{\text{PA}}^{\text{R}_s}(\tilde{\Phi}_{3,\hat{i}J}) \longrightarrow d\sigma_{\text{PA}}^{\text{R}_s}(\tilde{\Phi}_{3,\hat{i}J}) \Theta_{\text{cut}}(\tilde{\Phi}_{3,\hat{i}J} \mid k_{\hat{i}} = z_{\hat{i}J} \tilde{k}_{\hat{i}}, k = (1 - z_{\hat{i}J}) \tilde{p}_{\hat{i}}), \quad (7.24b)$$

$$d\sigma_{\text{PA}}^0(\tilde{\Phi}_{2,\hat{i}J}^{(ab)c}) \longrightarrow d\sigma_{\text{PA}}^0(\tilde{\Phi}_{2,\hat{i}J}^{(ab)c}) \Theta_{\text{cut}}(\tilde{\Phi}_{2,\hat{i}J}^{(ab)c} \mid \tilde{k}_{\hat{i}} = z_{\hat{i}J} \tilde{\tilde{k}}_{\hat{i}}, \tilde{k} = (1 - z_{\hat{i}J}) \tilde{\tilde{p}}_{\hat{i}}), \quad (7.24c)$$

where we have made explicit the cut-function for the computation of observables in the notation on the r.h.s. This modification induces additional convolution terms which we denote by “ $\bar{\text{R}}_{\text{ew}}$ ”,

$$\tilde{\sigma}_{\text{prod} \times \text{dec}}^{\text{V}_s \otimes \bar{\text{R}}_{\text{ew}}} = \int_2 d\sigma_{\text{PA}}^0 \otimes \left[2 \text{Re} \left\{ \delta_{\text{V}_s}^{V \bar{q}_a q_b} \right\} + \mathbf{I} \right] \int_0^1 dz \left[\bar{\mathcal{I}}^{\text{ew}}(z) \right]_+, \quad (7.25)$$

$$\tilde{\sigma}_{\text{prod} \times \text{dec}}^{\text{R}_s \otimes \bar{\text{R}}_{\text{ew}}} = \int_3 \left\{ d\sigma_{\text{PA}}^{\text{R}_s} - \sum_{\substack{\text{QCD} \\ \text{dipoles}}} d\sigma_{\text{PA}}^0 \otimes dV_{\text{dip}} \right\} \int_0^1 dz \left[\bar{\mathcal{I}}^{\text{ew}}(z) \right]_+, \quad (7.26)$$

$$\tilde{\sigma}_{\text{prod} \times \text{dec}}^{\text{C}_s \otimes \bar{\text{R}}_{\text{ew}}} = \int_0^1 dx \int_2 d\sigma_{\text{PA}}^0 \otimes (\mathbf{K} + \mathbf{P}) \int_0^1 dz \left[\bar{\mathcal{I}}^{\text{ew}}(z) \right]_+, \quad (7.27)$$

where $\bar{\mathcal{I}}^{\text{ew}}(z)$ is defined in Eq. (4.33).

7.3. Numerical results for the factorizable initial–final corrections

In this section we present the numerical results of the factorizable initial–final corrections in terms of relative correction factors to the LO prediction and, furthermore, compare these results to different predictions based on the naive factorization of NLO QCD and NLO EW corrections. The setup is identical to the NLO case in Sect. 4.5. We first introduce an alternative definition for the relative QCD factor defined by

$$\delta'_{\alpha_s} \equiv \frac{\Delta\sigma_{\text{pp}}^{\text{NLO}_s}}{\sigma_{\text{pp}}^{\text{LO}}}, \quad (7.28)$$

where $\sigma_{\text{pp}}^{\text{LO}}$ denotes the LO prediction and $\Delta\sigma_{\text{pp}}^{\text{NLO}_s}$ the genuine $\mathcal{O}(\alpha_s)$ contribution to the full NLO QCD prediction $\sigma_{\text{pp}}^{\text{NLO}_s}$. More details on the definition of the cross section contributions are given in Sect. 4.5.3 where they have been introduced. Note that the correction factor in Eq. (7.28) differs from the definition of Eq. (4.59) by the omission of the difference in the LO prediction induced by the transition from LO to NLO PDFs. The cross section definition based on the naive factorization ansatz $\sigma_{\text{pp,naive fact}}^{\text{NNLO}_{s\otimes\text{ew}}}$ was given in Eq. (4.61) which we compare to our best prediction based on the full NLO QCD and EW corrections improved by the factorizable initial–final $\mathcal{O}(\alpha_s\alpha)$ corrections $\Delta\sigma_{\text{pp,prod}\times\text{dec}}^{\text{NNLO}_{s\otimes\text{ew}}}$ calculated in this chapter,

$$\sigma_{\text{pp}}^{\text{NNLO}_{s\otimes\text{ew}}} = \sigma_{\text{pp}}^{\text{NLO}_s} + \Delta\sigma_{\text{pp}}^{\text{NLO}_{\text{ew}}} + \Delta\sigma_{\text{pp,prod}\times\text{dec}}^{\text{NNLO}_{s\otimes\text{ew}}}, \quad (7.29)$$

which is consistently evaluated with NLO PDFs. The non-factorizable corrections discussed in Chap. 6 were found to have a negligible impact on the cross section and are therefore not included here. Inspecting the relative difference of our best prediction with the factorized ansatz (4.61) normalized to the LO prediction,

$$\frac{\sigma_{\text{pp}}^{\text{NNLO}_{s\otimes\text{ew}}} - \sigma_{\text{pp,naive fact}}^{\text{NNLO}_{s\otimes\text{ew}}}}{\sigma_{\text{pp}}^{\text{LO}}} = \delta_{\alpha_s\alpha}^{\text{prod}\times\text{dec}} - \delta'_{\alpha_s}\delta_{\alpha}, \quad (7.30)$$

reveals that the proper comparison between the two cross section predictions should examine the two relative correction factors given by $\delta_{\alpha_s\alpha}^{\text{prod}\times\text{dec}} \equiv \Delta\sigma_{\text{pp,prod}\times\text{dec}}^{\text{NNLO}_{s\otimes\text{ew}}}/\sigma_{\text{pp}}^{\text{LO}}$ and the naive product $\delta'_{\alpha_s}\delta_{\alpha}$. Using the QCD correction factor defined in Eq. (4.59) instead, induces a mismatch that originates from the two different LO predictions $\sigma_{\text{pp}}^{\text{LO}}$ and σ_{pp}^0 that are evaluated with LO and NLO PDFs, respectively. The numerical impact of the two different choices in the QCD correction factors was discussed in the conference proceedings in Ref. [89]. The numerical results presented in the following comprise the corrections of the initial–final factorizable corrections and a comparison with the naive product of the NLO QCD and EW corrections. For the EW corrections we use two different versions: First, based on the full $\mathcal{O}(\alpha)$ correction (δ_{α}), and second, based on the dominant EW final-state correction of the PA ($\delta_{\alpha}^{\text{dec}}$). From the explicit calculation of the factorizable initial–final corrections presented in Sect. 7.1 we have observed that many parts of the calculation have the reducible form of a product of two NLO corrections. It is therefore compelling to examine in how far the naive product ansatz is able to capture the general features of the $\mathcal{O}(\alpha_s\alpha)$ corrections. Note, however, that the double-real emission corrections, and in particular their kinematics, cannot be approximated by the product of two NLO real-emission corrections. Any large deviations between $\delta_{\alpha_s\alpha}^{\text{prod}\times\text{dec}}$ and $\delta'_{\alpha_s}\delta_{\alpha}^{(\text{dec})}$ can be therefore attributed to these types of contributions.

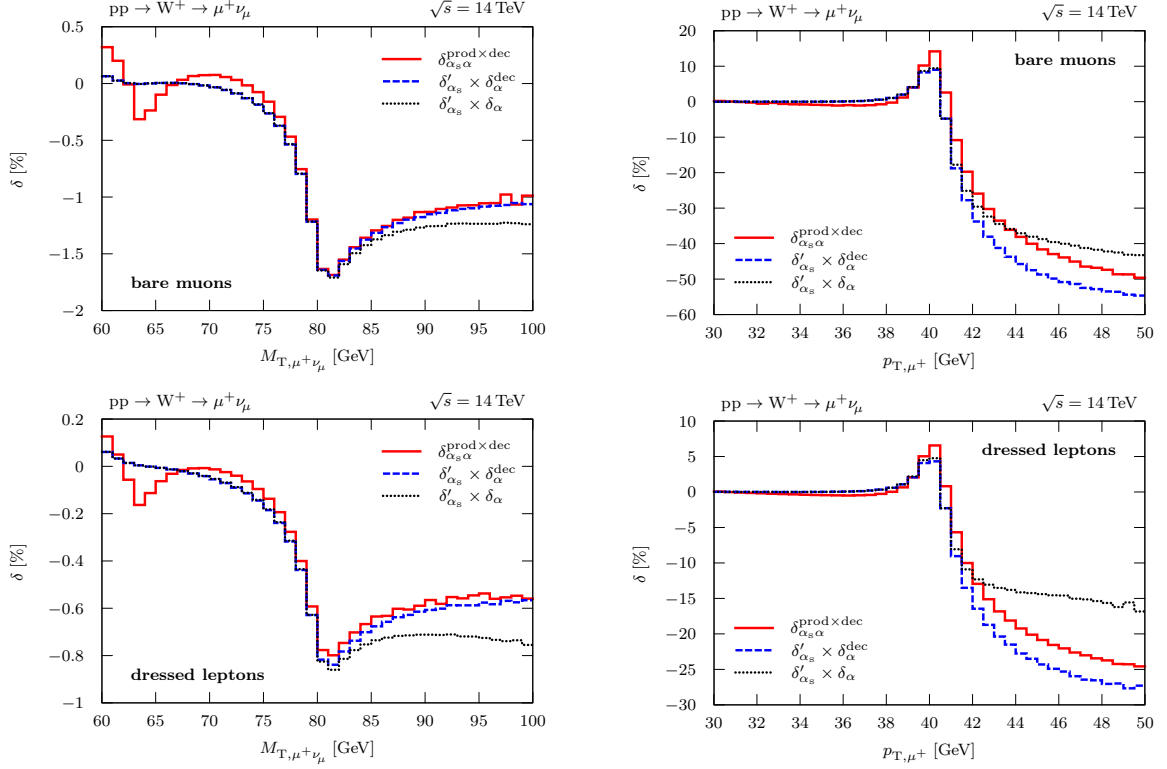


Figure 7.3.: Relative factorizable corrections of $\mathcal{O}(\alpha_s\alpha)$ induced by initial-state QCD and final-state EW contributions to the transverse-mass (left) and transverse-lepton-momentum (right) distributions for W^+ production at the LHC. The naive products of the NLO corrections factors δ'_{α_s} and δ_α are shown for comparison.

Figure 7.3 shows the numerical results for the corrections to the transverse-mass $M_{T,\nu\ell}$ and the transverse-lepton-momentum $p_{T,\ell}$ distributions for W^+ production at the LHC. The upper plots show the results for bare muons, the lower panels correspond to the corrections with photon recombination. The corrections amount to approximately -1.7% in the $M_{T,\nu\ell}$ distribution around the resonance for the case of bare muons and are approximated quite well by the product $\delta'_{\alpha_s} \delta_\alpha^{\text{dec}}$. The product $\delta'_{\alpha_s} \delta_\alpha$ also shows a good agreement in the region around and below the Jacobian peak which is dominated by resonant W production. However, we observe a departure from the other two curves for larger values of $M_{T,\nu\ell}$ reaching deviations at the per-mille level for $M_{T,\nu\ell} \approx 90$ GeV. The difference between the two versions of the naive products allows to assess the impact of the missing $\mathcal{O}(\alpha_s\alpha)$ corrections and therefore also provides an error estimate of the PA and the factorizable initial-final corrections in particular. The overall good agreement between the two naive products can be attributed to the property of the observable $M_{T,\nu\ell}$ that it is insensitive to initial-state radiation effects, as was already observed in the case of NLO corrections in Sect. 4.5. The structure observed in the correction $\delta_{\alpha_s\alpha}^{\text{prod} \times \text{dec}}$ around $M_{T,\nu\ell} \approx 62$ GeV can most likely be attributed to the interplay between the kinematics of the double-real emission corrections and the event selection cuts: Such an effect can already be seen in the NLO EW corrections shown in Fig. 4.8, where the corrections reach a turning point at around the same $M_{T,\nu\ell}$ value and become increasingly negative for smaller $M_{T,\nu\ell}$. This is a result of the event selection cuts $p_{T,\ell^\pm}, E_{rT}^{\text{miss}} > 25$ GeV which implies $M_{T,\nu\ell} > 50$ GeV for the

back-to-back kinematics of the non-radiating process. The additional emission of soft photons from the events close to the cut boundary can result in the rejection of the event due to a momentum loss of the lepton, thus leading to negative corrections. Such a sensitivity of the event selection criteria on soft radiation typically leads to artificially large corrections at cut boundaries and is most likely the origin of the structure that we observe in Fig. 7.3.

For the $p_{T,\ell}$ distribution we observe corrections that are small far below the Jacobian peak, but which rise to about 15 % on the Jacobian peak at $p_{T,\ell} \approx M_W/2$ and then display a steep drop reaching almost -50% at $p_{T,\ell} = 50\text{ GeV}$ in the case of bare muons. This enhancement stems from the large QCD corrections above the threshold for $V + \text{jet}$ production that was already observed in the NLO corrections shown in Fig. 4.8. Due to the sensitivity of this observable to initial-state radiation effects, the two naive products display larger deviations than in the $M_{T,\nu\ell}$ distribution shown above, which signals a larger impact of the missing $\mathcal{O}(\alpha_s\alpha)$ corrections. Furthermore, the strong influence of the recoil induced by initial-state radiation on the transverse momentum of the lepton also implies a larger effect of the double-real emission corrections on this distribution. Correspondingly, the naive product ansatz fails to describe the factorizable initial–final corrections in this observable and deviates by $5 - 10\%$ at the resonance, where the PA is expected to be the most accurate. Note, however, that a fixed-order prediction is not sufficient to describe this distribution around the peak region as we have already seen in Fig. 4.8 for the case of the NLO QCD corrections, and these deviations should be therefore interpreted with care.

The respective results to the $M_{T,\nu\ell}$ and $p_{T,\ell}$ distributions with photon recombination are shown in the lower panels of Fig. 7.3. They display the same general features as discussed above but are reduced by approximately a factor of two compared to the corresponding corrections for bare muons. This reduction is induced by the cancellation of the collinear singularities by restoring the level of inclusiveness required for the KLN theorem and a similar reduction was already observed at NLO in Sect. 4.5. The agreement between $\delta_{\alpha_s\alpha}^{\text{prod}\times\text{dec}}$ and $\delta'_{\alpha_s}\delta_\alpha^{\text{dec}}$ is better for the case of bare leptons which can be understood from the fact that the dominant part of the corrections stem from the collinear logarithms $\ln(m_\mu)$ which are known to factorize.

Figure 7.3 shows the results for the lepton-invariant-mass $M_{\ell\ell}$ and the transverse-lepton-momentum $p_{T,\ell}$ distributions for Z production at the LHC. The upper panels show the corrections for bare muons, the bottom plots show the corresponding results obtained with photon recombination. The relative corrections to the $p_{T,\ell}$ distributions show a similar behaviour as in the corresponding charged-current case with corrections ranging from almost 20 % at the Jacobian peak and reaching around -50% at $p_{T,\ell} \approx 50\text{ GeV}$ for bare muons. With the same reasoning from above, the sensitivity of the transverse momentum of the lepton on initial-state radiation results in a strong impact of the double-real emission contributions and thus spoils the naive factorization picture.

Although the invariant-mass distribution is completely unaffected by initial-state radiation effects, as indicated by the almost identical corrections obtained from the two versions of the product $\delta'_{\alpha_s}\delta_\alpha^{\text{dec}}$ and $\delta'_{\alpha_s}\delta_\alpha$, the naive factorized ansatz completely fails to reproduce the factorizable initial–final corrections in this observable already a little away from the resonance. On the resonance itself ($M_{\ell\ell} = M_Z$) and in the region above the resonance the discrepancy is not very large, however, the corrections are small in this invariant-mass range in any case. The largest corrections (up to 10 %) are observed below the resonance where the naive products display a completely different behaviour and even exhibit a sign change at $M_{\ell\ell} \approx 83\text{ GeV}$ which is not observed in $\delta_{\alpha_s\alpha}^{\text{prod}\times\text{dec}}$.

In order to locate the source for this large discrepancy we examine the individual correction

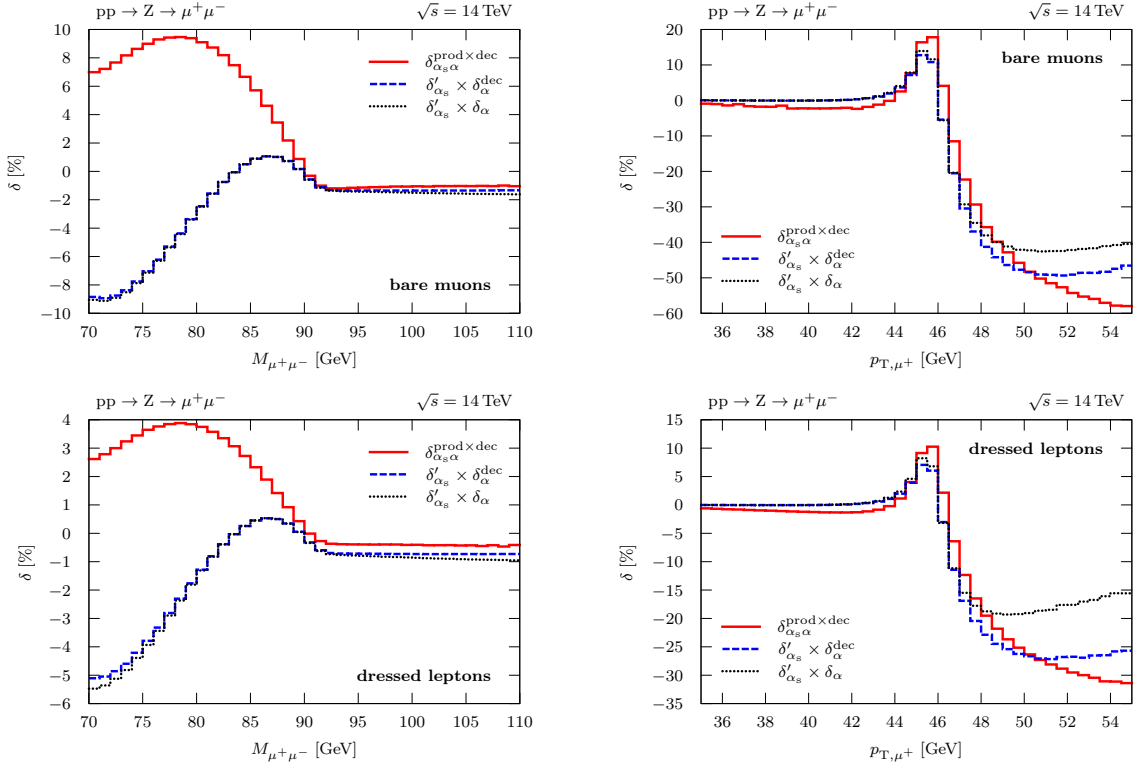


Figure 7.4.: Relative factorizable corrections of $\mathcal{O}(\alpha_s\alpha)$ induced by initial-state QCD and final-state EW contributions to the lepton-invariant-mass (left) and transverse-lepton-momentum (right) distributions for Z production at the LHC. The naive products of the NLO corrections factors δ'_{α_s} and δ_α are shown for comparison.

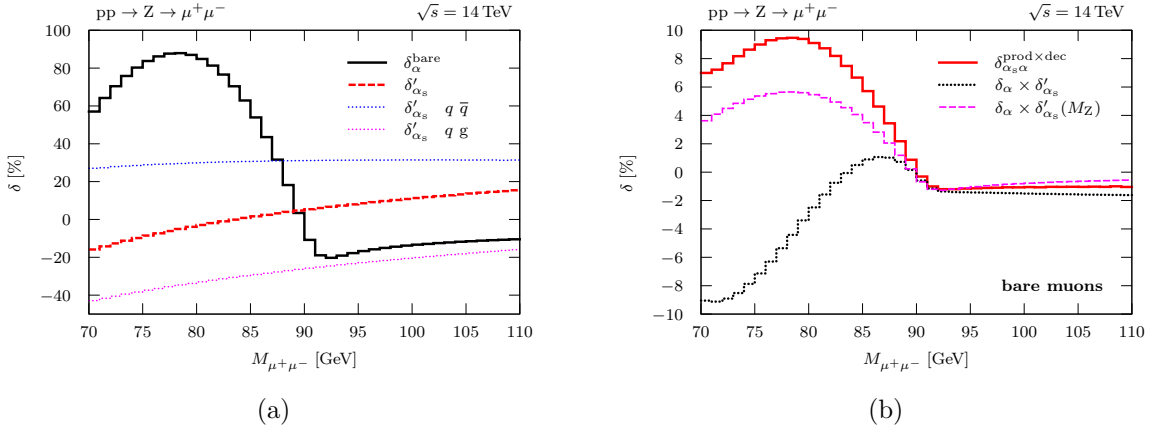


Figure 7.5.: The correction factors entering the naive product ansatz broken down into its individual contributions with the QCD corrections further divided into the quark and gluon-induced contributions (a). A comparison of the corrections shown in the upper left panel of Fig. 7.3 with the modified product using the value of the QCD corrections at the resonance $\delta'_{\alpha_s}(M_{\ell\ell} = M_Z) \approx 6.5\%$.

factors in more detail. We restrict ourselves to the case of bare muons here, but the same conclusions also hold for the case of dressed leptons. Furthermore, since the two versions of the EW correction factors $\delta_\alpha^{\text{dec}}$ and δ_α are almost identical for this observable, we only consider the full NLO EW correction δ_α in the following. First, we separate the two correction factors that enter the naive product $\delta'_{\alpha_s} \times \delta_\alpha^{\text{bare}}$ and further divide the QCD corrections into the $q\bar{q}$ and the gg induced contributions which are shown in Fig. 7.5(a). We observe that the two different quark- and gluon-induced channels individually receive large QCD corrections, however, they differ in sign so that large cancellations take place in the sum δ'_{α_s} . A small mismatch in the corrections of the individual channels can therefore quickly lead to a large effect in the QCD corrections which is then further enhanced by the large EW corrections they are multiplied with. Moreover, Fig. 7.5(a) reveals that the QCD correction factor δ'_{α_s} is responsible for the sign change at $M_{\ell\ell} \approx 83 \text{ GeV}$ which is the most striking feature in the naive product ansatz that differentiates it from the factorizable initial–final corrections. This zero crossing happens more than three widths below the resonance where the cross section is reduced by almost two orders of magnitudes compared to the resonance region and furthermore, will be very sensitive to event selection cuts since δ'_{α_s} arises from the cancellation of two large corrections as we have seen above. The EW correction shown in Fig. 7.5(a) is identical to the corresponding curve shown in Fig. 4.9 and its form reflects the well-known shift of the reconstructed invariant mass to lower values of $M_{\ell\ell}$ as a result of final-state photon radiation. The factorizable initial–final corrections display a very similar behaviour which indicates that the main corrections stem from a similar effect caused by final-state radiation. This picture therefore suggests that the large EW corrections below the resonance should be attributed to events near the Z pole that were redistributed to lower invariant masses by photon radiation. In contrast to this view, the naive product ansatz simply multiplies the corrections locally on a bin-by-bin basis and fails to account for such a migration of events in the distribution. Guided by this insight, we have modified the naive product and replaced the QCD correction δ'_{α_s} by its value at the resonance $\delta'_{\alpha_s}(M_{\ell\ell} = M_Z) \approx 6.5\%$, which corresponds to the location of the events that are responsible for the bulk of the large EW corrections below the resonance as argued above. The comparison of the previous results and this modified product is shown in Fig. 7.5(b) and clearly shows an improvement despite its very crude construction. This further supports our physical interpretation and explains the origin of the large discrepancy seen in the left plots of Fig. 7.4.

This immediately raises the question why the naive factorized approach shows such a good agreement in the case of the $M_{T,\nu\ell}$ distribution of the charged-current process shown in the left panels in Fig. 7.3. The reason lies in the fact that the whole range below the Jacobian peak $M_{T,\nu\ell} \lesssim M_W$ is dominated by resonant W production: As argued above, the naive product ansatz fails to take into account the redistribution of events due to final-state radiation which causes a mismatch in the correction factors that are multiplied with each other. The resulting discrepancy to the factorizable initial–final corrections is mostly driven by the events coming from the resonance, where the cross section is the largest. In case of the transverse-mass distribution, however, such a redistribution of events to lower $M_{T,\nu\ell}$ is simply overwhelmed by the events with resonant W bosons that already dominate the whole range below the Jacobian peak. Therefore, the positive EW corrections below resonance are almost invisible in contrast to the case of the invariant-mass distribution. The largest visible impact of the EW corrections to the $M_{T,\nu\ell}$ distribution is in the vicinity of the resonance itself which is not plagued by the mismatch of the correction factors. As a consequence, the simple products $\delta'_{\alpha_s} \delta_\alpha^{(\text{dec})}$ are able to approximate the factorizable initial–final corrections very well. It should be emphasized, however, that this is

not a general feature of the $M_{T,\nu\ell}$ distribution, but requires a careful case-by-case investigation. For instance, any event selection criteria that deplete events with resonant W bosons below the Jacobian peak will be much more sensitive to the effects of final-state radiation and can potentially lead to similarly large discrepancies as observed in the invariant-mass distribution.

Summary and outlook

The Drell–Yan-like W- and Z-boson production processes are one of the most precise probes of the Standard Model. They are theoretically well understood and can be experimentally measured to high precision, so that they represent one of the most important “standard candle” processes at hadron colliders, such as the LHC. Not only do they serve as key benchmark processes in detector calibration and luminosity monitoring, they also deliver crucial constraints in the fits of the parton distribution functions and can also contribute to searches for new physics. The investigation of the Drell–Yan processes in the resonance regions further allows for precision measurements of the W-boson mass and the effective weak mixing angle. This task of precision physics requires a further increase in the accuracy of the theoretical predictions, where the mixed QCD–electroweak corrections of $\mathcal{O}(\alpha_s\alpha)$ currently represent the largest unknown component of radiative corrections in terms of fixed-order predictions.

In this work we have established a framework for evaluating the $\mathcal{O}(\alpha_s\alpha)$ corrections to Drell–Yan processes in the pole approximation, which is based on the leading terms of a consistent expansion of the cross section about the resonance pole. It classifies the corrections in terms of factorizable and non-factorizable contributions: The former can be attributed to the W/Z production and decay sub-processes individually, while the latter link production and decay by soft-photon exchange. The corrections at this order are especially required in kinematic distributions around the resonances which motivates the use of the pole approximation. We have presented numerical results for the most important observables for the W-boson mass measurement: the transverse-mass and lepton-transverse-momentum distributions for W production. The results for the neutral-current process comprise the invariant-mass and the lepton-transverse-momentum distributions. These observables enter indirectly into the W-boson-mass measurement through the detector calibration as demonstrated by the measurements at the Tevatron [17,18], which appears to be an essential input in order to reach the experimental accuracy reported there.

In the first part of this thesis we have described the concept of the pole approximation and applied it to the electroweak next-to-leading-order corrections of $\mathcal{O}(\alpha)$. This was a necessary step in order to establish our methods as a preparation for the extension to the $\mathcal{O}(\alpha_s\alpha)$ corrections and, furthermore, to validate the pole approximation by comparing to the known full results.

For the treatment of infrared singularities that arise in radiative corrections involving massless particles, we have employed the phase-space-slicing method in the calculation of the non-factorizable corrections and the dipole subtraction formalism for the remaining corrections. The consistent application of the pole approximation to all parts of the calculation, in particular also the real-emission corrections, required the extension of the dipole subtraction formalism to cover decay kinematics. We have presented the construction of a universal subtraction term for decaying particles in QED in Chap. 3 which has been developed in the context of this work.

It turns out that at $\mathcal{O}(\alpha)$, the pole approximation works up to fractions of 1% near the resonance, i.e. at a phenomenologically satisfactory level. In detail, the factorizable corrections to the production process are mostly suppressed below the per-cent level, apart from off-shell tails in transverse-momentum distributions where the QCD recoil effects are overwhelming. The

non-factorizable contributions are also suppressed way below the per-cent level, and the bulk of the corrections near the resonance can be attributed to the factorizable corrections to the W/Z decay sub-processes.

In the second part of this work we have described how the mixed QCD–electroweak $\mathcal{O}(\alpha_s\alpha)$ corrections can be systematically calculated in the resonance region by establishing the concept of the pole approximation at this order. The quality of the approximation observed at NLO strongly supports our expectation that this approach is sufficient for the description of observables that are dominated by the resonances. The explicit calculation of the non-factorizable corrections has been presented in Chap. 6 which turn out to be phenomenologically negligible.

As a consequence, the $\mathcal{O}(\alpha_s\alpha)$ corrections almost entirely result from the corrections where the production and decay of the W/Z boson proceed independently. Guided by the insights that were obtained in the calculation of the pole approximation at NLO, we expect the factorizable corrections of “initial–final” type to constitute the most dominant contribution at $\mathcal{O}(\alpha_s\alpha)$. This part combines large QCD corrections to the production with large electroweak corrections to the decay sub-process and has been computed in Chap. 7. We have compared our results for the factorizable initial–final corrections to different versions of a naive product ansatz which were obtained by multiplying the NLO QCD and electroweak correction factors. We have demonstrated that the sensitivity of an observable to initial-state radiation, such as the transverse momentum of the lepton, also induces a strong impact of the double-real-emission part of the NNLO corrections. As a consequence, the naive products fail to capture the factorizable initial–final corrections in these distributions. We note that this does not imply that the stability of the observable with respect to initial-state radiation effects leads to a better agreement, but that it requires a careful investigation of the properties of the observable and the impact of event selection cuts. In particular, we have demonstrated that the naive products fail to capture the redistribution of events due to the real-emission corrections. If such a migration of events is responsible for the bulk of the corrections, such as in the invariant-mass distribution of the neutral-current process, large deviations are observed. On the other hand, if an observable is less affected by such a redistribution of events or is only affected by it in the vicinity of the resonance, such as the transverse-mass distribution of the charged-current process, the naive products are able to reproduce the factorizable initial–final corrections to a large extent.

The numerical results presented in this thesis have been obtained by a fully flexible Monte Carlo program which has been developed in the context of this work and allows to calculate total cross section predictions as well as arbitrary distributions in the form of histograms. In particular, our program includes the $\mathcal{O}(\alpha_s\alpha)$ corrections discussed in this work which are not available elsewhere and it will be used to prepare theory predictions for experimental analyses.

In the future it should be investigated to what extent a QED parton shower or a structure function approach for multi-photon radiation—which emulate the real emission of photons in the collinear approximation—applied to the NLO QCD corrections will be able to reproduce these corrections. Furthermore, in order to obtain a more realistic prediction for the lepton-transverse-momentum distributions it is desirable to perform QCD resummation or a matching to a parton shower.

Conventions and notation

A.1. General conventions

Lorentz vectors

The contravariant and covariant four-vectors are denoted with an upper and lower Lorentz index (greek letters by convention), respectively,

$$k^\mu = (k^0, \mathbf{k}), \quad k_\mu = (k_0, -\mathbf{k}), \quad (\text{A.1})$$

with $k^0 = k_0$ denoting the time-like component and the vector of the spatial components is written in boldface,

$$\mathbf{k} = (k^1, k^2, k^3) = |\mathbf{k}| (\sin \theta \cos \varphi, \sin \theta \sin \varphi, \cos \theta), \quad (\text{A.2})$$

where θ and φ denote the polar and azimuth angle in polar coordinates, respectively. Our metric definition is given by

$$g_{\mu\nu} = g^{\mu\nu} = \text{diag}(1, -1, -1, -1), \quad (\text{A.3})$$

and the scalar product between two four-vectors explicitly reads

$$p \cdot k = p_\mu k^\mu = g_{\mu\nu} p^\nu k^\mu = p^0 k^0 - \mathbf{p} \cdot \mathbf{k}. \quad (\text{A.4})$$

The space-time derivative is defined by

$$\partial_\mu = \frac{\partial}{\partial x^\mu} = \left(\frac{\partial}{\partial t}, \nabla \right) = \left(\frac{\partial}{\partial t}, \frac{\partial}{\partial x}, \frac{\partial}{\partial y}, \frac{\partial}{\partial z} \right). \quad (\text{A.5})$$

Finally, the totally anti-symmetric Levi-Civita tensor is defined as

$$\varepsilon^{\mu\nu\rho\sigma} = -\varepsilon_{\mu\nu\rho\sigma} = \begin{cases} +1, & \text{for even permutations of } \{\mu, \nu, \rho, \sigma\} = \{0, 1, 2, 3\}, \\ -1, & \text{for odd permutations of } \{\mu, \nu, \rho, \sigma\} = \{0, 1, 2, 3\}, \\ 0, & \text{otherwise.} \end{cases} \quad (\text{A.6})$$

Dirac algebra

The Dirac algebra is a special case of a Clifford algebra and the generators are given by the gamma matrices, which satisfy the following defining relation,

$$\{\gamma^\mu, \gamma^\nu\} = \gamma^\mu \gamma^\nu + \gamma^\nu \gamma^\mu = 2g^{\mu\nu} \mathbf{1}. \quad (\text{A.7})$$

One can further define the matrix γ^5 which anti-commutes with all other gamma matrices,

$$\gamma^5 = i\gamma^0\gamma^1\gamma^2\gamma^3 = -\frac{i}{4!}\varepsilon_{\mu\nu\rho\sigma}\gamma^\mu\gamma^\nu\gamma^\rho\gamma^\sigma, \quad \{\gamma^5, \gamma^\mu\} = 0, \quad (\text{A.8})$$

and which enters the definition of the right- and the left-handed chirality projectors

$$\omega_\pm = \frac{1}{2}(\mathbb{1} \pm \gamma^5). \quad (\text{A.9})$$

In the Weyl or chiral representation the gamma matrices are given by

$$\gamma^\mu = \begin{pmatrix} 0 & \bar{\sigma}^\mu \\ \sigma^\mu & 0 \end{pmatrix}, \quad \sigma^\mu = (\sigma^0, \boldsymbol{\sigma}), \quad \bar{\sigma}^\mu = (\sigma^0, -\boldsymbol{\sigma}), \quad (\text{A.10})$$

where $\sigma^0 = \mathbb{1}_{2 \times 2}$ is the unit matrix and $\boldsymbol{\sigma} = (\sigma^1, \sigma^2, \sigma^3)$ denotes the vector of the Pauli matrices,

$$\sigma^1 = \begin{pmatrix} 0 & 1 \\ 1 & 0 \end{pmatrix}, \quad \sigma^2 = \begin{pmatrix} 0 & -i \\ i & 0 \end{pmatrix}, \quad \sigma^3 = \begin{pmatrix} 1 & 0 \\ 0 & -1 \end{pmatrix}. \quad (\text{A.11})$$

In this representation γ^5 and the chirality projectors take a particularly simple form given by

$$\gamma^5 = \begin{pmatrix} 1 & 0 \\ 0 & -1 \end{pmatrix}, \quad \omega_+ = \begin{pmatrix} 1 & 0 \\ 0 & 0 \end{pmatrix}, \quad \omega_- = \begin{pmatrix} 0 & 0 \\ 0 & 1 \end{pmatrix}, \quad (\text{A.12})$$

so that the right(left) handed spinors can be identified by the first(last) two components of the Dirac spinor. Furthermore, we introduce the usual slashed notation for the contraction of four-vectors with a gamma matrix,

$$\not{p} = p_\mu \gamma^\mu. \quad (\text{A.13})$$

Finally, we note that the extension of the chirality matrix γ^5 to $d \neq 4$ space-time dimensions requires spacial care, which is discussed in more detail in Sect. 1.1.2.

Important functions

The Källén function

A function which appears repeatedly in kinematical equations is the Källén function (triangle function) which is defined by

$$\lambda(x, y, z) = x^2 + y^2 + z^2 - 2xy - 2yz - 2zx. \quad (\text{A.14})$$

The plus distribution

The plus prescription is used to regularize a function $f(x)$ which is singular at $x = 1$ by explicitly isolating the singularity at the endpoint. The plus distribution is defined as follows (see e.g. Ref [90])

$$[f(x)]_+ \equiv \lim_{\delta \rightarrow 0} \left[\theta(1 - x - \delta) f(x) - \delta(1 - x - \delta) \int_0^{1-\delta} dy f(y) \right], \quad (\text{A.15})$$

and can be equivalently defined in terms of an integral with a smooth test function $g(x)$,

$$\int_0^1 dx [f(x)]_+ g(x) = \int_0^1 dx f(x) [g(x) - g(1)]. \quad (\text{A.16})$$

The Gamma function

Euler's Gamma function is given by the definite integral

$$\Gamma(z) = \int_0^\infty t^{z-1} e^{-t} dt, \quad (\text{A.17})$$

and satisfies the following functional equation

$$\Gamma(1+z) = z \Gamma(z). \quad (\text{A.18})$$

In case the argument is a natural number, the Gamma function is related to the faculty as follows,

$$\Gamma(1+n) = n!. \quad (\text{A.19})$$

The series expansion of the Gamma function around 1 reads

$$\Gamma(1+\epsilon) = 1 - \gamma_E \epsilon + \left(\frac{1}{2} \gamma_E^2 + \frac{\pi^2}{12} \right) \epsilon^2 + \mathcal{O}(\epsilon^3), \quad (\text{A.20})$$

where γ_E is the Euler–Mascheroni constant with the numerical value

$$\gamma_E = 0.5772\dots \quad (\text{A.21})$$

The dilogarithm

The dilogarithm is defined as

$$\text{Li}_2(z) = \int_z^0 \frac{\ln(1-t)}{t} dt, \quad |\arg(1-z)| < \pi, \quad (\text{A.22})$$

and can be alternatively expressed as the following infinite sum,

$$\text{Li}_2(z) = \sum_{k=1}^{\infty} \frac{z^k}{k^2}, \quad |z| < 1. \quad (\text{A.23})$$

The polylogarithm

The dilogarithm defined above is a special case of the polylogarithms Li_n of order $n = 2$. The polylogarithm can be defined as a generalization of Eq. (A.23) by the following series representation

$$\text{Li}_n(z) = \sum_{k=1}^{\infty} \frac{z^k}{k^n}, \quad |z| < 1. \quad (\text{A.24})$$

In our calculations we will encounter polylogarithms up to order three, Li_3 , which is also called the trilogarithm.

The $SU(3)_C$ colour group

The eight generators in the fundamental representation of the $SU(3)_C$ Lie group are given by

$$t^a = \frac{\lambda^a}{2}, \quad a = 1, \dots, 8, \quad (\text{A.25})$$

where the matrices λ^a denote the Gell-Mann matrices which explicitly read

$$\begin{aligned} \lambda^1 &= \begin{pmatrix} 0 & 1 & 0 \\ 1 & 0 & 0 \\ 0 & 0 & 0 \end{pmatrix}, & \lambda^2 &= \begin{pmatrix} 0 & -i & 0 \\ i & 0 & 0 \\ 0 & 0 & 0 \end{pmatrix}, & \lambda^3 &= \begin{pmatrix} 1 & 0 & 0 \\ 0 & -1 & 0 \\ 0 & 0 & 0 \end{pmatrix}, \\ \lambda^4 &= \begin{pmatrix} 0 & 0 & 1 \\ 0 & 0 & 0 \\ 1 & 0 & 0 \end{pmatrix}, & \lambda^5 &= \begin{pmatrix} 0 & 0 & -i \\ 0 & 0 & 0 \\ i & 0 & 0 \end{pmatrix}, & \lambda^6 &= \begin{pmatrix} 0 & 0 & 0 \\ 0 & 0 & 1 \\ 0 & 1 & 0 \end{pmatrix}, \\ \lambda^7 &= \begin{pmatrix} 0 & 0 & 0 \\ 0 & 0 & -i \\ 0 & i & 0 \end{pmatrix}, & \lambda^8 &= \frac{1}{\sqrt{3}} \begin{pmatrix} 1 & 0 & 0 \\ 0 & 1 & 0 \\ 0 & 0 & -2 \end{pmatrix}. \end{aligned} \quad (\text{A.26})$$

The generator t^a are normalized as follows,

$$\text{Tr} [t^a t^b] = \frac{1}{2} \delta^{ab}, \quad (\text{A.27})$$

and satisfy the commutation relations

$$[t^a, t^b] = i f^{abc} t^c, \quad (\text{A.28})$$

where f^{abc} denote the structure constants of the algebra. The generators of the adjoint representation are defined through the structure constants as follows,

$$(T_{\text{adj}}^a)_{bc} = i f^{bac}. \quad (\text{A.29})$$

The quadratic Casimir operators of the two representations can be written as

$$\sum_{a=1}^8 t^a t^a = C_F \mathbb{1}_{3 \times 3}, \quad \sum_{a=1}^8 T_{\text{adj}}^a T_{\text{adj}}^a = C_A \mathbb{1}_{8 \times 8}, \quad (\text{A.30})$$

with $C_F = \frac{4}{3}$ and $C_A = 3$.

A.2. The Weyl–van-der-Waerden spinor formalism

This section provides a brief review of the Weyl–van-der-Waerden (WvdW) spinor formalism as presented in Ref. [165], which was employed in this work for the calculation of tree amplitudes, i.e. the LO and all real-emission amplitudes. We will restrict the presentation of this formalism

to the cases that are relevant for our calculation, i.e. to massless external fermions and vector bosons, and refer to Ref. [165] for a more comprehensive treatment. The direct computation of helicity amplitudes has the advantage that it allows to perform the squaring of the amplitudes and the subsequent summation over the polarizations numerically. As a result, the complexity of the analytical calculation involved in the helicity formalism only scales linearly with the number of contributing diagrams, in contrast to the quadratic scaling inherent to the conventional approach, where completeness relations of the external states and trace techniques are applied to sum over the external polarizations in the squared matrix element. Although each helicity configuration need to be computed separately, many of them give a vanishing contribution or can be related to other configurations using discrete symmetries, so that this additional complexity poses no problem in practice. The WvdW formalism further decomposes all objects that belong to higher-dimensional representations of the Lorentz group into the two-dimensional irreducible representations $D(\frac{1}{2}, 0)$ and $D(0, \frac{1}{2})$. This allows to treat all different Lorentz structures, such as Dirac spinors, Minkowski four-vectors, and polarization vectors on the same footing and simplifies the analytical calculation and the implementation in a computer code considerably. Owing to the close connection of the WvdW spinors to light-like momenta, this formalism is especially suited for the calculation involving massless external states and leads to particularly simple expressions in the final result.

Basic definitions and the Weyl–van-der-Waerden spinors

The basic building blocks in the WvdW formalism are the covariant and contravariant WvdW spinors which belong to the two-dimensional irreducible representations $D(\frac{1}{2}, 0)$ and $D(0, \frac{1}{2})$ and are denoted by ψ_A and $\psi^{\dot{A}}$, respectively. The transition between the two in-equivalent representations is accomplished by complex conjugation and a similarity transformation as follows,

$$\psi^{\dot{A}} = \epsilon^{\dot{A}\dot{B}} \psi_{\dot{B}} = \epsilon^{\dot{A}\dot{B}} (\psi_B)^*, \quad \psi_A = \psi^B \epsilon_{BA} = (\psi^{\dot{B}})^* \epsilon_{BA}, \quad (\text{A.31})$$

where complex conjugation is indicated by dotting or un-dotting the spinor index,

$$(\psi_A)^* = \psi_{\dot{A}}, \quad (\psi^{\dot{A}})^* = \psi^A, \quad (\text{A.32})$$

and the totally anti-symmetric tensor is given by

$$\epsilon_{AB} = \epsilon^{AB} = \epsilon^{\dot{A}\dot{B}} = \epsilon_{\dot{A}\dot{B}} = \begin{pmatrix} 0 & +1 \\ -1 & 0 \end{pmatrix}. \quad (\text{A.33})$$

The matrix ϵ further serves as a spinor metric and defines a Lorentz-invariant spinor product,

$$\langle \phi \psi \rangle = \phi_A \psi^A = \phi_A \epsilon^{AB} \psi_B, \quad \langle \phi \psi \rangle^* = \phi_{\dot{A}} \psi^{\dot{A}} = \phi_{\dot{A}} \epsilon^{\dot{B}\dot{A}} \psi^{\dot{B}}, \quad (\text{A.34})$$

$$\langle \phi \psi \rangle = -\langle \psi \phi \rangle, \quad \langle \phi \phi \rangle = 0, \quad (\text{A.35})$$

and defines the raising and lowering of spinor indices as indicated in Eqs. (A.31) and (A.34). The spinor metric further satisfies the Schouten identity

$$\epsilon^{AB} \epsilon^{CD} + \epsilon^{AC} \epsilon^{DB} + \epsilon^{AD} \epsilon^{BC} = 0, \quad (\text{A.36})$$

which can provide significant algebraic simplifications in the calculation.

The spinor representation of Minkowski four-vectors

The Minkowski four vectors (A.1) belong to the representation $D(\frac{1}{2}, \frac{1}{2})$ which decomposes into a product of the above representations according to $D(\frac{1}{2}, \frac{1}{2}) = D(\frac{1}{2}, 0) \otimes D(0, \frac{1}{2})$. The transition matrices are defined as, cf. Eqs. (A.10) and (A.11),

$$\sigma^{\mu, \dot{A}B} = \sigma^\mu = (\sigma^0, \boldsymbol{\sigma}), \quad \sigma_{\dot{A}B}^\mu = \bar{\sigma}^\mu = (\sigma^0, -\boldsymbol{\sigma}), \quad (\text{A.37})$$

and the spinor representation of the four-vector k^μ then reads

$$K_{\dot{A}B} = k_\mu \sigma_{\dot{A}B}^\mu = \begin{pmatrix} k^0 + k^3 & k^1 + ik^2 \\ k^1 - ik^2 & k^0 - k^3 \end{pmatrix}, \quad 2(k \cdot p) = 2k_\mu p^\mu = K_{\dot{A}B} P^{\dot{A}B}. \quad (\text{A.38})$$

In case of light-like momenta ($k^2 = 0$) the matrix $K_{\dot{A}B}$ factorizes into a product of two so-called *momentum spinors*,

$$K_{\dot{A}B} = k_A k_B, \quad k_A = \sqrt{2k^0} \begin{pmatrix} e^{-i\varphi} \cos \frac{\theta}{2} \\ \sin \frac{\theta}{2} \end{pmatrix}, \quad (\text{A.39})$$

with the polar and azimuth angles θ, φ defined in Eq. (A.2).

Spin- $\frac{1}{2}$ particles

The Dirac spinors Ψ belong to the representation $D(\frac{1}{2}, 0) \oplus D(0, \frac{1}{2})$ of the Lorentz group and can be directly constructed in the chiral representation (A.10) from two WvdW spinors as follows,

$$\Psi = \begin{pmatrix} \phi_A \\ \psi^{\dot{A}} \end{pmatrix}. \quad (\text{A.40})$$

Inserting the plane-wave ansatz for free particles $\Psi(x) = \exp(\mp i k x) \Psi^{(\pm)}(k)$ into the Dirac equation $((i\partial - m)\Psi(x) = 0)$ and further inserting the decomposition given in Eq. (A.40), we obtain

$$K_{\dot{A}B} \psi^{(\pm), \dot{B}}(k) = \pm m_f \phi_A^{(\pm)}(k), \quad K^{\dot{A}B} \phi_B^{(\pm)}(k) = \pm m_f \psi^{(\pm), \dot{A}}(k), \quad (\text{A.41})$$

where the Dirac spinors $\Psi^{(+)}$ and $\Psi^{(-)}$ correspond to fermions and anti-fermions, respectively. For massless fermions the above equations decouple into the *Weyl equations* for the helicity eigenstates which have the simple solutions

$$\Psi_+^{(+)}(k) = \Psi_-^{(-)}(k) = \begin{pmatrix} k_A \\ 0 \end{pmatrix}, \quad \Psi_-^{(+)}(k) = \Psi_+^{(-)}(k) = \begin{pmatrix} 0 \\ k^{\dot{A}} \end{pmatrix}, \quad (\text{A.42a})$$

$$\bar{\Psi}_+^{(+)}(k) = \bar{\Psi}_-^{(-)}(k) = (0, k_{\dot{A}}), \quad \bar{\Psi}_-^{(+)}(k) = \bar{\Psi}_+^{(-)}(k) = (k^A, 0). \quad (\text{A.42b})$$

Here, the subscript labels \pm indicate the helicity of the fermions, so that the spinor $\Psi_\tau^{(\pm)}$ corresponds to a fermion of helicity $\sigma = \frac{1}{2}\tau$.

Massless spin-1 particles

The polarization vectors $\varepsilon_\mu(k)$ for the spin-1 particles are transformed into the spinor representation in the same manner as the four-vector in Eq. (A.38). In case of massless spin-1 particles the additional freedom in the choice of the gauge manifests itself in the WvdW formalism by the arbitrary gauge spinors g_\pm ($\langle g_\pm k \rangle \neq 0$) in the definition of the polarization bi-spinors,

$$\varepsilon_{+,AB}(k) = \frac{\sqrt{2} g_{+,A} k_B}{\langle g_+ k \rangle^*}, \quad \varepsilon_{-,AB}(k) = \frac{\sqrt{2} k_{\dot{A}} g_{-,B}}{\langle g_- k \rangle}, \quad (\text{A.43a})$$

$$\varepsilon_{+,AB}^*(k) = \frac{\sqrt{2} k_{\dot{A}} g_{+B}}{\langle g_+ k \rangle}, \quad \varepsilon_{-,AB}^*(k) = \frac{\sqrt{2} g_{-,A} k_B}{\langle g_- k \rangle^*}, \quad (\text{A.43b})$$

where the labels \pm denote the helicities of the respective states.

Discrete symmetries

Discrete symmetries relate amplitudes of different processes and/or different helicities to each other. Here we will only give the recipes for the two symmetry transformations used in this work and refer to Ref. [165] for further details.

Crossing symmetry transforms incoming/outgoing particles into outgoing/ingoing anti-particles and vice versa. The transition $k^\mu \rightarrow -k^\mu$ can be consistently incorporated by a sign change for the dotted momentum spinors

$$k_{\dot{A}} \rightarrow -k_{\dot{A}}, \quad k_A \rightarrow k_A. \quad (\text{A.44})$$

In addition, the helicities of the crossed particles are reversed, i.e. an incoming left-handed fermion is transformed to an outgoing right-handed anti-fermion, etc. However, this rearrangement of the helicity configurations has no impact on unpolarized squared matrix elements since all particle helicities are summed over. Furthermore, an additional global factor -1 arises for each spin-1 field and each incoming(outgoing) left(right)-handed fermion involved in the crossing, which however represents an irrelevant phase factor that drops out in the squared amplitude. In this work, all amplitudes were calculated for the case of only incoming particles and the crossing relations were applied to obtain the amplitude of the desired process. Owing to the simple prescription (A.44), this crossing transformation can be easily performed inside the computer code by a flag that controls the direction of the particle. As a result, only one single implementation of the amplitude is necessary in order to obtain all squared matrix elements for the processes that are related to each other by crossing symmetry. Explicitly, we denote the crossing transformation by the operation $\mathcal{X} [X^\mp(p) \leftrightarrow X^\pm(k)]$,

$$\begin{aligned} & \mathcal{M}^{\dots \rightarrow X^\pm \dots} \left(\dots; \begin{bmatrix} k \\ h \end{bmatrix}, \dots \right) \\ &= \mathcal{X} [X^\mp(p) \rightarrow X^\pm(k)] \left\{ \mathcal{M}^{X^\mp \dots \rightarrow \dots} \left(\begin{bmatrix} p \\ h \end{bmatrix}, \dots; \dots \right) \right\} \\ &\equiv \mathcal{M}^{X^\mp \dots \rightarrow \dots} \left(\begin{bmatrix} -k \\ -h \end{bmatrix}, \dots; \dots \right) \times \begin{cases} -\text{sgn}(h), & X \text{ is a spin-}\frac{1}{2} \text{ particle,} \\ -1, & X \text{ is a spin-1 particle,} \end{cases} \quad (\text{A.45a}) \\ & \mathcal{M}^{X^\pm \dots \rightarrow \dots} \left(\begin{bmatrix} p \\ h \end{bmatrix}, \dots; \dots \right) \\ &= \mathcal{X} [X^\pm(p) \leftarrow X^\mp(k)] \left\{ \mathcal{M}^{\dots \rightarrow X^\mp \dots} \left(\begin{bmatrix} k \\ h \end{bmatrix}, \dots; \dots \right) \right\} \end{aligned}$$

$$\equiv \mathcal{M}^{\dots \rightarrow X^\mp \dots} \left(\dots; \begin{bmatrix} -p \\ -h \end{bmatrix}, \dots \right) \times \begin{cases} +\text{sgn}(h), & X \text{ is a spin-}\frac{1}{2} \text{ particle,} \\ -1, & X \text{ is a spin-1 particle,} \end{cases} \quad (\text{A.45b})$$

which transforms an incoming particle X^\mp with momentum p^μ into the corresponding outgoing anti-particle X^\pm with momentum k^μ and vice versa.

Parity establishes a relation between amplitudes with opposite helicities for all external particles and the additional inversion of the spatial components of the momenta. In the WvdW formalism this transformation amounts to the complex conjugation of the helicity amplitude, up to a global sign factor. In a chiral theory where parity is not conserved—as it is the case of the SM—an additional interchange of the couplings $C_{\dots}^\pm \rightarrow C_{\dots}^\mp$ is required (see Table A.5 for the chiral couplings of the SM). For an amplitude $i\mathcal{M}^{\dots}(\sigma_i, \lambda_j)$ involving n fermions and \bar{n} anti-fermions with helicities σ_i , and n_V vector bosons with helicities λ_j , the transformation explicitly reads

$$\begin{aligned} \mathcal{M}^{\dots}(\sigma_i, \lambda_j) &= \mathcal{P} \left\{ \mathcal{M}^{\dots}(-\sigma_i, -\lambda_j) \right\} \\ &\equiv (-1)^{\bar{n}} \text{sgn}(\sigma_1 \cdots \sigma_{n+\bar{n}}) \mathcal{M}^{\dots}(-\sigma_i, -\lambda_j)^* \Big|_{C_{\dots}^\pm \rightarrow C_{\dots}^\mp}. \end{aligned} \quad (\text{A.46})$$

Here, we have introduced the modified parity transformation, denoted by \mathcal{P} , which includes the exchange of the chiral couplings.

A.3. Feynman rules

This section collects all Feynman rules that appear in the calculation of the amplitudes of the Born and real-emission amplitudes. A complete list of the Feynman rules for the SM can be found e.g. in Appendix A of Ref. [108]. In addition to the Feynman rules given in terms of four-vectors and Dirac matrices, we further supply the respective expressions in the WvdW formalism discussed in the previous section that were obtained using the prescription outlined in Sect. 4.1 of Ref. [165].

The Feynman rules for the external legs correspond to the one-particle states which are given in Eqs. (A.42) and (A.43) for the case of massless spin- $\frac{1}{2}$ and spin-1 particles, respectively, and are collected in Tables A.1 and A.2. The propagators are listed in Table A.3 and the collection of the relevant vertices for this work are given in Table A.4. The chiral couplings $C_{V\bar{f}f'}^\pm$, appearing in the $V\bar{f}f$ -vertex are given in Table A.5, where the couplings g_f^\pm are defined as

$$g_f^+ = -\frac{s_w}{c_w} Q_f, \quad g_f^- = \frac{I_{w,f}^3 - s_w^2 Q_f}{s_w c_w}. \quad (\text{A.47})$$

The coupling constants $C_{V_1 V_2 V_3}$ appearing in the triple-gauge-boson vertex are given by

$$C_{\gamma W^+ W^-} = e, \quad C_{Z W^+ W^-} = -e \frac{c_w}{s_w}. \quad (\text{A.48})$$

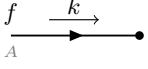
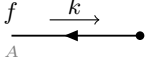
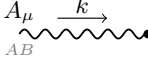
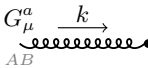
Incoming fields	Weyl-van-der-Waerden formalism		
	$\Psi_\tau^{(+)}(k)$	\longrightarrow	$\Psi_\tau^{(+)}(k) \stackrel{m_f=0}{=} \begin{cases} \begin{pmatrix} 0 \\ k^{\dot{A}} \end{pmatrix}, & \sigma = -\frac{1}{2}, \\ \begin{pmatrix} k^A \\ 0 \end{pmatrix}, & \sigma = +\frac{1}{2}. \end{cases}$
	$\bar{\Psi}_\tau^{(-)}(k)$	\longrightarrow	$\bar{\Psi}_\tau^{(-)}(k) \stackrel{m_f=0}{=} \begin{cases} (0, k_{\dot{A}}), & \sigma = -\frac{1}{2}, \\ (k^A, 0), & \sigma = +\frac{1}{2}. \end{cases}$
	$\varepsilon_{\lambda,\mu}(k)$	\longrightarrow	$\varepsilon_{\lambda,\dot{A}B}(k) = \begin{cases} \frac{\sqrt{2}k_{\dot{A}}g_{-,B}}{\langle g-k \rangle}, & \lambda = -1, \\ \frac{\sqrt{2}g_{+,\dot{A}}k_B}{\langle g+k \rangle^*}, & \lambda = +1. \end{cases}$
	$\varepsilon_{\lambda,\mu}^a(k)$	\longrightarrow	$\varepsilon_{\lambda,\dot{A}B}^a(k) = \begin{cases} \frac{\sqrt{2}k_{\dot{A}}g_{-,B}}{\langle g-k \rangle}, & \lambda = -1, \\ \frac{\sqrt{2}g_{+,\dot{A}}k_B}{\langle g+k \rangle^*}, & \lambda = +1. \end{cases}$

Table A.1.: Feynman rules for incoming particles. The label τ in the fermion states is related to the helicity σ via $\sigma = \frac{1}{2}\tau$.


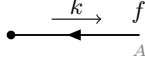
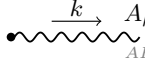
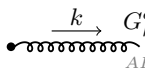
Outgoing fields	Weyl-van-der-Waerden formalism		
	$\bar{\Psi}_\tau^{(+)}(k)$	\longrightarrow	$\bar{\Psi}_\tau^{(+)}(k) \stackrel{m_f=0}{=} \begin{cases} (k^A, 0), & \sigma = -\frac{1}{2}, \\ (0, k_{\dot{A}}), & \sigma = +\frac{1}{2}. \end{cases}$
	$\Psi_\tau^{(-)}(k)$	\longrightarrow	$\Psi_\tau^{(-)}(k) \stackrel{m_f=0}{=} \begin{cases} \begin{pmatrix} k^A \\ 0 \end{pmatrix}, & \sigma = -\frac{1}{2}, \\ \begin{pmatrix} 0 \\ k^{\dot{A}} \end{pmatrix}, & \sigma = +\frac{1}{2}. \end{cases}$
	$\varepsilon_{\lambda,\mu}^*(k)$	\longrightarrow	$\varepsilon_{\lambda,\dot{A}B}^*(k) = \begin{cases} \frac{\sqrt{2}g_{-,\dot{A}}k_B}{\langle g-k \rangle^*}, & \lambda = -1, \\ \frac{\sqrt{2}k_{\dot{A}}g_{+,B}}{\langle g+k \rangle}, & \lambda = +1. \end{cases}$
	$\varepsilon_{\lambda,\mu}^{a*}(k)$	\longrightarrow	$\varepsilon_{\lambda,\dot{A}B}^{a*}(k) = \begin{cases} \frac{\sqrt{2}g_{-,\dot{A}}k_B}{\langle g-k \rangle^*}, & \lambda = -1, \\ \frac{\sqrt{2}k_{\dot{A}}g_{+,B}}{\langle g+k \rangle}, & \lambda = +1. \end{cases}$

Table A.2.: Feynman rules for outgoing particles. The label τ in the fermion states is related to the helicity σ via $\sigma = \frac{1}{2}\tau$.

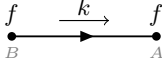
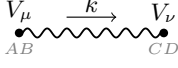
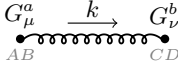
Propagators	Weyl–van-der-Waerden formalism	
	$\frac{i(\not{k}+m_f)}{k^2-m_f^2}$	$\longrightarrow \frac{i}{k^2-m_f^2} \begin{pmatrix} m_f \delta_A^B & K_{A\dot{B}} \\ K^{A\dot{B}} & m_f \delta_{\dot{B}}^A \end{pmatrix}$
	$\frac{-ig_{\mu\nu}}{k^2-M_V^2}$	$\longrightarrow \frac{-2i\epsilon_{\dot{A}\dot{C}}\epsilon^{BED}}{k^2-M_V^2}$
	$\frac{-i\delta^{ab}g_{\mu\nu}}{k^2}$	$\longrightarrow \frac{-2i\delta^{ab}\epsilon_{\dot{A}\dot{C}}\epsilon^{BED}}{k^2}$

Table A.3.: Feynman rules for the propagators.

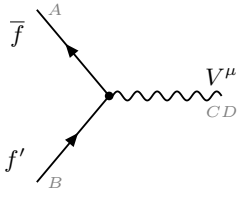
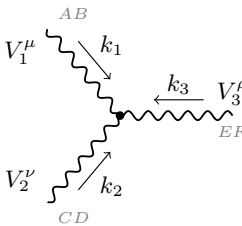
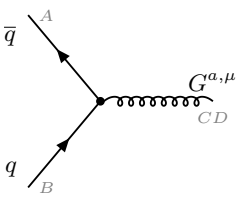
Vertices	Weyl–van-der-Waerden formalism	
	$ie\gamma^\mu C_{V\bar{f}f'}^\tau \omega_\tau$	$\longrightarrow ie \begin{pmatrix} 0 & C_{V\bar{f}f'}^-\delta_B^{\dot{C}}\delta_A^D \\ C_{V\bar{f}f'}^+\epsilon^{\dot{A}\dot{C}}\epsilon^{BD} & 0 \end{pmatrix}$
	$ieC_{V_1V_2V_3} [g^{\mu\nu}(k_1-k_2)^\rho + g^{\nu\rho}(k_2-k_3)^\mu + g^{\mu\rho}(k_3-k_1)^\nu]$	$\longrightarrow \frac{i}{4}eC_{V_1V_2V_3} \left[\epsilon^{\dot{A}\dot{C}}\epsilon^{BD}(K_1-K_2)^{\dot{E}F} \right. \\ \left. + \epsilon^{\dot{C}\dot{E}}\epsilon^{DF}(K_2-K_3)^{\dot{A}B} \right. \\ \left. + \epsilon^{\dot{A}\dot{E}}\epsilon^{BF}(K_3-K_1)^{\dot{C}D} \right]$
	$-ig_s t_{cc}^a \gamma^\mu$	$\longrightarrow -ig_s t_{cc}^a \begin{pmatrix} 0 & \delta_B^{\dot{C}}\delta_A^D \\ \epsilon^{\dot{A}\dot{C}}\epsilon^{BD} & 0 \end{pmatrix}$

Table A.4.: Feynman rules for the vertices.

$C_{V\bar{f}f'}^\pm$	$C_{\gamma\bar{f}f'}^\pm$	$C_{Z\bar{f}f'}^\pm$	$C_{W^+\bar{u}_i d_j}^\pm$	$C_{W^-\bar{d}_i u_j}^\pm$	$C_{W^+\bar{\nu}_i \ell_j}^\pm$	$C_{W^-\bar{\ell}_i \nu_j}^\pm$
$C_{V\bar{f}f'}^-$	$-Q_f \delta_{ff'}$	$-g_f^- \delta_{ff'}$	$\frac{1}{\sqrt{2}s_w} V_{ij}$	$\frac{1}{\sqrt{2}s_w} V_{ji}^*$	$\frac{1}{\sqrt{2}s_w} \delta_{ij}$	$\frac{1}{\sqrt{2}s_w} \delta_{ij}$
$C_{V\bar{f}f'}^+$	$-Q_f \delta_{ff'}$	$-g_f^+ \delta_{ff'}$	0	0	0	0

Table A.5.: Chiral coupling of the $V\bar{f}f$ -vertices.

A.4. Kinematics and phase-space integration

The differential cross section for a $2 \rightarrow n$ scattering process with the momentum assignment $p_a + p_b \rightarrow k_1 + \dots + k_n$, takes the following form,

$$d\sigma_{ab} = \frac{\langle |\mathcal{M}^{2 \rightarrow n}(p_a, p_b; k_1, \dots, k_n)|^2 \rangle}{F(p_a, p_b)} \frac{1}{S_{\{n\}}} d\phi(k_1, \dots, k_n; p_a + p_b), \quad (\text{A.49})$$

where the different contributions are given by:

- The squared matrix element $|\mathcal{M}|^2$ where the angle brackets $\langle \dots \rangle$ represents the possible average (sum) over initial (final) state degrees of freedom.
- The flux factor defined as

$$F(p_a, p_b) = 4\sqrt{(p_a \cdot p_b)^2 - m_a^2 m_b^2} \xrightarrow{m_{a,b}=0} 4(p_a \cdot p_b). \quad (\text{A.50})$$

- The symmetry factor given by

$$S_{\{n\}} = n_1! \dots, \quad (\text{A.51})$$

which is introduced to compensate the over-counting in the phase space for each set of n_i identical particles in the final state.

- The Lorentz invariant n -particle phase space defined as

$$\begin{aligned} d\phi(k_1, \dots, k_n; Q) &= \prod_{i=1}^n \left[\frac{d^4 k_i}{(2\pi)^4} (2\pi) \underbrace{\delta(k_i^2 - m_i^2) \theta(k_i^0)}_{\equiv \delta_+(k_i^2 - m_i^2)} \right] (2\pi)^4 \delta^{(4)} \left(\sum_{i=1}^n k_i - Q \right) \\ &= \prod_{i=1}^n \left[\frac{d^3 \mathbf{k}_i}{(2\pi)^3 2E_i} \right] (2\pi)^4 \delta^{(4)} \left(\sum_{i=1}^n k_i - Q \right), \quad E_i = \sqrt{\mathbf{k}_i^2 + m_i^2}. \end{aligned} \quad (\text{A.52})$$

The hadronic cross section is then obtained according to Eqs. (2.2) and (2.12) and involves the additional convolution with the respective PDFs. For the numerical integration of the phase space we employ the **Vegas** algorithm [147, 148] and a specific phase-space parametrization for each cross-section contribution. In order to achieve a fast converging and numerically stable evaluation of the integral, we introduce so-called *mappings* which smooth out the integrands and assist the **Vegas** algorithm in resolving narrow resonances and other regions of phase space where the integrand becomes large. Each cross section contribution is evaluated with an optimized phase-space parametrization which includes mappings that are specifically tailored for the respective integrands. For a detailed discussion on the generic construction of such phase-space parametrizations and an overview of the various mappings we refer to Appendix C in Ref. [166].

Virtual corrections

B.1. Scalar one-loop integrals

The general structure of one-loop integrals appearing in the virtual corrections at NLO is given by the N -point tensor integral defined by

$$T_{\mu_1 \dots \mu_P}^N(k_1, \dots, k_{N-1}, m_0, \dots, m_N) = \frac{(2\pi\mu)^{4-d}}{i\pi^2} \int d^d q \frac{q_{\mu_1} \dots q_{\mu_P}}{D_0 D_1 \dots D_{N-1}}, \quad (\text{B.1})$$

where N is the number of denominators and P corresponds to the number of loop momenta in the numerator. Here $d = (4 - 2\epsilon)$ is dimension of space-time and μ denotes the arbitrary scale of dimensional regularization as introduced in Sect. 1.1.2. The denominators are given by

$$D_0 = q^2 - m_0^2 + i0, \quad D_i = (q + k_i)^2 - m_i^2 + i0, \quad i = 1, \dots, N-1, \quad (\text{B.2})$$

where k_i is the internal momentum running through the propagator associated with D_i and $i0$ denotes the infinitesimal imaginary part of the propagator. Conventionally, the one-loop integral T^N is denoted by the N th letter of the alphabet, i.e. $T^1 \equiv A$, $T^2 \equiv B$, $T^3 \equiv C$, etc. The momentum and mass assignment that corresponds to the loop integral given in Eq. (B.1) is illustrated in Fig. B.1. The tensor integral of Eq. (B.1) can be further decomposed into Lorentz structures build from the momenta k_i and the metric tensor, where the Lorentz tensors are multiplied by the scalar tensor coefficient functions. Exploiting the fact that at one-loop order every scalar product between external momenta and the loop momentum can be expressed as a combination of propagators, the Passarino–Veltman reduction algorithm [167] allows to reduce all tensor-coefficient function into scalar integrals ($P = 0$) which are denoted with a subscript “0”.

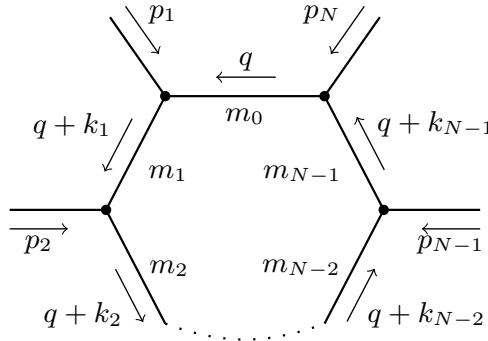


Figure B.1.: Momentum and mass assignment of the propagators in the one-loop integral of Eq. (B.1).

The evaluation of the scalar loop integrals starts by combining the the denominator factors D_i into a single denominator in order to perform the integration over the d -dimensional loop momentum in the next step. This can be accomplished by the identity

$$\begin{aligned} & \frac{1}{D_0^{\lambda_0} D_1^{\lambda_1} \cdots D_{N-1}^{\lambda_{N-1}}} \\ &= \frac{\Gamma\left(\sum_{i=0}^{N-1} \lambda_i\right)}{\prod_{i=0}^{N-1} \Gamma(\lambda_i)} \int_0^1 dx_0 \cdots \int_0^1 dx_{N-1} \prod_{i=0}^{N-1} x_i^{\lambda_i-1} \frac{\delta(1 - \sum_i x_i)}{\left[\sum_{i=0}^{N-1} x_i D_i\right]^{\sum_{i=0}^{N-1} \lambda_i}}, \end{aligned} \quad (\text{B.3})$$

where the integration variables x_i are called the *Feynman parameters* and $\Gamma(z)$ is the Euler Gamma function defined in Eq. (A.17). Once the denominators are combined, the integration over the loop momentum can be performed by first exploiting the translational invariance of the integral in order to eliminate all linear terms in the loop momentum and applying a *Wick rotation* into Euclidean space. Introducing polar coordinates in d dimensions and using the result

$$\int d^{d-1}\Omega = \frac{2\pi^{d/2}}{\Gamma(d/2)}, \quad (\text{B.4})$$

for the integration over solid angle in d dimensions, only the integration over the Feynman parameters remain,

$$\begin{aligned} T_0^N &= (-1)^N (4\pi\mu^2)^\epsilon \Gamma(N - d/2) \\ &\times \int_0^1 dx_0 \cdots \int_0^1 dx_{N-1} \delta\left(1 - \sum_{i=0}^{N-1} x_i\right) \left[- \left(\sum_{j=1}^{N-1} x_j k_j \right) - \sum_{j=0}^{N-1} x_j D_j \Big|_{q=0} \right]^{d/2-N}. \end{aligned} \quad (\text{B.5})$$

B.1.1. Mellin–Barnes method

In this section we briefly review the Mellin–Barnes method for computing scalar integrals and recite the main formulae. A more exhaustive discussion of this method in the application of Feynman integrals can be found, e.g., in Ref. [168]. The main identity underlying the Mellin–Barnes representation of a loop integral reads

$$\frac{1}{(A+B)^\lambda} = \frac{1}{\Gamma(\lambda)} \frac{1}{2\pi i} \int_{-i\infty}^{+i\infty} dz A^z B^{-z-\lambda} \Gamma(\lambda+z) \Gamma(-z), \quad (\text{B.6})$$

where the contour is chosen such that the poles of $\Gamma(\dots + z)$ are to the left (“left poles”) and the poles of $\Gamma(\dots - z)$ to the right (“right poles”) of the contour. Identity (B.6) can be further generalized to an arbitrary number of terms in the denominator,

$$\begin{aligned} (A_1 + \dots + A_n)^{-\lambda} &= \frac{1}{\Gamma(\lambda)} \frac{1}{(2\pi i)^{n-1}} \int_{-i\infty}^{+i\infty} dz_1 \cdots \int_{-i\infty}^{+i\infty} dz_{n-1} \\ &\times \Gamma(-z_1) \cdots \Gamma(-z_{n-1}) \Gamma(z_1 + \dots + z_{n-1} + \lambda) A_1^{z_1} \cdots A_{n-1}^{z_{n-1}} A_n^{-z_1 - \dots - z_{n-1} - \lambda}, \end{aligned} \quad (\text{B.7})$$

which can be shown by a successive application of identity (B.6). These representations can be used to convert the sums appearing inside the square brackets of Eq. (B.5) into products, so that all Feynman parameter integrals can be evaluated in terms of Gamma functions. The contour integrals over the complex variables z_i can be evaluated by closing the contour at infinity and summing up all residues. To this end, the Barnes' lemmas prove to be useful in evaluating integrals involving only Gamma functions. Barnes' first lemma states that

$$\begin{aligned} \frac{1}{2\pi i} \int_{-i\infty}^{+i\infty} dz \Gamma(a+z) \Gamma(b+z) \Gamma(c-z) \Gamma(d-z) \\ = \frac{\Gamma(a+c) \Gamma(a+d) \Gamma(b+c) \Gamma(b+d)}{\Gamma(a+b+c+d)}, \end{aligned} \quad (\text{B.8})$$

where it is required that none of the left poles coincides with a right pole. Barnes' second lemma reads

$$\begin{aligned} \frac{1}{2\pi i} \int_{-i\infty}^{+i\infty} dz \frac{\Gamma(a+z) \Gamma(b+z) \Gamma(c+z) \Gamma(d-z) \Gamma(e-z)}{\Gamma(a+b+c+d+e+z)} \\ = \frac{\Gamma(a+d) \Gamma(b+d) \Gamma(c+d) \Gamma(a+e) \Gamma(b+e) \Gamma(c+e)}{\Gamma(a+b+d+e) \Gamma(a+c+d+e) \Gamma(b+c+d+e)}. \end{aligned} \quad (\text{B.9})$$

From the formula given in Eq. (B.6) it becomes apparent that the Mellin–Barnes representation can be used to perform a systematic expansion of the loop integral. For instance, closing the contour to the left in Eq. (B.6) encloses the poles at $z = 0, -1, -2, \dots$ and the corresponding residues will result in an expansion in $1/A$.

B.1.2. Expansion of one-loop integrals

In the calculation of the EW $\mathcal{O}(\alpha)$ and $\mathcal{O}(\alpha_s \alpha)$ corrections to the charged-current process in the PA, contributions arise that can be attributed to both factorizable and non-factorizable corrections. They occur whenever the virtual photon attaches to the intermediate charged gauge-boson line. The non-factorizable part of these diagrams can be extracted in a gauge-invariant manner by first subtracting the factorizable contribution and then expanding the difference in the virtuality of the gauge boson as defined in Eqs. (4.9) and (6.20). To this end, performing an expansion in $\frac{p_V^2 - M_V^2}{M_V^2}$ of the scalar loop integrals using the Mellin–Barnes representation (B.7) allows to easily identify the factorizable and non-factorizable contributions. Here we summarize the results of the expansion of one-loop scalar integrals that are relevant for this work. A detailed application of the Mellin–Barnes method for the example of a two-loop integral is given in Sect. 6.1.2.

The scalar integrals considered in the following are shown in Fig. B.2 and are defined as

$$B_0(k_1^2, m_0, m_1) = \frac{(2\pi\mu)^{4-d}}{i\pi^2} \int \frac{d^d q}{[q^2 - m_0^2][(q+k_1)^2 - m_1^2]}, \quad (\text{B.10})$$

$$\begin{aligned} C_0(k_1^2, (k_2 - k_1)^2, k_2^2, m_0, m_1, m_2) \\ = \frac{(2\pi\mu)^{4-d}}{i\pi^2} \int \frac{d^d q}{[q^2 - m_0^2][(q+k_1)^2 - m_1^2][(q+k_2)^2 - m_2^2]}, \end{aligned} \quad (\text{B.11})$$

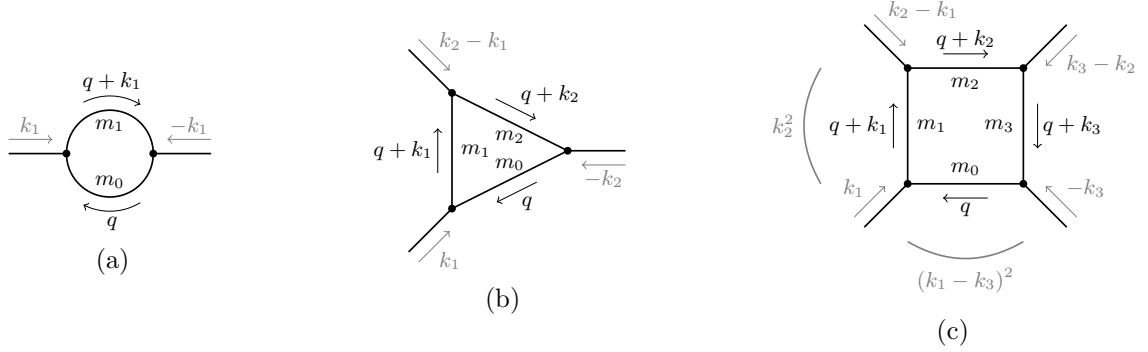


Figure B.2.: The kinematic variables of the scalar two-point (a), three-point (b), and four-point (c) integrals.

$$D_0(k_1^2, (k_2 - k_1)^2, (k_3 - k_2)^2, k_3^2, k_2^2, (k_3 - k_1)^2, m_0, m_1, m_2, m_3) \\ = \frac{(2\pi\mu)^{4-d}}{i\pi^2} \int \frac{d^d q}{[q^2 - m_0^2][(q + k_1)^2 - m_1^2][(q + k_2)^2 - m_2^2][(q + k_3)^2 - m_3^2]}, \quad (\text{B.12})$$

for the two-point, three-point, and four-point integrals, respectively. As explained in Sect. 4.2.1, the non-factorizable part of the not manifestly non-factorizable corrections arises from the non-commutativity of the on-shell limit and the IR regularization of the loop momentum. As a consequence, only IR-singular loop integrals contribute, and the non-factorizable parts always contain IR poles in ϵ accompanied by a threshold singularity of the form $\ln(p_V^2 - M^2)$.

We adopt the notation of Ref. [146] where over-lined variables are understood to receive a positive infinitesimal imaginary part, i.e. $\bar{s} \equiv s + i0$ etc. Furthermore, we introduce the abbreviation

$$c_\epsilon = (4\pi)^\epsilon \Gamma(1 + \epsilon), \quad (\text{B.13})$$

which commonly occurs in association with the poles in ϵ and is also related to the constants absorbed into the renormalization constants in the $\overline{\text{MS}}$ scheme, see Eq. (1.61).

Two-point integrals

As mentioned in Sect 1.3.1, at least three propagators are necessary in order to satisfy the conditions that lead to IR singularities and therefore, the scalar two-point integral B_0 is IR finite. However, derivatives of the two-point functions $B'_0 = \partial B_0(p^2)/\partial p^2$ arise in the expansion around the resonance, which effectively increases the number of denominators. As a consequence, the self-energy corrections to the W propagator contain non-factorizable contributions, and we isolate the non-factorizable parts (denoted with the label “nf”) using the Mellin–Barnes method described in Sect. B.1.1 and obtain

$$B'_0(p^2, 0, M) \equiv \frac{\partial}{\partial p^2} B_0(p^2, 0, M) \\ = B'_0(M^2, 0, M) + B_0^{\text{nf}}(p^2, 0, M) + \mathcal{O}(p^2 - M^2), \quad (\text{B.14})$$

$$B'_0(M^2, 0, M) = \frac{\partial}{\partial p^2} B_0(p^2, 0, M) \Big|_{p^2=M^2}$$

$$\begin{aligned}
&= -\frac{1}{2M^2} \frac{c_\epsilon}{\epsilon} \frac{1}{1-2\epsilon} \left(\frac{\mu^2}{M^2} \right)^\epsilon \\
&= -\frac{1}{2M^2} \left\{ \frac{c_\epsilon}{\epsilon} + 2 + \ln \left(\frac{\mu^2}{M^2} \right) + \mathcal{O}(\epsilon) \right\}, \tag{B.15}
\end{aligned}$$

$$\begin{aligned}
B_0^{\text{nf}}(s, 0, M) &= \frac{s - M^2}{2M^2} \frac{c_\epsilon}{\epsilon} \frac{1}{1-2\epsilon} \frac{\Gamma(1-\epsilon)\Gamma(1+2\epsilon)}{\Gamma(1+\epsilon)} \left(\frac{\mu^2}{M^2} \right)^\epsilon \left(\frac{M^2 - \bar{s}}{M^2} \right)^{-2\epsilon} \\
&= \frac{s - M^2}{2M^2} \left\{ \frac{c_\epsilon}{\epsilon} + 2 + \ln \left(\frac{\mu^2}{M^2} \right) - 2 \ln \left(\frac{M^2 - \bar{s}}{M^2} \right) + \mathcal{O}(\epsilon) \right\}. \tag{B.16}
\end{aligned}$$

Three-point integrals

The expansion of the $C_0(0, 0, s, 0, 0, M)$ function around $(s - M^2)$ is given by

$$C_0(0, 0, s, 0, 0, M) = C_0(0, 0, M^2, 0, 0, M) + C_0^{\text{nf}}(0, 0, s, 0, 0, M) + \mathcal{O}(s - M^2), \tag{B.17}$$

$$\begin{aligned}
C_0(0, 0, M^2, 0, 0, M) &= -\frac{1}{2M^2} \frac{c_\epsilon}{\epsilon^2} \left(\frac{\mu^2}{M^2} \right)^\epsilon \\
&= -\frac{1}{2M^2} \left\{ \frac{c_\epsilon}{\epsilon^2} + \frac{c_\epsilon}{\epsilon} \ln \left(\frac{\mu^2}{M^2} \right) + \frac{1}{2} \ln^2 \left(\frac{\mu^2}{M^2} \right) + \mathcal{O}(\epsilon) \right\}, \tag{B.18}
\end{aligned}$$

$$\begin{aligned}
C_0^{\text{nf}}(0, 0, s, 0, 0, M) &= \frac{1}{2M^2} \frac{c_\epsilon}{\epsilon^2} \frac{\Gamma(1-\epsilon)\Gamma(1+2\epsilon)}{\Gamma(1+\epsilon)} \left(\frac{\mu^2}{M^2} \right)^\epsilon \left(\frac{M^2 - \bar{s}}{M^2} \right)^{-2\epsilon} \\
&= \frac{1}{2M^2} \left\{ \frac{c_\epsilon}{\epsilon^2} + \frac{c_\epsilon}{\epsilon} \left[\ln \left(\frac{\mu^2}{M^2} \right) - 2 \ln \left(\frac{M^2 - \bar{s}}{M^2} \right) \right] \right. \\
&\quad \left. + \frac{1}{2} \left[\ln \left(\frac{\mu^2}{M^2} \right) - 2 \ln \left(\frac{M^2 - \bar{s}}{M^2} \right) \right]^2 + \frac{\pi^2}{3} + \mathcal{O}(\epsilon) \right\}. \tag{B.19}
\end{aligned}$$

Notice how the separation of the factorizable and non-factorizable corrections introduces spurious IR singularities in the respective terms which cancel exactly in the sum of Eq. (B.17).

In the $\mathcal{O}(\alpha_s \alpha)$ corrections the external quark legs can become off shell with the virtuality q^2 from the recoil of additional gluon emission. The expansion of the corresponding three-point integral reads

$$C_0(0, q^2, s, 0, 0, M) = C_0(0, q^2, M^2, 0, 0, M) + C_0^{\text{nf}}(0, q^2, s, 0, 0, M) + \mathcal{O}(s - M^2), \tag{B.20}$$

$$\begin{aligned}
C_0(0, q^2, M^2, 0, 0, M) &= \frac{1}{M^2 - q^2} \left\{ \frac{c_\epsilon}{2\epsilon^2} \left(\frac{\mu^2}{M^2} \right)^\epsilon - \frac{c_\epsilon}{\epsilon^2} \left(\frac{\mu^2}{M^2 - \bar{q}^2} \right)^\epsilon \right. \\
&\quad \left. + \text{Li}_2 \left(\frac{\bar{q}^2}{\bar{q}^2 - M^2} \right) + \mathcal{O}(\epsilon) \right\}
\end{aligned}$$

$$\begin{aligned}
&= -\frac{1}{2} \frac{1}{M^2 - q^2} \left\{ \frac{c_\epsilon}{\epsilon^2} + \frac{c_\epsilon}{\epsilon} \left[\ln \left(\frac{\mu^2}{M^2} \right) - 2 \ln \left(\frac{M^2}{M^2 - \bar{q}^2} \right) \right] \right. \\
&\quad \left. - \frac{1}{2} \ln^2 \left(\frac{\mu^2}{M^2} \right) + \ln^2 \left(\frac{M^2}{M^2 - \bar{q}^2} \right) + \mathcal{O}(\epsilon) \right\}, \tag{B.21}
\end{aligned}$$

$$\begin{aligned}
C_0^{\text{nf}}(0, q^2, s, 0, 0, M) &= \frac{1}{2} \frac{1}{M^2 - q^2} \frac{c_\epsilon}{\epsilon^2} \frac{\Gamma(1 - \epsilon) \Gamma(1 + 2\epsilon)}{\Gamma(1 + \epsilon)} \left(\frac{\mu^2}{M^2} \right)^\epsilon \left(\frac{M^2 - \bar{s}}{M^2} \right)^{-2\epsilon} \\
&= \frac{M^2}{M^2 - q^2} C_0^{\text{nf}}(0, 0, s, 0, 0, M). \tag{B.22}
\end{aligned}$$

For $q^2 \rightarrow 0$, Eq. (B.20) reduces to Eq. (B.17).

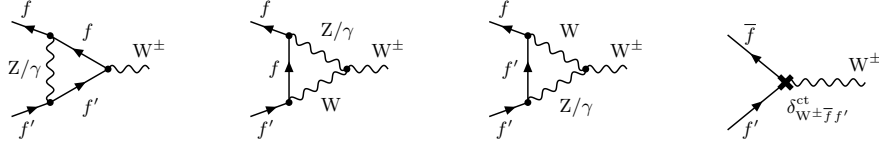
Four-point integrals

The four-point integrals only appear in the genuinely non-factorizable corrections, and therefore, do not require the expansion around the resonance for the extraction of the non-factorizable corrections. However, we give their results here which have been independently derived using the Mellin–Barnes method. The two four-point integrals relevant in the calculation of the non-factorizable corrections are given by

$$\begin{aligned}
&D_0(0, 0, 0, 0, s, t, 0, 0, M, 0) \\
&= \frac{1}{t(s - M^2)} \left\{ \frac{c_\epsilon}{\epsilon^2} \Gamma(1 - \epsilon)^2 \Gamma(1 + 2\epsilon) \left(\frac{\mu^2}{-t} \right)^\epsilon \left(\frac{M^2 - \bar{s}}{M^2} \right)^{-2\epsilon} \right. \\
&\quad \left. + \text{Li}_2 \left(1 + \frac{\bar{t}}{M^2} \right) - \frac{\pi^2}{6} + \mathcal{O}(\epsilon) \right\} \\
&= \frac{1}{t(s - M^2)} \left\{ \frac{c_\epsilon}{\epsilon^2} + \frac{c_\epsilon}{\epsilon} \left[\ln \left(\frac{\mu^2}{-t} \right) - 2 \ln \left(\frac{M^2 - \bar{s}}{M^2} \right) \right] + \text{Li}_2 \left(1 + \frac{\bar{t}}{M^2} \right) \right. \\
&\quad \left. + \frac{1}{2} \left[\ln \left(\frac{\mu^2}{-t} \right) - 2 \ln \left(\frac{M^2 - \bar{s}}{M^2} \right) \right]^2 + \frac{\pi^2}{3} + \mathcal{O}(\epsilon) \right\}, \tag{B.23}
\end{aligned}$$

and the case with the additional virtuality q^2 of one external leg,

$$\begin{aligned}
&D_0(0, q^2, 0, 0, s, t, 0, 0, M, 0) \\
&= \frac{1}{t(s - M^2)} \left\{ \frac{c_\epsilon}{\epsilon^2} \Gamma(1 - \epsilon)^2 \Gamma(1 + 2\epsilon) \left(\frac{\mu^2}{-t} \right)^\epsilon \left(\frac{M^2 - \bar{q}^2}{M^2} \right)^\epsilon \left(\frac{M^2 - \bar{s}}{M^2} \right)^{-2\epsilon} \right. \\
&\quad \left. + \text{Li}_2 \left(1 + \frac{t}{M^2 - \bar{q}^2} \right) - \frac{\pi^2}{6} + \mathcal{O}(\epsilon) \right\} \\
&= \frac{1}{t(s - M^2)} \left\{ \frac{c_\epsilon}{\epsilon^2} + \frac{c_\epsilon}{\epsilon} \left[\ln \left(\frac{\mu^2}{-t} \right) + \ln \left(\frac{M^2 - \bar{q}^2}{M^2} \right) - 2 \ln \left(\frac{M^2 - \bar{s}}{M^2} \right) \right] \right.
\end{aligned}$$

Figure B.3.: Virtual corrections to the $W^\pm \bar{f} f'$ vertex.

$$\begin{aligned}
& + \frac{1}{2} \left[\ln \left(\frac{\mu^2}{-t} \right) + \ln \left(\frac{M^2 - \bar{q}^2}{M^2} \right) - 2 \ln \left(\frac{M^2 - \bar{s}}{M^2} \right) \right]^2 \\
& + \text{Li}_2 \left(1 + \frac{t}{M^2 - \bar{q}^2} \right) + \frac{\pi^2}{3} + \mathcal{O}(\epsilon) \Big\}. \tag{B.24}
\end{aligned}$$

Equation (B.24) reduces to Eq. (B.12) in the limit $q^2 \rightarrow 0$.

B.2. Electroweak vertex corrections

In this section we recite the known analytic results of the EW vertex corrections which can be found, e.g., in Refs. [37, 45]. The EW corrections to the $V \bar{f} f'$ vertex are given in terms of renormalized form factors denoted by $\hat{F}_{V \bar{f} f'}^\tau$, with the label τ denoting the sign appearing in the chiral coupling C_{\dots}^\pm of the tree-level vertex expression, see Table A.4.

B.2.1. Charged-current interactions

The corrections to the $W^\pm \bar{f} f'$ vertex enter the calculation of the charged-current process and can be found, e.g., in Ref. [37]. They are given by the virtual loop corrections and the counterterm contributions shown in Fig. B.3,

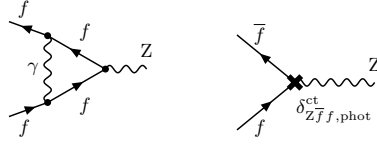
$$\hat{F}_{W^\pm \bar{f} f'}^\tau(\hat{s}) = F_{W^\pm \bar{f} f'}^\tau(\hat{s}) + \delta_{W^\pm \bar{f} f'}^{\text{ct}, \tau}. \tag{B.25}$$

In the case of the chiral charged-current interactions, the form factor for the case $\tau = +$ vanishes, $\hat{F}_{W^\pm \bar{f} f'}^+ = 0$. For the left-chiral ($\tau = -$) case the counterterm is given by

$$\delta_{W^\pm \bar{f} f'}^{\text{ct}, -} = \delta Z_e - \frac{\delta s_w}{s_w} + \frac{1}{2} (\delta Z_W + \delta Z_f^- + \delta Z_{f'}^-), \tag{B.26}$$

and the unrenormalized vertex form factor reads

$$\begin{aligned}
F_{W^\pm \bar{f} f'}^-(\hat{s}) = & \frac{\alpha}{16\pi} \left\{ \frac{2(1 - 2s_w^2 - 4Q_f Q_{f'} s_w^2)}{c_w^2 s_w^2} + \frac{4}{s_w^2} \left(2 + \frac{M_W^2}{\hat{s}} \right) B_0(0, 0, M_W) \right. \\
& + \frac{2}{c_w^2 s_w^2} (1 - 2s_w^2 + 2Q_f^2 s_w^4 + 2Q_{f'}^2 s_w^4) \left(2 + \frac{M_Z^2}{\hat{s}} \right) B_0(0, 0, M_Z) \\
& \left. - 4 \left(1 + \frac{M_W^2}{\hat{s}} \right) B_0(\hat{s}, 0, M_W) - \frac{4c_w^2}{s_w^2} \left(1 + \frac{M_W^2 + M_Z^2}{\hat{s}} \right) B_0(\hat{s}, M_W, M_Z) \right\}
\end{aligned}$$

Figure B.4.: Virtual photonic corrections to the $Z\bar{f}f$ vertex.

$$\begin{aligned}
& + \frac{1}{c_w^2 s_w^2} \left[2 \frac{M_Z^2}{\hat{s}} (Q_f - Q_{f'} - 2Q_f s_w^2)(Q_f - Q_{f'} + 2Q_{f'} s_w^2) \right. \\
& \quad \left. + 3(1 - 2s_w^2 - 4Q_f Q_{f'} s_w^2) \right] B_0(\hat{s}, 0, 0) \\
& + 8(Q_f^2 + Q_{f'}^2) B_0(0, 0, 0) - 8Q_f Q_{f'} \hat{s} C_0(0, 0, \hat{s}, 0, 0, 0) \\
& + 8M_W^2 C_0(0, 0, \hat{s}, 0, 0, M_W) \\
& + \frac{8c_w^2}{s_w^2} \left(M_W^2 + M_Z^2 + \frac{M_W^2 M_Z^2}{\hat{s}} \right) C_0(0, 0, \hat{s}, M_W, 0, M_Z) \\
& + \frac{2}{c_w^2 s_w^2} (Q_f - Q_{f'} - 2Q_f s_w^2)(Q_f - Q_{f'} + 2Q_{f'} s_w^2) \\
& \quad \times \left(1 + \frac{M_Z^2}{\hat{s}} \right)^2 \hat{s} C_0(0, 0, \hat{s}, 0, M_Z, 0) \Big\}. \tag{B.27}
\end{aligned}$$

The definition of the renormalization constants is given in Sect. 1.1.2.

B.2.2. Neutral-current interactions

For the neutral-current interactions, the photonic corrections constitute a gauge-invariant subset and can be discussed separately,

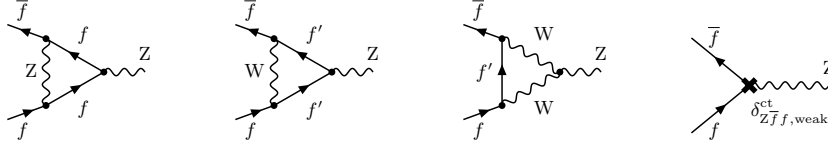
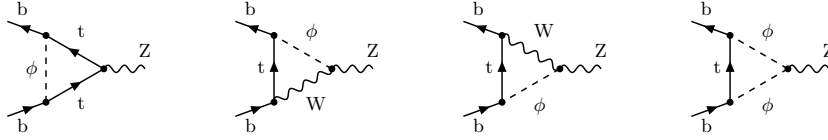
$$\hat{F}_{Z\bar{f}f}^\tau(\hat{s}) = \hat{F}_{Z\bar{f}f,\text{phot}}^\tau(\hat{s}) + \hat{F}_{Z\bar{f}f,\text{weak}}^\tau(\hat{s}). \tag{B.28}$$

The results given here can be found, e.g., in Ref. [45].

Photonic corrections

The Feynman diagrams for the photonic corrections to the $Z\bar{f}f$ vertex are shown in Fig. B.4 and the corresponding renormalized form factor is explicitly given by

$$\begin{aligned}
\hat{F}_{Z\bar{f}f,\text{phot}}^\tau(\hat{s}) & = F_{Z\bar{f}f,\text{phot}}^\tau(\hat{s}) + \delta Z_{f,\text{phot}}, \\
& = -\frac{\alpha}{2\pi} Q_f^2 \left\{ \frac{c_\epsilon}{\epsilon^2} + \frac{c_\epsilon}{\epsilon} \left[\ln \left(\frac{\mu^2}{-\hat{s} + i0} \right) + \frac{3}{2} \right] \right. \\
& \quad \left. + \frac{1}{2} \ln^2 \left(\frac{\mu^2}{-\hat{s} + i0} \right) + \frac{3}{2} \ln \left(\frac{\mu^2}{-\hat{s} + i0} \right) - \frac{\pi^2}{6} + 4 \right\}. \tag{B.29}
\end{aligned}$$

(a) Virtual weak corrections to the $Z \bar{f} f$ vertex for light fermions.

(b) Additional virtual weak corrections in case of external bottom quarks.

Figure B.5.: Virtual weak corrections to the $Z \bar{f} f$ vertex. The fermion f' appearing inside the loop diagrams in (a) denotes the weak isospin partner of f . In case of external bottom quarks, the isospin partner t is massive and additional diagrams contribute (b).

Weak corrections

The purely weak corrections to the $Z \bar{f} f$ vertex are shown in Fig. B.5(a) and comprise the unrenormalized on-loop corrections and the counterterms,

$$\hat{F}_{Z \bar{f} f, \text{weak}}^\tau(\hat{s}) = F_{Z \bar{f} f, \text{weak}}^\tau(\hat{s}) + \delta_{Z \bar{f} f, \text{weak}}^{\text{ct}, \tau}. \quad (\text{B.30})$$

The counterterm contribution is given by

$$\delta_{Z \bar{f} f, \text{weak}}^{\text{ct}, \tau} = \frac{\delta g_f^\tau}{g_f^\tau} + \frac{1}{2} \delta Z_{ZZ} + \delta Z_{f, \text{weak}}^\tau - \frac{1}{2} \frac{Q_f}{g_f^\tau} \delta Z_{AZ}, \quad (\text{B.31})$$

with

$$\delta g_f^+ = -\frac{s_w}{c_w} Q_f \left(\delta Z_e + \frac{1}{c_w^2} \frac{\delta s_w}{s_w} \right), \quad \delta g_f^- = \frac{I_{w, f}^3}{s_w c_w} \left(\delta Z_e + \frac{s_w^2 - c_w^2}{c_w^2} \frac{\delta s_w}{s_w} \right) + \delta g_{Z \bar{f} f}^+. \quad (\text{B.32})$$

The unrenormalized vertex form factors read

$$\begin{aligned} F_{Z \bar{f} f, \text{weak}}^-(\hat{s}) = & \frac{\alpha}{8\pi} \left\{ \frac{1}{\hat{s} s_w^2 (I_{w, f}^3 - Q_f s_w^2)} \left[2(I_{w, f}^3 - Q_f s_w^2)(2\hat{s} + M_W^2) B_0(0, 0, M_W) \right. \right. \\ & + (I_{w, f}^3 c_w^2 - I_{w, f}^3 s_w^2 + Q_f s_w^2) (2\hat{s} + (3\hat{s} + 2M_W^2) B_0(\hat{s}, 0, 0) \\ & + 2(\hat{s} + M_W^2)^2 C_0(0, 0, \hat{s}, 0, M_W, 0)) \\ & - 2c_w^2 I_{w, f}^3 ((\hat{s} + 2M_W^2) B_0(\hat{s}, M_W, M_W) \\ & \left. \left. - 2M_W^2 (2\hat{s} + M_W^2) C_0(0, 0, \hat{s}, M_W, 0, M_W)) \right] \right\} \\ & + \frac{(I_{w, f}^3 - Q_f s_w^2)^2}{\hat{s} c_w^2 s_w^2} \left[-4\hat{s} + 4(2\hat{s} + M_Z^2) B_0(0, 0, M_Z) \right] \end{aligned}$$

$$- 2(3\hat{s} + 2M_Z^2)B_0(\hat{s}, 0, 0) - 4(\hat{s} + M_Z^2)^2 C_0(0, 0, \hat{s}, 0, M_Z, 0) \Big] \Big\}. \quad (\text{B.33})$$

$$F_{Z\bar{f}f, \text{weak}}^+(\hat{s}) = -\frac{\alpha}{4\pi} \frac{Q_f^2 s_w^2}{c_w^2} \left\{ 2 - \frac{2(M_Z^2 + 2\hat{s})}{\hat{s}} B_0(0, 0, M_Z) + \frac{3\hat{s} + 2M_Z^2}{\hat{s}} B_0(\hat{s}, 0, 0) \right. \\ \left. + \frac{2(M_Z^2 + \hat{s})^2}{\hat{s}} C_0(0, 0, \hat{s}, 0, M_Z, 0) \right\}. \quad (\text{B.34})$$

In case of external bottom quarks, the non-vanishing mass of the isospin partner (t) requires a modification of the form factor above and, furthermore, additional diagrams need to be considered which are shown in Fig. B.5(b). In summary, the following term needs to be added to the vertex form factor (4.1) in case of external bottom quarks,

$$\delta F_{Z\bar{b}b, \text{weak}}^-(\hat{s}) = \frac{\alpha}{8\pi} \left\{ -\frac{1}{(2s_w^2 - 3)\hat{s}s_w^2} \left[2(2\hat{s} + M_W^2)(2s_w^2 - 3) \right. \right. \\ \times \left(B_0(0, 0, M_W) - B_0(0, m_t, M_W) \right) \\ + (3\hat{s} + 2M_W^2)(4s_w^2 - 3) \left(B_0(\hat{s}, 0, 0) - B_0(\hat{s}, m_t, m_t) \right) \\ - 12c_w^2 M_W^2 (2\hat{s} + M_W^2) \\ \times \left(C_0(0, 0, \hat{s}, M_W, 0, M_W) - C_0(0, 0, \hat{s}, M_W, m_t, M_W) \right) \\ + 2(4s_w^2 - 3)(\hat{s} + M_W^2)^2 \\ \times \left. \left(C_0(0, 0, \hat{s}, 0, M_W, 0) - C_0(0, 0, \hat{s}, m_t, M_W, m_t) \right) \right] \\ - \frac{m_t^2}{(2s_w^2 - 3)\hat{s}s_w^2 M_W^2} \left[(m_t^2 + M_W^2) \left(4B_0(\hat{s}, m_t, m_t) s_w^2 \right. \right. \\ - 3B_0(\hat{s}, M_W, M_W)(s_w^2 - c_w^2) + B_0(0, m_t, M_W)(2s_w^2 - 3) \\ + (2\hat{s}s_w^2 - 6M_W^2)B_0(\hat{s}, m_t, m_t) + \hat{s} \left(\frac{3}{2} - 5s_w^2 \right) \\ + \left(6M_W^2 - \frac{3}{2}\hat{s}(s_w^2 - c_w^2) \right) B_0(\hat{s}, M_W, M_W) \\ - 12\hat{s}M_W^2 C_0(0, 0, \hat{s}, m_t, M_W, m_t) \\ - 3(4M_W^4 - 2m_t^2 M_W^2 - m_t^2 \hat{s}) \\ \times \left(C_0(0, 0, \hat{s}, m_t, M_W, m_t) + C_0(0, 0, \hat{s}, M_W, m_t, M_W) \right) \\ - 3(3M_W^4 - m_t^4) C_0(0, 0, \hat{s}, M_W, m_t, M_W) \\ + 2s_w^2 (M_W^2(2\hat{s} + 3M_W^2) - m_t^2(m_t^2 + \hat{s})) \\ \times \left. \left. \left(2C_0(0, 0, \hat{s}, m_t, M_W, m_t) + 3C_0(0, 0, \hat{s}, M_W, m_t, M_W) \right) \right] \right\}, \quad (\text{B.35})$$

$$\delta F_{Z\bar{b}b, \text{weak}}^+(\hat{s}) = 0. \quad (\text{B.36})$$

B.3. Non-factorizable corrections

After neglecting all non-resonant contributions as described in Sect. 4.2.1, the one-loop integrals appearing in the the virtual non-factorizable corrections reduces to scalar integrals only. For the not manifestly non-factorizable corrections that contribute to both factorizable and non-factorizable corrections, e.g. given by the diagram in Fig. 4.3(b), the non-factorizable part is defined as the difference given in Eq. (4.9). Using the results for the expansion of the corresponding scalar integrals given in Sect. B.1.2, the factorizable corrections can be identified immediately and the non-factorizable corrections arise from the terms labelled by “nf” in the expansion. Furthermore, the corrections factorize from the lower-order cross section owing to the soft nature of these corrections.

The relative correction factor for the non-factorizable corrections to the process $\bar{q}_a q_b \rightarrow \ell_1 \bar{\ell}_2$ is then given by

$$\delta_{\text{nf}}^{\bar{q}_a q_b \rightarrow \ell_1 \bar{\ell}_2} = \frac{\alpha}{2\pi} \left\{ \begin{aligned} & -Q_{q_a} Q_{\ell_1} (-t_{a1}) (s_{12} - M_V^2) \\ & \quad \times D_0(0, 0, 0, 0, s_{12}, t_{a1}, 0, 0, M_V, 0) \quad \left\{ \begin{array}{c} \text{Diagram 1: } \bar{q}_a \text{ and } q_b \text{ exchange a photon } \gamma \text{ and a vector } V \text{ to produce } \ell_1 \text{ and } \bar{\ell}_2. \end{array} \right. \\ & + Q_{q_a} Q_{\ell_2} (-t_{a2}) (s_{12} - M_V^2) \\ & \quad \times D_0(0, 0, 0, 0, s_{12}, t_{a2}, 0, 0, M_V, 0) \quad \left\{ \begin{array}{c} \text{Diagram 2: } \bar{q}_a \text{ and } q_b \text{ exchange a photon } \gamma \text{ and a vector } V \text{ to produce } \ell_1 \text{ and } \bar{\ell}_2. \end{array} \right. \\ & - Q_{q_b} Q_{\ell_2} (-t_{b2}) (s_{12} - M_V^2) \\ & \quad \times D_0(0, 0, 0, 0, s_{12}, t_{b2}, 0, 0, M_V, 0) \quad \left\{ \begin{array}{c} \text{Diagram 3: } \bar{q}_a \text{ and } q_b \text{ exchange a vector } V \text{ and a photon } \gamma \text{ to produce } \ell_1 \text{ and } \bar{\ell}_2. \end{array} \right. \\ & + Q_{q_b} Q_{\ell_1} (-t_{b1}) (s_{12} - M_V^2) \\ & \quad \times D_0(0, 0, 0, 0, s_{12}, t_{b1}, 0, 0, M_V, 0) \quad \left\{ \begin{array}{c} \text{Diagram 4: } \bar{q}_a \text{ and } q_b \text{ exchange a vector } V \text{ and a photon } \gamma \text{ to produce } \ell_1 \text{ and } \bar{\ell}_2. \end{array} \right. \\ & + 2(Q_{q_b} - Q_{q_a})(Q_{\ell_1} - Q_{\ell_2})M_V^2 \\ & \quad \times C_0^{\text{nf}}(0, 0, s_{12}, 0, 0, M_V) \quad \left\{ \begin{array}{c} \text{Diagram 5: Two diagrams showing } \bar{q}_a \text{ and } q_b \text{ interacting via } V \text{ and } \gamma \text{ to produce } \ell_1 \text{ and } \bar{\ell}_2. \end{array} \right. \\ & + 2(Q_{q_b} - Q_{q_a})(Q_{\ell_1} - Q_{\ell_2})M_V^2 \\ & \quad \times B_0^{\text{nf}}(s_{12}, 0, M_V) \quad \left\{ \begin{array}{c} \text{Diagram 6: Two diagrams showing } \bar{q}_a \text{ and } q_b \text{ interacting via } V \text{ and } \gamma \text{ to produce } \ell_1 \text{ and } \bar{\ell}_2. \end{array} \right. \end{aligned} \right\}, \quad (\text{B.37})$$

where the one-loop diagrams contributing to each term are shown to the right. Note that no

counterterm contributions remain after taking the difference in Eq. (4.9).

The non-factorizable corrections to the process $\bar{q}_a q_b \rightarrow \ell_1 \bar{\ell}_2 g$ can be calculated in an analogous manner and explicitly read

$$\begin{aligned}
 \delta_{\text{nf}}^{\bar{q}_a q_b \rightarrow \ell_1 \bar{\ell}_2 g} = \frac{\alpha}{2\pi} \Big\{ & \\
 & - Q_{q_a} Q_{\ell_1} (-t_{a1}) (s_{12} - M_V^2) \\
 & \quad \times D_0(0, t_{bg}, 0, 0, s_{12}, t_{a1}, 0, 0, M_V, 0) \quad \left\{ \begin{array}{c} \text{Diagram 1} \end{array} \right. \\
 & + Q_{q_a} Q_{\ell_2} (-t_{a2}) (s_{12} - M_V^2) \\
 & \quad \times D_0(0, t_{bg}, 0, 0, s_{12}, t_{a2}, 0, 0, M_V, 0) \quad \left\{ \begin{array}{c} \text{Diagram 2} \end{array} \right. \\
 & - Q_{q_b} Q_{\ell_2} (-t_{b2}) (s_{12} - M_V^2) \\
 & \quad \times D_0(0, t_{ag}, 0, 0, s_{12}, t_{b2}, 0, 0, M_V, 0) \quad \left\{ \begin{array}{c} \text{Diagram 3} \end{array} \right. \\
 & + Q_{q_b} Q_{\ell_1} (-t_{b1}) (s_{12} - M_V^2) \\
 & \quad \times D_0(0, t_{ag}, 0, 0, s_{12}, t_{b1}, 0, 0, M_V, 0) \quad \left\{ \begin{array}{c} \text{Diagram 4} \end{array} \right. \\
 & - Q_{q_a} (Q_{\ell_1} - Q_{\ell_2}) (M_V^2 - t_{bg}) \\
 & \quad \times C_0^{\text{nf}}(0, t_{bg}, s_{12}, 0, 0, M_V) \quad \left\{ \begin{array}{c} \text{Diagram 5} \end{array} \right. \\
 & + Q_{q_b} (Q_{\ell_1} - Q_{\ell_2}) (M_V^2 - t_{ag}) \\
 & \quad \times C_0^{\text{nf}}(0, t_{ag}, s_{12}, 0, 0, M_V) \quad \left\{ \begin{array}{c} \text{Diagram 6} \end{array} \right. \\
 & + (Q_{q_b} - Q_{q_a}) (Q_{\ell_1} - Q_{\ell_2}) M_V^2 \\
 & \quad \times C_0^{\text{nf}}(0, 0, s_{12}, 0, 0, M_V) \quad \left\{ \begin{array}{c} \text{Diagram 7} \end{array} \right. \\
 & + 2(Q_{q_b} - Q_{q_a}) (Q_{\ell_1} - Q_{\ell_2}) M_V^2 \\
 & \quad \times B_0^{\text{nf}}(s_{12}, 0, M_V) \quad \left\{ \begin{array}{c} \text{Diagram 8} \end{array} \right. \\
 & \Big\}.
 \end{aligned} \tag{B.38}$$

The additional gluon emission and the resulting recoil of the quarks translates into the additional kinematic dependence on the virtuality of the respective quark. In the soft-gluon limit $k_g \rightarrow 0$ Eq. (B.38) reduces to Eq. (B.37). The corresponding correction factors for the gluon-induced channels are obtained by applying crossing relations and their final results are given in Eqs. (6.34).

The soft phase-space slicing method

In this appendix we collect the relevant formulae for the phase-space slicing method that was employed in the calculation of the non-factorizable corrections in Chap. 4 and 6. The results given here can be found, e.g., in Refs. [108, 169] and are summarized here for completeness. The general idea of the slicing method was briefly sketched in Sect. 2.2 (see also Ref. [170]). The non-factorizable corrections only contain soft singularities, and therefore a cut on the photon energy $k^0 > \Delta E > 0$ is sufficient to render the integration over the hard real-emission corrections finite.

For sufficiently small values of the cut parameter ΔE ($\Delta E \ll \Gamma_V$ in the case of the Drell–Yan processes), the real-emission matrix element can be replaced by its eikonal approximation (1.89) in the remaining integral over the soft-singular phase space. Furthermore, the phase space factorizes in the soft limit according to

$$d\Phi_{n+\gamma}|_{k^0 < \Delta E} \rightarrow d\Phi_n d\Phi_{\text{soft}}(\Delta E), \quad (\text{C.1})$$

and the soft-slicing terms can be expressed in terms of the basic integrals defined as

$$\begin{aligned} & -e^2 \mu^{2\epsilon} \int d\Phi_{\text{soft}}(\Delta E) \frac{1}{(p_i \cdot k)(p_j \cdot k)} \\ & \equiv -e^2 \mu^{2\epsilon} \int_{k^0=|\mathbf{k}| \leq \Delta E} \frac{d^{d-1}\mathbf{k}}{(2\pi)^{d-1} 2k^0} \frac{1}{(p_i \cdot k)(p_j \cdot k)} \\ & = \frac{\alpha}{4\pi^2} \frac{\Gamma(1-\epsilon)}{\Gamma(1-2\epsilon)\Gamma(1+\epsilon)} \frac{c_\epsilon}{\epsilon} \left(\frac{2\Delta E}{\mu} \right)^{-2\epsilon} \int_0^\pi d\theta (\sin \theta)^{1-2\epsilon} \int_0^\pi d\phi (\sin \phi)^{-2\epsilon} \\ & \quad \times \frac{(E_i - |\mathbf{p}_i| \cos \theta)^{-1}}{E_j - |\mathbf{p}_j|(\cos \theta_{ij} \cos \theta + \sin \theta_{ij} \sin \theta \cos \phi)}, \end{aligned} \quad (\text{C.2})$$

where the angles are defined in Fig. C.1. Details on their calculation can be found, e.g., in Refs. [108, 171]. The analytical results of the three integrals relevant in this work are given in the following:

- $p_i^2 = p_j^2 = 0$:

$$\begin{aligned} \hat{\mathcal{E}}_{ij}(p_i, p_j; \Delta E) & \equiv -e^2 \mu^{2\epsilon} \int d\Phi_{\text{soft}}(\Delta E) \frac{p_i \cdot p_j}{(p_i \cdot k)(p_j \cdot k)} \\ & = -\frac{\alpha}{2\pi} \left\{ \frac{c_\epsilon}{\epsilon^2} - \frac{c_\epsilon}{\epsilon} \left[2 \ln \left(\frac{2\Delta E}{\mu} \right) + \ln \left(\frac{2(p_i \cdot p_j)}{4E_i E_j} \right) \right] - \text{Li}_2 \left(1 - \frac{4E_i E_j}{2(p_i \cdot p_j)} \right) \right. \\ & \quad \left. + 2 \ln^2 \left(\frac{2\Delta E}{\mu} \right) + 2 \ln \left(\frac{2\Delta E}{\mu} \right) \ln \left(\frac{2(p_i \cdot p_j)}{4E_i E_j} \right) - \frac{\pi^2}{3} + \mathcal{O}(\epsilon) \right\}, \end{aligned} \quad (\text{C.3})$$

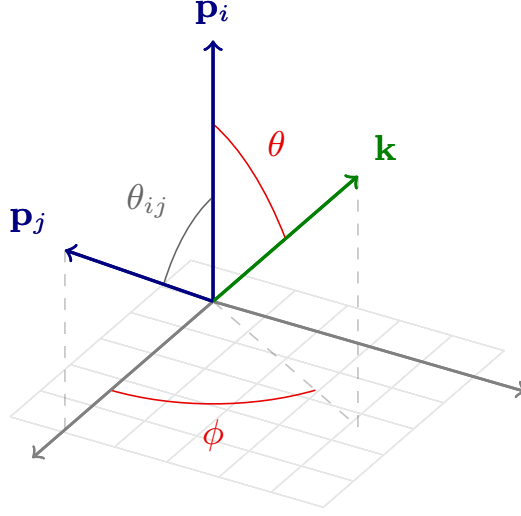


Figure C.1.: Definition of the angles appearing in Eq. (C.2).

- $p_i^2 = 0, \quad p_j^2 = M^2$:

$$\begin{aligned}
 \bar{\mathcal{E}}_{ij}(p_i, p_j; \Delta E) &\equiv -e^2 \mu^{2\epsilon} \int d\Phi_{\text{soft}}(\Delta E) \frac{p_i \cdot p_j}{(p_i \cdot k)(p_j \cdot k)} \\
 &= -\frac{\alpha}{2\pi} \left\{ \frac{c_\epsilon}{2\epsilon^2} - \frac{c_\epsilon}{\epsilon} \left[\ln \left(\frac{2\Delta E}{\mu} \right) + \ln \left(\frac{2(p_i \cdot p_j)}{2E_i M} \right) \right] - \frac{1}{4} \ln^2 \left(\frac{E_j + |\mathbf{p}_j|}{E_j - |\mathbf{p}_j|} \right) \right. \\
 &\quad - \text{Li}_2 \left(1 - \frac{2E_i(E_j + |\mathbf{p}_j|)}{2(p_i \cdot p_j)} \right) - \text{Li}_2 \left(1 - \frac{2E_i(E_j - |\mathbf{p}_j|)}{2(p_i \cdot p_j)} \right) \\
 &\quad \left. + \ln^2 \left(\frac{2\Delta E}{\mu} \right) + 2 \ln \left(\frac{2\Delta E}{\mu} \right) \ln \left(\frac{2(p_i \cdot p_j)}{2E_i M} \right) - \frac{\pi^2}{6} + \mathcal{O}(\epsilon) \right\}, \quad (\text{C.4})
 \end{aligned}$$

- $p_i = p_j \equiv p, \quad p^2 = M^2$:

$$\begin{aligned}
 \tilde{\mathcal{E}}_{ii}(p; \Delta E) &\equiv -e^2 \mu^{2\epsilon} \int d\Phi_{\text{soft}}(\Delta E) \frac{M^2}{(p \cdot k)^2} \\
 &= \frac{\alpha}{2\pi} \left\{ \frac{c_\epsilon}{\epsilon} - 2 \ln \left(\frac{2\Delta E}{\mu} \right) + \underbrace{\frac{E}{|\mathbf{p}|} \ln \left(\frac{E + |\mathbf{p}|}{E - |\mathbf{p}|} \right)}_{\xrightarrow{|\mathbf{p}| \rightarrow 0} +2} + \mathcal{O}(\epsilon) \right\}. \quad (\text{C.5})
 \end{aligned}$$

Explicit form of the IR-safe contributions to $\mathcal{O}(\alpha_s\alpha)$ corrections in the PA

In this appendix we collect the explicit expressions for the IR-safe cross-section contributions to the $\mathcal{O}(\alpha_s\alpha)$ corrections in the PA. We restrict ourselves to the quark–anti-quark and the quark–gluon channels, and the respective expressions for the gluon–anti-quark channel follow analogously.

D.1. Non-factorizable corrections

In this section we provide the explicit expressions for each of the contributions to the non-factorizable corrections in our master formula (6.47).

The double-virtual corrections (6.48) and the (virtual QCD) \times (real photonic) corrections (6.49) are obtained by dressing the virtual part of the NLO QCD corrections in Eq. (4.46a) with the appropriate non-factorizable EW correction factors, i.e. with the sum of the virtual corrections (4.11) and the integrated soft-slicing factor (4.37) and with the real-correction factor (4.22), respectively,

$$\tilde{\sigma}_{\bar{q}_a q_b, \text{nf}}^{\text{Vs} \otimes \text{Vew}} = \int_2 \left\{ d\sigma_{\bar{q}_a q_b, \text{PA}}^{\text{Vs}} + d\sigma_{\bar{q}_a q_b, \text{PA}}^0 \otimes \mathbf{I} \right\} \left[2 \operatorname{Re} \left\{ \delta_{\text{Vew}, \text{nf}}^{\bar{q}_a q_b \rightarrow \ell_1 \bar{\ell}_2} \right\} + \delta_{\text{soft}}^{\bar{q}_a q_b \rightarrow \ell_1 \bar{\ell}_2}(\Delta E) \right], \quad (\text{D.1a})$$

$$\tilde{\sigma}_{\bar{q}_a q_b, \text{nf}}^{\text{Vs} \otimes \text{Rew}} = \iint_{\substack{2+\gamma \\ E_\gamma > \Delta E}} \left\{ d\sigma_{\bar{q}_a q_b, \text{PA}}^{\text{Vs}} + d\sigma_{\bar{q}_a q_b, \text{PA}}^0 \otimes \mathbf{I} \right\} \delta_{\text{Rew}, \text{nf}}^{\bar{q}_a q_b \rightarrow \ell_1 \bar{\ell}_2 \gamma}. \quad (\text{D.1b})$$

As in the NLO QCD corrections, only the quark–anti-quark induced channel receives a non-vanishing contribution.

The IR-regularized (real QCD) \times (virtual EW) corrections (6.50) and the double-real corrections (6.51) are obtained from the real-emission part of the NLO QCD cross sections (4.46) by multiplying with the appropriate EW correction factors, i.e. the sum of the virtual corrections and the integrated slicing factors given in Eqs. (6.39) and (6.34), and the real corrections (6.38), respectively. For the quark–anti-quark channel, the explicit expressions are

$$\begin{aligned} \tilde{\sigma}_{\bar{q}_a q_b, \text{nf}}^{\text{Rs} \otimes \text{Vew}} = & \int_3 \left\{ d\sigma_{\bar{q}_a q_b, \text{PA}}^{\text{Rs}} \left[2 \operatorname{Re} \left\{ \delta_{\text{Vew}, \text{nf}}^{\bar{q}_a q_b \rightarrow \ell_1 \bar{\ell}_2 g} \right\} + \delta_{\text{soft}}^{\bar{q}_a q_b \rightarrow \ell_1 \bar{\ell}_2 g}(\Delta E) \right] \right. \\ & \left. - d\sigma_{\bar{q}_a q_b, \text{PA}}^0(\tilde{\Phi}_{2, (\bar{q}_a g) q_b}) \left[2 \operatorname{Re} \left\{ \delta_{\text{Vew}, \text{nf}}^{\bar{q}_a q_b \rightarrow \ell_1 \bar{\ell}_2} \right\} + \delta_{\text{soft}, \Lambda_z(x_g, \bar{q}_a q_b, 1)}^{\bar{q}_a q_b \rightarrow \ell_1 \bar{\ell}_2}(\Delta E) \right] \otimes dV_{\text{dip}}^{\bar{q}_a, \bar{q}_a} \right. \end{aligned}$$

$$-d\sigma_{\bar{q}_a q_b, \text{PA}}^0(\tilde{\Phi}_{2, (q_b g) \bar{q}_a}) \left[2 \text{Re} \left\{ \delta_{\text{Vew, nf}}^{\bar{q}_a q_b \rightarrow \ell_1 \bar{\ell}_2} \right\} + \delta_{\text{soft}, \Lambda_z(1, x_{g, q_b \bar{q}_a})}^{\bar{q}_a q_b \rightarrow \ell_1 \bar{\ell}_2}(\Delta E) \right] \otimes dV_{\text{dip}}^{q_b, q_b} \Big\}, \quad (\text{D.2a})$$

$$\begin{aligned} \tilde{\sigma}_{\bar{q}_a q_b, \text{nf}}^{\text{Rs} \otimes \text{Rew}} &= \iint_{\substack{3+\gamma \\ E_\gamma > \Delta E}} \left\{ d\sigma_{\bar{q}_a q_b, \text{PA}}^{\text{Rs}} \delta_{\text{Rew, nf}}^{\bar{q}_a q_b \rightarrow \ell_1 \bar{\ell}_2 \gamma g} \right. \\ &\quad - d\sigma_{\bar{q}_a q_b, \text{PA}}^0(\tilde{\Phi}_{2+\gamma, (\bar{q}_a g) q_b}) \delta_{\text{Rew, nf}}^{\bar{q}_a q_b \rightarrow \ell_1 \bar{\ell}_2 \gamma} \otimes dV_{\text{dip}}^{\bar{q}_a, \bar{q}_a} \\ &\quad \left. - d\sigma_{\bar{q}_a q_b, \text{PA}}^0(\tilde{\Phi}_{2+\gamma, (q_b g) \bar{q}_a}) \delta_{\text{Rew, nf}}^{\bar{q}_a q_b \rightarrow \ell_1 \bar{\ell}_2 \gamma} \otimes dV_{\text{dip}}^{q_b, q_b} \right\}. \end{aligned} \quad (\text{D.2b})$$

Note that it is implied that the correction factors are evaluated on the same phase space as the differential cross section they multiply. In particular, the two correction factors that appear as the second and third terms inside the curly braces in Eq. (D.2a) are not identical, as they are evaluated for different kinematics that correspond to the two possible initial-state splittings of the incoming quarks. The integrated slicing factors of the subtraction terms correspond to the boosted variants given in Eq. (6.41), where the boost along the beam axis is determined by the dipole-variable $x_{i,ab}$ defined in Eq. (4.47a). The corresponding expressions for the quark–gluon-initiated sub-processes read

$$\begin{aligned} \tilde{\sigma}_{g q_b, \text{nf}}^{\text{Rs} \otimes \text{Vew}} &= \int_3 \left\{ d\sigma_{g q_b, \text{PA}}^{\text{Rs}} \left[2 \text{Re} \left\{ \delta_{\text{Vew, nf}}^{g q_b \rightarrow \ell_1 \bar{\ell}_2 q_a} \right\} + \delta_{\text{soft}}^{g q_b \rightarrow \ell_1 \bar{\ell}_2 q_a}(\Delta E) \right] \right. \\ &\quad \left. - d\sigma_{\bar{q}_a q_b, \text{PA}}^0(\tilde{\Phi}_{2, (g q_a) q_b}) \left[2 \text{Re} \left\{ \delta_{\text{Vew, nf}}^{\bar{q}_a q_b \rightarrow \ell_1 \bar{\ell}_2} \right\} + \delta_{\text{soft}, \Lambda_z(x_{q_a, g q_b}, 1)}^{\bar{q}_a q_b \rightarrow \ell_1 \bar{\ell}_2}(\Delta E) \right] \otimes dV_{\text{dip}}^{g, \bar{q}_a} \right\}, \end{aligned} \quad (\text{D.3a})$$

$$\begin{aligned} \tilde{\sigma}_{g q_b, \text{nf}}^{\text{Rs} \otimes \text{Rew}} &= \iint_{\substack{3+\gamma \\ E_\gamma > \Delta E}} \left\{ d\sigma_{g q_b, \text{PA}}^{\text{Rs}} \delta_{\text{Rew, nf}}^{g q_b \rightarrow \ell_1 \bar{\ell}_2 \gamma q_a} - d\sigma_{\bar{q}_a q_b, \text{PA}}^0(\tilde{\Phi}_{2+\gamma, (g q_a) q_b}) \delta_{\text{Rew, nf}}^{\bar{q}_a q_b \rightarrow \ell_1 \bar{\ell}_2 \gamma} \otimes dV_{\text{dip}}^{g, \bar{q}_a} \right\}. \end{aligned} \quad (\text{D.3b})$$

The collinear counterterms with additional virtual EW (6.52) and real photonic (6.53) corrections are constructed from the corresponding term in Eq. (4.46) by dressing it with the respective non-factorizable correction factors,

$$\begin{aligned} \tilde{\sigma}_{\bar{q}_a q_b, \text{nf}}^{\text{Cs} \otimes \text{Vew}} &= \int_0^1 dx \int_2 d\sigma_{\bar{q}_a q_b, \text{PA}}^0(x p_a, p_b) \\ &\quad \times \left[2 \text{Re} \left\{ \delta_{\text{Vew, nf}}^{\bar{q}_a q_b \rightarrow \ell_1 \bar{\ell}_2} \right\} + \delta_{\text{soft}, \Lambda_z(x, 1)}^{\bar{q}_a q_b \rightarrow \ell_1 \bar{\ell}_2}(\Delta E) \right] \otimes (\mathbf{K} + \mathbf{P})^{\bar{q}_a, \bar{q}_a} \\ &\quad + \int_0^1 dx \int_2 d\sigma_{\bar{q}_a q_b, \text{PA}}^0(p_a, x p_b) \\ &\quad \times \left[2 \text{Re} \left\{ \delta_{\text{Vew, nf}}^{\bar{q}_a q_b \rightarrow \ell_1 \bar{\ell}_2} \right\} + \delta_{\text{soft}, \Lambda_z(1, x)}^{\bar{q}_a q_b \rightarrow \ell_1 \bar{\ell}_2}(\Delta E) \right] \otimes (\mathbf{K} + \mathbf{P})^{q_b, q_b}, \end{aligned} \quad (\text{D.4a})$$

$$\begin{aligned} \tilde{\sigma}_{\bar{q}_a q_b, \text{nf}}^{\text{Cs} \otimes \text{Rew}} &= \int_0^1 dx \iint_{\substack{2+\gamma \\ E_\gamma > \Delta E}} d\sigma_{\bar{q}_a q_b, \text{PA}}^0(x p_a, p_b) \delta_{\text{Rew, nf}}^{\bar{q}_a q_b \rightarrow \ell_1 \bar{\ell}_2 \gamma} \otimes (\mathbf{K} + \mathbf{P})^{\bar{q}_a, \bar{q}_a} \end{aligned}$$

$$+ \int_0^1 dx \iint_{\substack{2+\gamma \\ E_\gamma > \Delta E}} d\sigma_{\bar{q}_a q_b, \text{PA}}^0(p_a, xp_b) \delta_{\text{Rew, nf}}^{\bar{q}_a q_b \rightarrow \ell_1 \bar{\ell}_2 \gamma} \otimes (\mathbf{K} + \mathbf{P})^{q_b, q_b}. \quad (\text{D.4b})$$

As discussed in Sect. 6.2, the boosted variants of the soft-slicing factor in Eq. (D.4a) arise from the choice of the frame of reference, in which the photon-energy cut $E_\gamma > \Delta E$ in Eq. (D.4b) is applied. The corresponding formulas for the gluon–quark channel read

$$\begin{aligned} \tilde{\sigma}_{g q_b, \text{nf}}^{C_s \otimes V_{\text{ew}}} &= \int_0^1 dx \int_2 d\sigma_{\bar{q}_a q_b, \text{PA}}^0(xp_g, p_b) \\ &\times \left[2 \operatorname{Re} \left\{ \delta_{V_{\text{ew}, \text{nf}}}^{\bar{q}_a q_b \rightarrow \ell_1 \bar{\ell}_2} \right\} + \delta_{\text{soft}, \Lambda_z(x, 1)}^{\bar{q}_a q_b \rightarrow \ell_1 \bar{\ell}_2}(\Delta E) \right] \otimes (\mathbf{K} + \mathbf{P})^{g, \bar{q}_a}, \end{aligned} \quad (\text{D.5a})$$

$$\tilde{\sigma}_{g q_b, \text{nf}}^{C_s \otimes R_{\text{ew}}} = \int_0^1 dx \iint_{\substack{2+\gamma \\ E_\gamma > \Delta E}} d\sigma_{\bar{q}_a q_b, \text{PA}}^0(xp_g, p_b) \delta_{\text{Rew, nf}}^{\bar{q}_a q_b \rightarrow \ell_1 \bar{\ell}_2 \gamma} \otimes (\mathbf{K} + \mathbf{P})^{g, \bar{q}_a}. \quad (\text{D.5b})$$

D.2. Factorizable initial–final corrections

In this section we provide the explicit expressions for each of the contributions to the factorizable initial–final corrections in our master formula (7.15).

The double-virtual corrections (7.16) and the (virtual QCD) \times (real photonic) corrections (7.17) are obtained by dressing the virtual part of the NLO QCD corrections in Eq. (4.46a) with the factorizable final-state EW corrections (4.27),

$$\tilde{\sigma}_{\bar{q}_a q_b, \text{prod} \times \text{dec}}^{V_s \otimes V_{\text{ew}}} = \int_2 \left[2 \operatorname{Re} \left\{ \delta_{V_{\text{ew}}(\tau_\ell)}^{\text{dec}} \right\} + I^{\text{ew}} \right] d\sigma_{\bar{q}_a q_b, \text{PA}}^0 \otimes \left[2 \operatorname{Re} \left\{ \delta_{V_s}^{V \bar{q}_a q_b} \right\} + \mathbf{I} \right], \quad (\text{D.6a})$$

$$\begin{aligned} \tilde{\sigma}_{\bar{q}_a q_b, \text{prod} \times \text{dec}}^{V_s \otimes R_{\text{ew}}} &= \iint_{2+\gamma} \left\{ d\sigma_{\text{dec}}^{R_{\text{ew}}} + 4\pi\alpha Q_{\ell_1} \left[(Q_{\ell_1} - Q_{\ell_2}) d_{\ell_1 V}^{(\text{sub})} d\sigma_{\bar{q}_a q_b, \text{PA}}^0(\tilde{\Phi}_{2, \ell_1 V}) \right. \right. \\ &\quad \left. \left. + Q_{\ell_2} g_{\ell_1 \bar{\ell}_2}^{(\text{sub})} d\sigma_{\bar{q}_a q_b, \text{PA}}^0(\tilde{\Phi}_{2, \ell_1 \bar{\ell}_2}) \right] \otimes \left[2 \operatorname{Re} \left\{ \delta_{V_s}^{V \bar{q}_a q_b} \right\} + \mathbf{I} \right] + (\ell_1 \leftrightarrow \bar{\ell}_2) \right\}, \end{aligned} \quad (\text{D.6b})$$

where the integrated counterpart of the QED dipoles I^{ew} is defined in Eq. (4.30). As in the NLO QCD corrections, only the quark–anti-quark induced channel receives a non-vanishing contribution.

The IR-regularized (real QCD) \times (virtual EW) corrections (7.18) and the double-real corrections (7.19) are obtained by dressing the real-emission part of the NLO QCD cross sections (4.46) with the final-state factorizable corrections (4.27). Note the two-fold application of the dipole subtraction formalism in case of the double-real corrections. For the quark–anti-quark channel, the explicit expressions are

$$\begin{aligned} \tilde{\sigma}_{\bar{q}_a q_b, \text{prod} \times \text{dec}}^{R_s \otimes V_{\text{ew}}} &= \int_3 \left[2 \operatorname{Re} \left\{ \delta_{V_{\text{ew}}(\tau_\ell)}^{\text{dec}} \right\} + I^{\text{ew}} \right] \\ &\times \left\{ d\sigma_{\bar{q}_a q_b, \text{PA}}^{R_s} - d\sigma_{\bar{q}_a q_b, \text{PA}}^0(\tilde{\Phi}_{n, (\bar{q}_a g) q_b}) \otimes dV_{\text{dip}}^{\bar{q}_a, \bar{q}_a} - d\sigma_{\bar{q}_a q_b, \text{PA}}^0(\tilde{\Phi}_{n, (q_b g) \bar{q}_a}) \otimes dV_{\text{dip}}^{q_b, q_b} \right\}, \end{aligned} \quad (\text{D.7a})$$

$$\begin{aligned}
\tilde{\sigma}_{\bar{q}_a q_b, \text{prod} \times \text{dec}}^{\text{R}_s \otimes \text{R}_{\text{ew}}} = & \iint_{3+\gamma} \left\{ d\sigma_{\bar{q}_a q_b, \text{prod} \times \text{dec}}^{\text{R}_s \otimes \text{R}_{\text{ew}}} \right. \\
& - d\sigma_{\bar{q}_a q_b, \text{dec}}^{\text{R}_{\text{ew}}} \left(\tilde{\Phi}_{2+\gamma, (\bar{q}_a g) q_b} \right) \otimes dV_{\text{dip}}^{\bar{q}_a, \bar{q}_a} \\
& - d\sigma_{\bar{q}_a q_b, \text{dec}}^{\text{R}_{\text{ew}}} \left(\tilde{\Phi}_{2+\gamma, (q_b g) \bar{q}_a} \right) \otimes dV_{\text{dip}}^{q_b, q_b} \\
& + 4\pi\alpha Q_{\ell_1} \left[(Q_{\ell_1} - Q_{\ell_2}) d_{\ell_1 V}^{(\text{sub})} d\sigma_{\bar{q}_a q_b, \text{PA}}^{\text{R}_s} \left(\tilde{\Phi}_{3, \ell_1 V} \right) \right. \\
& \quad \left. + Q_{\ell_2} g_{\ell_1 \bar{\ell}_2}^{(\text{sub})} d\sigma_{\bar{q}_a q_b, \text{PA}}^{\text{R}_s} \left(\tilde{\Phi}_{3, \ell_1 \bar{\ell}_2} \right) \right] + (\ell_1 \leftrightarrow \bar{\ell}_2) \\
& - 4\pi\alpha Q_{\ell_1} \left[(Q_{\ell_1} - Q_{\ell_2}) d_{\ell_1 V}^{(\text{sub})} d\sigma_{\bar{q}_a q_b, \text{PA}}^0 \left(\tilde{\Phi}_{2, \ell_1 V}^{(\bar{q}_a g) q_b} \right) \otimes dV_{\text{dip}}^{\bar{q}_a, \bar{q}_a} \right. \\
& \quad + (Q_{\ell_1} - Q_{\ell_2}) d_{\ell_1 V}^{(\text{sub})} d\sigma_{\bar{q}_a q_b, \text{PA}}^0 \left(\tilde{\Phi}_{2, \ell_1 V}^{(q_b g) \bar{q}_a} \right) \otimes dV_{\text{dip}}^{q_b, q_b} \\
& \quad + Q_{\ell_2} g_{\ell_1 \bar{\ell}_2}^{(\text{sub})} d\sigma_{\bar{q}_a q_b, \text{PA}}^0 \left(\tilde{\Phi}_{2, \ell_1 \bar{\ell}_2}^{(\bar{q}_a g) q_b} \right) \otimes dV_{\text{dip}}^{\bar{q}_a, \bar{q}_a} \\
& \quad \left. + Q_{\ell_2} g_{\ell_1 \bar{\ell}_2}^{(\text{sub})} d\sigma_{\bar{q}_a q_b, \text{PA}}^0 \left(\tilde{\Phi}_{2, \ell_1 \bar{\ell}_2}^{(q_b g) \bar{q}_a} \right) \otimes dV_{\text{dip}}^{q_b, q_b} \right] + (\ell_1 \leftrightarrow \bar{\ell}_2) \Big\}. \tag{D.7b}
\end{aligned}$$

A detailed discussion of the behaviour of the individual terms of the double-real corrections in the various singular regions is given in Sect. 7.2. The corresponding expressions for the quark–gluon-initiated sub-processes read

$$\tilde{\sigma}_{g q_b, \text{prod} \times \text{dec}}^{\text{R}_s \otimes \text{V}_{\text{ew}}} = \int_3 \left[2 \text{Re} \left\{ \delta_{\text{V}_{\text{ew}}}^{\text{dec}}(\tau_\ell) \right\} + I^{\text{ew}} \right] \left\{ d\sigma_{g q_b, \text{PA}}^{\text{R}_s} - d\sigma_{\bar{q}_a q_b, \text{PA}}^0 \left(\tilde{\Phi}_{n, (g q_a) q_b} \right) \otimes dV_{\text{dip}}^{g, \bar{q}_a} \right\}, \tag{D.8a}$$

$$\begin{aligned}
\tilde{\sigma}_{g q_b, \text{prod} \times \text{dec}}^{\text{R}_s \otimes \text{R}_{\text{ew}}} = & \iint_{3+\gamma} \left\{ d\sigma_{g q_b, \text{prod} \times \text{dec}}^{\text{R}_s \otimes \text{R}_{\text{ew}}} - d\sigma_{\bar{q}_a q_b, \text{dec}}^{\text{R}_{\text{ew}}} \left(\tilde{\Phi}_{2+\gamma, (g q_a) q_b} \right) \otimes dV_{\text{dip}}^{g, \bar{q}_a} \right. \\
& + 4\pi\alpha Q_{\ell_1} \left[(Q_{\ell_1} - Q_{\ell_2}) d_{\ell_1 V}^{(\text{sub})} d\sigma_{g q_b, \text{PA}}^{\text{R}_s} \left(\tilde{\Phi}_{3, \ell_1 V} \right) \right. \\
& \quad \left. + Q_{\ell_2} g_{\ell_1 \bar{\ell}_2}^{(\text{sub})} d\sigma_{g q_b, \text{PA}}^{\text{R}_s} \left(\tilde{\Phi}_{3, \ell_1 \bar{\ell}_2} \right) \right] + (\ell_1 \leftrightarrow \bar{\ell}_2) \\
& - 4\pi\alpha Q_{\ell_1} \left[(Q_{\ell_1} - Q_{\ell_2}) d_{\ell_1 V}^{(\text{sub})} d\sigma_{\bar{q}_a q_b, \text{PA}}^0 \left(\tilde{\Phi}_{2, \ell_1 V}^{(g q_a) q_b} \right) \otimes dV_{\text{dip}}^{g, \bar{q}_a} \right. \\
& \quad \left. + Q_{\ell_2} g_{\ell_1 \bar{\ell}_2}^{(\text{sub})} d\sigma_{\bar{q}_a q_b, \text{PA}}^0 \left(\tilde{\Phi}_{2, \ell_1 \bar{\ell}_2}^{(g q_a) q_b} \right) \otimes dV_{\text{dip}}^{g, \bar{q}_a} \right] + (\ell_1 \leftrightarrow \bar{\ell}_2) \Big\}. \tag{D.8b}
\end{aligned}$$

The collinear counterterms with additional virtual EW (7.22) and real-photonic (7.23) corrections are constructed from the corresponding term in Eq. (4.46) by dressing it with the respective factorizable final-state corrections,

$$\tilde{\sigma}_{\bar{q}_a q_b, \text{prod} \times \text{dec}}^{\text{C}_s \otimes \text{V}_{\text{ew}}} = \int_0^1 dx \int_2 \left[2 \text{Re} \left\{ \delta_{\text{V}_{\text{ew}}}^{\text{dec}}(\tau_\ell) \right\} + I^{\text{ew}} \right] d\sigma_{\bar{q}_a q_b, \text{PA}}^0(x p_a, p_b) \otimes (\mathbf{K} + \mathbf{P})^{\bar{q}_a, \bar{q}_a}$$

$$+ \int_0^1 dx \int_2 \left[2 \operatorname{Re} \left\{ \delta_{V_{\text{ew}}(\tau_\ell)}^{\text{dec}} \right\} + I^{\text{ew}} \right] d\sigma_{\bar{q}_a q_b, \text{PA}}^0(p_a, xp_b) \otimes (\mathbf{K} + \mathbf{P})^{q_b, q_b}, \quad (\text{D.9a})$$

$$\begin{aligned} \tilde{\sigma}_{\bar{q}_a q_b, \text{prod} \times \text{dec}}^{\text{Cs} \otimes \text{R}_{\text{ew}}} &= \int_0^1 dx \iint_{2+\gamma} \left\{ d\sigma_{\bar{q}_a q_b, \text{dec}}^{\text{R}_{\text{ew}}}(xp_a, pb) \right. \\ &\quad + 4\pi\alpha Q_{\ell_1} \left[(Q_{\ell_1} - Q_{\ell_2}) d_{\ell_1 V}^{(\text{sub})} d\sigma_{\bar{q}_a q_b, \text{PA}}^0(\tilde{\Phi}_{2, \ell_1 V}(xp_a, pb)) \right. \\ &\quad \left. \left. + Q_{\ell_2} g_{\ell_1 \bar{\ell}_2}^{(\text{sub})} d\sigma_{\bar{q}_a q_b, \text{PA}}^0(\tilde{\Phi}_{2, \ell_1 \bar{\ell}_2}(xp_a, pb)) \right] + (\ell_1 \leftrightarrow \bar{\ell}_2) \right\} \otimes (\mathbf{K} + \mathbf{P})^{\bar{q}_a, \bar{q}_a} \\ &+ \int_0^1 dx \iint_{2+\gamma} \left\{ d\sigma_{\bar{q}_a q_b, \text{dec}}^{\text{R}_{\text{ew}}}(p_a, xp_b) \right. \\ &\quad + 4\pi\alpha Q_{\ell_1} \left[(Q_{\ell_1} - Q_{\ell_2}) d_{\ell_1 V}^{(\text{sub})} d\sigma_{\bar{q}_a q_b, \text{PA}}^0(\tilde{\Phi}_{2, \ell_1 V}(p_a, xp_b)) \right. \\ &\quad \left. \left. + Q_{\ell_2} g_{\ell_1 \bar{\ell}_2}^{(\text{sub})} d\sigma_{\bar{q}_a q_b, \text{PA}}^0(\tilde{\Phi}_{2, \ell_1 \bar{\ell}_2}(p_a, xp_b)) \right] + (\ell_1 \leftrightarrow \bar{\ell}_2) \right\} \otimes (\mathbf{K} + \mathbf{P})^{q_b, q_b}. \end{aligned} \quad (\text{D.9b})$$

The corresponding formulae for the gluon–quark channel read

$$\tilde{\sigma}_{g q_b, \text{prod} \times \text{dec}}^{\text{Cs} \otimes V_{\text{ew}}} = \int_0^1 dx \int_2 \left[2 \operatorname{Re} \left\{ \delta_{V_{\text{ew}}(\tau_\ell)}^{\text{dec}} \right\} + I^{\text{ew}} \right] d\sigma_{\bar{q}_a q_b, \text{PA}}^0(xp_g, pb) \otimes (\mathbf{K} + \mathbf{P})^{g, \bar{q}_a}, \quad (\text{D.10a})$$

$$\begin{aligned} \tilde{\sigma}_{g q_b, \text{prod} \times \text{dec}}^{\text{Cs} \otimes \text{R}_{\text{ew}}} &= \int_0^1 dx \iint_{2+\gamma} \left\{ d\sigma_{\bar{q}_a q_b, \text{dec}}^{\text{R}_{\text{ew}}}(xp_g, pb) \right. \\ &\quad + 4\pi\alpha Q_{\ell_1} \left[(Q_{\ell_1} - Q_{\ell_2}) d_{\ell_1 V}^{(\text{sub})} d\sigma_{\bar{q}_a q_b, \text{PA}}^0(\tilde{\Phi}_{2, \ell_1 V}(xp_g, pb)) \right. \\ &\quad \left. \left. + Q_{\ell_2} g_{\ell_1 \bar{\ell}_2}^{(\text{sub})} d\sigma_{\bar{q}_a q_b, \text{PA}}^0(\tilde{\Phi}_{2, \ell_1 \bar{\ell}_2}(xp_g, pb)) \right] + (\ell_1 \leftrightarrow \bar{\ell}_2) \right\} \otimes (\mathbf{K} + \mathbf{P})^{g, \bar{q}_a}. \end{aligned} \quad (\text{D.10b})$$

Here we have included the dependence on the momenta of the incoming partons in order to indicate which particle undergoes a collinear splitting with the momentum fraction given by the convolution variable x .

Non-collinear-safe observables

For non-collinear-safe observables an additional term arises which is obtained by the convolution of the NLO QCD corrections (4.46a) with the function $\tilde{\mathcal{I}}^{\text{ew}}$ defined in Eq. (4.33). The contribution with virtual QCD corrections is given by

$$\tilde{\sigma}_{\bar{q}_a q_b, \text{prod} \times \text{dec}}^{V_s \otimes \bar{\text{R}}_{\text{ew}}} = \int_0^1 dz \int_2 \left[\tilde{\mathcal{I}}^{\text{ew}}(z) \right]_+ d\sigma_{\bar{q}_a q_b, \text{PA}}^0 \otimes \left[2 \operatorname{Re} \left\{ \delta_{V_s}^{V \bar{q}_a q_b} \right\} + \mathbf{I} \right], \quad (\text{D.11})$$

and the real-emission corrections for the quark–anti-quark and gluon–quark induced contributions read

$$\begin{aligned} \tilde{\sigma}_{\bar{q}_a q_b, \text{prod} \times \text{dec}}^{\text{R}_s \otimes \bar{\text{R}}_{\text{ew}}} &= \int_0^1 dz \int_3 [\bar{\mathcal{I}}^{\text{ew}}(z)]_+ \left\{ d\sigma_{\bar{q}_a q_b, \text{PA}}^{\text{R}_s} - d\sigma_{\bar{q}_a q_b, \text{PA}}^0 \left(\tilde{\Phi}_{n, (\bar{q}_a g) q_b} \right) \otimes dV_{\text{dip}}^{\bar{q}_a, \bar{q}_a} \right. \\ &\quad \left. - d\sigma_{\bar{q}_a q_b, \text{PA}}^0 \left(\tilde{\Phi}_{n, (q_b g) \bar{q}_a} \right) \otimes dV_{\text{dip}}^{q_b, q_b} \right\}, \end{aligned} \quad (\text{D.12})$$

$$\tilde{\sigma}_{g q_b, \text{prod} \times \text{dec}}^{\text{R}_s \otimes \bar{\text{R}}_{\text{ew}}} = \int_0^1 dz \int_3 [\bar{\mathcal{I}}^{\text{ew}}(z)]_+ \left\{ d\sigma_{g q_b, \text{PA}}^{\text{R}_s} - d\sigma_{g q_b, \text{PA}}^0 \left(\tilde{\Phi}_{n, (g q_a) q_b} \right) \otimes dV_{\text{dip}}^{g, \bar{q}_a} \right\}. \quad (\text{D.13})$$

The \mathbf{K} and \mathbf{P} operators contain an additional convolution over the momentum fractions of the incoming partons and can be written in the following form,

$$\begin{aligned} \tilde{\sigma}_{\bar{q}_a q_b, \text{prod} \times \text{dec}}^{\text{C}_s \otimes \bar{\text{R}}_{\text{ew}}} &= \int_0^1 dx \int_0^1 dz \int_2 [\bar{\mathcal{I}}^{\text{ew}}(z)]_+ d\sigma_{\bar{q}_a q_b, \text{PA}}^0(x p_a, p_b) \otimes (\mathbf{K} + \mathbf{P})^{\bar{q}_a, \bar{q}_a} \\ &\quad + \int_0^1 dx \int_0^1 dz \int_2 [\bar{\mathcal{I}}^{\text{ew}}(z)]_+ d\sigma_{\bar{q}_a q_b, \text{PA}}^0(p_a, x p_b) \otimes (\mathbf{K} + \mathbf{P})^{q_b, q_b}, \end{aligned} \quad (\text{D.14})$$

$$\tilde{\sigma}_{g q_b, \text{prod} \times \text{dec}}^{\text{C}_s \otimes \bar{\text{R}}_{\text{ew}}} = \int_0^1 dx \int_0^1 dz \int_2 [\bar{\mathcal{I}}^{\text{ew}}(z)]_+ d\sigma_{g q_b, \text{PA}}^0(x p_g, p_b) \otimes (\mathbf{K} + \mathbf{P})^{g, \bar{q}_a}. \quad (\text{D.15})$$

Note that the \mathbf{K} and \mathbf{P} operators, in general, contain plus distributions with respect to the variable x , and the above equations need to be properly evaluated in combination with the plus distribution $[\bar{\mathcal{I}}^{\text{ew}}(z)]_+$ that acts on the z integration variable.

The convolution variable z represents the energy fraction of the charged lepton ℓ^\pm that undergoes a collinear splitting $\ell^\pm \rightarrow \ell^\pm + \gamma$ as described by the observable definition

$$\Theta_{\text{cut}} \left(\tilde{\Phi}_n \mid k_{\ell^\pm} = z \tilde{k}_{\ell^\pm}, \ k = (1-z) \tilde{k}_{\ell^\pm} \right), \quad (\text{D.16})$$

which appears in the definition of $\bar{\mathcal{I}}^{\text{ew}}$ given in Eq. (4.33).

Bibliography

- [1] S. Glashow, Nucl.Phys. **22** (1961) 579.
- [2] S. Weinberg, Phys.Rev.Lett. **19** (1967) 1264.
- [3] A. Salam, Conf.Proc. **C680519** (1968) 367.
- [4] UA1 Collaboration, G. Arnison *et al.*, Phys.Lett. **B122** (1983) 103.
- [5] UA2 Collaboration, M. Banner *et al.*, Phys.Lett. **B122** (1983) 476.
- [6] UA1 Collaboration, G. Arnison *et al.*, Phys.Lett. **B126** (1983) 398.
- [7] UA2 Collaboration, P. Bagnaia *et al.*, Phys.Lett. **B129** (1983) 130.
- [8] ATLAS Collaboration, G. Aad *et al.*, Phys.Lett. **B716** (2012) 1, [arXiv:1207.7214 \[hep-ex\]](#).
- [9] CMS Collaboration, S. Chatrchyan *et al.*, Phys.Lett. **B716** (2012) 30, [arXiv:1207.7235 \[hep-ex\]](#).
- [10] D. J. Gross and F. Wilczek, Phys.Rev.Lett. **30** (1973) 1343.
- [11] H. D. Politzer, Phys.Rev.Lett. **30** (1973) 1346.
- [12] Supernova Cosmology Project, M. Kowalski *et al.*, Astrophys.J. **686** (2008) 749, [arXiv:0804.4142 \[astro-ph\]](#).
- [13] S. Drell and T.-M. Yan, Annals Phys. **66** (1971) 578.
- [14] T.-M. Yan and S. D. Drell, [arXiv:1409.0051 \[hep-ph\]](#).
- [15] TeV4LHC-Top and Electroweak Working Group, C. Gerber *et al.*, [arXiv:0705.3251 \[hep-ph\]](#).
- [16] TeV4LHC Working Group, S. Abdullin *et al.*, [arXiv:hep-ph/0608322 \[hep-ph\]](#).
- [17] CDF Collaboration, T. Aaltonen *et al.*, Phys.Rev.Lett. **108** (2012) 151803, [arXiv:1203.0275 \[hep-ex\]](#).
- [18] D0 Collaboration, V. M. Abazov *et al.*, Phys.Rev.Lett. **108** (2012) 151804, [arXiv:1203.0293 \[hep-ex\]](#).
- [19] M. Boonekamp, F. Chevallier, C. Royon, and L. Schoeffel, Acta Phys.Polon. **B40** (2009) 2239, [arXiv:0902.1678 \[hep-ph\]](#).
- [20] ATLAS Collaboration, G. Aad *et al.*, Phys.Rev.Lett. **109** (2012) 012001, [arXiv:1203.4051 \[hep-ex\]](#).

- [21] S. Haywood *et al.*, [arXiv:hep-ph/0003275](#) [[hep-ph](#)].
- [22] CDF Collaboration, D0 Collaboration, T. A. Aaltonen *et al.*, *Phys.Rev.* **D88** (2013) 5, 052018, [arXiv:1307.7627](#) [[hep-ex](#)].
- [23] ALEPH Collaboration, DELPHI Collaboration, L3 Collaboration, OPAL Collaboration, LEP Electroweak Working Group, J. Alcaraz *et al.*, [arXiv:hep-ex/0612034](#) [[hep-ex](#)].
- [24] ATLAS Collaboration, N. Besson, M. Boonekamp, E. Klinkby, S. Mehlhase, and T. Petersen, *Eur.Phys.J.* **C57** (2008) 627, [arXiv:0805.2093](#) [[hep-ex](#)].
- [25] M. Baak *et al.*, [arXiv:1310.6708](#) [[hep-ph](#)].
- [26] R. Hamberg, W. van Neerven, and T. Matsuura, *Nucl.Phys.* **B359** (1991) 343. [Erratum-*ibid.* B **644** (2002) 403].
- [27] R. V. Harlander and W. B. Kilgore, *Phys.Rev.Lett.* **88** (2002) 201801, [arXiv:hep-ph/0201206](#) [[hep-ph](#)].
- [28] C. Anastasiou, L. J. Dixon, K. Melnikov, and F. Petriello, *Phys.Rev.* **D69** (2004) 094008, [arXiv:hep-ph/0312266](#) [[hep-ph](#)].
- [29] K. Melnikov and F. Petriello, *Phys.Rev.Lett.* **96** (2006) 231803, [arXiv:hep-ph/0603182](#) [[hep-ph](#)].
- [30] K. Melnikov and F. Petriello, *Phys.Rev.* **D74** (2006) 114017, [arXiv:hep-ph/0609070](#) [[hep-ph](#)].
- [31] S. Catani, L. Cieri, G. Ferrera, D. de Florian, and M. Grazzini, *Phys.Rev.Lett.* **103** (2009) 082001, [arXiv:0903.2120](#) [[hep-ph](#)].
- [32] R. Gavin, Y. Li, F. Petriello, and S. Quackenbush, *Comput.Phys.Commun.* **182** (2011) 2388, [arXiv:1011.3540](#) [[hep-ph](#)].
- [33] R. Gavin, Y. Li, F. Petriello, and S. Quackenbush, *Comput.Phys.Commun.* **184** (2013) 208, [arXiv:1201.5896](#) [[hep-ph](#)].
- [34] U. Baur, S. Keller, and W. Sakumoto, *Phys.Rev.* **D57** (1998) 199, [arXiv:hep-ph/9707301](#) [[hep-ph](#)].
- [35] V. Zykunov, *Eur.Phys.J.direct* **C3** (2001) 9, [arXiv:hep-ph/0107059](#) [[hep-ph](#)].
- [36] U. Baur, O. Brein, W. Hollik, C. Schappacher, and D. Wackerroth, *Phys.Rev.* **D65** (2002) 033007, [arXiv:hep-ph/0108274](#) [[hep-ph](#)].
- [37] S. Dittmaier and M. Krämer, *Phys. Rev.* **D65** (2002) 073007, [hep-ph/0109062](#).
- [38] U. Baur and D. Wackerroth, *Phys.Rev.* **D70** (2004) 073015, [arXiv:hep-ph/0405191](#) [[hep-ph](#)].
- [39] A. Arbuzov *et al.*, *Eur.Phys.J.* **C46** (2006) 407, [arXiv:hep-ph/0506110](#) [[hep-ph](#)].
- [40] C. Carloni Calame, G. Montagna, O. Nicrosini, and A. Vicini, *JHEP* **0612** (2006) 016, [arXiv:hep-ph/0609170](#) [[hep-ph](#)].

- [41] V. Zykunov, Phys.Rev. **D75** (2007) 073019, [arXiv:hep-ph/0509315](#) [hep-ph].
- [42] C. Carloni Calame, G. Montagna, O. Nicrosini, and A. Vicini, JHEP **0710** (2007) 109, [arXiv:0710.1722](#) [hep-ph].
- [43] A. Arbuzov *et al.*, Eur.Phys.J. **C54** (2008) 451, [arXiv:0711.0625](#) [hep-ph].
- [44] S. Brensing, S. Dittmaier, M. Krämer, and A. Mück, Phys.Rev. **D77** (2008) 073006, [arXiv:0710.3309](#) [hep-ph].
- [45] S. Dittmaier and M. Huber, JHEP **1001** (2010) 060, [arXiv:0911.2329](#) [hep-ph].
- [46] R. Boughezal, Y. Li, and F. Petriello, Phys.Rev. **D89** (2014) 034030, [arXiv:1312.3972](#) [hep-ph].
- [47] U. Baur and T. Stelzer, Phys.Rev. **D61** (2000) 073007, [arXiv:hep-ph/9910206](#) [hep-ph].
- [48] W. Placzek and S. Jadach, Eur.Phys.J. **C29** (2003) 325, [arXiv:hep-ph/0302065](#) [hep-ph].
- [49] C. Carloni Calame, G. Montagna, O. Nicrosini, and M. Treccani, Phys.Rev. **D69** (2004) 037301, [arXiv:hep-ph/0303102](#) [hep-ph].
- [50] S. Moch, J. Vermaseren, and A. Vogt, Nucl.Phys. **B726** (2005) 317, [arXiv:hep-ph/0506288](#) [hep-ph].
- [51] E. Laenen and L. Magnea, Phys.Lett. **B632** (2006) 270, [arXiv:hep-ph/0508284](#) [hep-ph].
- [52] A. Idilbi and X.-d. Ji, Phys.Rev. **D72** (2005) 054016, [arXiv:hep-ph/0501006](#) [hep-ph].
- [53] V. Ravindran and J. Smith, Phys.Rev. **D76** (2007) 114004, [arXiv:0708.1689](#) [hep-ph].
- [54] S. Frixione and B. R. Webber, [arXiv:hep-ph/0612272](#) [hep-ph].
- [55] S. Alioli, P. Nason, C. Oleari, and E. Re, JHEP **0807** (2008) 060, [arXiv:0805.4802](#) [hep-ph].
- [56] K. Hamilton, P. Richardson, and J. Tully, JHEP **0810** (2008) 015, [arXiv:0806.0290](#) [hep-ph].
- [57] C. Balazs and C. Yuan, Phys.Rev. **D56** (1997) 5558, [arXiv:hep-ph/9704258](#) [hep-ph].
- [58] F. Landry, R. Brock, P. M. Nadolsky, and C. Yuan, Phys.Rev. **D67** (2003) 073016, [arXiv:hep-ph/0212159](#) [hep-ph].
- [59] G. Bozzi, S. Catani, G. Ferrera, D. de Florian, and M. Grazzini, Phys.Lett. **B696** (2011) 207, [arXiv:1007.2351](#) [hep-ph].
- [60] S. Mantry and F. Petriello, Phys.Rev. **D83** (2011) 053007, [arXiv:1007.3773](#) [hep-ph].
- [61] T. Becher, M. Neubert, and D. Wilhelm, JHEP **1202** (2012) 124, [arXiv:1109.6027](#) [hep-ph].

- [62] Q.-H. Cao and C. Yuan, Phys.Rev.Lett. **93** (2004) 042001, [arXiv:hep-ph/0401026](#) [hep-ph].
- [63] P. Richardson, R. Sadykov, A. Saproinov, M. Seymour, and P. Skands, JHEP **1206** (2012) 090, [arXiv:1011.5444](#) [hep-ph].
- [64] C. Bernaciak and D. Wackerroth, Phys.Rev. **D85** (2012) 093003, [arXiv:1201.4804](#) [hep-ph].
- [65] L. Barzè, G. Montagna, P. Nason, O. Nicrosini, and F. Piccinini, JHEP **1204** (2012) 037, [arXiv:1202.0465](#) [hep-ph].
- [66] Y. Li and F. Petriello, Phys.Rev. **D86** (2012) 094034, [arXiv:1208.5967](#) [hep-ph].
- [67] L. Barzè *et al.*, Eur.Phys.J. **C73** (2013) 2474, [arXiv:1302.4606](#) [hep-ph].
- [68] G. Balossini *et al.*, JHEP **1001** (2010) 013, [arXiv:0907.0276](#) [hep-ph].
- [69] A. Kotikov, J. H. Kühn, and O. Veretin, Nucl.Phys. **B788** (2008) 47, [arXiv:hep-ph/0703013](#) [HEP-PH].
- [70] W. B. Kilgore and C. Sturm, Phys.Rev. **D85** (2012) 033005, [arXiv:1107.4798](#) [hep-ph].
- [71] R. Bonciani, PoS **EPS-HEP2011** (2011) 365.
- [72] A. Czarnecki and J. H. Kühn, Phys.Rev.Lett. **77** (1996) 3955, [arXiv:hep-ph/9608366](#) [hep-ph].
- [73] D. Kara, Nucl.Phys. **B877** (2013) 683, [arXiv:1307.7190](#).
- [74] J. H. Kühn, A. Kulesza, S. Pozzorini, and M. Schulze, Nucl.Phys. **B727** (2005) 368, [arXiv:hep-ph/0507178](#) [hep-ph].
- [75] J. H. Kühn, A. Kulesza, S. Pozzorini, and M. Schulze, Nucl.Phys. **B797** (2008) 27, [arXiv:0708.0476](#) [hep-ph].
- [76] W. Hollik, T. Kasprzik, and B. Kniehl, Nucl.Phys. **B790** (2008) 138, [arXiv:0707.2553](#) [hep-ph].
- [77] A. Denner, S. Dittmaier, T. Kasprzik, and A. Mück, JHEP **0908** (2009) 075, [arXiv:0906.1656](#) [hep-ph].
- [78] A. Denner, S. Dittmaier, T. Kasprzik, and A. Mück, JHEP **1106** (2011) 069, [arXiv:1103.0914](#) [hep-ph].
- [79] A. Denner, S. Dittmaier, T. Kasprzik, and A. Mück, Eur.Phys.J. **C73** (2013) 2297, [arXiv:1211.5078](#) [hep-ph].
- [80] J. Smith, D. Thomas, and W. van Neerven, Z.Phys. **C44** (1989) 267.
- [81] J. Ohnemus, Phys.Rev. **D47** (1993) 940.
- [82] J. Ohnemus, Phys.Rev. **D51** (1995) 1068, [arXiv:hep-ph/9407370](#) [hep-ph].

- [83] L. J. Dixon, Z. Kunszt, and A. Signer, Nucl.Phys. **B531** (1998) 3, [arXiv:hep-ph/9803250 \[hep-ph\]](#).
- [84] J. M. Campbell and R. K. Ellis, Phys.Rev. **D60** (1999) 113006, [arXiv:hep-ph/9905386 \[hep-ph\]](#).
- [85] D. De Florian and A. Signer, Eur.Phys.J. **C16** (2000) 105, [arXiv:hep-ph/0002138 \[hep-ph\]](#).
- [86] J. M. Campbell, R. K. Ellis, and C. Williams, JHEP **1107** (2011) 018, [arXiv:1105.0020 \[hep-ph\]](#).
- [87] S. Dittmaier, A. Huss, and C. Schwinn, Nucl.Phys. **B885** (2014) 318, [arXiv:1403.3216 \[hep-ph\]](#).
- [88] S. Dittmaier, A. Huss, and C. Schwinn, PoS **RADCOR2013** (2013) 020.
- [89] S. Dittmaier, A. Huss, and C. Schwinn, [arXiv:1405.6897 \[hep-ph\]](#).
- [90] M. Böhm, A. Denner, and H. Joos, *Gauge theories of strong and electroweak interactions; 3rd ed.* B. G. Teubner, Stuttgart, 2001.
- [91] M. E. Peskin and D. V. Schroeder, *An Introduction to Quantum Field Theory; 1995 ed.* Westview, Boulder, CO, 1995.
- [92] H. Fritzsch and M. Gell-Mann, eConf **C720906V2** (1972) 135, [arXiv:hep-ph/0208010 \[hep-ph\]](#).
- [93] H. Fritzsch, M. Gell-Mann, and H. Leutwyler, Phys.Lett. **B47** (1973) 365.
- [94] Y. Nambu, Phys.Rev. **117** (1960) 648.
- [95] J. Goldstone, Nuovo Cim. **19** (1961) 154.
- [96] P. W. Higgs, Phys.Lett. **12** (1964) 132.
- [97] P. W. Higgs, Phys.Rev.Lett. **13** (1964) 508.
- [98] F. Englert and R. Brout, Phys.Rev.Lett. **13** (1964) 321.
- [99] G. Guralnik, C. Hagen, and T. Kibble, Phys.Rev.Lett. **13** (1964) 585.
- [100] S. M. Bilenky and S. Petcov, Rev.Mod.Phys. **59** (1987) 671.
- [101] N. Cabibbo, Phys.Rev.Lett. **10** (1963) 531.
- [102] M. Kobayashi and T. Maskawa, Prog.Theor.Phys. **49** (1973) 652.
- [103] L. Faddeev and V. Popov, Phys.Lett. **B25** (1967) 29.
- [104] C. Becchi, A. Rouet, and R. Stora, Phys.Lett. **B52** (1974) 344.
- [105] C. Becchi, A. Rouet, and R. Stora, Commun.Math.Phys. **42** (1975) 127.
- [106] H. Lehmann, K. Symanzik, and W. Zimmermann, Nuovo Cim. **1** (1955) 205.

- [107] G. 't Hooft, Nucl.Phys. **B35** (1971) 167.
- [108] A. Denner, Fortsch.Phys. **41** (1993) 307, [arXiv:0709.1075 \[hep-ph\]](#).
- [109] G. 't Hooft and M. Veltman, Nucl.Phys. **B44** (1972) 189.
- [110] C. Bollini and J. Giambiagi, Nuovo Cim. **B12** (1972) 20.
- [111] J. C. Collins, *Renormalization: an introduction to renormalization, the renormalization group, and the operator-product expansion*. Cambridge monographs on mathematical physics. Cambridge Univ. Press, Cambridge, 1984.
- [112] M. S. Chanowitz, M. Furman, and I. Hinchliffe, Nucl.Phys. **B159** (1979) 225.
- [113] F. Jegerlehner, Eur.Phys.J. **C18** (2001) 673, [arXiv:hep-th/0005255 \[hep-th\]](#).
- [114] R. K. Ellis, W. J. Stirling, and B. R. Webber, *QCD and Collider Physics*. Cambridge monographs on particle physics, nuclear physics, and cosmology. Cambridge Univ. Press, Cambridge, 2003.
- [115] S. Eidelman and F. Jegerlehner, Z.Phys. **C67** (1995) 585, [arXiv:hep-ph/9502298 \[hep-ph\]](#).
- [116] A. Sirlin, Phys.Rev. **D22** (1980) 971.
- [117] M. Veltman, Acta Phys.Polon. **B8** (1977) 475.
- [118] A. Sirlin, Phys.Rev.Lett. **67** (1991) 2127.
- [119] R. G. Stuart, Phys. Lett. **B262** (1991) 113.
- [120] A. Sirlin, Phys.Lett. **B267** (1991) 240.
- [121] T. Bhattacharya and S. Willenbrock, Phys.Rev. **D47** (1993) 4022.
- [122] M. Veltman, Physica **29** (1963) 186.
- [123] Particle Data Group, J. Beringer *et al.*, Phys.Rev. **D86** (2012) 010001.
- [124] J. Butterworth *et al.*, [arXiv:1405.1067 \[hep-ph\]](#).
- [125] L. Landau, Nucl.Phys. **13** (1959) 181.
- [126] T. Kinoshita, J.Math.Phys. **3** (1962) 650.
- [127] T. Lee and M. Nauenberg, Phys.Rev. **133** (1964) B1549.
- [128] S. Dittmaier, Nucl.Phys. **B675** (2003) 447, [arXiv:hep-ph/0308246 \[hep-ph\]](#).
- [129] S. Catani and M. Seymour, Nucl.Phys. **B485** (1997) 291, [arXiv:hep-ph/9605323 \[hep-ph\]](#).
- [130] S. Catani, S. Dittmaier, and Z. Trocsanyi, Phys.Lett. **B500** (2001) 149, [arXiv:hep-ph/0011222 \[hep-ph\]](#).

- [131] D. Yennie, S. C. Frautschi, and H. Suura, *Annals Phys.* **13** (1961) 379.
- [132] F. A. Berends *et al.*, *Nucl.Phys.* **B206** (1982) 61.
- [133] S. Dittmaier, *Nucl. Phys.* **B565** (2000) 69, [hep-ph/9904440](#).
- [134] S. Dittmaier, A. Kabelschacht, and T. Kasprzik, *Nucl.Phys.* **B800** (2008) 146, [arXiv:0802.1405 \[hep-ph\]](#).
- [135] R. P. Feynman, *Phys.Rev.Lett.* **23** (1969) 1415.
- [136] J. Bjorken and E. A. Paschos, *Phys.Rev.* **185** (1969) 1975.
- [137] J. C. Collins, D. E. Soper, and G. F. Sterman, *Adv.Ser.Direct.High Energy Phys.* **5** (1988) 1, [arXiv:hep-ph/0409313 \[hep-ph\]](#).
- [138] V. Gribov and L. Lipatov, *Sov.J.Nucl.Phys.* **15** (1972) 438.
- [139] G. Altarelli and G. Parisi, *Nucl.Phys.* **B126** (1977) 298.
- [140] Y. L. Dokshitzer, *Sov.Phys.JETP* **46** (1977) 641.
- [141] K.-P. Diener, S. Dittmaier, and W. Hollik, *Phys.Rev.* **D72** (2005) 093002, [arXiv:hep-ph/0509084 \[hep-ph\]](#).
- [142] NNPDF, R. D. Ball *et al.*, *Nucl.Phys.* **B877** (2013) 2, 290, [arXiv:1308.0598 \[hep-ph\]](#).
- [143] R. D. Ball *et al.*, *Nucl.Phys.* **B867** (2013) 244, [arXiv:1207.1303 \[hep-ph\]](#).
- [144] A. Denner, S. Dittmaier, and L. Hofer, [arXiv:1407.0087 \[hep-ph\]](#).
- [145] A. Denner and S. Dittmaier, *Nucl.Phys.* **B734** (2006) 62, [arXiv:hep-ph/0509141 \[hep-ph\]](#).
- [146] A. Denner and S. Dittmaier, *Nucl.Phys.* **B844** (2011) 199, [arXiv:1005.2076 \[hep-ph\]](#).
- [147] G. P. Lepage, *J.Comput.Phys.* **27** (1978) 192.
- [148] G. P. Lepage, Cornell preprint CLNS-80/447 (1980) .
- [149] S. Catani, S. Dittmaier, M. H. Seymour, and Z. Trocsanyi, *Nucl.Phys.* **B627** (2002) 189, [arXiv:hep-ph/0201036 \[hep-ph\]](#).
- [150] L. Phaf and S. Weinzierl, *JHEP* **0104** (2001) 006, [arXiv:hep-ph/0102207 \[hep-ph\]](#).
- [151] K. Melnikov, A. Scharf, and M. Schulze, *Phys.Rev.* **D85** (2012) 054002, [arXiv:1111.4991 \[hep-ph\]](#).
- [152] J. M. Campbell, R. K. Ellis, and F. Tramontano, *Phys.Rev.* **D70** (2004) 094012, [arXiv:hep-ph/0408158 \[hep-ph\]](#).
- [153] A. Aeppli, G. J. van Oldenborgh, and D. Wyler, *Nucl. Phys.* **B428** (1994) 126, [hep-ph/9312212](#).
- [154] D. Wackeroth and W. Hollik, *Phys. Rev.* **D55** (1997) 6788, [hep-ph/9606398](#).

- [155] U. Baur, S. Keller, and D. Wackeroth, Phys.Rev. **D59** (1999) 013002, [arXiv:hep-ph/9807417](#) [hep-ph].
- [156] A. Denner, S. Dittmaier, and M. Roth, Nucl. Phys. **B519** (1998) 39, [hep-ph/9710521](#).
- [157] P. Gambino and P. A. Grassi, Phys.Rev. **D62** (2000) 076002, [arXiv:hep-ph/9907254](#) [hep-ph].
- [158] P. A. Grassi, B. A. Kniehl, and A. Sirlin, Phys.Rev. **D65** (2002) 085001, [arXiv:hep-ph/0109228](#) [hep-ph].
- [159] A. Denner, S. Dittmaier, M. Roth, and D. Wackeroth, Nucl.Phys. **B560** (1999) 33, [arXiv:hep-ph/9904472](#) [hep-ph].
- [160] A. Denner, S. Dittmaier, M. Roth, and L. Wieders, Nucl.Phys. **B724** (2005) 247, [arXiv:hep-ph/0505042](#) [hep-ph].
- [161] A. Denner, S. Dittmaier, and M. Roth, Phys.Lett. **B429** (1998) 145, [arXiv:hep-ph/9803306](#) [hep-ph].
- [162] W. Beenakker, A. P. Chapovsky, and F. A. Berends, Phys. Lett. **B411** (1997) 203, [hep-ph/9706339](#).
- [163] W. Beenakker, A. P. Chapovsky, and F. A. Berends, Nucl. Phys. **B508** (1997) 17, [hep-ph/9707326](#).
- [164] K. Melnikov and O. I. Yakovlev, Nucl. Phys. **B471** (1996) 90, [hep-ph/9501358](#).
- [165] S. Dittmaier, Phys.Rev. **D59** (1998) 016007, [arXiv:hep-ph/9805445](#) [hep-ph].
- [166] M. Roth, [arXiv:hep-ph/0008033](#) [hep-ph].
- [167] G. Passarino and M. Veltman, Nucl.Phys. **B160** (1979) 151.
- [168] V. Smirnov, *Feynman integral calculus*. Springer, 2006.
- [169] W. Beenakker, H. Kuijf, W. van Neerven, and J. Smith, Phys.Rev. **D40** (1989) 54.
- [170] B. Harris and J. Owens, Phys.Rev. **D65** (2002) 094032, [arXiv:hep-ph/0102128](#) [hep-ph].
- [171] G. 't Hooft and M. Veltman, Nucl.Phys. **B153** (1979) 365.

Acknowledgements

I would like to express my greatest gratitude to the people who have helped and supported me throughout my PhD studies.

First and foremost, I want to thank my supervisor Stefan Dittmaier for the opportunity to work under his guidance and for providing me with this interesting topic. I was able to profit immensely from his expertise in the field of particle physics and collider phenomenology and he always took the time to answer my question and gave me the decisive hints that lead me into the right direction. Furthermore, I want to thank him for the meticulous suggestions and comments on this dissertation.

I would like to offer my special thanks to Christian Schwinn for a fruitful collaboration on this project and for proof reading this manuscript. His broad knowledge in physics always led to very enlightening discussions and I thank him for his inexhaustible patience when I came to him with my questions.

I would also like to thank the current and former members of our research group who have supported me in many different ways over the last years. Each one of them contributed to creating a stimulating working environment and a positive atmosphere which has been a constant source of encouragement, especially at times when progress did not come easily. The many helpful discussions and constructive comments in particular during our weekly meetings were greatly appreciated.

Last but not least, I would like to extend my deepest gratitude to my family. Without their encouragement and support, this work would have not been possible.

List of publications

Parts of the results presented in this work have been published prior to submission of the thesis: Chapters 4 and 6 on the application of the PA to the EW corrections and the non-factorizable $\mathcal{O}(\alpha_s\alpha)$ corrections are largely based on the following publications:

- S. Dittmaier, A. Huss, and C. Schwinn, “Mixed QCD–electroweak $\mathcal{O}(\alpha_s\alpha)$ corrections to Drell–Yan processes in the resonance region: pole approximation and non-factorizable corrections”, Nucl.Phys. **B885** (2014) 318, [arXiv:1403.3216 \[hep-ph\]](#).
- S. Dittmaier, A. Huss, and C. Schwinn, “ $\mathcal{O}(\alpha_s\alpha)$ Corrections to Drell–Yan Processes in the Resonance Region”, PoS **RADCOR2013** (2013) 020.

First preliminary numerical results for the factorizable initial–final corrections presented in Chap. 7 were shown in conference proceedings

- S. Dittmaier, A. Huss, and C. Schwinn, “ $\mathcal{O}(\alpha_s\alpha)$ corrections to Drell–Yan processes in the resonance region”, PoS **LL2014** (2014) 045, [arXiv:1405.6897 \[hep-ph\]](#).

Other publications:

- S. Moch *et al.*, “High precision fundamental constants at the TeV scale”, proceedings of the MITP 2014 scientific program, [arXiv:1405.4781 \[hep-ph\]](#).
- J. Butterworth *et al.*, “Les Houches 2013: Physics at TeV Colliders: Standard Model Working Group Report”, Les Houches Workshop 2013: Standard Model Working Group, [arXiv:1405.1067 \[hep-ph\]](#).
- J. M. Campbell *et al.*, “Report of the Snowmass 2013 energy frontier QCD working group”, Snowmass 2013 Working Group Report: QCD, [arXiv:1310.5189 \[hep-ph\]](#).
- K. Mishra *et al.*, “Electroweak Corrections at High Energies”, Snowmass 2013 white paper on QCD, [arXiv:1308.1430 \[hep-ph\]](#).
- S. Dittmaier, A. Huss, and C. Speckner, “Weak radiative corrections to dijet production at the LHC”, PoS **DIS2013** (2013) 283, [arXiv:1306.6298 \[hep-ph\]](#).
- S. Dittmaier, A. Huss, and C. Speckner, “Weak radiative corrections to dijet production at hadron colliders”, JHEP **1211** (2012) 095, [arXiv:1210.0438 \[hep-ph\]](#).